EJA
European Journal of Anatomy
Volume 26 - Number 5 September 2022

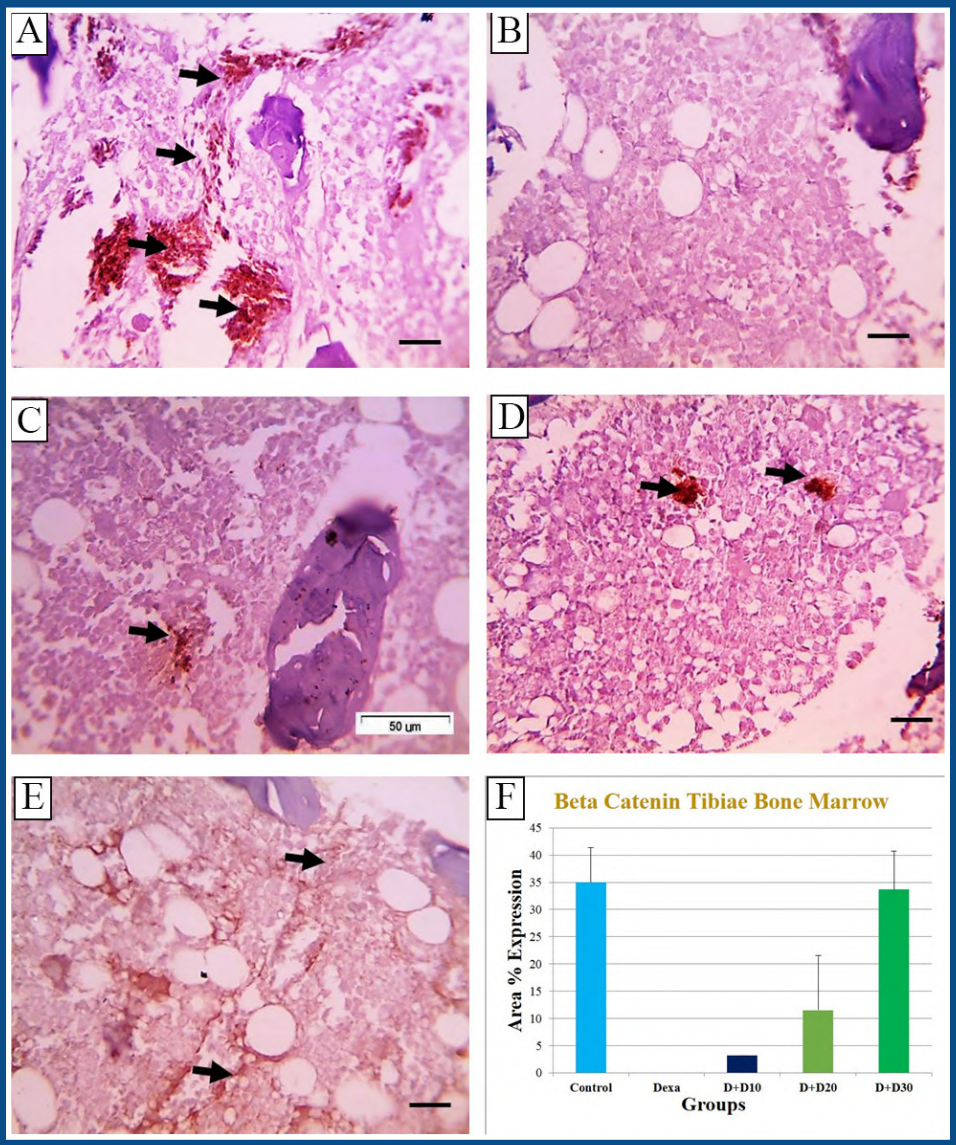

Indexed in:

CLARIVATE
• JCR:2020
• Q4 (21/23)
• I.F. J.C.I.: 0.19
DIALNET
EMBASE / Excerpta Medica

SCOPUS
• SJCR: 2020
• Q4 (31/39)
• I.F.: 0.162
Emerging Sources Citation Index
LATINDEX. Catálogo v1.0 (2002-2017)

Official Journal of the Spanish Society of Anatomy

www.eurjanat.com

European Journal of Anatomy

Volume 26 - Number 5 September 2022

The height of the sinuses of Valsalva depending on anthropometric data among Ukrainian population

Uliana Pidvalna[1], Vassyl A. Lonchyna[2], Dmytro Beshley [1,3,4], Lesya Mateshuk-Vatseba[1]

[1] *Danylo Halytsky Lviv National Medical University*
[2] *University of Chicago Pritzker School of Medicine*
[3] *Ukrainian-Polish Heart Center "Lviv"*
[4] *Lviv Regional Clinical Hospital*

SUMMARY

Sinuses of Valsalva height is an important parameter in planning cardiac surgery, percutaneous coronary intervention and transcatheter aortic valve implantation (TAVI). The aim of the study is to analyze the height of the sinuses of Valsalva depending on height, weight, body mass index, body surface area, and sex using computed tomography angiography images in Ukrainian population. 59 chest computed tomography angiography examination for non-cardiac reasons were retrospectively evaluated. Data were collected from Ukrainian citizen. The height of the Sinuses of Valsalva was measured as the distance between aortic annulus and sinotubular junction.

All three sinuses of Valsalva height were higher in men than in women ($p<0.001$). In men, three Sinuses of Valsalva had a correlation with height and body surface area (BSA) ($p<0.05$). In women, a correlation has been confirmed only between anthropometric measurements and the height of left and right coronary sinuses ($p<0,05$). The left coronary sinus height had a correlation with height, weight, body mass index (BMI) and BSA ($p<0,05$). The right coronary sinus height had a correlation with weight, BMI, and BSA ($p<0.05$). The parameters of the non-coronary sinus in women do not have confirmed direct correlations with any anthropometric measurements observed. The sinuses of Valsalva height is higher in males. The most significant confirmed correlations were between height and left and right coronary sinuses in men and women. Increased size of sinuses in men correlated with an increase of height, weight and decrease of BMI and BSA values.

Keywords: Aortic Anatomy – Aortic root – Sinuses of Valsalva – Height – Computed Tomographic Angiography

INTRODUCTION

The sinuses of Valsalva are components of the aortic root. It is differentiated into the right aortic sinus (RAS), the left aortic sinus (LAS) and the posterior or non-coronary sinus (NAS). The names of the Valsalva sinuses correspond to the right, left, and posterior (non-coronary) semilunar leaflets of the aortic valve (Razzolini et al., 2011). Semilunar leaflets of the aortic valve are

Corresponding author:
Uliana Pidvalna. Department of Anatomy, Danylo Halytsky Lviv National Medical University, Pekarska st, 69, Lviv, Ukraine, 79010. Phone: +380963551782. E-mail: uljaska.p@gmail.com

Submitted: March 21, 2022. **Accepted:** May 2, 2022

https://doi.org/10.52083/IYMG4367

named according to their corresponding location in the fetus. Postnatally, the names of the leaflets do not change, but their location does. The right semilunar leaflet is located in the anterior part, the left semilunar leaflet has a posterior-left position, and the posterior semilunar leaflet has a posterior-right position. Correspondently, the right aortic sinus is also known as the anterior aortic sinus, the left as the left posterior aortic sinus, and the posterior as the right posterior aortic sinus (Nasr and El Tahlawi, 2018). In clinical medicine the names are determined by the coronary artery ostia normally contained in these sinuses: the right coronary, the left coronary and the non-coronary sinuses (Ho, 2009). The height of the sinus of Valsalva is defined as the distance from the aortic annulus to the sinotubular junction (Hennessey et al., 2020). Syntopy of the sinuses of Valsalva occurs with the aortic valve leaflets, the leaflet attachments and the interleaflet trigones (Berdajs, 2016). The morphology of the sinuses of Valsalva correlates with the functioning of the aortic valve and the corresponding coronary artery blood supply to the left ventricle (Ho, 2009).

Classical cardiac surgery (using a sternotomy or mini-thoracotomy), endovascular procedures (coronary angiography, coronary artery stenting, transcatheter aortic valve implantation (TAVI)) and hybrid procedures require thorough knowledge of all components of the aortic root. Preoperative planning which takes into account the morphometric parameters of the aortic root allow for successful intervention and reduces the risk of possible complications (Freeman et al., 2013; Hennessey et al., 2020).

Within the general structure of the heart and main vessels, there are gender differences (Merz & Cheng, 2016; Taqueti, 2018) that must be taken into consideration. Gender differences affect the clinical findings, diagnostics and choice of treatment tactics (Merz and Cheng, 2016). The height of the person also influences the state of the cardiovascular system, especially in coronary artery disease (Nelson et al., 2015; Silventoinen et al., 2006). Studies have shown that people of short stature have a 50% higher risk of coronary artery disease and a higher mortality rate (Plonek et al., 2019; Rosenberg et al., 2014).

The aim of the study is to use computed tomography angiography (CTA) to compare the height of the right, left and posterior sinuses of Valsalva in men and women without any pathology of the heart and ascending aorta.

MATERIALS AND METHODS

Patient population. Patients of the Ukrainian-Polish Heart Center "Lviv" (Lviv, Ukraine) were involved in the given study. Inclusion criteria: patients without any signs of heart or ascending aorta disease undergoing contrast-enhanced Computed Tomography (CT) chest examination. Exclusion criteria: improper visualization of the aortic root, incomplete clinical data, refusal to be involved in the study, patients with anomalies of the heart, ascending aorta or coronary vessels. All patients signed the informed consent (signed by the patient or official representative) according to the Declaration of Helsinki and the national legal regulations (Ethics Committee Approval: Bioethics Commission of Danylo Halytsky Lviv National Medical University, protocol No. 10, 20 December 2021).

CTA images of 59 patients were selected with the following gender distribution: 43 men and 16 women. The patients were scanned using the MDCT scanner LightSpeed VCT XT, GE (General Electric, USA) with 64-row chest CT with administration of the contrast agent Ultravist 470 (Bayer Healthcare, Germany). CT angiography images were evaluated on a dedicated CT workstation (General Electric, USA) by two independent observers with experience in assessment of contrast-enhanced CT images of the chest. The following parameters were measured: the distance between the aortic annulus and the sinotubular junction, labeled as the height of the right, left and non-coronary sinuses. All measurements were done according to the updated 2019 Guidelines (Blanke et al., 2019). Each aortic cusp was first identified and then the height of each sinus of Valsalva was measured. The body surface area (BSA) was calculated as the square root of the height multiplied by the weight divided by 3600 (Mosteller formula). The body mass index was calculated as weight (in kilograms) divided by the height in meters squared.

The results of the study were analyzed using the methods of descriptive and analytical statistics. The statistical analysis was conducted using the SPSS version 22.0 for Windows (IBM Corp., Armonk, NY, USA). The normality of data distribution was assessed using Shapiro-Francia test. Values are presented in mean ± standard deviation. Student's *t*-test was performed to compare means. P-value of <0.05 was considered significant. The correlation between the observed variables has been calculated using Pearson's linear correlation method (r). Multiple correlation and regression analysis have been performed in Statistica 10, allowing for accurate calculations and their visual presentations.

RESULTS

A total of 59 CTA examinations were collected from adults of both sexes and same ages: 43 (73%) males, aged 53 ± 14 years, and 16 (37%) females, aged 56 ± 13 (p = 0.33). All patients were free of structural heart and ascending aortic disease. Men's height differed significantly from that of women: men 1.76 ± 0.07 m and women 1.63 ± 0.04 m (p <0.001). Clinical characteristics of patients are presented in Table 1.

Table 1. Characteristics of the patients.

Parameters	Male (n=43)	Female (n-16)	P value
Age (y)	52.56±13.52	56.38±13.34	0.33
Height (m)	1.76±0.07	1.63±0.04	<0.001*
Weight (kg)	84.74±14.14	76.5±13.48	0.04*
BMI (kg/m^2)	27.54±4.74	28.79±5.19	0.40
BSA (m^2)	2.03±0.18	1.85±0.17	0.001*

BMI: Body mass index; BSA: Body surface area; * P-value of <0.05 was considered significant

CTA images received in the course of the study were analyzed in double oblique multiplanar reconstruction. The height of the sinuses of Valsalva was measured from the level of the aortic annulus to the sinotubular junction. All measurements were performed on a perpendicular plane to the long axis of the vessel.

There is a statistically significant difference in the height of the sinuses of Valsalva (as measured between the aortic annulus and the sinotubular junction) in men and women. The height of the anterior (right) sinus of Valsalva was 24.27 ± 3.83 mm in men and 18.59 ± 2.25 mm in women. This was 5.68 mm higher (1.3 times) in men than in women (p <0.001). The height of the left sinus of Valsalva in men is 4.62 mm higher (1.31 times) (p <0.001) than in women (23.49 ± 3.33 mm and 17.87 ± 1.82 mm respectively). The height of the non-coronary sinus of Valsalva in men is 1.26 times higher (p <0.001) than in women (24.83 ± 3.59 mm and 19.71 ± 2.17 mm respectively) (Fig. 1).

In view of the abovementioned, it appeared reasonable to study the correlation between sinuses of Valsalva height and anthropometric measurements of men and women. For this purpose, multiple correlation and regression analysis have been used. Key impact factors have been selected based on Pearson's correlation analysis. Essential independent variables are presented in Tables 2, 3.

Correlation analysis has confirmed a correlation between height and BSA and sinuses of Valsalva measurements in men: strong direct correlation with height (r = from +0.71 to +0.75, p<0.05) and moderate direct correlation with BSA (r = from +0.31 to +0.42, p<0.05). In women, a correlation has been confirmed only between anthropometric measurements and the sizes of left and right coronary sinuses. Left coronary sinus size has a moderate direct correlation with height (r=+0.41, p<0.05), weight (r=+0.52, p<0.05), BMI (r=+0.40, p<0.05) and BSA (r=+0.57, p<0.05); right coronary sinus size has a correlation with weight (r=+0.33, p<0.05), BMI (r=+0.31, p<0.05) and BSA (r=+0.32, p<0.05). The parameters of the non-coronary sinus in women do not have confirmed direct correlations with any anthropometric measurements observed. It has been additionally established that there is no confirmed correlation between age and the height of sinuses of Valsalva in men and women.

Based on the findings obtained, multiple correlation coefficient R has been calculated, which points to the strength of correlation between the dependent variables (sinuses of Valsalva) and the combination of independent variables (height, weight, BMI, BSA) (Table 4).

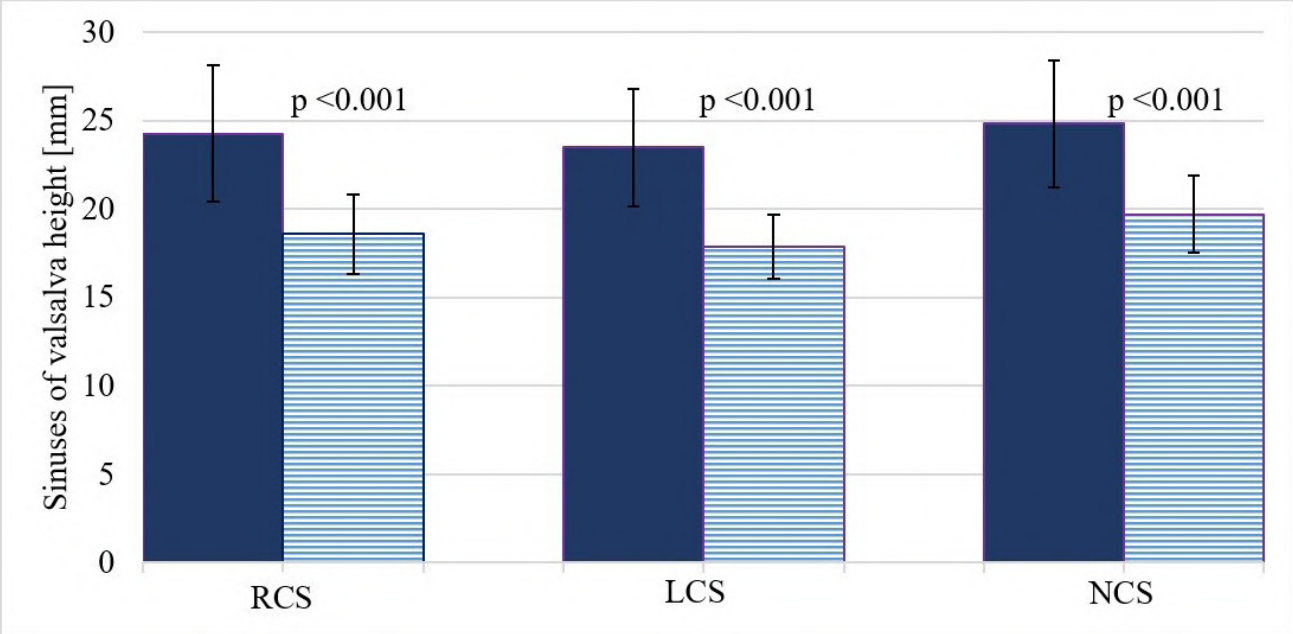

Fig. 1.- Differences between the height of the sinuses of Valsalva in the male *(solid bar)* and female *(striped bar)* cohorts. Values are presented as mean ± standard deviation. See measurements in Tables 2 and 3. *RCS*, Right coronary sinus; *LCS*, Left coronary sinus; *NCS*, Non-coronary sinus.

Table 2. Correlation relationship (r) between anthropometric measurements and sinus of Valsalva height in men.

Parameters	Age (y)	Height (m)	Weight (kg)	BMI (kg/m²)	BSA (m²)	LCS (mm)	RCS (mm)	NCS (mm)
Age (y)	-	-0.28	0.03	0.14	-0.03	-0.10	-0.06	-0.30
Height (m)	-0.28	-	0.18	-0.27	0.40*	0.75*	0.71*	0.74*
Weight (kg)	0.03	0.18	-	0.90*	0.97*	0.27	0.16	0.20
BMI (kg/m²)	0.14	-0.27	0.90*	-	0.78*	-0.07	-0.16	-0.13
BSA (m²)	-0.03	0.40*	0.97*	0.78*	-	0.42*	0.31*	0.35*
LCS (mm)	-0.10	0.75*	0.27	-0.07	0.42*	-	0.86*	0.74*
RCS (mm)	-0.06	0.71*	0.16	-0.16	0.31*	0.86*	-	0.63*
NCS (mm)	-0.30	0.74*	0.20	-0.13	0.35*	0.74*	0.63*	-

BMI: Body mass index; BSA: Body surface area; RCS: Right Coronary Sinus; LCS: Left Coronary Sinus; NCS: Non-Coronary Sinus.
Note. * - confirmed (p<0.05) correlation

Table 3. Correlation relationship (r) between anthropometric measurements and sinus of Valsalva height in women.

Parameters	Age (y)	Height (m)	Weight (kg)	BMI (kg/m²)	BSA (m²)	LCS (mm)	RCS (mm)	NCS (mm)
Age (y)	-	-0.12	0.00	0.03	0.02	0.14	-0.12	-0.14
Height (m)	-0.12	-	0.06	-0.22	0.20	0.41*	0.06	0.25
Weight (kg)	0.00	0.06	-	0.96*	0.99*	0.52*	0.33*	0.01
BMI (kg/m²)	0.03	-0.22	0.96*	-	0.91*	0.40*	0.31*	-0.06
BSA (m²)	0.02	0.20	0.99*	0.91*	-	0.57*	0.32*	0.03
LCS (mm)	0.14	0.41*	0.52*	0.40*	0.57*	-	0.56*	0.24
RCS (mm)	-0.12	0.06	0.33*	0.31*	0.32*	0.56*	-	0.43*
NCS (mm)	-0.14	0.25	0.01	-0.06	0.03	0.24	0.43*	-

BMI: Body mass index; BSA: Body surface area; RCS: Right Coronary Sinus; LCS: Left Coronary Sinus; NCS: Non-Coronary Sinus.
Note. * - confirmed (p<0.05) correlation

Table 4. Results of calculations for multiple correlation and regression analysis of the sinuses of Valsalva height and anthropometric measurements observed in men and women.

Parameters	Males		Females	
	R	p	R	p
NCS (mm)	0.76	0.00001	0.46	0.75
LCS (mm)	0.77	0.000002	0.72	0.014
RCS (mm)	0.73	0.00002	0.36	0.90

NCS: Non-Coronary Sinus; LCS: Left Coronary Sinus; RCS: Right Coronary Sinus.

A strong direct correlation has been identified in men between the anthropometric measurements observed and the sinuses of Valsalva height indicators (R = from +0.73 to +0.77, p<0.001). Increased size of sinuses in men correlated with an increase of height, weight and a decrease of BMI and BSA values.

Within the group of women, multiple correlation and regression of independent variables (anthropometric data) have been confirmed only for the dependent variable «left coronary sinus» (R=+0.72, p=0.014), while for other sinuses the correlation was insufficient (p>0.05). The size (increase) of the left coronary sinus in women was affected by the increase of height and BMI and decreased BSA. Fig. 2 and Fig. 3 visualize the above-described correlations between left coronary sinus parameters and anthropometric data in men and women.

DISCUSSION

The present study represents a single-center data of the height of the sinuses of Valsalva in subjects without heart disease or ascending aorta disease undergoing contrast-enhanced CT. Data assessed by CTA is considered the fastest and one of the most accurate methods of measuring the aorta, with very high spatial resolution (Blondheim et al., 2016). We studied the relationship of variations with sex and height. Patients were distributed by gender (43 men vs 16 women).

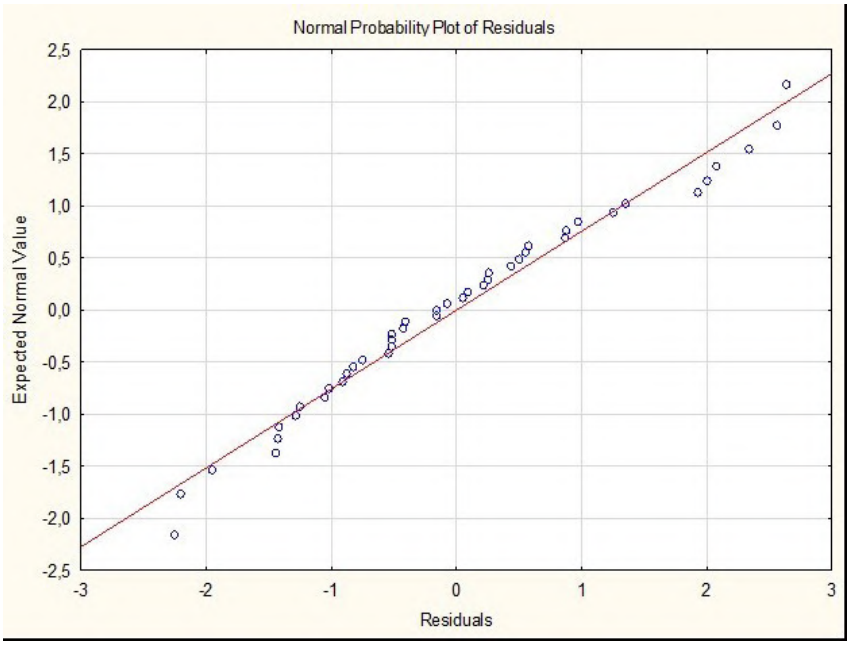

Fig. 2.- Visualization of multiple correlation and regression analysis of the left coronary sinus of Valsalva and anthropometric measurements observed in men.

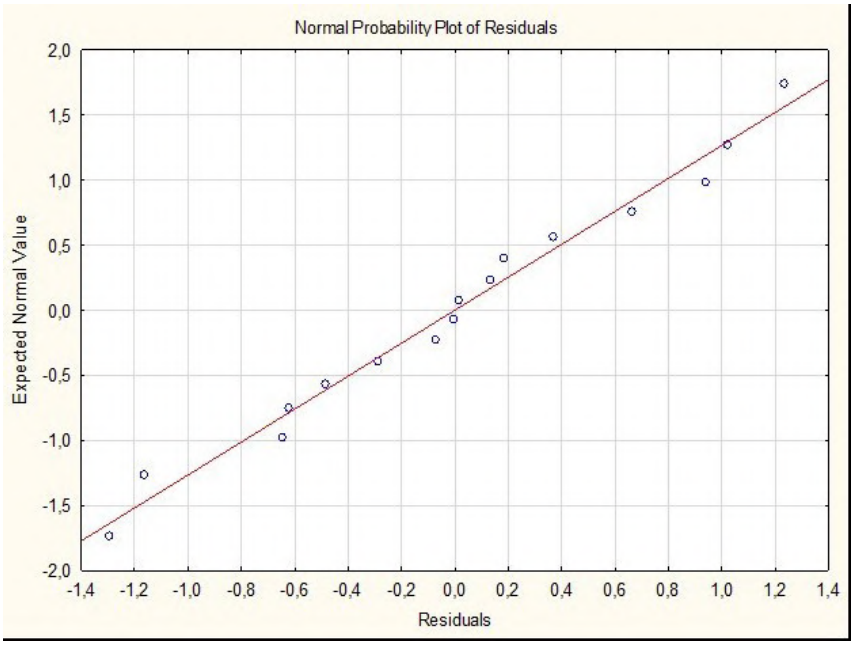

Fig. 3.- Visualisation of multiple correlation and regression analysis of the left coronary sinus of Valsalva and anthropometric factors observed in women.

We found a constant difference in the size of the right, left coronary and non-coronary sinuses of Valsalva in the male as compared to the female cohort. The sinuses of Valsalva are higher in men than in women ($p < 0.001$). The left sinus of Valsalva in men is 1.31 times higher than in women, and almost the same difference is observed in the height of the right (1.3 times) and the non-coronary sinus of Valsalva (1.26 times). Our results are in general agreement with published studies, i.e., that right and left coronary sinuses of Valsalva are greater in males (Knight et al., 2009; Stolzmann et al., 2009). Those publications reporting differences in both the left and the right coronary sinuses omitted measurement of the non-coronary sinus of Valsalva. It could be explained by their focus on precise location of the coronary artery ostia only. The shorter the right sinus of Valsalva, the lower the location of the right coronary artery ostium. This is an important consideration in patients undergoing aortic valve surgery. A high location of the right coronary artery ostium with a sufficient height of the right coronary sinus allows for easier and safer aortic valve replacement. It is, however, a frequent location of air embolism occurrence during the de-aeration stage of cardiac surgery, which can lead to sudden life-threatening arrhythmias. The height of the left coronary sinus is important because of the location of the left main coronary artery ostium.

The anatomy of the non-coronary sinus of Valsalva should not be omitted in measurements. The reason is that the posterior sinus of Valsalva lies in the interatrial groove, thus bordering with right and left atrium simultaneously. Additionally, the height of the non-coronary sinus is important in clinical practice, as in choosing the type of aortic valve prosthesis, the position of implantation (annular, sub- or supra-annular), and the method of suturing the aortic valve prosthesis. Low height of the non-coronary sinus is always identified with the higher percentage of the intraoperative conduction disturbances, as the length of the aortic-mitral junction decreases and, as a result, the conduction bundle passes closer to the aortic annulus in the projection of the non-coronary sinus (Charitos and Sievers, 2013). With the bicuspid aortic valve and the sagittal location of the effective orifice (Sievers type I), the plane of the non-coronary sinus is 1/3 lower than the other fused sinus (Stephens et al., 2015). Thus, surgeons have to take into account the given anatomical feature to prevent the displacement of the plane

of the implanted aortic valve prosthesis towards the left ventricle outflow tract. The height of the non-coronary sinus is also crucial for the choice of patch height in patients with a narrow aortic annulus in the aortic root dilatation operations (Nicks and Manouguian techniques) (Massias et al., 2021). In the present study, the non-coronary sinus in men correlates with height and BSA, and does not have confirmed direct correlations with any anthropometric measurements in women.

The geometry of the sinuses of Valsalva is of the considerable importance in surgery aiming at the aortic root reimplantation into the vascular prosthesis (David I-V operations) (Miller, 2003) as well as in aortic root remodeling (Yacoub Procedure, Urbanski operation) (Yacoub et al., 2018), because the most accurate restoration of all the anatomical structures of the aortic root ensures appropriate and long-term functioning of the aortic valve. The length and height of the aortic root sinuses are the main indicators in the operation of neocuspidation of the aortic valve (Ozaki operation) (Alhan, 2019).

Authors have reported that age (Vriz et al., 2013) and gender (Koepke et al., 2018) have an impact on the cardiovascular system. With age, the number of collagen fibers increases and replace the elastin fibers changing the histological structure of aorta (Komutrattananont et al., 2019). Many authors pay attention to increasing aortic diameter with age (Bahlmann et al., 2011; Komutrattananont et al., 2019; Vriz et al., 2013). Changes in the geometry and diameter of the sinuses of Valsalva affect the hemodynamics and the nature of the flow at the aortic root (Kivi et al., 2020). The results of the present study do not confirm a correlation between age and the height of sinuses of Valsalva in both gender groups. It should be noted that the previously published studies compare horizontal measurements (diameter) of the aorta. The probable aging changes in the height of the sinuses of Valsalva require further investigation.

Height correlates with the cardiovascular events. Tall people have lower incidence and mortality rate from the coronary heart disease (Nelson et al., 2015; Rosenberg et al., 2014; Silventoinen et al., 2006). Short stature has an association with a higher incidence of cardiovascular disease events (Paajanen et al., 2010). Therefore, the patient's height is one of the indicators that might be considered to predict risks of cardiovascular disease. The current study confirms a strong direct correlation between height and the size of all the three sinuses of Valsalva in men. In female cohorts only the size of the left coronary sinus of Valsalva has a moderate direct correlation with height. The impact of gender on the aortic root anatomy may be considered an additional factor. Interestingly, the degree of correlation in women is lower than in men.

BMI and BSA, which are calculated with formulas using height and weight, have a different correlation with the sinuses of Valsalva measurements in two groups. In men, correlation analysis has confirmed a moderate direct correlation between BSA and right, left and non-coronary sinus. In female cohorts, left and right coronary sinus size have a moderate direct correlation with BMI and BSA.

Multiple correlation coefficient R, which was used to point to the strength of correlation, showed a strong direct correlation in men between the anthropometric measurements (height, weight, BMI, BSA) and the sinuses of Valsalva height indicators ($p<0.001$). Increased size of sinuses in men correlated with an increase of height, weight and decrease of BMI and BSA values. Within the group of women, the increased size of the left coronary sinus was affected by the increase of height and BMI and decreased BSA.

In conclusion, we found an association between gender and patient height and the height of the sinuses of Valsalva. The sinuses of Valsalva height is higher in males. The most significant confirmed correlations were between height and left and right coronary sinuses in men and women. Increased size of sinuses in men correlated with an increase of height, weight and decrease of BMI and BSA values.

Limitations of the study

The study design was limited to a group of patients consisting of Ukrainians and was not repeated with different ethnic groups. Intra- and inter-group variability of the sinuses of

Valsalva height was measured only with CTA, and no comparison was made with other possible diagnostic methods (ECHO, MRI, IVUS).

Sources of Funding

The study was conducted within the scientific research program of the Department of Normal Anatomy at Danylo Halytsky Lviv National Medical University (Lviv, Ukraine) according to the research topic "Morphofunctional features of organs in pre- and post-natal ontogenetic periods under the influence of opioids, food additives, reconstructive surgeries and obesity"; the research program is funded from the State Budget of The Ministry of Health of Ukraine.

REFERENCES

ALHAN C (2019) Ozaki Procedure. *Turkish J Thorac Cardiovasc Surg*, 27(4): 451-453.

BAHLMANN E, NIENABER CA, CRAMARIUC D, GOHLKE-BAERWOLF C, RAY S, DEVEREUX RB, WACHTELL K, KUCK KH, DAVIDSEN E, GERDTS E (2011) Aortic root geometry in aortic stenosis patients (a SEAS substudy). *Eur J Echocardiogr*, 12(8): 585-590.

BERDAJS DA (2016) Aortic root morphology: a paradigm for successful reconstruction. *Interact Cardiovasc Thorac Surg*, 22(1): 85-91.

BLANKE P, WEIR-MCCALL JR, ACHENBACH S, DELGADO V, HAUSLEITER J, JILAIHAWI H, MARWAN M, NORGAARD BL, PIAZZA N, SCHOENHAGEN P, LEIPSIC JA (2019) Computed tomography imaging in the context of transcatheter aortic valve implantation (TAVI) / transcatheter aortic valve replacement (TAVR): An expert consensus document of the Society of Cardiovascular Computed Tomography. *J Cardiovasc Computed Tomography*, 13(1): 1-20.

BLONDHEIM DS, VASSILENKO L, GLICK Y, ASIF A, NACHTIGAL A, MEISEL SR, SHOCHAT M, SHOTAN A, ZEINA A (2016) Aortic dimensions by multi-detector computed tomography vs. echocardiography. *J Cardiol*, 67(4): 365-370.

CHARITOS E, SIEVERS H (2013) Anatomy of the aortic root: implications for valve-sparing surgery. *Ann Cardiothorac Surg*, 2(1): 53-56.

FREEMAN L, YOUNG P, FOLEY T, WILLIAMSON E, BRUCE C, GREASON K (2013) CT and MRI assessment of the aortic root and ascending aorta. *Am J Roentgenol*, 200(6): 581-592.

HENNESSEY B, VERA-URQUIZA R, MEJÍA-RENTERÍA H, GONZALO N, ESCANED J (2020) Contemporary use of coronary computed tomography angiography in the planning of percutaneous coronary intervention. *Int J Cardiovasc Imaging*, 36(12): 2441-2459.

HO S (2009) Structure and anatomy of the aortic root. *Eur J Echocardiogr*, 10(1): 3-10.

KIVI A, SEDAGHATIZADEH N, CAZZOLATO B, ZANDER A, NELSON A, ROBERTS-THOMSON R, YOGANATHAN A, ARJOMANDI M (2020) Hemodynamics of a stenosed aortic valve: Effects of the geometry of the sinuses and the positions of the coronary ostia. *Int J Mechan Sci*, 188: 106015.

KNIGHT J, KURTCUOGLU V, MUFFLY K, MARSHALL W, STOLZMANN P, DESBIOLLES L, SEIFERT B, POULIKAKOS D, ALKADHI H (2009) Ex vivo and in vivo coronary ostial locations in humans. *Surg Radiol Anat*, 31(8): 597-604.

KOEPKE N, FLORIS J, PFISTER C, RÜHLI F, STAUB K (2018) Ladies first: Female and male adult height in Switzerland, 1770-1930. *Economics Human Biol*, 29: 76-87.

KOMUTRATTANANONT P, MAHAKKANUKRAUH P, DAS S (2019) Morphology of the human aorta and age-related changes: anatomical facts. *Anat Cell Biol,* 52(2): 109-114.

MASSIAS S, PITTAMS A, MOHAMED M, AHMED S, YOUNAS H, HARKY A (2021) Aortic root enlargement: When and how. *J Cardiac Surg*, 36(1): 229-235.

MERZ A, CHENG S (2016) Sex differences in cardiovascular ageing. *Heart*, 102(11): 825-831.

MILLER D (2003) Valve-sparing aortic root replacement in patients with the Marfan syndrome. *J Thorac Cardiovasc Surg*, 125(4): 773-778.

NASR A, EL TAHLAWI M (2018) Anatomical and radiological angiographic study of the coronary ostia in the adult human hearts and their clinical significance. *Anat Cell Biol*, 51(3): 164-173.

NELSON C, HAMBY S, SALEHEEN D, HOPEWELL J, ZENG L, ASSIMES T, KANONI S, WILLENBORG C, BURGESS S, AMOUYEL P, ANAND S, BLANKENBERG S, BOEHM B, CLARKE R, COLLINS R, DEDOUSSIS G, FARRALL M, FRANKS P, GROOP L, SAMANI N (2015) Genetically determined height and coronary artery disease. *New Engl J Med*, 372(17): 1608-1618.

PAAJANEN T, OKSALA N, KUUKASJÄRVI P, KARHUNEN P (2010) Short stature is associated with coronary heart disease: a systematic review of the literature and a meta-analysis. *Eur Heart J*, 31(14): 1802-1809.

PLONEK T, BEREZOWSKI M, BOCHENEK M, FILIP G, RYLSKI B, GOLESWORTHY T, JASINSKI M (2019) A comparison of aortic root measurements by echocardiography and computed tomography. *J Thorac Cardiovasc Surg*, 157(2): 479-486.

RAZZOLINI R, LONGHI S, TARANTINI G, RIZZO S, NAPODANO M, ABATE E, FRACCARO C, THIENE G, ILICETO S, GEROSA G, BASSO C (2011) Relation of aortic valve weight to severity of aortic stenosis. *Am J Cardiol*, 107(5): 741-746.

ROSENBERG M, LOPEZ F, BŮŽKOVÁ P, ADABAG S, CHEN L, SOTOODEHNIA N, KRONMAL R, SISCOVICK D, ALONSO A, BUXTON A, FOLSOM A, MUKAMAL K (2014) Height and risk of sudden cardiac death: the atherosclerosis risk in communities and cardiovascular health studies. *Ann Epidemiol*, 24(3): 174-179.e2.

SILVENTOINEN K, ZDRAVKOVIC S, SKYTTHE A, MCCARRON P, HERSKIND A, KOSKENVUO M, DE FAIRE U, PEDERSEN N, CHRISTENSEN K, KAPRIO J (2006) Association between height and coronary heart disease mortality: a prospective study of 35,000 twin pairs. *Am J Epidemiol*, 163(7): 615-621.

STEPHENS E, HOPE T, KARI F, KVITTING J, LIANG D, HERFKENS R, MILLER D (2015) Greater asymmetric wall shear stress in Sievers' type 1/LR compared with 0/LAT bicuspid aortic valves after valve-sparing aortic root replacement. *J Thorac Cardiovasc Surg*, 150(1): 59-68.

STOLZMANN P, KNIGHT J, DESBIOLLES L, MAIER W, SCHEFFEL H, PLASS A, KURTCUOGLU V, LESCHKA S, POULIKAKOS D, MARINCEK B, ALKADHI H (2009) Remodelling of the aortic root in severe tricuspid aortic stenosis: implications for transcatheter aortic valve implantation. *Eur Radiol*, 19(6): 1316-1323.

TAQUETI V (2018) Sex differences in the coronary system. *Adv Exp Med Biol*, 1065: 257-278.

VRIZ O, DRIUSSI C, BETTIO M, FERRARA F, D'ANDREA A, BOSSONE E (2013) Aortic root dimensions and stiffness in healthy subjects. *Am J Cardiol*, 112(8): 1224-1229.

YACOUB M, AGUIB H, GAMRAH M, SHEHATA N, NAGY M, DONIA M, AGUIB Y, SAAD H, ROMEIH S, TORII R, AFIFI A, LEE S (2018) Aortic root dynamism, geometry, and function after the remodeling operation: Clinical relevance. *J Thorac Cardiovasc Surg*, 156(3): 951-962.

MO11 and MS06 ameliorated cadmium chloride-induced neuro-inflammation, hyperplasia and apoptosis via NF-kB/ Caspase-3/p53 pathway and down-regulated sVEGFR in rats

Adelaja Akinlolu[1], Mubarak Ameen[2], Gabriel Ebito[3], Nnaemeka Asogwa[4], Raheem Akindele[5], Bamidele Fagbounka[6], Temitope Akintunde[7], Fatimah Odunola[7], Simisola Osibowale[7], Muhideen Adepeju[7]

[1] Department of Anatomy, Faculty of Basic Medical Sciences, University of Medical Sciences Ondo, Ondo State, Nigeria

[2] Department of Chemistry, Faculty of Physical Sciences, University of Ilorin, Kwara State, Nigeria

[3] Department of Anatomy, Faculty of Basic Medical Sciences, Ekiti State University, Ekiti State, Nigeria

[4] Central Research Laboratory, Tanke, Ilorin, Kwara State, Nigeria

[5] Department of Physiology, Faculty of Basic Medical Sciences, Babcock University, Ogun State, Nigeria

[6] Department of Biochemistry, Faculty of Basic Medical Sciences, Olabisi Onabanjo University, Ogun State, Nigeria

[7] Department of Anatomy, Faculty of Basic Medical Sciences, Olabisi Onabanjo University, Ogun State, Nigeria

SUMMARY

Cadmium is a neurotoxin, carcinogen and a suspected agent in aetiology of Parkinson's disease and Alzheimer's disease (AD). Furthermore, upregulations of Caspase-3 and p53 were reported in brains of AD patients. This study evaluated the neuroprotective potentials of MO11 (isolated from *Moringa oleifera* leaves) and MS06 (isolated from *Musa sapientum* suckers) in Cadmium Chloride (CdCl)-induced neurotoxicity in the cerebrum of rats.

Twenty-eight adult male wistar rats (average weight of 155 g) were randomly divided into 7 groups (n = 4). Group 1 received physiological saline. Groups 2-4 and 7 received single 1.5 mg/Kg bodyweight of CdCl (i.p.) (Day 1). Groups 3-4 and 7 were post-treated with 15 mg/Kg bodyweight of MO11, 15 mg/Kg bodyweight of MO11 + 7 mg/Kg bodyweight of MSF1 and 3.35 mg/Kg bodyweight of Doxorubicin respectively (Days 1-17). Groups 5-6 received only MO11 and Vegetable Oil (vehicle) respectively (Days 1-17). Cerebral histopathology (Cresyl Fast Violet method) was evaluated in rats. ELISA evaluations of biomarkers of pro-inflammation (IL-1β, IL-6, IL-8 and NF-kB), anti-inflammation (IL-4 and IL-10), apoptosis (Caspase-3 and p53), proliferation (Ki67) and angiogenesis (sVEGFR) in cerebral homogenates of rats were also conducted.

Histopathological evaluations showed a high number of chromatolytic cells in Group 2, compared with Groups 1 and 3-7. Post-

Corresponding author:
Adelaja Akinlolu. Department of Anatomy, Faculty of Basic Medical Sciences, University of Medical Sciences Ondo, Ondo State, Nigeria. Phone: +2348062765308. E-mail: aadelaja@unimed.edu.ng

Submitted: December 10, 2021. **Accepted:** May 5, 2022

https://doi.org/10.52083/UUTB8311

treatments of CdCl-induced neurotoxicity with MO11 and MS06 resulted in decreased levels of IL-1β, IL-6, IL-8, NF-kB, Caspase-3, Ki67, p53 and sVEGFR, but increased levels of IL-4 and IL-10 in Groups 3-4, compared with Group 2. Therefore, MO11 and MS06 possess neuroprotective, neuroregenerative, anti-AD, anti-inflammatory and anticancer potentials.

Key words: Cadmium – Neurotoxicity – Alzheimer's disease – *Moringa oleifera* – *Musa sapientum* – Neuroprotection – Neuroregeneration

INTRODUCTION

Cadmium (Cd), according to the World Health Organization, is one of the 10 chemicals of concern for human health (Andjelkovic et al., 2019). Cd was classified as a human carcinogen by the National Toxicology program (Wang and Du, 2013) and the International Agency for Research on Cancer (Huff et al., 2007). Cd-induced toxicity resulted in systemic dysfunctions such as neurotoxicity (Wang and Du, 2013; Batool et al., 2019), skin alopecia and ulceration (Lansdown et al., 2001), inflammation and hepatotoxicity (Bernhoft, 2013; Wang and Du, 2013; Andjelkovic et al., 2019).

Human Cd-exposure is associated with dysfunctions of the nervous system resulting in symptoms such as impaired learning capacity, headache and vertigo, decreased cognitive functions, olfactory dysfunction, poor vasomotor functioning, parkinsonian-like symptoms, peripheral neuropathy and poor equilibrium and balance co-ordination (Wang and Du, 2013). Cd-exposure has also been suspected as an etiological factor in the development of Parkinson's disease (PD) and Alzheimer's disease (AD) (Wang and Du, 2013). Increased concentrations in total Cd-exposure was associated with dyslexia or learning difficulties, decreased visual motor capacity and mental retardation in children (Wang and Du, 2013). It is, therefore, scientifically relevant to develop drug candidates from plants or other sources which can prevent or eliminate resulting dysfunctions of the nervous system due to Cd-induced neurotoxicity.

Moringa oleifera (MO) and *Musa sapientum* (MS) are ethno-medicinal plants that are well grown in Nigeria (Akinlolu et al., 2021). Furthermore, MOF6, which was fractionated from MO leaves using column chromatography methods, showed significant antioxidant and neuro-protective potentials against Cuprizone-induced cerebellar damage in rats (Omotoso et al., 2018), as well as neuro-protective potentials against dysregulated Acetylcholinesterase concentrations in Sodium arsenite-induced neurotoxicity in rats (Akinlolu et al., 2020a). MOF6 equally showed hepato-protective, anti-proliferation and anti-drug resistance potentials in 7,12-Dimethylbenz[a]anthracene-induced hepato-toxicity in rats (Akinlolu et al., 2021). Similarly, MSF1, which was fractionated from MS sucker using column chromatography methods possesses hepatoprotective, antiproliferation and antidrug resistance potentials in 7,12-Dimethylbenz[a]anthracene-induced hepato-toxicity in rats (Akinlolu et al., 2021).

Cd-induced neuro-toxicity has been suggested to result from increased oxidative stress, dysregulation and dysfunction of neurotransmitters, estrogen-like effect, interactions with heavy metals such as zinc and cobalt and epigenetic effects (Wang and Du, 2013; Batool et al., 2019). The mechanism underlying Cd-induced neurotoxicity remains poorly understood and unresolved till date. What mechanism underlies Cd-induced neuroinflammation? What is the relationship between Cd-induced neuroinflammation and neuronal cell death? Cd is an established carcinogen (Wang and Du, 2013; Batool et al., 2019), and mutagenesis is associated with increased angiogenesis (Batchelor et al., 2009). What type of relationship exists amongst Cd-induced apoptosis, hyperplasia, angiogenesis and mutagenesis? Finally, what are the effects of post-treatments with MO and MS on the possible mechanisms underlying Cd-induced neurotoxicity, neuroinflammation, apoptosis, hyperplasia, angiogenesis and mutagenesis?

Cd generally exists as a divalent cation, complexed with other elements, such as Cadmium Chloride (CdCl) (Bernhoft, 2013; Andjelkovic et al., 2019). Cd-induced neurotoxicity possibly results from increased oxidative stress, and neuronal cell death (apoptosis) are cell-specific, with cerebral cortical neurons as main targets (Wang and Du,

2013). In this study, the most active antioxidant and antimicrobial cytotoxic compounds were isolated from MO leaves (MO11) and MS suckers (MS06) respectively. Therefore, in order to further understand the mechanisms underlying Cd-induced neurotoxicity and in order to determine the neuroprotective potentials of MO and MS, this study evaluated the effects of MO11 and MS06 on CdCl-induced neuroinflammation, apoptosis, hyperplasia, angiogenesis, mutagenesis and neurodegeneration in the cerebral cortices of adult male Wistar rats.

MATERIALS AND METHODS

Ethical Approval

Ethical approval for this study was sought and received from the Ethical Review Committee of the University of Ilorin, Nigeria. Appropriate measures were observed to ensure minimal pain or discomfort of rats used in this study. The ethical approval number is UERC/ASN/2018/1161. Furthermore, this research study was conducted in accordance with the internationally accepted principles for laboratory animal use and care as provided in the European Community guidelines (EEC Directive of 1986; 86/609/EEC), the Directive 2010/63/Eu of the European Parliament and of the Council of 22 September 2010 on the protection of animals used for scientific purposes and the Guidelines of the U.S. Public Health Service and NIH regarding the care and use of animals for experimentation (NIH publication #85-23, revised in 985).

Collection, authentication and deposition of *Moringa oleifera* (MO) leaves and *Musa sapientum* (MS) suckers

Freshly cut MO leaves and MS suckers were obtained locally from forest reserves in Ilorin and samples identified and authenticated by a Pharmaceutical Botanist of the Department of Botany, Faculty of Life Sciences, University of Ilorin, Ilorin, Nigeria. Samples of MO leaves and MS suckers were deposited at the herbarium of the Department of Botany, Faculty of Life Sciences, University of Ilorin, and assigned Herbarium Identification Numbers UILH/001/1249 and UILH/002/1182 respectively.

Extraction and partitioning of fractions of MO leaves and MS suckers

MO leaves were air-dried, grinded, weighed and stored in an air tight container until further analysis. 4.0 Kg weight of the MO leaves were powdered, extracted with distilled ethanol and concentrated on a rotary evaporator. Similarly, MS suckers were air-dried, grinded, weighed and stored in an air tight container until further analysis. 5.2 kg weight of the MS suckers were powdered, extracted with distilled ethanol and concentrated on a rotary evaporator. The crude extract (210.2 g) of MO leaves was successively partitioned into n-hexane (NH), dichloromethane (DCM), ethyl acetate (EA) and methanol (MeOH) soluble fractions in an increasing order of polarity to afford 12 fractions (MO1 – MO12). Similarly, the crude extract (159.32 g) of MS suckers was successively partitioned into n-hexane (NH), dichloromethane (DCM), ethyl acetate (EA) and methanol (MeOH) soluble fractions in an increasing order of polarity to afford 8 fractions (MS01 – MS08). Phytochemical screening of MS showed the presence of saponins, saponin glycosides, tannins, alkaloids and indole alkaloids.

Column Chromatography

Column chromatography of the MO and MS fractions was carried out on silica gel (70 – 230 and 240 – 300 mesh size, Merck, Germany), Merck alumina (70 – 230 mesh ASTM). Thin Layer Chromatography (TLC) was carried out on pre-coated silica gel 60 F_{254} aluminium foil (Merck, Germany) for the establishment of the purity of isolates. Spots on TLC were examined with an ultraviolet lamp operating at a wavelength of 366 nm for fluorescence and at 254 nm for fluorescence quenching spots.

Evaluations of antioxidant and antimicrobial activities of MO and MS fractions

Antioxidant activities of plants' extracts and fractions were evaluated using modified 2,2-diphenyl-1-picrylhydrazyl method as previously described by Chaves et al. (2020). In addition, antimicrobial activities of plants' extracts and fractions were evaluated by testing the cyto-toxic potentials of each fraction against the growths of *Escherichia*

coli and *Salmonella tiphimurium* as previously described by Elisha et al. (2017).

Purification of MO fractions

The antioxidant and antimicrobial activities of the obtained 12 MO fractions (MO1 – MO12) were determined. MO8 and MO11 fractions, which had the best antioxidant and antimicrobial potentials, were selected and further purified on a silica gel open column, using NH, DCM, EA and MeOH in an increasing order of polarity until the most active antioxidant and antimicrobial drug candidates ($MO11_{8,3}$ and $MO11_{8,4}$) were obtained. Phytochemical screenings of $MO11_{8,3}$ and $MO11_{8,4}$ showed the presence of flavonoids, saponin, tannins, alkaloids, glycosides and steroids. The resulting grams of $MO11_{8,3}$ and $MO11_{8,4}$ were mixed together as 1.43 g of MO11, which was used for the evaluations of neuro-protective potentials of MO against CdCl-induced neurotoxicity.

Purification of MS fractions

The antioxidant and antimicrobial activities of the obtained 8 MS fractions (MS01 – MS08) were determined. MS06, which had the best antioxidant and antimicrobial potential, was selected and further purified on a silica gel open column, using NH, DCM, EA and MeOH in an increasing order of polarity to afford seven fractions ($MS06_{1-7}$). $MS06_5$ showed the best antioxidant and antimicrobial potential out of the seven fractions. The resulting 1.24 g of $MS06_5$ was used for the evaluations of neuro-protective potentials of MS against CdCl-induced neurotoxicity.

Chemicals and Reagents

Cadmium Chloride (CdCl) was a product of Sigma-Aldrich Japan Co. (Tokyo, Japan), and was purchased from Bristol Scientific Company, Lagos State, Nigeria. Normal Saline, Doxorubicin and Vegetable Oil were purchased from Olabisi Onabanjo University Teaching Hospital pharmacy, Sagamu, Ogun State, Nigeria. Sucrose crystal produced by Qualikems and Methylated spirit produced by Samstella Industry Nigeria Limited, Abule- Oba, Ogun State, Nigeria were purchased from local suppliers.

Animal care and feeding

28 adult male Wistar rats (average weight of 155 g and 2 months of age) were purchased from a colony breed at Badagry in Lagos state, Nigeria. The rats were randomly divided into 7 groups with 4 rats per group. The rats were acclimatized for a week at the animal house of the Faculty of Pharmacy of Olabisi Onabanjo University, Sagamu campus, Ogun State, Nigeria before the beginning of experimental procedures. The rats were kept under standard conditions and allowed free access to food and drinking water ad libitum. The experimental procedure lasted for 18 Days. The bodyweights of the rats were measured and recorded on daily bases using electronic compact scale (SF-400C weighs in gram) weighing scale; a product of Valid Enterprise, Kalbadevi, Mumbai, India.

Grouping of rats and extracts/drugs administration

MO11 and MS11 were dissolved in Vegetable Oil (vehicle). Rats of Control Group 1 (Baseline Control) received physiological saline only for 17 Days (Days 1-17). Each rat of Experimental Groups 2–4 and 7 received single intra-peritoneal administration of 1.5 mg/Kg bodyweight CdCl on Day 1. Rats of Group 2 (Negative Control) were left untreated throughout experimental procedure for 17 Days (Days 1-17). Thereafter, rats of Group 3 were post-treated with 15 mg/Kg bodyweight of MO11 for 17 Days (Days 1-17). Rats of Group 4 were post-treated with combined mixture of 15 mg/Kg bodyweight of MO11 and 7 mg/Kg bodyweight of MS06 for 17 Days (Days 1-17). Rats of Group 5 received only 15 mg/Kg bodyweight of MO11 for 17 Days (Days 1-17). Rats of Group 6 received only 1 ml/Kg bodyweight of Vegetable Oil (vehicle) for 17 Days (Days 1-17). Rats of Group 7 were post-treated with 3.35 mg/Kg bodyweight of Doxorubicin (standard anticancer drug – Positive Control) for 17 Days (Days 1-17).

Histopathological evaluations of the cerebral cortex

Twenty-four hours after the last day of administration of drugs and extracts on Day 17 and following animal sacrifice, the cranium of each rat was exposed and the cerebrum removed. Each cerebrum was divided into two hemispheres. One cerebral hemisphere was fixed in 10% formalin and

processed for light microscopy using conventional histological procedures. Slices were stained with Cresyl fast violet and examined under the microscope for histopathological changes as earlier described (Omotoso et al., 2018). Photomicrographs of the slides were prepared.

Evaluations of concentrations of IL-1β, IL-4, IL-6, IL-8, IL-10, NF-kB, Caspase-3, Ki67, p53 and sVEGFR in homogenates of cerebral hemispheres of rats using enzyme linked immunosorbent assay (ELISA)

The second cerebral hemisphere from each rat was isolated and then subjected to thorough homogenization using porcelain mortar and pestle in ice-cold 0.25 M sucrose, in the proportion of 1 g to 4 ml of 0.25 M sucrose solution. The tissue homogenates were filled up to 5 ml with additional sucrose, and collected in a 5 ml serum bottle. Homogenates were thereafter centrifuged at 3000 revolution per minute (rpm) for 15 minutes using a centrifuge (Model 90-1). The supernatant was collected with Pasteur pipettes and placed in a freezer at -4°C, and thereafter assayed for concentrations of IL-1β, IL-4, IL-6, IL-8, IL-10, NF-kB, Caspase-3, Ki67, p53 and sVEGFR in the cerebral cortices of all rats of Control Group 1 and Experimental Groups 2 – 7 using ELISA technique as previously described (Akinlolu et al., 2021).

Statistical analyses

Statistical analyses were conducted using the 2019 Statistical Package for the Social Science software Version 23.0. Computed data of concentrations of each biomarker was expressed as arithmetic means ± standard error of mean, and were subjected to statistical analyses using One-way Analysis of Variance to test for significant difference amongst Groups 1-7. Degree of freedom (*df*): (between groups and within groups) and *F*-values were computed. Significant difference was confirmed at 95% confidence interval with associated *P* -value of less than 0.05 ($P \leq 0.05$). In addition, Scheffe Post-hoc analysis was used for separation of Mean values amongst Groups 1-7. The statistical comparison of the concentration of each biomarker between two groups was considered significant only at $P \leq 0.05$.

RESULTS

Histopathological evaluations of the pre-frontal cortices of rats

Histopathological evaluations showed normal histoarchitectures of the prefrontal cortices of rats of Control Group 1 and Experimental Groups 5 and 6 (Figs. 1A, 1B and 5A-6B), with normal staining intensity of Nissl substance, cellular density and delineation. Normal staining neurons (black arrows) present with intensively stained soma both peripherally and centrally. Chromatolytic neurons (red arrows) present with reduced staining intensity in the central or peripheral aspect of the soma of neuron. In contrast to normal stained neurons of rats of Control Group 1 and Experimental Groups 5 and 6 (Figs. 5A-6B), histopathological analyses of prefrontal cortices of rats of Experimental Group 2 showed Nissl substance with reduced staining intensity and high number of chromatolytic cells (Figs. 2A and 2B). In addition, histopathological analyses of prefrontal cortices of rats of Experimental Groups 3, 4 and 7 showed normal staining intensity of Nissl substance and cellular delineation but reduced cellular density and few chromatolytic cells (Figs. 3A-4B and 7A-7B).

Concentrations of IL-1β, IL-4, IL-6, IL-8, IL-10 and NF-kB in cerebral cortices of rats: CdCl-only treated Group 2 versus Normal Saline-only Control Group 1

Results showed statistically significant higher ($P \leq 0.05$) levels of IL-1β (df = 6,14, F = 52.34, $P < 0.001$), IL-6 (df = 6,16, F = 59.22, $P < 0.001$), IL-8 (df = 6,16, F = 127.64, $P < 0.001$) and NF-KB (df = 6,19, F = 36.41, $P < 0.001$) in rats of Group 2, when compared with Control Group 1 (Table 1, Figs. 8, 9, 10 and 11). In addition, results showed statistically non-significant lower ($P \geq 0.05$) levels of IL-4 (df = 6,16, F = 272.42, P = 0.74), but significant lower ($P \leq 0.05$) levels of IL-10 (df = 6,16, F = 272.42, $P < 0.001$) in rats of Group 2, when compared with Control Group 1 (Table 1, Figs. 12 and 13).

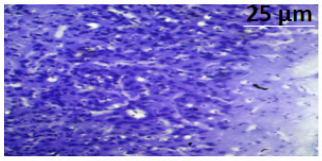

Figure 1A

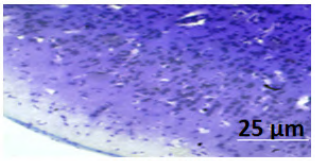

Figure 2A

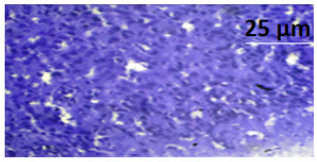

Figure 3A

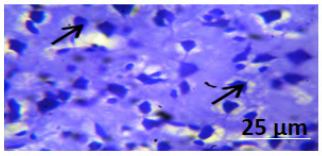

Figure 1B

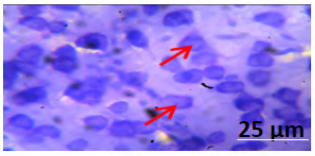

Figure 2B

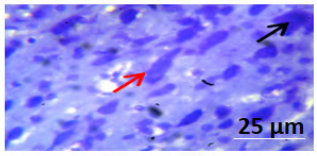

Figure 3B

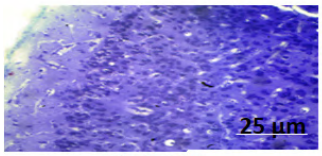

Figure 4A

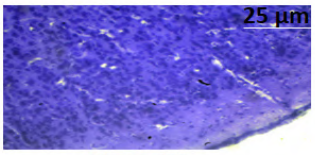

Figure 5A

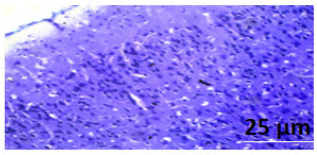

Figure 6A

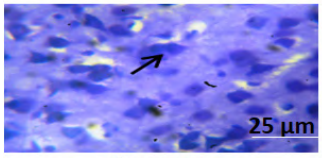

Figure 4B

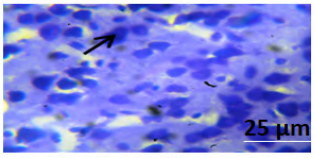

Figure 5B

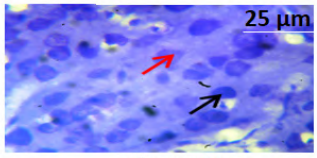

Figure 6B

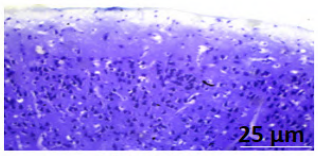

Figure 7A

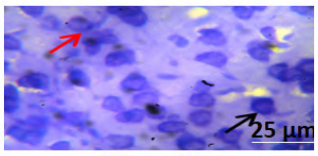

Figure 7B

Fig. 1.- Section of the dorsolateral prefrontal cortex of rats of control Group 1 which received only normal saline. This figure shows (**A**) Cresyl fast Violet x100; (**B**) Cresyl fast Violet x400. Black arrows represent normal neurons. Histopathological evaluation shows normal staining intensity of Nissl substance, cellular density and delineation. Scale bars = 25 µm. **Fig. 2.**- Section of the dorsolateral prefrontal cortex of rats of experimental Group 2 which received intraperitoneal (i.p.) injection of 1.5m/kg bodyweight of CdCl only. This figure shows (**A**) Cresyl fast Violet x100; (**B**) Cresyl fastViolet x400. Red arrows represent chromatolytic neurons. Histopathological evaluation shows Nissl substance with reduced staining intensity, but high number of chromatolytic cells. Scale bars = 25 µm. **Fig. 3.**- Dorsolateral prefrontal cortex of rats of experimental Group 3 which received 1.5 mg/kg bodyweight of CdCl (i.p.) and post-treatment with 15 mg/kg bodyweight of MO11. This figure shows (**A**) Cresyl fast Violet x100; (**B**) Cresyl fast Violet x400. Black arrow represents a normal neuron while red arrow represents a chromatolytic neuron. Histopathological evaluation shows normal staining intensity of Nissl substance but reduced cellular density and few chromatolytic cells. Scale bars = 25 µm. **Fig. 4.**- Section of the dorsolateral prefrontal cortex of rats of experimental Group 4 which received 1.5 mg/kg bodyweight of CdCl (i.p.) and post-treatment with 15 mg/kg bodyweight of MO11 + 7 mg/kg bodyweight of MS06. This figure shows (**A**) Cresyl fast Violet x100; (**B**) Cresyl fast Violet x400. Black arrow represents a normal neuron. Histopathological evaluation shows normal staining intensity of Nissl substance and cellular delineation but reduced cellular density and few chromatolytic cells. Scale bars = 25 µm. **Fig. 5.**- Section of the dorsolateral prefrontal cortex of rats of experimental Group 5 which received 15 mg/kg bodyweight of MO11 only. This figure shows (**A**) Cresyl fast Violet x100; (**B**) Cresyl fast Violet x400. Black arrow represents a normal neuron. Histopathological evaluation shows normal staining intensity of Nissl substance, cellular density and delineation. Scale bars = 25 µm. **Fig. 6.**- Section of the dorsolateral prefrontal cortex of rats of experimental Group 6 which received 1 ml/kg bodyweight of Vegetable Oil only. This figure shows (**A**) Cresyl fast Violet x100; (**B**) Cresyl fast Violet x400. Black arrow represents a normal neuron while red arrow represents a chromatolytic neuron. Histopathological evaluation shows normal staining intensity of Nissl substance, cellular density and delineation. Scale bars = 25 µm. **Fig. 7.**- Section of the dorsolateral prefrontal cortex of rats of experimental Group 7 which received 1.5 mg/kg bodyweight of CdCl (i.p.) and post-treatment with 3.35 mg/kg bodyweight of Doxorubicin. This figure shows (**A**) Cresyl fast Violet x100; (**B**) Cresyl fast Violet x400. Black arrow represents a normal neuron while red arrow represents a chromatolytic neuron. Histopathological evaluation shows normal staining intensity of Nissl substance, but reduced cellular density and few chromatolytic cells. Scale bars = 25 µm.

Table 1. Concentrations (ng/ml) of IL-1β, IL-4, IL-6, IL-8, IL-10 and NF-kB in cerebral cortices of rats.

Drug/Extract administered	IL-1β	IL-4	IL-6	IL-8	IL-10	NF-kB
Normal Saline only	80.83±5.75^{c}	31.54±4.11^{c}	99.26±3.99^{b}	63.79±6.22^{b}	35.75±3.44^{ab}	38.29±1.66^{c}
CdCl only	481.25±41.37^{a}	19.31±0.58^{c}	125.18±2.33^{a}	84.82±2.16^{a}	17.68±0.35^{d}	56.82±1.78^{a}
CdCl-exposure + MO11 post-treated group	312.75±8.13^{b}	24.56±0.84^{c}	97.52±0.99^{b}	65.67±1.03^{b}	6.48±0.88^{e}	39.12±1.5^{b}
CdCl-exposure + MO11 + MS06 post-treated group	302.38±4.84^{b}	32.88±1.07^{c}	100.25±2.51^{b}	29.43±1.58^{d}	28.91±1.97^{b}	39.32±1.71^{b}
MO11 only	293.67±21.36^{b}	154.57±13.09^{a}	97.72±1.48^{b}	58.73±3.05^{b}	58.88±3.11^{a}	38.5±1.31^{c}
Vegetable Oil only	249.75±40.62^{b}	109.03±11.27^{b}	97.68±1.43^{b}	44.18±1.49^{c}	25.34±2.01^{c}	37.5±1.13^{c}
CdCl-exposure + Doxorubicin post-treated group	291.33±27.54^{b}	15.65±2.35^{c}	101.71±1.78^{b}	62.3±0.43^{b}	2.4±0.21^{e}	44.98±4.54^{ab}

Results of One-way ANOVA from Days 1-17. Mean ± SEM across the columns between groups are significantly different with a>ab>b>c>d>e. (n = 4 per group).

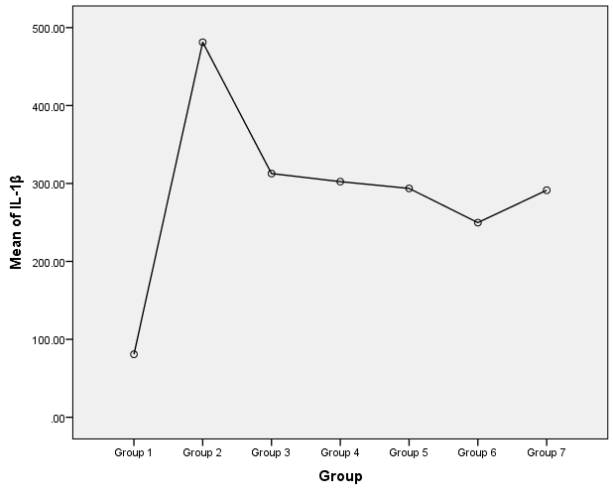

Figure 8.

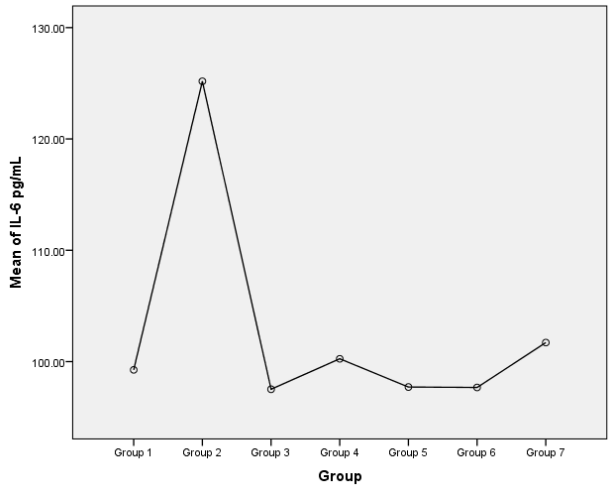

Figure 9.

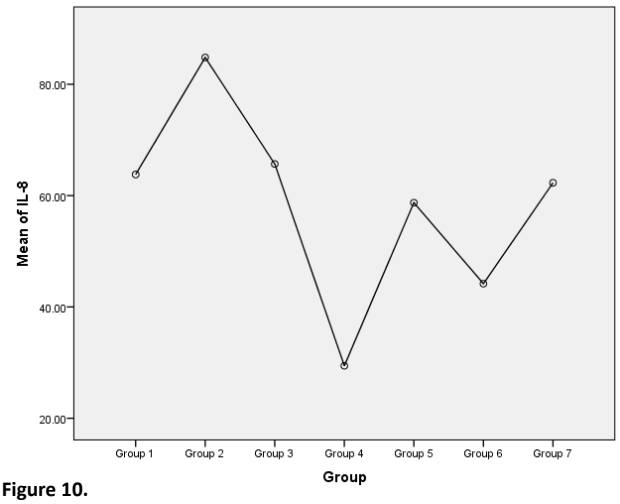

Figure 10.

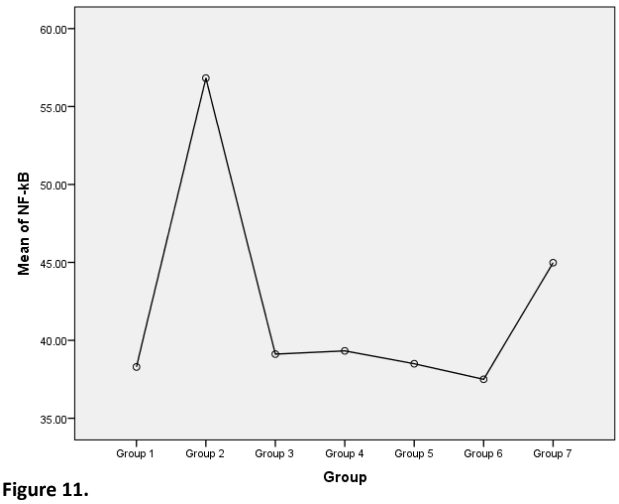

Figure 11.

Fig. 8.- Concentration (ng/ml) of IL-1β in cerebral cortices of rats. Group 1: Normal Saline-only treated group. Group 2: CdCl-only treated group. Group 3: CdCl-exposure + MO11 post-treated group. Group 4: CdCl-exposure + MO11 + MS06 post-treated group. Group 5: MO11-only treated group. Group 6: Vegetable Oil-only treated group. Group 7: CdCl-exposure + Doxorubicin post-treated group.

Fig. 9.- Concentration (ng/ml) of IL-6 in cerebral cortices of rats. Group 1: Normal Saline-only treated group. Group 2: CdCl-only treated group. Group 3: CdCl-exposure + MO11 post-treated group. Group 4: CdCl-exposure + MO11 + MS06 post-treated group. Group 5: MO11-only treated group. Group 6: Vegetable Oil-only treated group. Group 7: CdCl-exposure + Doxorubicin post-treated group.

Fig. 10.- Concentration (ng/ml) of IL-8 in cerebral cortices of rats. Group 1: Normal Saline-only treated group. Group 2: CdCl-only treated group. Group 3: CdCl-exposure + MO11 post-treated group. Group 4: CdCl-exposure + MO11 + MS06 post-treated group. Group 5: MO11-only treated group. Group 6: Vegetable Oil-only treated group. Group 7: CdCl-exposure + Doxorubicin post-treated group.

Fig. 11.- Concentration (ng/ml) of NF-kB in cerebral cortices of rats. Group 1: Normal Saline-only treated group. Group 2: CdCl-only treated group. Group 3: CdCl-exposure + MO11 post-treated group. Group 4: CdCl-exposure + MO11 + MS06 post-treated group. Group 5: MO11-only treated group. Group 6: Vegetable Oil-only treated group. Group 7: CdCl-exposure + Doxorubicin post-treated group.

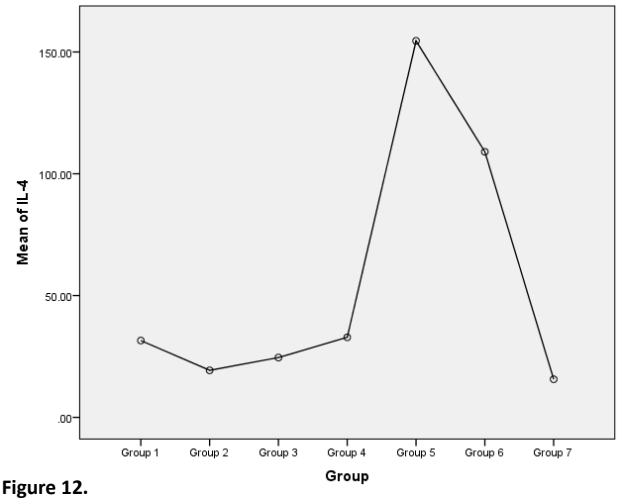

Figure 12.

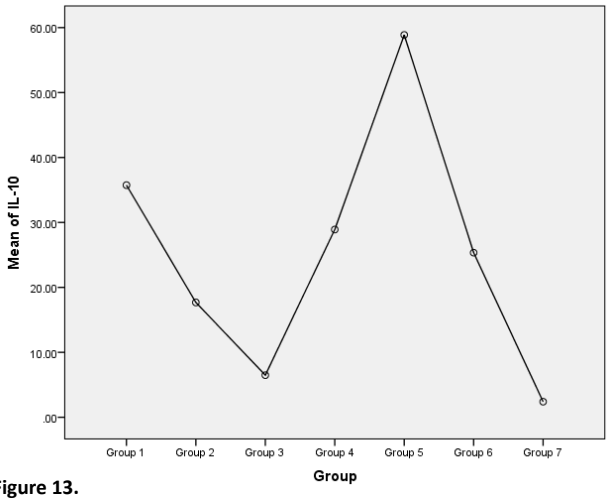

Figure 13.

Fig. 12.- Concentration (ng/ml) of IL-4 in cerebral cortices of rats. Group 1: Normal Saline-only treated group. Group 2: CdCl-only treated group. Group 3: CdCl-exposure + MO11 post-treated group. Group 4: CdCl-exposure + MO11 + MS06 post-treated group. Group 5: MO11-only treated group. Group 6: Vegetable Oil-only treated group. Group 7: CdCl-exposure + Doxorubicin post-treated group.

Fig. 13.- Concentration (ng/ml) of IL-10 in cerebral cortices of rats. Group 1: Normal Saline-only treated group. Group 2: CdCl-only treated group. Group 3: CdCl-exposure + MO11 post-treated group. Group 4: CdCl-exposure + MO11 + MS06 post-treated group. Group 5: MO11-only treated group. Group 6: Vegetable Oil-only treated group. Group 7: CdCl-exposure + Doxorubicin post-treated group.

Concentrations of Caspase-3, Ki67, p53 and sVEGFR in cerebral cortices of rats: CdCl-only treated Group 2 versus Normal Saline-only Control Group 1

Results showed statistically significant higher ($P \leq 0.05$) levels of Caspase-3 (df = 6,18, F = 21.11, $P<0.001$), Ki67 (df = 6,11, F = 8.95, P = 0.01) and sVEGFR (df = 6,20, F = 386.68, $P<0.001$), but statistically non-significant higher ($P \geq 0.05$) levels of p53 (df = 6,13, F = 8.54, P = 0.74) in rats of Group 2, when compared with Control Group 1 (Table 2 and Figs. 14-16).

Concentrations of IL-1β, IL-4, IL-6, IL-8, IL-10 and NF-kB in cerebral cortices of rats: CdCl-only treated Group 2 versus CdCl-exposure + MO11 post-treated Group 3 and CdCl-exposure + MO11 + MS06 post-treated Group 4

Results showed statistically significant higher ($P \leq 0.05$) levels of IL-1β (df = 6,14, F = 52.34, $P<0.001$) and (df = 6,14, F = 52.34, $P<0.001$), IL-6 (df = 6,16, F = 59.22, $P<0.001$) and (df = 6,16, F = 59.22, $P<0.001$), IL-8 (df = 6,16, F = 127.64, $P<0.001$) and (df = 6,16, F = 127.64, $P<0.001$) and NF-KB (df = 6,19, F = 36.41, $P<0.001$) and (df = 6,19, F = 36.41, $P<0.001$) in rats of Group 2, when

Table 2. Concentrations (ng/ml) of Caspase-3, Ki67, p53 and sVEGFR in cerebral cortices of rats.

Drug/Extract administered	Caspase-3	Ki67	p53	sVEGFR
Normal Saline only	121.56±23.71^{c}	1.94±1.05^{b}	4.58±0.37^{b}	114.21±7.53^{b}
CdCl only	799.22±9.86^{a}	5.13±0.61^{a}	18.31±10.80^{ab}	440.04±11.47^{a}
CdCl-exposure + MO11 post-treated group	396.25±281.18^{c}	2.88±0.07^{ab}	3.36±0.79^{b}	105.46±7.56^{b}
CdCl-exposure + MO11 + MS06 post-treated group	662.5±12.76^{ab}	2.51±0.10^{b}	6.42±2.36^{b}	104±11.48^{b}
MO11 only	643.28±35.52^{ab}	1.46±0.67^{b}	23.61±0.82^{ab}	87.33±10.10^{c}
Vegetable Oil only	452.19±14.93^{b}	4.0±0.51^{ab}	14.94±1.28^{ab}	102.13±14.54^{b}
CdCl-exposure + Doxorubicin post-treated group	657.29±44.26^{ab}	2.23±0.67^{b}	27.94±3.91^{a}	302.75±29.06^{ab}

Results of One-way ANOVA from Days 1-17. Mean ± SEM across the columns between groups are significantly different with a>ab>b>c>d>e. (n = 4 per group).

compared with Groups 3 and 4 respectively (Table 1 and Figs. 8-11). In addition, results showed statistically non-significant lower ($P \geq 0.05$) levels of IL-4 in rats of Group 2, when compared with Group 3 ($df = 6,16$, $F = 204.89$, $P = 0.99$) and Group 4 ($df = 6,16$, $F = 204.89$, $P = 0.59$) (Table 1 and Fig. 12). Furthermore, results showed statistically significant lower ($P \leq 0.05$) levels of IL-10 in rats of Group 2, when compared Group 3 ($df = 6,16$, $F = 272.42$, $P = 0.003$) and Group 4 ($df = 6,16$, $F = 272.42$, $P = 0.02$) (Table 1 and Fig. 13).

Concentrations of IL-1β, IL-4, IL-6, IL-8, IL-10 and NF-kB in cerebral cortices of rats: CdCl-only treated Group 2 versus CdCl-exposure + Doxorubicin post-treated Group 7

Results showed statistically significant higher ($P \leq 0.05$) levels of IL-1β ($df = 6,14$, $F = 52.34$, $P < 0.001$), IL-6 ($df = 6,16$, $F = 59.22$, $P < 0.001$), IL-8 ($df = 6,16$, $F = 127.64$, $P < 0.001$), IL-10 ($df = 6,16$, $F = 272.42$, $P < 0.001$) and NF-KB ($df = 6,19$, $F = 36.41$, $P < 0.001$), but non-significant higher ($P \geq 0.05$) levels of IL-4 ($df = 6,16$, $F = 272.42$, $P = 0.99$), in rats of Group 2, when compared with Group 7 (Table 1 and Figs. 8-13).

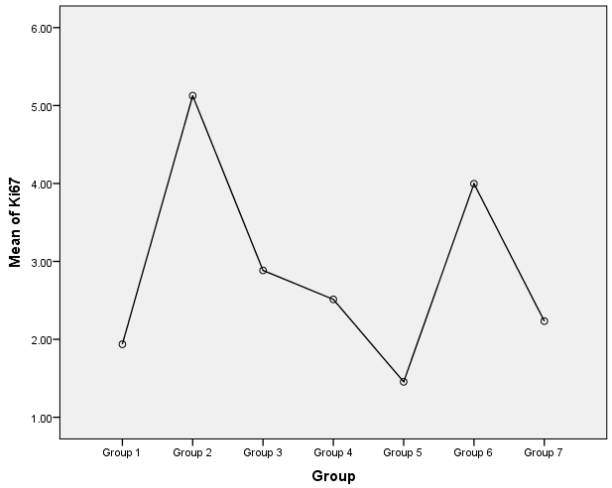

Figure 14.

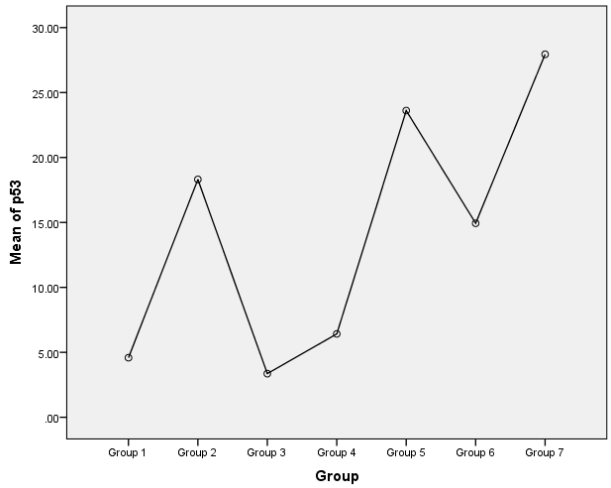

Figure 15.

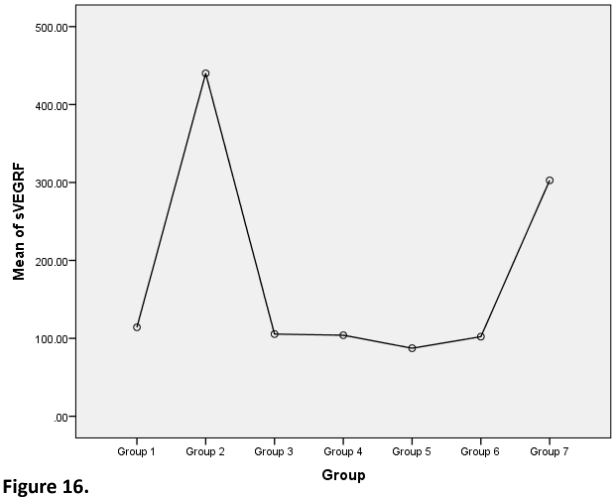

Figure 16.

Fig. 14.- Concentration (ng/ml) of Ki67 in cerebral cortices of rats. Group 1: Normal Saline-only treated group. Group 2: CdCl-only treated group. Group 3: CdCl-exposure + MO11 post-treated group. Group 4: CdCl-exposure + MO11 + MS06 post-treated group. Group 5: MO11-only treated group. Group 6: Vegetable Oil-only treated group. Group 7: CdCl-exposure + Doxorubicin post-treated group.

Fig. 15.- Concentration (ng/ml) of p53 in cerebral cortices of rats. Group 1: Normal Saline-only treated group. Group 2: CdCl-only treated group. Group 3: CdCl-exposure + MO11 post-treated group. Group 4: CdCl-exposure + MO11 + MS06 post-treated group. Group 5: MO11-only treated group. Group 6: Vegetable Oil-only treated group. Group 7: CdCl-exposure + Doxorubicin post-treated group.

Fig. 16.- Concentration sVEGFR in cerebral cortices of rats. Group 1: Normal Saline-only treated group. Group 2: CdCl-only treated group. Group 3: CdCl-exposure + MO11 post-treated group. Group 4: CdCl-exposure + MO11 + MS06 post-treated group. Group 5: MO11-only treated group. Group 6: Vegetable Oil-only treated group. Group 7: CdCl-exposure + Doxorubicin post- treated group.

Concentrations of Caspase-3, Ki67, p53 and sVEGFR in cerebral cortices of rats: CdCl-only treated Group 2 versus CdCl-exposure + MO11 post-treated Group 3 and CdCl-exposure + MO11 + MS06 post-treated Group 4

Results showed statistically significant higher ($P \leq 0.05$) levels of Caspase-3 ($df = 6,18$, $F = 21.11$, $P = 0.04$) and non-significant higher ($P \geq 0.05$) levels of Caspase-3 ($df = 6,18$, $F = 21.11$, $P = 0.75$) in rats of Group 2, when compared with Groups 3 and 4 respectively (Table 2 and Fig. 17). In addition, results showed statistically non-significant higher ($P \geq 0.05$) levels of Ki67 ($df = 6,11$, $F = 8.95$, $P = 0.17$) and ($df = 6,11$, $F = 8.95$, $P = 0.08$); and p53 ($df = 6,13$, $F = 8.54$, $P = 0.23$) and ($df = 6,13$, $F = 8.54$, $P = 0.46$) in rats of Group 2, when compared with Groups 3 and 4 respectively (Table 2 and Figs. 14-15). Furthermore, results showed statistically significant higher ($P \leq 0.05$) levels of sVEGFR in rats of Group 2, when compared with Group 3 ($df = 6,20$, $F = 386.68$, $P < 0.001$) and Group 4 ($df = 6,20$, $F = 386.68$, $P < 0.001$) (Table 2 and Fig. 16).

Concentrations of Caspase-3, Ki67, p53 and sVEGFR in cerebral cortices of rats: CdCl-only treated Group 2 versus CdCl-exposure + Doxorubicin post-treated Group 7

Results showed statistically non-significant higher ($P \geq 0.05$) levels of Caspase-3 ($df = 6,18$, $F = 21.11$, $P = 0.72$), in rats of Group 2, when compared with Group 7 (Table 2 and Fig. 17). Furthermore, results showed statistically significant higher ($P \leq 0.05$) levels of Ki67 ($df = 6,11$, $F = 8.95$, $P = 0.03$) and sVEGFR ($df = 6,20$, $F = 386.68$, $P < 0.001$), but statistically significant lower ($P \leq 0.05$) levels of p53 ($df = 6,13$, $F = 8.54$, $P = 0.47$) in rats of Group 2, when compared with Group 7 (Table 2 and Figs. 14-16).

DISCUSSION

Chromatolysis of neurons involves the dispersal and redistribution of rough endoplasmic reticulum and polyribosomes (Nissl substance) from the central to the periphery of the perikaryon for

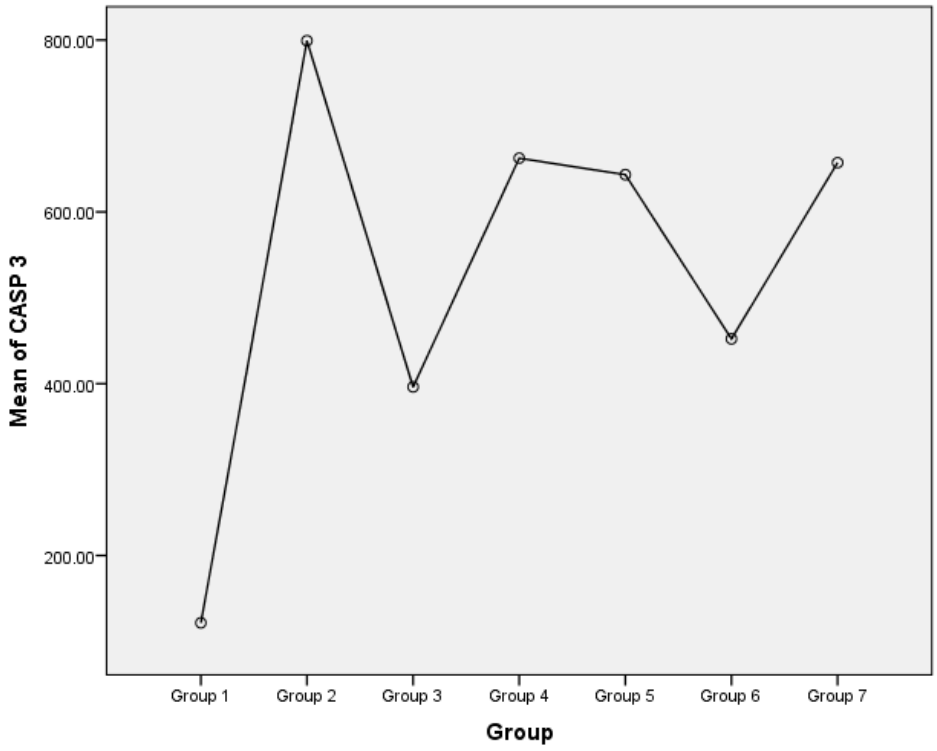

Fig. 17.- Concentration (ng/ml) of Caspase-3 in cerebral cortices of rats. Group 1: Normal Saline-only treated group. Group 2: CdCl-only treated group. Group 3: CdCl-exposure + MO11 post- treated group. Group 4: CdCl-exposure + MO11 + MS06 post-treated group. Group 5: MO11-only treated group. Group 6: Vegetable Oil-only treated group. Group 7: CdCl-exposure + Doxorubicin post-treated group.

increased protein synthesis in response to disruption of axonal transport, axotomy, metabolic nerve injuries, trauma or response to regenerative stimuli (Hanz and Fainzilber, 2006; Bhuiyan et al., 2018). The observed increase in number of chromatolytic cells in the prefrontal cortices of rats of CdCl-only treated Group 2 (Figs. 2A and 2B) confirms CdCl-induced neurotoxicity, chromatolysis and neurodegeneration. In addition, the decreased number of chromatolytic cells in the prefrontal cortices of rats post-treated with MO11 (Group 3), MO11 + MS06 (Group 4) and Doxorubicin (Group 7) (Figs. 3A – 4B and 7A – 7B) following CdCl-exposure indicates that MO11, MS06 and Doxorubicin possess neuroprotective potentials and were able to gradually reverse CdCl-induced chromatolysis and neurodegeneration within 17 days.

Is CdCl-induced chromatolysis associated with neuro-inflammation? Hanz and Fainzilber (2006) opined that axotomy of peripheral nerve resulted in increased expressions of ciliary neurotrophic factor and interleukins (LIF and IL-6) and activation of the JAK-STAT3 signalling pathway. Results showed significant upregulation of IL-6 in rats of CdCl-only treated Group 2, when compared with Normal saline-only treated Control Group 1, CdCl-exposure + MO11 post-treated Group 3, CdCl-exposure + MO11 + MS06 post-treated Group 4 and CdCl-exposure + Doxorubicin post-treated Group 7 (Table 1 and Fig. 9). Chromatolysis is associated with axotomy, hence these observations possibly indicate the involvement of IL-6 in CdCl-induced chromatolysis. It is equally possible that the observed anti-chromatolytic potentials of MO11, MS06 and Doxorubicin are associated with the regulation of IL-6 expression.

What mechanism underlies CdCl-induced neuroinflammation? Neuroinflammation involves the actuation of microglia cells leading to the release of pro-inflammatory cytokines such as IL-1β, IL-6, IL-8, TNFα and NF-kB (Shih et al., 2015; Akinlolu et al., 2020b). NF-kB upregulation results in the release and increased levels of other pro-inflammatory cytokines; hence NF-kB is opined to be the central regulator of neuroinflammation (Shih et al., 2015). Furthermore, the central nervous system environment is anti-inflammatory with high levels of anti-inflammatory cytokines such as IL-4 and IL-10. IL-4 and IL-10 inhibit the release of NF-kB and pro-inflammatory cytokines, and are involved in the resolution of neuroinflammation (Shih et al., 2015). Previous studies reported Cd-induction of inflammation via upregulations of IL-1β, IL-6 and IL-8 in rats, but downregulations of IL-4 in mice (Ebrahimi et al., 2020).

Similarly, results of this study showed significant upregulations of IL-1β, IL-6, IL-8 and NF-kB, but downregulations of IL-4 and IL-10 in rats of CdCl-only treated Group 2, when compared with Normal saline-only treated Control Group 1 (Table 1 and Figs. 8-13). These observations confirm CdCl-induction of neuro-inflammation, and equally indicate that CdCl-induced neuroinflammation possibly occurs via the NF-kB pathway.

Do MO11, MS06 and Doxorubicin have neuroprotective potentials against CdCl-induced neuroinflammation? Post-treatments of CdCl-induced neuroinflammation in rats with MO11 (Group 3), MO11 + MS06 (Group 4) and Doxorubicin (Group 7) resulted in significant downregulations of pro-inflammatory cytokines (IL-1β, IL-6, IL-8 and NF-kB), but upregulations of anti-inflammatory cytokines (IL-4 and IL-10), when compared with CdCl-only treated Group 2 (Table 1 and Figs. 8-13). These observations indicate that MO11, MS06 and Doxorubicin possess anti-neuro-inflammatory potentials which were possibly mediated via the NF-kB pathway.

What is the relationship between Cd-induced neuro-inflammation and neuronal cell death (apoptosis)? NF-kB is pro-apoptotic and its upregulation is associated with increased release of p53 and c-myc as well as induction of apoptosis (Barkett and Gilmore, 1999). Ryan et al., 2000 noted that loss or blockage of NF-kB activities resulted in loss of p53-induction of apoptosis, confirming the role of NF-kB in p53-induced apoptosis. In addition, significant upregulation of Caspase-3 is associated with activation of both the intrinsic mitochondrial pathway and the extrinsic death-receptor pathway of apoptosis (Akinlolu et al., 2020b). Hence, significant upregulation of Caspase-3 is associated with promotion of apoptosis. In addition, Genchi et al. (2020) reported Cd-induction of significant upregulation

of Caspase-3, while Huff et al. (2007) reported significant upregulation of p53 in Cd-induced toxicity in *in vivo* and *in vitro* experimental studies.

The findings of this study showed significant upregulations of NF-kB, Caspase-3 and p53 in CdCl-only treated Group 2, when compared with Normal Saline-only treated Control Group 1 (Tables 1, 2 , Figs. 11, 15 and 17). These observations indicate CDCl-induction of apoptosis via the NF-kB/Caspase-3/p53 pathway.

Do MO11 and MS06 have neuro-protective potentials against CdCl-induced neuro-apoptosis? Post-treatments of CdCl-induced neuro-apoptosis in rats with MO11 (Group 3) and MO11 + MS06 (Group 4) resulted in downregulations of NF-kB, Caspase-3 and p53 (Tables 1, 2 and Figs. 11, 15 and 17). These observations indicate that MO11 and MS06 resolved CdCl-induced apoptosis via the NF-kB/Caspase-3/p53 pathway. In addition, these observations indicate that MO11 and MS06 are possible anticancer drug compounds of clinical interest, as opined by Barkett and Gilmore (1999), who noted that drug compounds which interfere with the apoptotic role of Rel/NF-kB transcription factors could have therapeutic and clinical anticancer potentials.

Is there any possible association between CdCl-induced neuronal cell death and neuro-degeneration? Previous studies reported upregulations of Caspase-3 and p53 in brain of AD patients (Seo and Park, 2020). The observed upregulations of Caspase-3 and p53 in rats of CdCl-only treated Group 2, when compared with Normal Saline-only treated Control Group 1 (Table 2, Figs. 15 and 17) confirm Cd-induced toxicity as a possible aetiological factor in the development of AD and neurodegenerative diseases.

Can MO11 and MS06 reverse CdCl-induced neuro-degeneration? The observed downregulations of Caspase-3 and p53 in CdCl-exposed rats post-treated with MO11 (Group 3) and MO11 + MS06 (Group 4), when compared with CdCl-only treated Group 2 (Table 2, Figs. 15 and 17) indicate that MO11 and MS06 reversed CdCl-induced neurodegeneration and possess neuroregenerative potentials.

Does Doxorubicin have neuroprotective potentials against CdCl-induced p-53 dependent apoptosis and neurodegeneration? Results showed significant upregulation of p53 in rats of Doxorubicin-treated group 7, when compared with CdCl-only treated Group 2 (Table 2 and Fig. 15). These observations indicate that Doxorubicin did not reverse CdCl-induced p-53 dependent apoptosis and neurodegeneration.

Is there any relationship between CdCl-induced apoptosis, hyperplasia and mutagenesis? Genchi et al. (2020) noted that Cd-induced apoptosis is p-53 dependent. However, Genchi et al. (2020) equally reported that, while some Cd-treated cells undergo apoptosis, the remaining cells acquire apoptotic resistant capability resulting in increased development of pre-neoplastic cells, neoplastic cells and hyperplasia. Similarly, Prajapati et al. (2014) reported Cd-induced increased Ki67-index and hyperplasia in rats. The results of this study showed upregulation of Ki67 in rats of Cdcl-only treated Group 2, when compared with Normal Saline-only treated Control Group 1 (Table 2 and Fig. 14). This observation confirms CdCl-induction of hyperplasia and mutagenesis, and equally confirms that CdCl-induced hyperplasia, mutagenesis and apoptosis are intimately related.

Do MO11 and MS06 and Doxorubicin have neuroprotective potentials against CdCl-induced hyperplasia and mutagenesis? Post-treatments of CdCl-induced neuroapoptosis in rats with MO11 (Group 3) and MO11 + MS06 (Group 4) resulted in downregulations of Ki67 (Table 2 and Fig. 14). These observations indicate that MO11, MS06 and Doxorubicin possess anti-proliferation potentials.

Cd is an established carcinogen (Wang and Du, 2013; Batool et al., 2019), and mutagenesis is associated with increased angiogenesis (Batchelor et al., 2009). What then is the relationship between Cd-induced mutagenesis and increased angiogenesis in the cerebrum? VEGF is an established angiogenic factor, and abnormal VEGF upregulation is associated with increased angiogenesis, cancer, metastasis, ischemia and inflammation (Mahoney et al., 2021). Results showed significant upregulation of VEGFR in rats of CdCl-only treated Group 2, when compared with Normal Saline-only treated rats Control Group 1 (Table 2 and Fig. 16). This observation confirms

CdCl-induced promotion of angiogenesis, and equally confirms a relationship between CdCl-induced mutagenesis and angiogenesis.

Do MO11, MS06 and Doxorubicin have neuro-protective potentials against CdCl-induced increased angiogenesis? Results showed significant upregulation of sVEGFR in rats of CdCl-only treated Group 2, when compared with rats post-treated with MO11 (Group 3), MO11 + MS06 (Group 4) and Doxorubicin (Group 7) following CdCl-exposure (Table 2 and Fig. 16). These observations indicate that MO11, MS06 and Doxorubicin possess neuro-protective and anti-angiogenesis potentials.

CONCLUSION

The findings of this study suggest that post-treatments with MO11 (isolated from *Moringa oleifera* leaves) and MS06 (isolated from *Musa sapientum* suckers) conferred a degree of neuro-protection against CdCl-induced neurotoxicity and resulted in decreased levels of IL-1β, IL-6, IL-8, NF-kB, Caspase-3, Ki67, p53 and sVEGFR, but increased levels of IL-4 and IL-10 in rats. These observations indicate that MO11 and MS06 ameliorated CdCl-induced neurotoxicity, neuroinflammation, apoptosis, hyperplasia, angiogenesis, mutagenesis and neurodegeneration via the NF-kB/Caspase-3/p53 pathway. Hence, MO11 and MS06 possess neuroprotective potentials and are recommended for further evaluations as potential drug candidates for the treatments of neuroinflammatory and neurodegenerative diseases, as well as cancers.

However, post-treatments of CdCl-induced neurotoxicity with standard anticancer drug Doxorubicin resulted in decreased levels of IL-1β, IL-6, IL-8, NF-kB, Caspase-3, Ki67 and sVEGFR, but increased levels of p53, IL-4 and IL-10 in rats. These observations indicate that Doxorubicin ameliorated CdCl-induced neurotoxicity, neuroinflammation, hyperplasia, angiogenesis, but not p53-dependent apoptosis and neurodegeneration. Therefore, MO11 and MS06 possess better neuroprotective potentials against CdCl-induced neurotoxicity, when compared with Doxorubicin.

ACKNOWLEDGEMENTS

The authors acknowledge the technical support of Laboratory staff members of the Department of Chemistry of the University of Ilorin, Nigeria, the Central Research Laboratory, Ilorin, Nigeria and Department of Mathematics, University of Medical Sciences Ondo, Nigeria (where statistical analyses were conducted).

REFERENCES

AKINLOLU AA, AMEEN M, QUADRI T, ODUBELA O, OMOTOSO G, YAHYA R, BILIAMINU S, ADEYANJU M, EBITO G, OTULANA J (2020a) Extraction, isolation and evaluation of anti-toxic principles from *Moringa oleifera* (MOF_6) and *Myristica fragrans* (Trimyristin) upregulated acetylcholinesterase concentrations in sodium arsenite-induced neurotoxicity in rats. *J Phytomed Therap*, 19(2): 503-519.

AKINLOLU AA, SULAIMAN FA, TAJUDEEN S, SULEIMAN SK, ABDULSALAM AA, ASOGWA NT (2020b) *Cajanus cajan* drives apoptosis via activation of caspase3/p53 pathway and possesses re-myelination and anti-gliosis potentials in ethidium bromide-induced neurotoxicity in rats. *Nig J Sci Res*, 19(4): 286-293.

AKINLOLU AA, OYEWOPO AO, KADIR RE, LAWAL A, ADEMILOYE J, JUBRIL A, AMEEN MO, EBITO GE (2021) *Moringa oleifera* and *Musa sapientum* ameliorated 7,12-dimethylbenz[a]anthracene-induced upregulations of Ki67 and multidrug resistance1 genes in rats. *Intern J Health Sci*, 15(3): 26-33.

ANDJELKOVIC M, BUHA DA, ANTONIJEVIC E, ANTONIJEVIC B, STANIC M, KOTUR-STEVULJEVIC J, SPASOJEVIC-KALIMANOVSKA V, JOVANOVIC M, BORICIC N, WALLACE D, BULAT Z (2019) Toxic effect of acute cadmium and lead exposure in rat blood, liver, and kidney. *Intern J Env Res Pub Health*, 16(2): 274.

BATCHELOR TT, PRISCILLA K, BRASTIANO MD (2009) VEGF inhibitors in brain tumours. *Clinical Adv Hematol Oncol*, 7(11): 753-768.

BATOOL Z, AGHA F, TABASSUM S, BATOOL TS, SIDDIQUI RA, HAIDER S (2019) Prevention of cadmiuminduced neurotoxicity in rats by essential nutrients present in nuts. *Acta Neurobiol Exp*, 79: 169-183.

BERNHOFT RA (2013) Cadmium toxicity and treatment. *Scientific World J,* Article ID394652: 7. http://dx.doi.org/10.1155/2013/394652.

BHUIYAN PS, RAJGOPAL L, SHYAMKISHORE K (2018) *Indebir Singh's Textbook of Human Neuroanatomy*. Jaypee Brothers Medical Publishers (P) Limited, India.

CHAVES N, ANTONIO S, JUAN CA (2020) Quantification of the antioxidant activity of plant extracts: analysis of sensitivity and hierarchization based on the method used. *Antioxidants*, 9(1): 76.

EBRAHIMI M, KHALILI N, RAZI S, KESHAVARZ-FATHI M, KHALILI N, REZAEI N (2020) Effects of lead and cadmium on the immune system and cancer progression. *J Env Health Sci Eng,* 18: 335343.

ELISHA IL, BOTHA FS, MCGAW LJ, ELOFF JN (2017) The antibacterial activity of extracts of nine plant species with good activity against *Escherichia coli* against five other bacteria and cytotoxicity of extracts. *BMC Complement Altern Med*, 17(1): 133.

GENCHI G, SINICROPI MS, LAURIA G, CAROCCI A, CATALANO A (2020) The effects of Cadmium toxicity. *Int J Env Res Public Health*, 17: 3782.

HANZ S, FAINZILBER M (2006) Retrograde signaling in injured nerve – the axon reaction revisited. *J Neurochem*, 99: 13-19.

LANSDOWN AB, KING H, AUBERT RE (2001) Experimental observations in the rat on the influence of cadmium on skin wound repair. *Intern J Exp Pathol*, 82(1): 35-41.

RYAN KM, ERNST MK, RICE NR, VOUSDEN KH (2000) Role of NF-kB in p53-mediated programmed cell death. *Nature*, 404: 892-896.

MAHONEY ER, DUMITRESCU L, MOORE AM, CAMBRONERO FE, DE JAGER PL, KORAN MEI, PETYUK VA, ROBINSON RAS, GOYAL S, SCHNEIDER JA, BENNETT DA, JEFFERSON AL, HOHMAN TJ (2021) Brain expression of the vascular endothelial growth factor gene family in cognitive aging and Alzheimer's disease. *Mol Psych*, 26: 888-896.

BARKETT M, GILMORE TD (1999) Control of apoptosis by Rel/NF-kB transcription factors. *Oncogene*, 18: 6910-6924.

OMOTOSO GO, KADIR ER, LEWU SF, GBADAMOSI IT, AKINLOLU AA, ADUNMO GO, KOLO RM, LAWAL MO, AMEEN MO (2018) *Moringa oleifera* ameliorates cuprizone-induced cerebellar damage in adult female rats. *Res J Health Sci*, 6(1): 13-25.

PRAJAPATI A, RAO A, PATEL J, GUPTA S, GUPTA S (2014) A single low dose of cadmium exposure induces benign prostate hyperplasia like condition in rat: A novel benign prostate hyperplasia rodent model. *Exp Biol Med (Maywood)*, 239(7): 829-841.

SHIH R-H, WANG C-Y, YANG C-M (2015) NF-kappaB signalling pathways in neurological inflammation: a mini review. *Front Mol Neurosci*, 8: 77.

SEO J, PARK M (2020) Molecular crosstalk between cancer and neurodegenerative diseases. *Cell Mol Life Sci*, 77: 2659-2680.

WANG B, DU Y (2013) Cadmium and its neurotoxic effects. *Oxid Med Cellular Long*, 2013: 898034.

Potential benefits of dihydroartemisinin in suppression of dexamethasone induced osteoporosis, osteoclast formation and RANKL induced signaling pathways in adult female albino rat

Omnia S. Erfan[1], Yassmin G. Salem[1], Mona A. El-Shahat[1], Walaa F. Awadin[2], Huda Eltahry[1], Mamdouh Eldesoqui[1]

[1] *Department of Anatomy and Embryology, Faculty of Medicine, Mansoura University, Egypt*

[2] *Department of Pathology, Faculty of Veterinary Medicine, Mansoura University, Egypt*

SUMMARY

Osteoporosis is a musculoskeletal disorder characterized by reduced bone density and increased susceptibility to fractures. Fractures cause a considerable increase in mortality, disability, and morbidity incidence. Artemisia annua is a medicinal plant, used for long time in Asian countries and its active metabolite is Dihydroartemisinin (DHA). It is proven to possess anti-inflammatory and antioxidant effects. The present study is the first to investigate the role of different doses of DHA in treatment of Dexamethasone (Dexa)-induced osteoporosis. Thirty female Wister adult rats were divided into three groups for three months. Control and Dexa groups were both six in number. Dihydroartemisinin treated groups, eighteen in number, received intramuscular injection of Dexamethasone and intraperitoneal injection of DHA, then subdivided in three different groups according to DHA doses (10, 20 and 30 mg/kg body wight). Blood level of Ca, P, calcitonin, alkaline and acid phosphatase, and Tissue MDA, GSH were estimated. Tibiae were stained with H&E, Masson-Goldner, and immunological examination of β catenin and RANKL was done. Then, one-way ANOVA test, followed by Tukey's post-hoc test, was used in order to compare groups, and P value <0.05 was considered statistically significant.

A highest dose of DHA showed normalization of blood parameter and oxidative stress markers. Also, bone histology improvement, reduced RANKL and increased β catenin expression were recorded. Treatment with DHA has significantly improved the oxidative stress, biochemical parameters, and bone histology. Dihydroartemisinin might represent a novel approach for modulation of osteoporosis induced by glucocorticoid.

Key words: Dihydroartemisinin – RANKL – Osteoporosis – Dexamethasone – β-catenin

Corresponding author:
Omnia Sameer Erfan. Department of Anatomy and Embryology, Faculty of Medicine, Mansoura University, Egypt. Phone: 00201552523630. E-mail: Omnia.sameer@gmail.com

Submitted: February 4, 2022. **Accepted:** May 3, 2022

https://doi.org/10.52083/ITUY9072

INTRODUCTION

Osteoporosis is a musculoskeletal disorder characterized by reduced bone density and enhanced susceptibility to fractures. Osteoporosis is a silent disease without any apparent symptoms till a fracture occurs (Sozen and Ozer, 2017). These fractures lead to significant mortality and morbidity and result in socio-economic costs, including direct medical and indirect expenses resulting from decreased quality of life and disabilities (Willson et al., 2015).

Osteopetrosis results from the disturbance in the balance between bone formation by osteoblasts and bone resorption by osteoclasts (Ahmadzadeh et al., 2016). Osteoclast formation and activation is primarily regulated by the receptor activator of nuclear factor kappa-B ligand (RANKL). The interaction between RANKL and its receptor RANK activates several transcription factors that in turn activate the expression of genes regulating osteoclast differentiation and function (Zhou et al., 2016). Proliferation and differentiation of osteoblastic precursors, and maintenance of mature osteoblasts ar regulated by the Wnt/β-catenin pathway (Baron et al., 2006).

Glucocorticoids represent the first option used during treatment of various chronic and autoimmune diseases, and in organ transplantation (Fang et al., 2021). Osteoporosis is one of the major sequels following treatment with glucocorticoid (GC), known as secondary osteoporosis (Hartmann et al., 2016). Glucocorticoid therapy suppresses osteoblast function and bone formation; on the other hand, it boosts bone resorption, reduces calcium absorption and inhibits endogenous gonadal steroids, all of which lead to enhanced bone loss (Ioannidis et al., 2014).

Appropriate nutrition, weight bearing exercise, calcium, vitamin D supplements, and pharmacological therapies could minimize bone loss (Gallagher and Sai, 2010). Lee et al. (2017) reported that long-term use of pharmacological therapies possesses different adverse effects, such as bisphosphonates (osteonecrosis of the jaw and nephrotoxicity), estrogen replacement therapy, (risk of cardiovascular disease and breast cancer), teriparatide, (temporary rises in serum and urine calcium levels), and denosumab, (reduce serum calcium level).

Artemisia annua is a medicinal plant, which has been used for a long time to treat different diseases in Asian countries (Katiyar et al., 2012). It has been used safely for treatment of malaria, as it acts by killing plasmodium parasites through induction of iron-dependent oxidative stress (Cabello et al., 2012). Many studies used Artemisia annua extract and its active compound artemisinin to develop more effective drug against malaria (Chaturvedi et al., 2010). Artemisinins have proven to have anti-inflammatory, antioxidant, anti-cancer and anti-microbial activities (Ferreira et al., 2010). Dihydroartemisinin (DHA) is known to be the active ingredient of the artemisinin compounds. The present experiment aimed to investigate the role of DHA in the management of Dexamethasone (Dexa)-induced osteoporosis.

MATERIALS AND METHODS

Experimental animals

Thirty adult female Wister albino rats (12-14 weeks old) weighting 200-250 g were used in this study. Rats were kept under controlled condition of temperature (23±3 °C), and relative humidity throughout the whole study period, with stable 12/12-hours light/dark cycle. Three animals were housed per cage, with free access to water and *ad libitum* diet. The housing of the rats was conducted in the Faculty of Medicine, Mansoura University. The experiment was conducted in accordance with the Animals' Experimentation Committee at Mansoura University and was authorized by Mansoura Faculty of Medicine, Institutional Research Board under the number of (MDP. 18.12.15.R1.R2). Significant efforts were made to minimize the number of animals used.

Experimental design and treatments

Rats were randomly allocated into three groups: Control group (n = 6): injected intraperitoneal with saline every 2 days; Dexamethasone (Dexa)-treated group (n=6): injected intramuscularly by Dexamethasone with dose of 1 mg/kg/BWT every 3 days (Liu et al., 2011); Dihydroartemisinin-treated

(D+D) groups (n=18): injected intramuscularly by Dexamethasone (1 mg/kg / BWT every 3 days), as well as intraperitoneal injection of dihydroartemisinin dissolved in saline every 2 days. They were divided into three subgroups according to the dose of dihydroartemisinin: D+D10 group (n = 6) received 10 mg/kg (Zhou et al., 2016), D+D20 group (n = 6) received 20 mg/kg, and D+D30 group (n = 6) received 30 mg/kg (Ge et al., 2018). The experiments lasted for three months.

Body weight measurement

At the end of the experiment, the weight of each animal was recorded with a digital electrical balance.

Blood collection

After three months, a retro-orbital blood sample was withdrawn from all animals, then centrifuged to separate serum. The serum was used to measure calcium, phosphorus, calcitonin, alkaline phosphatase, and acid phosphatase levels.

Bone specimen

The animals were anaesthetized deeply by intraperitoneal ketamine (90 mg/kg) and xylazine (15 mg/kg) just before scarification. From each animal, right tibiae were dissected out and cleaned from muscle and soft tissues. Also, left tibiae were dissected out from each animal then homogenized for quantitative analysis of oxidative stress markers (Sözen et al., 2017).

Biochemical studies

Serum was separated by centrifugation at 4000 rpm for 15 minutes for use in the biochemical assay. The serum was stored at −20°C before analysis, using a Synchron cx5 autoanalyzer (Beckman, CA, USA). Concentrations of calcium (Ca), phosphorus (P), alkaline phosphatase and acid phosphatase in the serum were determined spectrophotometrically using specific diagnostic reagent kits (Biodiagnostic kits, Giza, Egypt) and an Olympus AU 2700 analyzer (Mishima, Japan) (Chen et al., 2019). Calcitonin (CT) was determined in serum using ELISA kits obtained from Life Span Bioscience, Inc. (LSBio).

Evaluation of oxidative stress

Malondialdehyde (MDA) and reduced glutathione (GSH) were assessed in Bone homogenate of left tibiae, using colorimetric method applying the suitable kits (Biodiagnostic kits, Giza, Egypt) (El Wakf et al., 2014).

Histological and immunohistochemical stains

From each animal in each group, the collected tibiae were fixed for 4 days using 10% buffered formal saline, then decalcified with Ethylenediamine Tetra-acetic acid (EDTA) (Ge et al., 2018) for nearly 14 days, and then blocks of paraffin were prepared. Longitudinal sections of tibiae, with the thickness of 5 µm, were stained by hematoxylin and eosin (H&E) to evaluate bone histological changes, Masson Goldner to assess development of new bone, bone formation and resorption immunohistochemical marks (β-catenin and RANKL, respectively) supplied by New Test Company, Cairo, Egypt.

For immunohistochemical staining, sections on positively charged glass slides were de-paraffinized and rehydrated. Then sections were washed with distilled water, blocked in 0.1% hydrogen peroxide, and then rinsed for three times with phosphate-buffered saline (PBS). Protein block was used (5 minutes) to block nonspecific background. Then sections were rinsed by distilled water after that, and they were washed in PBS for three times. The different primary antibodies were incubated with slides overnight at 4° C. The used primary antibodies were rabbit polyclonal anti-RANKL (DF7006, Affinity Bioscience, USA, at 1/200 dilution) and rabbit monoclonal anti-Beta catenin antibody (IGX4794R-3, Gene Tex International Corporation, USA at 1/100 dilution). Following washing for three times by PBS for 5 minutes, the slides were incubated with biotinylated goat antipolyvent for 20 min. After that, slides were then incubated for 10 minutes together with conjugated streptavidin and rinsed out over again with PBS. Following that, slides were incubated with DAB substrate (diaminobenzidine) for 3 minutes (Mouse and

rabbit HRP/DAB (ABC) detection IHC kit, ab64264, Abcam, UK). Lastly, sections were counterstained using Mayer's hematoxylin for one minute.

Statistical analysis and measurements

Morphometric studies were done using Image J program (version 1.48, Wayne Rasband, National Institutes of Health, Bethesda, MD, USA), matching with the program instructions. Five sections of tibiae cut at different levels stained by H&E or immunostained were examined from five rats in every group. In H&E-stained slides, the bony trabeculae were assessed at their midpoint away from their branched areas. In every section, the mean trabecular thickness of five non-overlapping fields (at magnification x100) was estimated. The mean area percentage of immune positive reaction was calculated using five non overlapping fields (at magnification x400; area: 0.071 mm^2) for every RANKL and β-catenin stained- section (Shaalan et al., 2020).

Data were analyzed using computer program SPSS (Statistical Package for Social Science), version 22 (IBM, USA). Data were expressed as Mean ± Standard deviation. One-way ANOVA test, and then Tukey's post-hoc test were applied in order to compare different groups. The statistically significant rate was judged when P value below 0.05. All graphical data descriptions were performed with Microsoft Excel® for windows® (Microsoft Inc., USA).

RESULTS

Body weight

At the time of sacrifice, the body weight of Dexa group was highly significantly decreased compared to that of control group, and only the highest dose of DHA (D+D30) normalized the body weight, while both D+D10- and D+D20-treated groups showed a highly significant increase as compared to Dexa group (Fig. 1A).

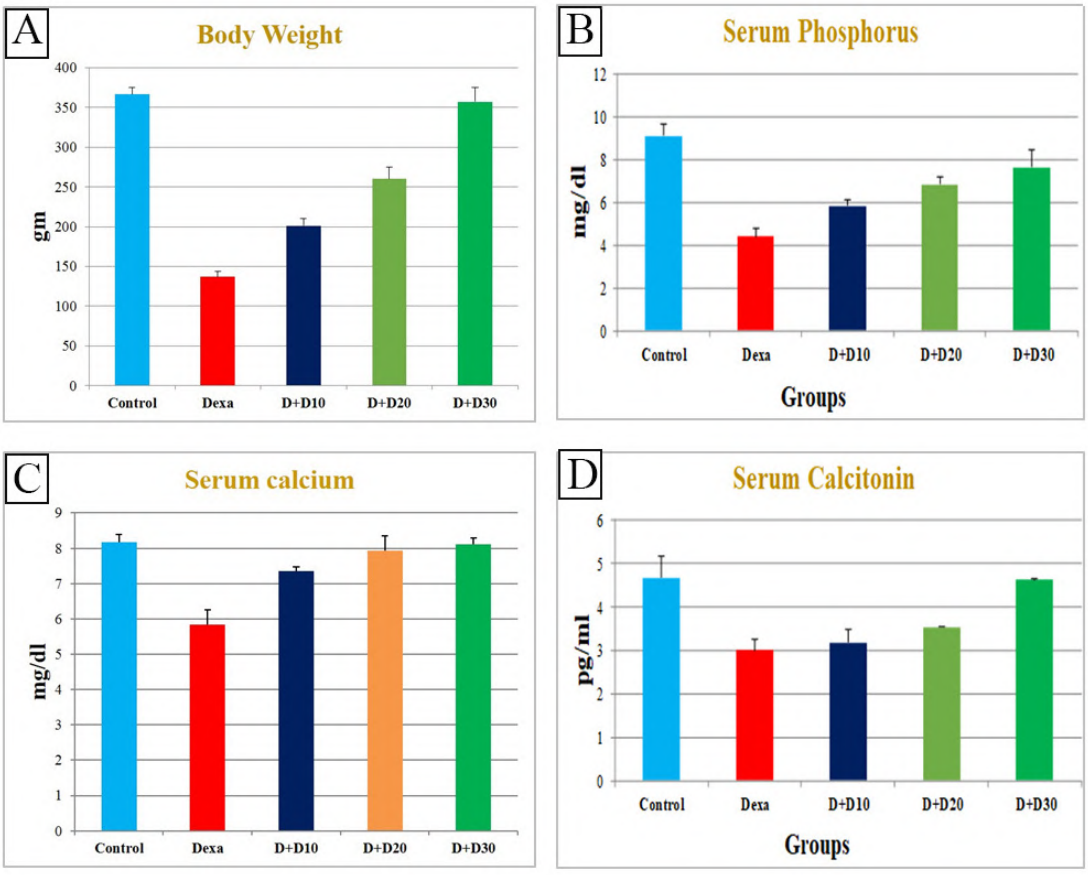

Fig. 1.- Body weight at the time of sacrifice in different groups (**1A**), Serum level of phosphorus in different groups (**1B**), Serum level of calcium in different groups (**1C**) and Serum level of calcitonin in different groups (**1D**).

Biochemical tests

Serum level of P in Dexa group was highly significantly decreased compared to that of control group, and all three doses of DHA showed a high significant increased compared to Dexa group (Fig. 1B). Serum level of Ca of the Dexa group was highly significantly decreased compared to that of control group. While compared to control, both doses of DHA 20 and 30 normalized the serum level of Ca, while the lower dose (D+D10) showed a high significant increase compared to Dexa-treated group (Fig. 1C).

Serum level of calcitonin of Dexa group was highly significantly decreased compared to that of control group, and only the high dose (D+D30) normalized serum level of calcitonin, while both D+D10- and D+D20-treated groups showed highly significant increased compared to Dexa group (Fig. 1D).

Serum level of alkaline and acid phosphatase of Dexa group was highly significantly increased compared to that of control group. Only the highest dose of DHA normalized serum both levels of alkaline and acid phosphatase while both D+D10 and D+D20 groups significantly decreased compared to that of Dexa group (Figs. 2C, 2D).

Oxidative stress markers

Bone tissue level of GSH in Dexa group was highly significantly decreased in comparison to the control group. Compared with control rats, only the high dose (D+D30) normalized the GSH level, although in both D+D10 and D+D20 groups this was increased highly significantly compared to Dexa group (Fig. 2A).

Bone tissue level of MDA of Dexa group was highly significantly increased compared to that of the control group. Only the highest dose normalized the bone tissue level of MDA, althoughin both D+D10 and D+D20 groups this was highly significantly decreased compared to that of Dexa group (Fig. 2B).

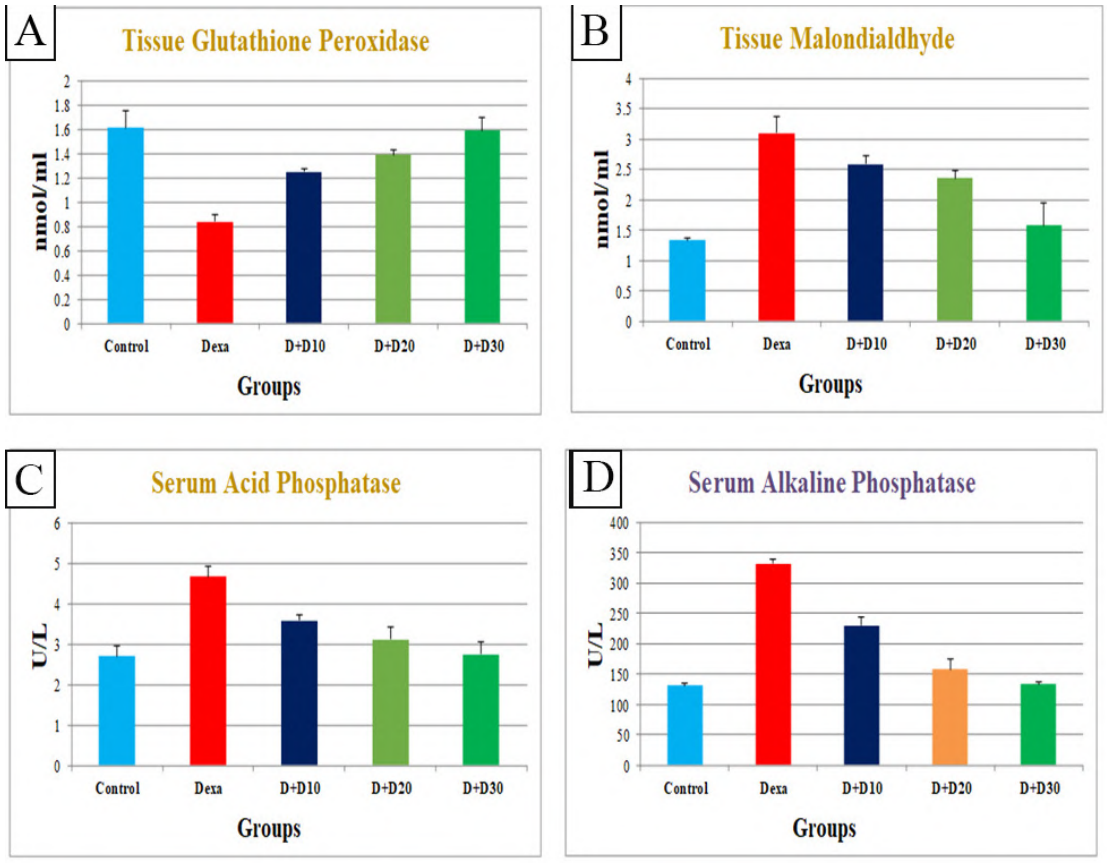

Fig. 2.- Bone tissue level of glutathione peroxidase in different groups (**2A**), Bone tissue level of MDA in different groups (**2B**), Serum level of acid phosphatase in different groups (**2C**) and Serum level of alkaline phosphatase in different groups (**2D**).

Histological Examination

Hematoxylin and Eosin-stained sections

The epiphysis of the tibia in the control group showed cancellous bone formed of bony trabecular networks separated by interconnecting spaces containing bone marrow formed of hemopoietic tissue, scattered adipocytes and seeming normal numbers of osteoclasts (Fig. 3A). Epiphysis of Dexa group showed apparent increase of the adipocytes in bone marrow as compared with control rats, with clear trabecular bone resorption indicated by widely separated thin bone spicules. Increased numbers of bone marrow adipocytes and osteoclasts were also observed (Fig. 3B). The effect of Dexa gradually reversed in DHA-treated groups with increasing dose from 10 to 30, as shown in gradual increase of the trabecular thickness, reduction of adipocytes and osteoclasts numbers contrasted to the Dexa-treated rats (Figs. 3C, D and E). Statically, the trabecular bone thickness in the epiphysis of the Dexa group was significantly decreased compared to that of the control group. Trabecular bone thickness in the epiphysis of D+D30-treated group was highly significantly increased compared to that of Dexa group and both groups (D+D10 and D+D20) showed a significant increase compared to that of Dexa group. Moreover, the three doses of DHA normalized the trabecular bone thickness (Fig. 3F).

The diaphysis of control group sections showed compact bone covered from outside by regular periosteum, and from inside by smooth endosteal surface (Fig. 4A). Osteocytes inside their lacunae and osteoblasts on bone surface and regularly arranged collagen fibers were seen. the diaphysis from the Dexa group (Fig. 4B) showed irregularly eroded endosteal surface. Empty lacunae, osteoclast housed in the eroded area in bone surface with faintly stained matrix were observed. the diaphysis from the D+D10 group showed compact bone with regular periosteum and endosteum with some empty lacunae. Higher magnification showed regularly arranged collagen fibers and some osteocytes inside their lacunae (Fig. 4C). The diaphysis from D+D20 and D+D30 groups showed compact bone with regular periosteum and endosteum (Fig. 4D, E).

Masson Goldner-stained sections

Masson Goldner-stained sections of tibia diaphysis (Fig. 5A) in the control group showed compact bone and tibia epiphysis (Fig. 6A), cancellous bone with regular appearance of mature bone, which is stained green, and average amount of red stained newly formed bone (Fig. 5A). In the Dexa group, a significant decline in red-stained newly formed bone was noticed (Figs. 5, 6B). The consequence of Dexa gradually inverted in treated groups, D+D corresponding to increasing dose from 10 to 30 mg, with noticeable rise of the red-stained newly formed bone in comparison to the Dexa treated rats (Figs. 5, 6C, D and E).

Immunostained sections

RANKL-stained sections

RANKL expression was nonexistent almost in bone marrow of control rats (Fig. 7A). Highly significant potent RANKL expression was observed in bone marrow of the Dexa-treated rats compared to that of the control group (Figs. 7B, F). Expression of RANKL in bone marrow significantly diminished with all DHA doses, D+D10 (Figs. 7C and F), D+D20 (Figs. 7D and F), and D+D30 (Figs. 7E and F), and both doses D+D20 and D+D30 restored the normal RANKL expression (Figs. 7C, D, E and F).

β *catenin-stained sections*

β-catenin expression was identified in the bone marrow of control rats (Fig. 8A). In Dexa-treated animals, β-catenin expression was not detected in bone marrow, with a significant high ($P < 0.001$) reduction in area percentage in comparison with control sections (Fig. 8B and F). β-catenin expression gradually raised in bone marrows of groups treated with D+D10, D+D20, and D+D30 when compared with the Dexa group. Also, it significantly ($P<0.001$) enhanced in comparison to the Dexa rats in both D+D20, and D+D30, but was non-significantly increased in D+D10 group (Figs. 8C, D, E and F).

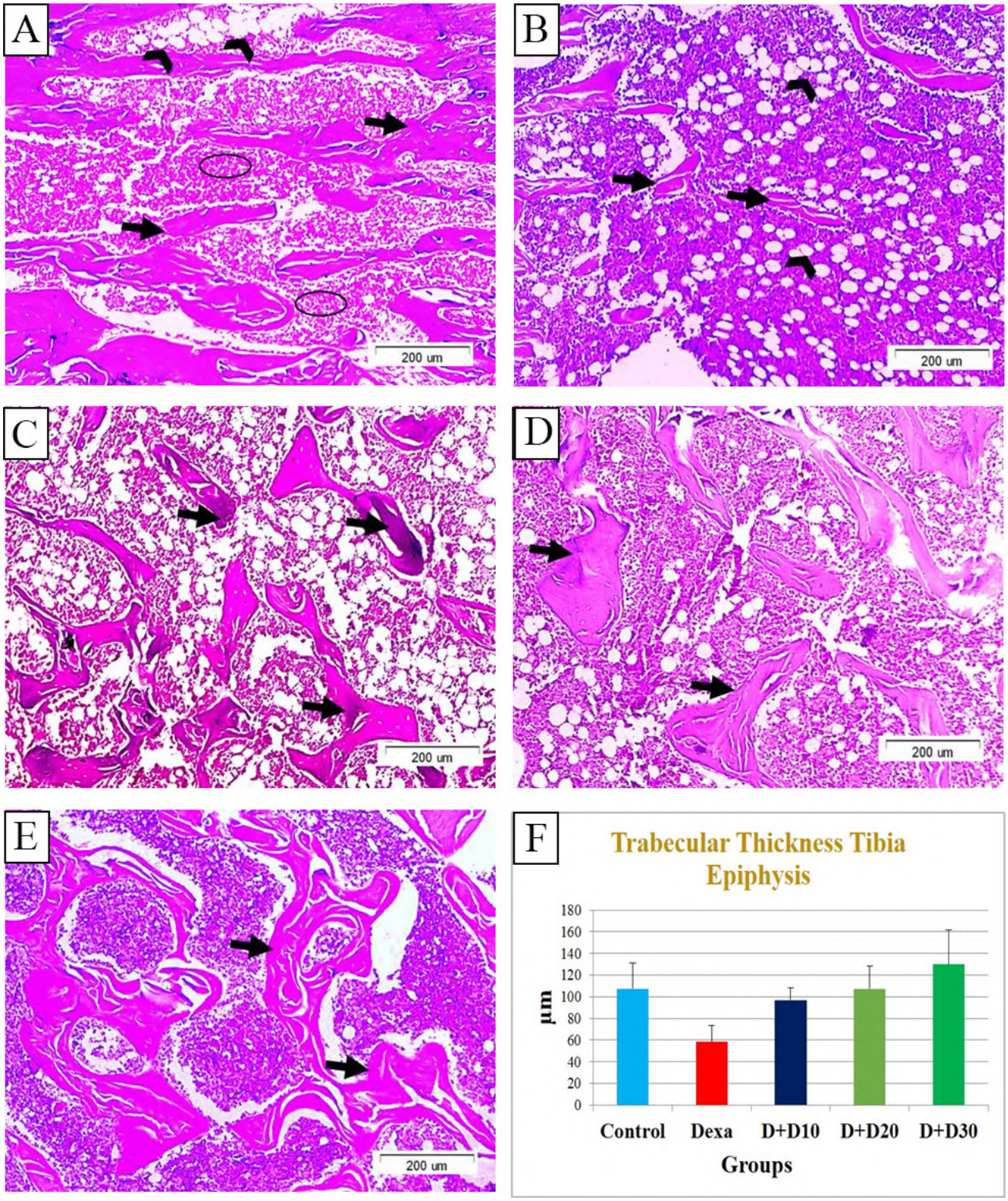

Fig. 3.- Tibia section from epiphysis stained with H&E the control group (**3A**) displaying cancellous bone arranged as networks of bony trabeculae (black arrows) separated by bone marrow interconnecting spaces made by hemopoietic tissue (circles) and dispersed adipocytes (arrowheads). The Dexa group (**3B**) showing apparent increase in the bone marrow adipocytes (arrowheads) compared to control sections. Significant trabecular bone resorption is seen and revealed as widely separated thin bone spicules (black arrows). The D+D10 group (**3C**) showing a slight increase in trabecular thickness (black arrows) as compared to Dexa group. The group treated with D+D20 (**3D**) showed an increase in trabecular thickness (black arrows) as compared to Dexa group and D+D10-treated group. The group treated with D+D30 (**3E**) showed a marked increase in trabecular thickness (black arrows) as compared to Dexa group and D+D10-treated groups, with well-developed thickened trabeculae when compared with the co group. (H&E, x100, scale bar = 200 µm). Trabecular bone thickness in the epiphysis of different groups (**3F**).

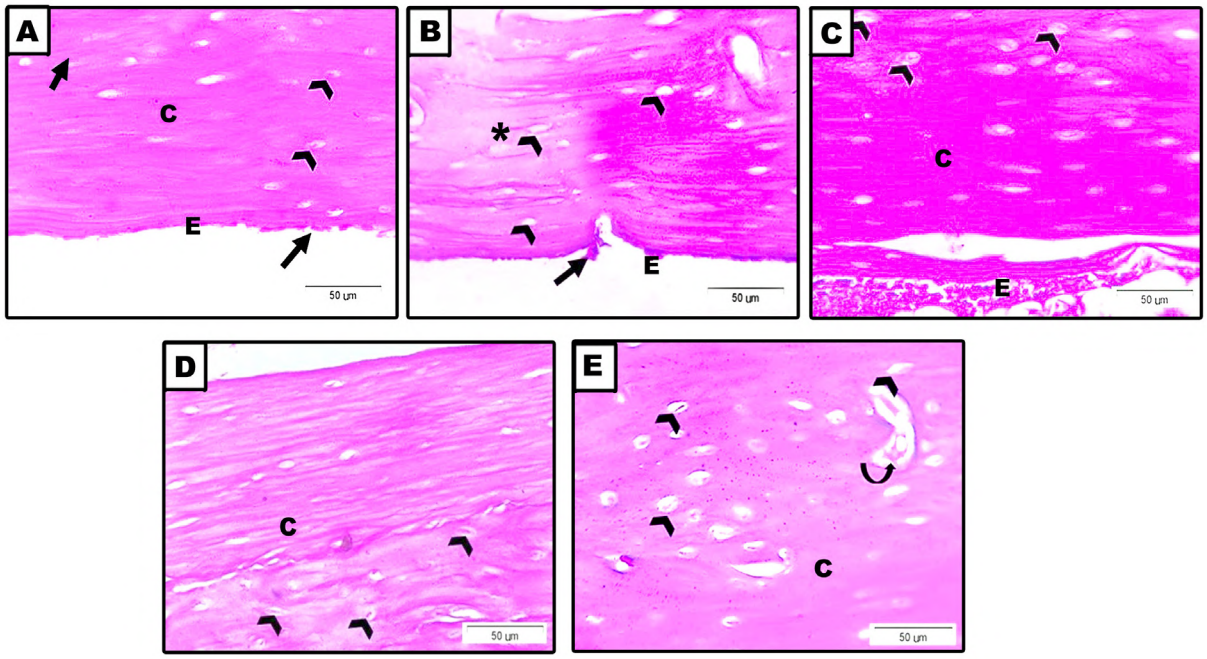

Fig. 4.- Tibia section from diaphysis of control group (**4A**) stained with H&E showing osteocytes inside their lacunae (arrowheads), smooth endosteal surface (E) lined with osteoblasts (black arrow) and regularly arranged collagen fibers (C). Dexa group (**4B**) showing empty lacunae (arrowheads), osteoclast housed in the eroded area in bone surface (black arrows) with faintly stained matrix (*) irregularly and eroded endosteal surface (E). D+D10 (**4C**) stained with H&E showing compact bone with regular arrangement of collagenous fibers of matrix (C) and osteocytes inside their lacunae (arrowheads). D+D20 (**4D**) stained with H&E showing compact bone with regularly arranged collagenous fibers of matrix (C) and osteocytes inside their lacunae (arrowheads). D+D30 (**4E**) group stained with H&E showing compact bone with regularly arranged collagenous fibers of matrix (C) and osteocytes within their lacunae (arrowheads). Blood vessel (curved arrow) is seen. (H&E, x400, scale bar = 50 µm).

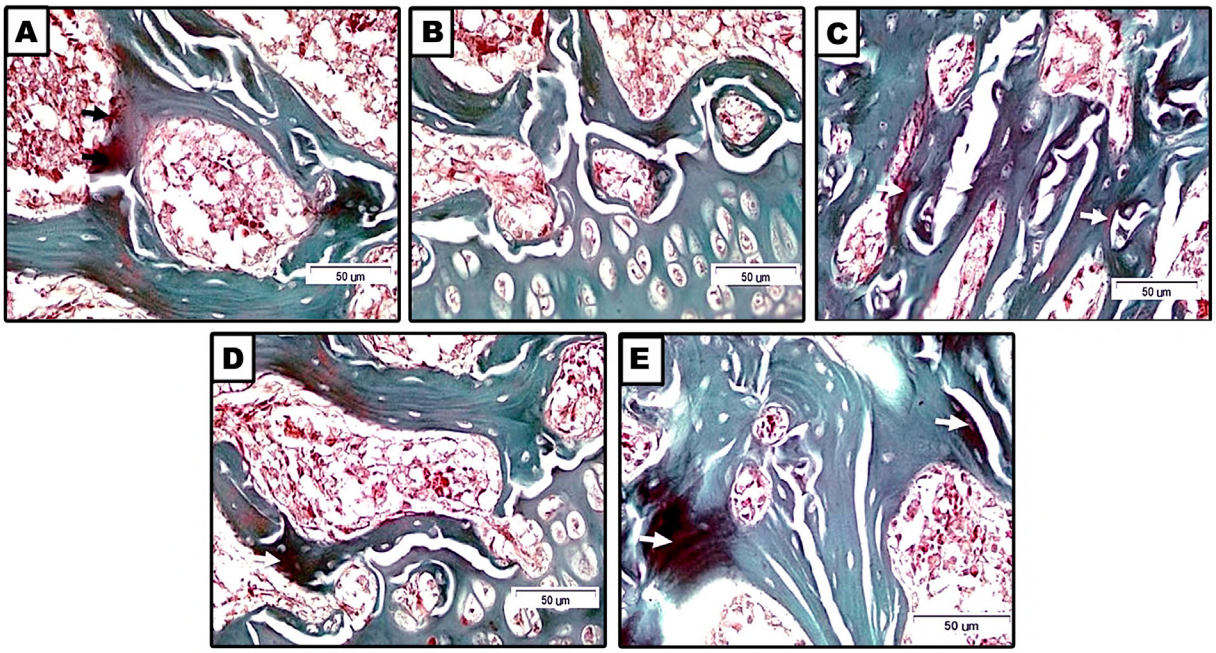

Fig. 5.- Masson Goldner-stained tibia section of the epiphysis of control group (**5A**) showing typical green stained mature compact bone look and average amount of red stained newly formed bone. The epiphysis of Dexa group (**5B**) showing significant decrease of red stained newly constructed bone. The epiphysis of D+D10 group (**5C**) showing enhanced red stained newly formed bone in comparison with Dexa-treated rats. The epiphysis of D+D20 group (**5D**) showing increased red stained newly formed bone as compared to Dexa-treated rats. Epiphysis of D+D30 group (**5E**) showing markedly enhanced red stained newly formed bone (white arrows) in comparison to Dexa section. (Masson Goldner, x400, scale bar = 50 µm).

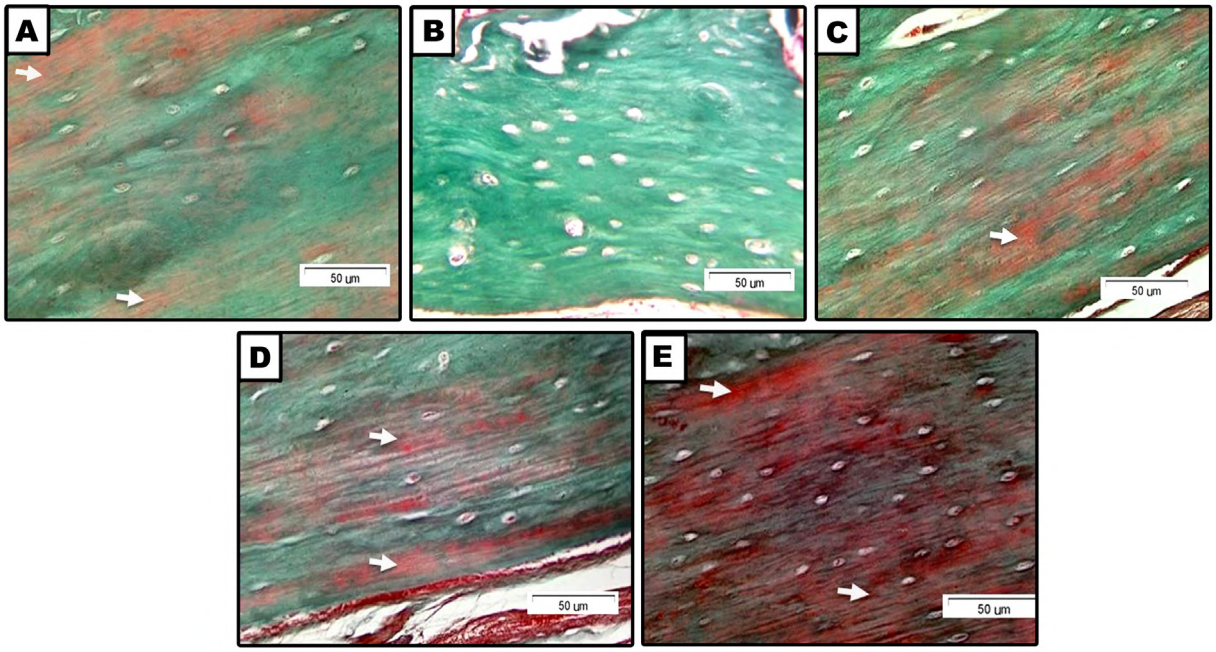

Fig. 6.- Masson Goldner stained of tibia diaphysis control group (**6A**) showing typical look of green colored mature compact bone with average amount of newly formed bone which is stained red. Dexa group (**6B**) showing noticeable decrease of red colored newly formed bone. D+D10 group (**6C**) showing enhanced red colored newly formed bone in comparison to Dexa sections. D+D20 rats (**6D**) showing elevated amount of red colored newly formed bone when compared to Dexa-treated rats. D+D30 group (**6E**) showing significantly enhanced red colored newly formed bone when compared to Dexa treated animals (Masson Goldner, x400, scale bar = 50 µm).

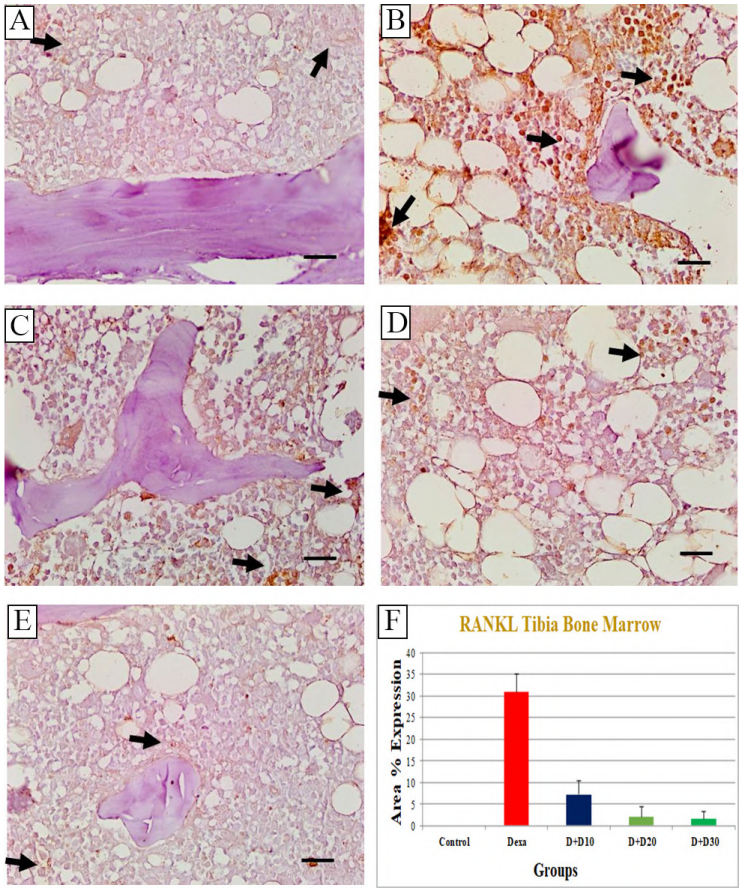

Fig. 7.- Tibia section immunostained against RANKL control group (**7A**) showing weak RANKL expression (black arrows) in bone marrow. Dexa group (**7B**) showing strong expression (black arrows) against RANKL in the bone marrow. D+D10 group (**7C**) showing moderate RANKL expression (black arrows) against as compared to Dexa group. D+D20 group (**7D**) showing mild expression (black arrows) against RANKL as compared to Dexa group. D+D30 group (**7E**) showing mild expression (black arrows) against RANKL in the bone marrow as compared to Dexa group. (RANKL immunohistochemistry, x400, bar = 50 µm). RANKL expression by area % in Dexa group (**7F**).

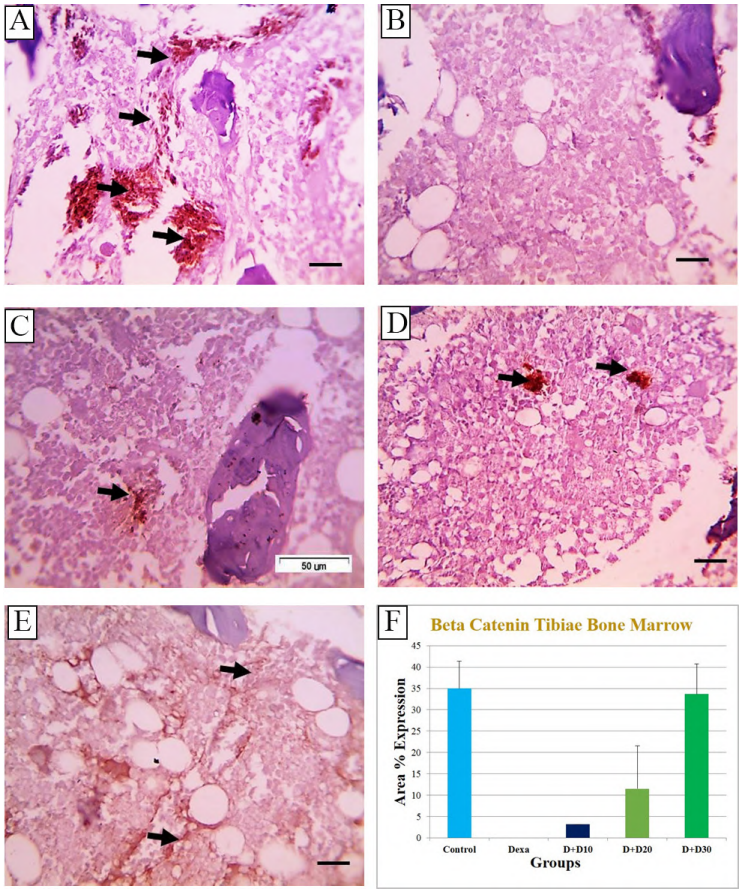

Fig. 8.- Tibia section immunostained against β catenin, control group (**8A**) showing strong β catenin expression in the bone marrow. Dexa-treated rats (**8B**) showing nearly absent expression in the bone marrow. D+D10 group (**8C**) showing mild increase of β catenin expression (black arrow) in the bone marrow as compared with Dexa group. D+D20 group (**8D**) showing moderate increase of β catenin expression (black arrow) in the bone marrow as compared with Dexa group. D+D30 group (**8E**) showing marked increase of β catenin expression (black arrows) in the bone marrow as compared with Dexa group. (β catenin immunohistochemistry, x400, scale bar = 50 µm). β catenin expression by area % in different groups (**8F**).

DISCUSSION

In this study, we used the glucocorticoid osteoporotic rat model to elucidate the protective effect of the antimalarial active compound in Artemisia Annua plant, the artemisinin against the development of osteoporosis. Glucocorticoids (GCs) induce osteoporosis via multiple mechanisms; they decrease bone formation, suppress the production of bone matrix, enhance apoptosis of the osteoblasts (Gohel et al., 1999) and increase resorption of bone by increase the numbers of the osteoclasts (Frenkel et al., 2015). Corticosteroids-induced oxidative stress provoke apoptosis, osteonecrosis and osteoporosis (Kerachian et al., 2006). Reactive oxygen species (ROS) can induce necrosis or apoptosis through Bcl-2 family proteins, mitochondrial dysfunction, and caspase stimulation. In addition, ROS can promote osteoclast differentiation (Callaway et al., 2015).

Corticosteroids induce bone resorption through the expression of receptor activator RANKL cytokine, which is necessary for osteoclast development. On the other hand, GCs downregulate the osteoprotegerin receptor (OPG) that blocks RANKL binding to RANK (Sivagurunathan et al., 2005). Kondo et al. (2008) reported that Osteoprotegerin impedes osteoclast differentiation, survival, and function in vitro and bone resorption in vivo. The imbalance between RANKL and OPG eventually results in a state of increased osteoclastogenesis and accelerated the rate of bone resorption (Boyce and Xing, 2008).

Osteoblasts and adipocytes originate from common mesenchymal progenitors (Prockop, 1997). The GCs inhibit bone formation through suppression of osteoblast proliferation, and it directs the mesenchymal progenitor cells in the direction of adipocyte lineage (Canalis

et al., 2007). The Wnt/ß-catenin signaling is the determining factor of the cell fate of pre-osteoblasts (Song et al., 2012). Activation of Wnt/ß-catenin stimulates the differentiation of osteoblasts, enhances the osteoblastogenesis and prevents their apoptosis (Duan and Bonewald, 2016). On the other hand, activation of Wnt/ß-catenin signaling inhibits adipogenesis from the mesenchymal precursors (Krishnan et al., 2006). Wnt/ß-catenin signals in osteoblasts induce OPG expression and thereby suppress the osteoclast differentiation (Kondo et al., 2008). Naito et al. (2012) reported that Corticosteroids can suppress Wnt/b-catenin activity via activation of GSK3b and downregulating ß-catenin. In addition, GCs induced RANKL signalling also increase degradation and inhibit synthesis of ß-catenin (Chen et al., 2018).

Many studies have demonstrated that Artemisia-annua-derived compounds, artemisinins (ARS), protects from bone loss in several animal models of induced bone loss. As in mouse model of different diseases, ovariectomized mice (Lee et al., 2017), lipopolysaccharide (LPS)-induced bone loss model (Wei et al., 2018), titanium-particle induced osteolysis (Feng et al., 2016), and in rat model of inflammatory bowel disease-related bone loss (Ge et al., 2018).

Up to our knowledge, this is the first study which use dihydroartemisinin (DHA) in treatment of Dexa-induced osteoporosis, and it showed increasing effects with dose increment as proven histological, immunohistochemical and biochemical tests. Also, thickness of bony trabeculae increased with new bone formation and in the bone marrow, expression of RANKL decreased while β-catenin was raised. The serum levels of Ca, P and calcitonin increased while alkaline phosphatase and acid phosphatase decreased. In bony tissue homogenate, the lipid peroxidation was reduced as indicated by the decrease of MDA, and the oxidative stress state decreased as was evident by the elevation of GSH.

The antioxidant effects of Artemisia annua is believed to be related to its flavonoids contents, which are capable of neutralizing free radicals present in the cell environment, and prevent their damaging effects (Lang et al., 2019). Flavonoids likewise prevent lipid peroxidation and increase the activity of antioxidant system (Kim et al., 2003). Artemisia plant extract also hinders activity of heme oxygenase, therefore reducing free radicals creation (Jafari Dinani et al., 2007).

In the current study, DHA markedly inhibited the expression of receptor activator of nuclear factor-κB ligand (RANKL) in the bone marrow. Thus, RANKL-stimulated osteoclast differentiation in bone-marrow-derived macrophages is supressed by diminished osteoclastogenesis and suppressed bone resorption. These repressing effects might be facilitated by inhibitions of multiple signalling pathways such as decreased expression of c-Fos and nuclear factor of activated T-cells (NFATc1) (Lee et al., 2017), nuclear factor kappa-B (NF-κB) (Wei et al., 2018), mitogen-activated protein kinases (MAPKs) (Wu et al., 2018), phospholipase Cγ1 (PLCγ1)-Ca2+-NFATc1 (Zeng et al., 2017), and protein kinase B (PKB/AKT)/SRC (Feng et al., 2016). Lee et al. (2017) suggested that Artemisia annua extract may reduce bone loss through inhibiting RANKL-induced osteoclast differentiation, instead of controlling RANKL and/or OPG production in proinflammatory cytokine-stimulated osteoblastic cells.

In a mouse model of lipopolysaccharide (LPS)-induced bone loss, artesunate suppressed osteoclastogenesis and bone resorption. However, it did not affect osteoblast mediated bone formation (Wei et al., 2018). In particular, ARS compounds might induce oxidative damage in osteoclasts that have higher intracellular iron level than other cells (Zhang, 2020). Intracellular iron may trigger ARS compounds, causing release of huge amount of free radical (Chaturvedi et al., 2010). Any reason able to increases ROS may lead to oxidative damage to osteoclasts which already have increased level of ROS (Domazetovic et al., 2017). Accumulation of ROS increases cytochrome c and AIF release from mitochondria to the cytosol, with the stimulation of caspase-3 and rise of the Bax/Bcl-2 ratio (Dou et al., 2016).

However, Fang et al. (2021) demonstrated that artemisinin treatment increased survival of bone marrow mesenchymal stromal cells by suppression of ROS production that associated with the reduction of caspase-3 activation, and

apoptosis induced by Dexa. This may be related to the decreased oxidative stress in bone-marrow mesenchymal cells prior to their differentiation into osteoclasts, which cause them to be less vulnerable to DHA-stimulated apoptosis (Dou et al., 2016).

Moreover, in this research, DHA improved the expression of β-catenin in bone marrow, which may indicate stimulation of osteoblastogenesis. This was manifested by new formations in both the trabecular and cancellous bone as detected by Masson Goldner stain. (Nemeth et al., 2009). Tay et al. (2017) showed that ß-catenin deficient bone marrow exhibited decreased numbers of osteoblasts in vitro and in vivo, with diminished production of the hematopoietic regulatory factors; basic fibroblast growth factor (bFGF), SCF, and VCAM-1. ß-catenin is essential for production of osteoblasts and the preservation of hematopoietic progenitors in the adult bone marrow (Nemeth et al., 2009). The Wnt canonical pathway regulates the proliferation and differentiation of osteoblastic precursors and retains mature osteoblasts (Baron et al., 2006).

In conclusion, this study showed that treatment with DHA to Dexa-induced model of osteoporosis significantly improved the oxidative stress, biochemical and histological bone indices. It exerted its effects through stimulation of the Wnt-β catenin and inhibition of RANKL pathways, which is reflected on stimulation of osteoblastogenesis and inhibition of osteoclastogenesis. Dihydroartemisinin may be a new treatment approach to avoid glucocorticoid-induced osteoporosis.

REFERENCES

AHMADZADEH A, NOROZI F, SHAHRABI S, SHAHJAHANI M, SAKI N (2016) Wnt/β-catenin signaling in bone marrow niche. *Cell Tissue Res,* 363(2): 321-335.

BARON R, RAWADI G, ROMAN-ROMAN S (2006) Wnt signaling: a key regulator of bone mass. *Curr Top Dev Biol,* 76: 103-127.

BOYCE BF, XING L (2008) Functions of RANKL/RANK/OPG in bone modeling and remodeling. *Arch Biochem Biophys,* 473(2): 139-146.

CABELLO CM, LAMORE SD, BAIR WB 3RD, QIAO S, AZIMIAN S, LESSON JL, WONDRAK GT (2012) The redox antimalarial dihydroartemisinin targets human metastatic melanoma cells but not primary melanocytes with induction of NOXA-dependent apoptosis. *Invest New Drugs,* 30(4): 1289-1301.

CALLAWAY DA, JIANG JX (2015) Reactive oxygen species and oxidative stress in osteoclastogenesis, skeletal aging and bone diseases. *J Bone Miner Metab,* 33(4): 359-370.

CANALIS E, MAZZIOTTI G, GIUSTINA A, BILEZIKIAN JP (2007) Glucocorticoid-induced osteoporosis: pathophysiology and therapy. *Osteoporos Int,* 18(10): 1319-1328.

CHATURVEDI D, GOSWAMI A, SAIKIA PP, BARUA NC, RAO PG (2010) Artemisinin and its derivatives: a novel class of anti-malarial and anti-cancer agents. *Chem Soc Rev,* 39(2): 435-454.

CHEN C, ZHENG H, QI S (2019) Genistein and silicon synergistically protects against ovariectomy-induced bone loss through upregulating OPG/RANKL ratio. *Biol Trace Elem Res,* 188(2): 441-450.

CHEN X, ZHI X, WANG J, SU J (2018) RANKL signaling in bone marrow mesenchymal stem cells negatively regulates osteoblastic bone formation. *Bone Res,* 27(6): 34.

DOMAZETOVIC V, MARCUCCI G, IANTOMASI T, BRANDI ML, VINCENZINI MT (2017) Oxidative stress in bone remodeling: role of antioxidants. *Clin Cases Miner Bone Metab,* 14(2): 209-216.

DOU C, DING N, XING J, ZHAO C, KANG F, HOU T, QUAN H, CHEN Y, DAI Q, LUO F, XU J, DONG S (2016) Dihydroartemisinin attenuates lipopolysaccharide-induced osteoclastogenesis and bone loss via the mitochondria-dependent apoptosis pathway. *Cell Death Dis,* 7(3): e2162.

DUAN P, BONEWALD LF (2016) The role of the wnt/β-catenin signaling pathway in formation and maintenance of bone and teeth. *Int J Biochem Cell Biol,* 77(Pt A): 23-29.

EL WAKF AM, HASSAN HA, GHARIB NS (2014) Osteoprotective effect of soybean and sesame oils in ovariectomized rats via estrogen-like mechanism. *Cytotechnology,* 66(2): 335-343.

FANG J, SILVA M, LIN R, ZHOU W, CHEN Y, ZHENG W (2021) Artemisinin reverses glucocorticoid-induced injury in bone marrow-derived mesenchymal stem cells through regulation of ERK1/2-CREB signaling pathway. *Oxid Med Cell Longev,* 2021: 5574932.

FENG MX, HONG JX, WANG Q, FAN YY, YUAN CT, LEI XH, ZHU M, QIN A, CHEN HX, HONG D (2016) Dihydroartemisinin prevents breast cancer-induced osteolysis via inhibiting both breast caner cells and osteoclasts. *Sci Rep,* 6: 19074.

FERREIRA JF, LUTHRIA DL, SASAKI T, HEYERICK A (2010) Flavonoids from Artemisia annua L. as antioxidants and their potential synergism with artemisinin against malaria and cancer. *Molecules,* 15(5): 3135-3170.

FRENKEL B, WHITE W, TUCKERMANN J (2015) Glucocorticoid-induced osteoporosis. *Adv Exp Med Biol,* 872: 179-215.

GALLAGHER JC, SAI AJ (2010) Molecular biology of bone remodeling: implications for new therapeutic targets for osteoporosis. *Maturitas.* 65(4): 301-307.

GE X, CHEN Z, XU Z, LV F, ZHANG K, YANG Y (2018) The effects of dihydroartemisinin on inflammatory bowel disease-related bone loss in a rat model. *Exp Biol Med (Maywood),* 243(8): 715-724.

GOHEL A, MCCARTHY MB, GRONOWICZ G (1999) Estrogen prevents glucocorticoid-induced apoptosis in osteoblasts in vivo and in vitro. *Endocrinology,* 140(11): 5339-5347.

HARTMANN K, KOENEN M, SCHAUER S, WITTIG-BLAICH S, AHMAD M, BASCHANT U, TUCKERMANN JP (2016) Molecular actions of glucocorticoids in cartilage and bone during health, disease, and steroid therapy. *Physiol Rev,* 96(2): 409-447.

IOANNIDIS G, PALLAN S, PAPAIOANNOU A, MULGUND M, RIOS L, MA J, THABANE L, DAVISON KS, JOSSE RG, KOVACS CS, KREIGER N, OLSZYNSKI WP, PRIOR JC, TOWHEED T, ADACHI JD; CAMOS RESEARCH GROUP (2014) Glucocorticoids predict 10-year fragility fracture risk in a population-based ambulatory cohort of men and women: Canadian Multicentre Osteoporosis Study (CaMos). *Arch Osteoporos,* 9: 169.

JAFARI DINANI N, ASGARY S, MADANI H, MAHZONI P, NADERI G (2007) Effect of *Artemisia aucheri e*xtract on atherogenic lipids and atherogenesis in hypercholesterolemic rabbits. *J Med Plants,* 6(23): 20-28.

KATIYAR C, GUPTA A, KANJILAL S, KATIYAR S (2012) Drug discovery from plant sources: An integrated approach. *Ayu,* 33(1): 10-19.

KERACHIAN MA, HARVEY EJ, COURNOYER D, CHOW TY, SÉGUIN C (2006) Avascular necrosis of the femoral head: vascular hypotheses. *Endothelium,* 13(4): 237-244.

KIM KS, LEE S, LEE YS, JUNG SH, PARK Y, SHIN KH, KIM BK (2003) Anti-oxidant activities of the extracts from the herbs of Artemisia apiacea. *J Ethnopharmacol,* 85(1): 69-72.

KONDO T, KITAZAWA R, YAMAGUCHI A, KITAZAWA S (2008) Dexamethasone promotes osteoclastogenesis by inhibiting osteoprotegerin through multiple levels. *J Cell Biochem,* 1;103(1): 335-345.

KRISHNAN V, BRYANT HU, MACDOUGALD OA (2006) Regulation of bone mass by Wnt signaling. *J Clin Invest,* 116(5): 1202-1209.

LANG SJ, SCHMIECH M, HAFNER S, PAETZ C, STEINBORN C, HUBER R, GAAFARY ME, WERNER K, SCHMIDT CQ, SYROVETS T, SIMMET T (2019) Antitumor activity of an Artemisia annua herbal preparation and identification of active ingredients. *Phytomedicine,* 62: 152962.

LEE SK, KIM H, PARK J, KIM HJ, KIM KR, SON SH, PARK KK, CHUNG WY (2017) Artemisia annua extract prevents ovariectomy-induced bone loss by blocking receptor activator of nuclear factor kappa-B ligand-induced differentiation of osteoclasts. *Sci Rep,* 7(1): 17332.

LIU Y, CHEN Y, ZHAO H, ZHONG L, WU L, CUI L (2011) Effects of different doses of dexamethasone on bone qualities in rats. S*heng Wu Yi Xue Gong Cheng Xue Za Zhi,* 28(4): 737-743.

NAITO M, OMOTEYAMA K, MIKAMI Y, TAKAHASHI T, TAKAGI M (2012) Inhibition of Wnt/β-catenin signaling by dexamethasone promotes adipocyte differentiation in mesenchymal progenitor cells, ROB-C26. *Histochem Cell Biol,* 138(6): 833-845.

NEMETH MJ, MAK KK, YANG Y, BODINE DM (2009) beta-Catenin expression in the bone marrow microenvironment is required for long-term maintenance of primitive hematopoietic cells. *Stem Cells,* 27(5): 1109-1119.

PROCKOP DJ (1997) Marrow stromal cells as stem cells for nonhematopoietic tissues. *Science,* 276(5309): 717-724.

SHAALAN AAM, EL-SHERBINY M, EL-ABASERI TB, SHOAEIR MZ, ABDEL-AZIZ TM, MOHAMED MI, ZAITONE SA, MOHAMMAD HMF (2020) Supplement with calcium or alendronate suppresses osteopenia due to long term rabeprazole treatment in female mice: influence on bone TRAP and osteopontin levels. *Front Pharmacol,* 13(11): 583.

SIVAGURUNATHAN S, MUIR MM, BRENNAN TC, SEALE JP, MASON RS (2005) Influence of glucocorticoids on human osteoclast generation and activity. *J Bone Miner Res,* 20(3): 390-398.

SONG L, LIU M, ONO N, BRINGHURST FR, KRONENBERG HM, GUO J (2012) Loss of wnt/β-catenin signaling causes cell fate shift of preosteoblasts from osteoblasts to adipocytes. *J Bone Miner Res,* 27(11): 2344-2358.

SOZEN E, OZER NK (2017) Impact of high cholesterol and endoplasmic reticulum stress on metabolic diseases: An updated mini-review. *Redox Biol,* 12: 456-461.

SÖZEN T, ÖZIŞIK L, BAŞARAN NÇ (2017) An overview and management of osteoporosis. *Eur J Rheumatol,* 4(1): 46-56.

TAY J, LEVESQUE JP, WINKLER IG (2017) Cellular players of hematopoietic stem cell mobilization in the bone marrow niche. *Int J Hematol,* 105(2): 129-140.

WEI CM, LIU Q, SONG FM, LIN XX, SU YJ, XU J, HUANG L, ZONG SH, ZHAO JM (2018) Artesunate inhibits RANKL-induced osteoclastogenesis and bone resorption in vitro and prevents LPS-induced bone loss in vivo. *J Cell Physiol,* 233(1): 476-485.

WILLSON T, NELSON SD, NEWBOLD J, NELSON RE, LAFLEUR J (2015) The clinical epidemiology of male osteoporosis: a review of the recent literature. *Clin Epidemiol,* 9(7): 65-76.

WU H, HU B, ZHOU X, ZHOU C, MENG J, YANG Y, ZHAO X, SHI Z, YAN S (2018) Artemether attenuates LPS-induced inflammatory bone loss by inhibiting osteoclastogenesis and bone resorption via suppression of MAPK signaling pathway. *Cell Death Dis,* 9(5): 498.

ZENG X, ZHANG Y, WANG S, WANG K, TAO L, ZOU M, CHEN N, XU J, LIU S, LI XJBP (2017) Artesunate suppresses RANKL-induced osteoclastogenesis through inhibition of PLCγ1-Ca2+–NFATc1 signaling pathway and prevents ovariectomy-induced bone loss. *Biochem Pharmacol,* 15(124): 57-68.

ZHANG J (2020) The osteoprotective effects of artemisinin compounds and the possible mechanisms associated with intracellular iron: A review of in vivo and in vitro studies. *Environ Toxicol Pharmacol,* 76: 103358.

Is there a relationship between sella turcica calcification and thyroid cartilage calcification? A random study using lateral cephalometric radiography

Andrea Garrido[1,3], Alaa Alsafadi[1,3], Iván Menéndez[1,3], Ramón Cobo[1,2,3], Teresa Cobo[1,3]

[1] *University of Oviedo, Spain*

[2] *Marqués de Valdecilla University Hospital, Santander, Spain*

[3] *Instituto Asturiano de Odontología, Oviedo, Spain*

SUMMARY

Thyroid cartilage changes begin in the second decade of life with the horn of the thyroid cartilage, and spread throughout the individual's lifetime to other cartilage plates. However, the objective of the present study is to assess if there is an association between thyroid calcification (TC) and sella turcica bridging (STB). Forty patients, 11 men and 29 women, aged between 40 and 62 years with a mean age of 48.6 years were studied. The sample inclusion criteria of this study were age in the fourth decade, no craniofacial deformities, no history of craniofacial surgical intervention, good-quality lateral cephalometric radiographs, and good visualization of the sella turcica (ST). A total of 40 registered patients were included in the assessment of calcification of the thyroid cartilage. Of these, 75% presented with thyroid calcifications, and 25% did not. Data on sex was available for all 40 registered patients. A total of 72.5% were female, and 27.5% were male. While in a comparison between calcification of the thyroid and calcification of the sella turcica, no statistical relationship was observed between the two variables. Thyroid cartilage calcification could be considered a normal part of the ageing process, while STB could appear on lateral radiographs due to superimposition of the anatomical structures. In this study, we found no relationship between thyroid cartilage calcification and STB, and a larger patient sample is required for evaluating calcification of the thyroid and STB.

Keywords: Sella turcica bridging – Thyroid cartilage calcification – Lateral cephalometry

INTRODUCTION

Lateral radiography, introduced by Broadbent in 1931, has played an essential role in orthodontic assessment and treatment planning (Durão et al., 2015). The main goals of lateral cephalometric radiography (LCR) are to provide detailed views of the patient's skeletal, dental, and soft-tissue morphology, to evaluate skeletal maturation and to assess a patient's progressive response to treatment. The sella turcica (ST) is an essential structural reference in cephalometric

Corresponding author:
Teresa Cobo. Instituto Asturiano de Odontologia, C/ Catedrático José Serrano 10 bajo, 33006 Oviedo, Spain. Phone: +34 650 389 074. E-mail: dracobo@iaodontologia.com

Submitted: April 26, 2022. **Accepted:** May 6, 2022

https://doi.org/10.52083/AESO9994

analysis. A sellar point is determined from this structure, usually located at the centre of the ST, and is considered an essential landmark in cephalometric studies (Shatyanarayana et al, 2013). The ST is a saddle-shaped bony structure located anatomically on the intracranial surface of the body of the sphenoid bone (Kaya et al., 2021). Radiographically, the size of the ST can be assessed through either linear or various area and volume measurement methods. Usually, it ranges from 4 to 12 mm in the vertical dimensions and 15 to 16 mm in the anteroposterior dimensions (Kaya et al., 2021).

The hypophysis is located within this anatomical space. Any change in the size of the ST is more frequently associated with pathology; thus, the relationship between dimensional and morphological variations in the ST and various syndromes and disorders, skeletal patterns (Alkofide, 2007; Meyer-Marcotty et al., 2010), and dental anomalies has been investigated in previous studies using lateral radiography. Axelsson et al. (2004) and Acevedo et al. (2021), distinguished five different morphological variations for the ST: STB, double floor contour, oblique anterior wall, pyramidal shape of the dorsum sella (DS), and irregularity in the posterior (DS). These structures may fuse and form osseous bridges due to an abnormal development of the anterior and posterior walls of the clinoid processes (Leonardi et al., 2011; Scribante et al., 2017). On LCR, many crucial anatomic structures can be observed, such as the laryngeal cartilage, in which ossification and calcification have been investigated widely since 1882 (Aramaki et al., 2017). When ossification begins with the lamina or cornua, the thyroid cartilage is visible on lateral cephalometric and lateral neck radiographs (Mupparapu et al., 2005). The thyroid cartilage is made up of hyaline cartilage, as well as other structures such as cricoid and arytenoid cartilage; the hyaline cartilages calcify and ossify as part of the ageing process (Aramaki et al., 2017). These changes begin in the second decade of life with the horn of the thyroid cartilage, and spread throughout the individual's lifetime to other cartilage plates (Aramaki et al., 2017; Garvin, 2008; Tabatabaee et al., 2020). The present study aims to evaluate the relationship between STB and calcification of the thyroid cartilage.

MATERIALS AND METHODS

This study included 40 patients, 11 men and 29 women, aged between 40 and 62 years with a mean age of 48.6 years. The sample inclusion criteria of this study were age in the fourth decade, no craniofacial deformities, no history of craniofacial surgical intervention, good-quality lateral cephalometric radiographs, and good visualization of the sella turcica. The cephalometric measurements were realized using Dolphin software 11.95.67 and performed by one observer with six years of orthodontic experience. On lateral radiography and after radiograph calibration, a series of specific cephalometric analysis measurements were conducted after identifying the following anatomical structures: nasion (N), sella (S), sella diameter (from the tuberculum sella (TS) to the DS), deepest point of the sella floor (SF), farthest point on the inner sellar wall (SW), most anterior point of the hyoid bone, base of the styloid process, glossal point, A point, pogonion point (Pg), anterior nasal spine (ANS) and posterior nasal spine (PNS) (Fig. 1). The intersection of the palatal plane with the S-N plane, the perpendicular distance between A point and the S-N plane, the perpendicular distance between Pg and the S-N plane, and the plane formed by the stylohyoid, styloglossal, and hyoidglossal planes were evaluated. A total of 14 values were evaluated from lateral radiography. Through radiograph assessment, scores were assigned for bridging of the sella turcica (no bridging = 0, partial bridging = 1, complete bridging = 2) (Fig. 1) and calcification of the thyroid cartilage (no calcification = 0, calcification = 1) (Fig. 2).

This study was conducted in accordance with the ethics defined in the Declaration of Helsinki, and approval was obtained from the research ethics committee of the Instituto Asturiano de Odontología (Ref. IAO-21-0621).

Informed consent was obtained from all subjects and/or their legal guardian(s).

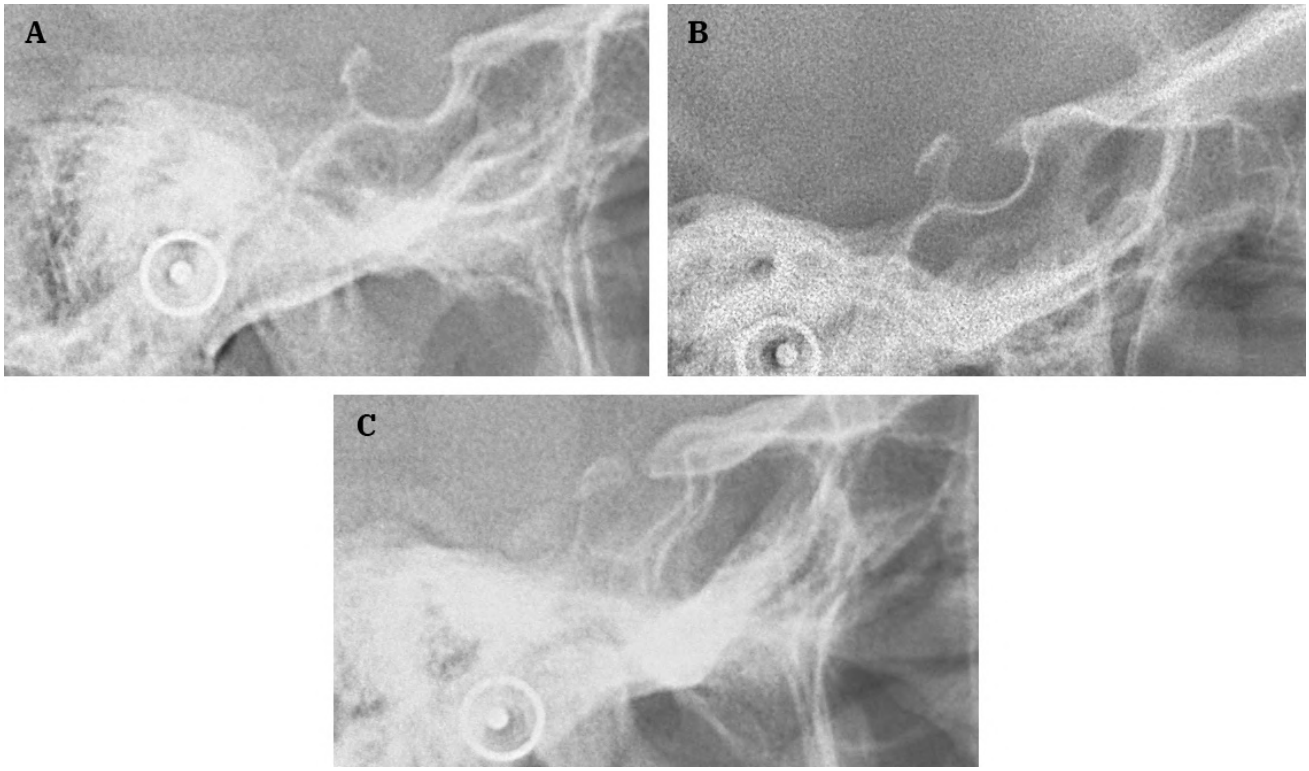

Fig. 1.- Sella Turcica and thyroid cartilage classification. **A**- Sella Turcica non bridging. **B-** Patient with partial Sella turcica bridging. **C-** Sella turcica with complete bridging.

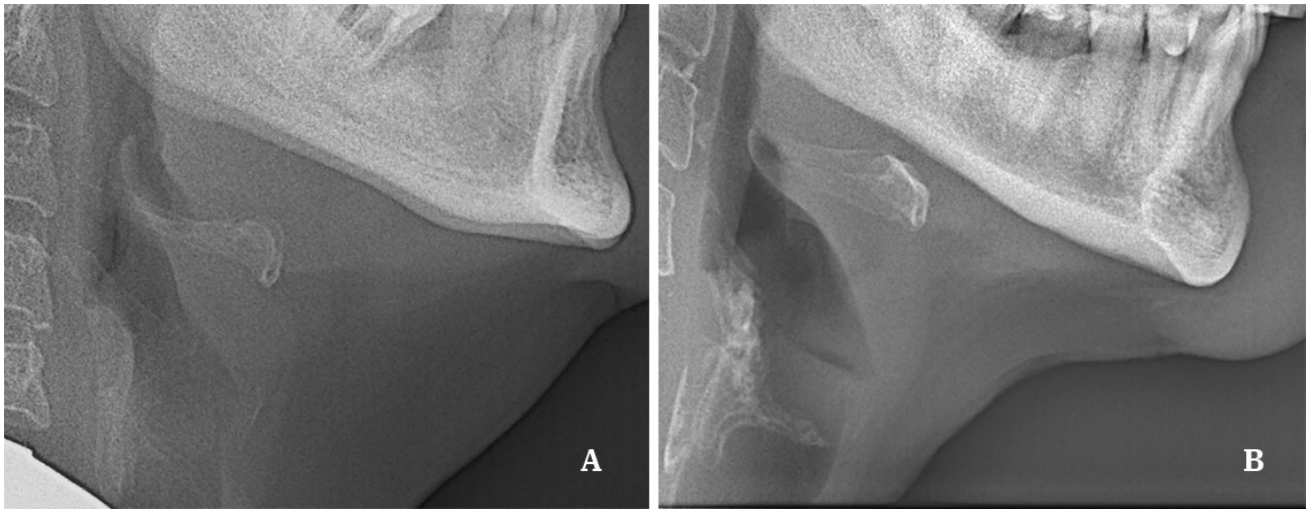

Fig. 2.- Thyroid cartilage classification. **A-** Thyroid cartilage calcification. **B-** Thyroid cartilage with no calcification.

Statistical study

Quantitative variables are described as the mean and standard deviation, and qualitative variables are described as the absolute and relative frequencies. The Pearson or Spearman correlation coefficients were calculated with significance testing depending on whether the normality hypothesis was verified. The relationships between qualitative variables were evaluated with Pearson's or Fisher's chi-square test depending on whether the hypothesis about expected frequencies was fulfilled. The differences in quantitative variables between two groups were assessed using Student's t test or the Wilcoxon test for independent samples, depending on whether the normality was verified.

Table 1. Summary values for the measured quantitative variables.

	n	Median	SD	Percentile (%)				
				0	25	50	75	100
Age	40	48.65	6.11	32.00	45.00	48.00	53.00	62.00
Long	40	8.88	2.42	3.00	7.00	8.50	11.00	15.00
Sella turica depth	40	8.72	1.52	6.00	8.00	9.00	10.00	13.00
Diam	40	11.93	1.80	6.00	11.00	12.00	13.00	15.00
SN-A	40	55.75	4.73	50.00	52.00	55.00	60.00	68.00
SN-Pg	40	105.58	10.29	59.00	100.00	105.00	111.25	120.00
SN	40	67.12	3.74	60.00	65.00	66.00	69.25	75.00
Palatine plane angle	40	9.62	2.65	4.00	7.75	10.00	12.00	16.00
Stylohyoid distance	40	80.20	8.95	63.00	74.75	75.60	86.50	100.00
Styloglossal distance	40	94.17	6.17	82.00	90.00	95.00	98.00	108.00
Hyoglossal distance	40	36.08	5.53	20.00	38.00	38.00	40.25	50.00

Finally, linear models were constructed to study whether calcification influenced the variables collected, adjusting for sex and age.

The level of significance used was 0.05. Statistical analysis was carried out using the R program (R Development Core Team), version 3.6.3. Entries to include in the bibliography (R and libraries used):

- R Core Team (2020). A: Language and environment for statistical computing. R Foundation for Statistical Computing, Vienna, Austria.
- Corrplot. Taiyun Wei and Viliam Simko (2017). R package corrplot: Visualization of a correlation matrix (Version 0.84).

RESULTS

A summary of the measured quantitative variables is presented below: the number of available data, mean, standard deviation, zero percentile or minimum value, 25th percentile or first quartile, 50th percentile or median, 75th or third percentile, quartile, and 100th percentile or maximum value (Table 1).

A total of 40 registered patients were included in the assessment of calcification of the thyroid cartilage. Of these, 75% presented with thyroid calcifications, and 25% did not (Table 2).

Table 2. Calcification or no calcification of the thyroid cartilage variable.

	Frequency	%
Calcification	10	25
No calcification	30	75
Total	40	100

Data on sex were available for all 40 registered patients. A total of 72.5% were female, and 27.5% were male (Table 3).

Table 3. Patient sex classification.

	Frequency	%
Male	11	27.5
Female	29	72.5
Total	40	100

Moreover, in a comparison between calcification of the thyroid and calcification of the sella turcica, no statistical relationship was observed between the two variables (Fisher's test, p value = 0.135) (Table 4).

Table 4. Calcification of the thyroid and calcification of the sella turcica.

	n	%	n	%
No	6	60.00	9	30.00
Yes	4	40.00	21	70.00

To determine whether the behaviour of the depth from the sella turcica to the SF differs between sexes, various comparisons were made, as detailed in the table. Given that the normality hypothesis was not rejected for all modalities (Shapiro–Wilk test: Male, p value = 0.111; Female, p value = 0.067) and that the hypothesis of equality of the two population variances was not rejected (F test of variances, p value = 0.97), the hypothesis of equality of population means cannot be rejected (Student's t test, p value = 0.824) (Table 5).

Table 5. The depth from the sella turcica to the SF and patient sex.

	n	Mean	Median	SD	P25	P75
Male	11	8.64	9.00	1.50	7.50	9.00
Female	29	8.76	9.00	1.55	8.00	10.00

To determine whether the behaviour of the anteroposterior maximum diameter of the TS to the most posterior point of the sella turcica differs according to sex, various comparisons were conducted, as detailed in the table. Given that the normality hypothesis was rejected for some of the modalities (Shapiro–Wilk test: Male, p value = 0.312; Female, p value = 0.039) and the reduced sample size, the hypothesis that the averages are equal cannot be rejected (Wilcoxon test, p value = 0.547) (Table 6).

Table 6. Anteroposterior maximum diameter of the TS to the most posterior point of the sella turcica and patient sex.

	n	Mean	Median	SD	P25	P75
Male	11	11.82	12.00	1.47	11.00	12.50
Female	29	11.97	12.00	1.94	11.00	13.00

Furthermore, to determine if the behaviour of the perpendicular SN-distance differs according to sex, various tests were conducted, as detailed in Table 7. Given that the normality hypothesis was rejected for some of the modalities (Shapiro–Wilk test: Male, p value = 0.01; Female, p value = 0.001) and the reduced size of the sample, the hypothesis that the averages are equal can be rejected (Wilcoxon test, p value <0.001).

Table 7. The perpendicular SN-distance differs according to sex.

	n	Mean	Median	SD	P25	P75
Male	11	70.45	70.00	3.33	68.00	12.50
Female	29	65.86	66.00	3.08	64.00	13.00

Likewise, to determine whether the S-N distance differs according to sex, various tests were conducted, as detailed in Table 8 below. Given that the normality hypothesis was not rejected for all modalities (Shapiro–Wilk test: Male, p value = 0.276; Female, p value = 0.246) and the hypothesis of equality of the two population variances (F test of variances, p value = 0.704), the hypothesis of equality of population means can be rejected (Student's t test, p value <0.001).

Table 8. The S-N distance and patient sex.

	n	Mean	Median	SD	P25	P75
Male	11	91.73	90.00	6.34	90.00	95.00
Female	29	75.83	75.00	5.03	74.00	78.00

To determine wheher the behaviour of the stylogenian distance differs according to sex, various tests were conducted, as detailed in Table 9. Since the hypothesis of normality was not rejected for all modalities (Shapiro–Wilk test, Male, p value = 0.228; Female, p value = 0.379) and that the hypothesis of equality of the two population variances was not rejected (F test of variances, p value = 0.159), the hypothesis of equality of population means can be rejected (Student's t test, p value = 0.001).

Table 9. The stylogenian and patient sex.

	n	Mean	Median	SD	P25	P75
Male	11	99.00	98.00	3.87	95.50	101.00
Female	29	92.34	92.00	5.92	90.00	95.00

To determine whether the behaviour of age differs according to the TCscore, various tests were conducted, which are detailed in Table 10. Considering the sufficient sample size and the

result of the normality test (Shapiro–Wilk test, no thyroid calcifications: p value = 0.043), the hypothesis that the means are equal can be rejected (Wilcoxon test, p value = 0.042).

Table 10. The thyroid calcification and no calcification.

	n	Mean	Median	SD	P25	P75
No thyroid calcification	10	51.50	53.00	4.25	48.50	53.75
Thyroid calcification	30	47.70	46.50	6.40	44.25	51.00

Moreover, to determine whether the behaviour of the depth from the sella turcica to the SF differs according to the TCscore, various tests were conducted, as detailed in Table 11. Considering the sufficient sample size, that the hypothesis of normality was not rejected in all modalities (Shapiro–Wilk test, no thyroid calcifications: p value = 0.119) and that the hypothesis of equality of the two population variances was not rejected (F test of variances, p value = 0.893), the hypothesis of equality of population means cannot be rejected (Student's t test, p value = 0.374).

Table 11. The depth from the sella turcica to the SF differs according to the thyroid calcification score.

	n	Mean	Median	SD	P25	P75
No thyroid calcification	10	9.10	9.00	1.45	9.00	9.75
Thyroid calcification	30	8.60	8.50	1.54	8.00	9.75

To determine whether the behaviour of the ante-post maximum diameter TS- most posterior point differs according to the thyroid calcification score, various tests were conducted, as detailed in Table 12. Considering the sufficient sample size, that the hypothesis of normality was not rejected for all modalities (Shapiro–Wilk test, no thyroid calcifications: p value = 0.151) and that the hypothesis of equality of the two population variances was not rejected (F test of variances, 12 p values = 0.384), the hypothesis of equality of population means can be accepted (Student's t test, p value = 0.076).

To determine whether the behaviour of the stylohyoid distance differs according to the thyroid calcification score, various tests were conducted, as detailed in Table 13. Considering the sufficient sample size, that the hypothesis of normality was not rejected for all modalities (Shapiro–Wilk test, no thyroid calcifications: p value = 0.136) and that the hypothesis of equality of the two population variances was not rejected (F test of variances, p value = 0.103), the hypothesis of equality of population means can be rejected (Student's t test, p value <0.001).

Table 12. Ante-post maximum diameter TS- most posterior point according to the thyroid calcification score.

	n	Mean	Median	SD	P25	P75
No thyroid calcification	10	12.80	13.00	1.40	12.00	13.00
Thyroid calcification	30	11.63	12.00	1.85	11.00	13.00

Table 13. Stylohyoid distance according to the thyroid calcification score.

	n	Mean	Median	SD	P25	P75
No thyroid calcification	10	88.60	92.50	9.94	8000	95.99
Thyroid calcification	30	77.40	75.00	6.69	74.00	82.25

To determine whether the behaviour of the greater anteroposterior DS-TS length differs according to the sella turcica calcification score, various comparisons were conducted, as detailed in Table 14. Given that the normality hypothesis was not rejected for all modalities (Shapiro–Wilk test: No, p value = 0.216; Yes, p value = 0.217) and that the hypothesis of equality of the two population variances was not rejected (F test of variances, p value = 0.402), the hypothesis of equality of population means can be rejected (Student's t test, p value <0.001).

Table 14. Anteroposterior DS-TS length according to the sella turcica calcification score.

	n	Mean	Median	SD	P25	P75
No	15	10.73	11.00	2.19	10.00	11.50
Yes	25	7.76	8.00	1.81	7.00	9.00

To determine whether the depth from the maximum anterior-posterior diameter of the

TS to the most posterior point of the TS differs according to the calcification of the sella turcica, various comparisons were conducted, as detailed in Table 15. Since the hypothesis of normality was rejected for some of the modalities (Shapiro–Wilk test: No, p value = 0.287; Yes, p value = 0.025), and the reduced sample size, the hypothesis that the averages are equal can be rejected (Wilcoxon test, p value = 0.018).

Table 15. The maximum anterior-posterior diameter of the TS to the most posterior point of the TS differs according to the calcification of the sella turcica.

	n	Mean	Median	SD	P25	P75
No	15	12.80	13.00	1.52	12.00	13.50
Yes	25	11.40	11.00	1.78	11.00	12.00

To determine whether the behaviour of the stylogenian distance differs according to the calcification of the sella turcica, various tests were conducted, as detailed in the table 16. Given that the normality hypothesis was not rejected for all modalities (Shapiro–Wilk test: No, p value = 0.645; Yes, p value = 0.559) and that the hypothesis of equality of the two population variances was not rejected (F test of variances, p value = 0.372), the hypothesis of equality of population means can be rejected (Student's t test, p value = 0.026).

Table 16. The stylogenian distance according to the calcification of the sella turcica.

	n	Mean	Median	SD	P25	P75
No	15	96.93	95.00	6.58	95.00	101.00
Yes	25	92.52	93.00	5.38	90.00	96.00

DISCUSSION

The lateral cephalometric radiograph provides a specialized lateral skull view that allows clinicians to investigate facial type, growth pattern, the relationship of the jaw and teeth and the anatomy of the anatomical positioning of cervical vertebral hyoid bone and, on occasion, the laryngeal cartilage. After adolescence, human thyroid cartilage typically undergoes terminal differentiation and mineralization (Kirsch et al., 2000). Most of the previously cartilaginous human skeletal elements ossify by this point, and the epiphyseal disks close (Kirsch et al., 2000). In both sexes, ossification begins at the posterior border, the lower margin and the inferior horn of the thyroid cartilage (Mupparapu et al., 2002). Most male thyroid cartilage ossifies by approximately age 70, but female cartilage never completely ossifies, leaving the ventral half cartilaginous (Mupparapu et al., 2002). When ossification of the thyroid cartilage is seen on a lateral cephalometric radiograph at a young age, further imaging with ultrasound (US), computerized tomography (CT) or magnetic resonance imaging (MRI) may help rule out parathyroid adenomas (Mupparapu et al., 2002).

The degree and frequency of thyroid cartilage ossification are lower in females than in males, especially in the anterior aspect. However, the degree and frequency of cricoid calcification are also lower in females than in males (Mupparapu et al., 2002). For both sexes, however, the degree of ossification of the thyroid and cricoid increases with age. Furthermore, ossification begins in the posterior region of the thyroid cartilage in both sexes at 18 to 20 years. According to the present study, a higher incidence of thyroid cartilage was observed in females than in males; this phenomenon could be related to many factors, such as hormonal factors, especially for women in the fourth decade of life, a history of hyperthyroidism or a previous history of cancer.

STB is described as calcification of the clinoid processes without apparent clinical signs, and symptoms should be considered a standard variant of sella turcica anatomy (Scribante et al., 2017; Baidas et al., 2018). Moreover, Suleyman et al. (2019), believed that STB could be considered a developmental anomaly. Bridging of the sella turcica can be induced by a variety of factors, the most common of which is the appearance of fusion between the anterior and posterior structures on lateral radiography due to superposition of the structures despite the absence of genuine bone fusion (Suleyman et al., 2019).

Several 2D radiographic studies have investigated the phenomena of STB. Müller (1952) reported an incidence of 3.8%, while Cederberg et al. (2003), reported an incidence of 8% in a study of

225 subjects. Furthermore, Jewett (1920) reported an incidence of 13% in a study of 100 normal subjects. The increased frequency of complete bridging on lateral cephalometric radiography can be partly explained by the 2D view provided, which makes it difficult to discriminate between true STB and the appearance of fusion between the clinoid process because of radiographic superimposition (Acevedo et al., 2021). Through this study, 37.5% of subjects showed no STB, 57.5% of subjects showed partial STB, and 5% showed complete STB. Our results coincide with other surveys. A study conducted by Cederberg et al. (2003), on 255 patients showed that the percentage of partial sella turcica calcification was 68.8% on lateral radiographs.

The objective of this study was to assess whether there was a relationship between thyroid cartilage calcification and STB. However, the results of statistical analysis showed that there was no relationship between these structures.

Additionally, statistical analysis revealed that regarding the anterior-posterior dimension (DS-TS) of the sella turcica, there was no relationship with sex (P value = 0.358). Similarly, we found that there was no relationship between the depth of the sella turcica sex (P value = 0.824). However, an analysis of the stylohyoid distance and sex showed a significant relationship in women (P value = 0.06) but not in men (p value = 0.2).

Whether age plays a role in calcification remains controversial; thus, the pathologies that occur in the human body have been assessed in many studies in terms of the relationship with age. In this study, we also evaluated the relationship between age and calcification of the thyroid cartilage. Statistical analyses showed a significant relationship between age and TC (p value = 0.04). This result coincides with other studies, which indicate that calcification of the thyroid cartilage starts in the 25th year and that by the 65th year, the cartilage has become completely ossified (Mupparapu et al., 2005). Furthermore, a significant result was obtained when we compared calcification of the thyroid cartilage and stylohyoid and stylogenic calcification (p value = 0.01, P value = 0.01), respectively.

Due to the lack of studies on the relationship between calcification of both the sella turcica and thyroid cartilage, a large sample size and advanced radiographic techniques such as CBCT are required to fully evaluate both structures. This study was limited by the patient sample size and the radiographic 2D technique used in this study. Thyroid cartilage calcification could be considered a normal part of the ageing process, while STB could appear on lateral radiographs due to superimposition of the anatomical structures. In this study, we found no relationship between thyroid cartilage calcification and STB, and large patient sample is required for evaluating calcification of the thyroid and STB.

AUTHORS' CONTRIBUTIONS

Andrea Garrido analysed the data and carried out the work; Alaa Alsafadi directed the structure; Iván Menéndez performed the literature review; Ramón Cobo provided, as an otolaryngologist, knowledge of thyroid calcification, cephalometry and sella turcica, Teresa Cobo conceived the idea and the development approach.

ACKNOWLEDGEMENTS

The authors would like to appreciate the Statistical Consulting Unit of the University of Oviedo for helping with the statistical analyses.

REFERENCES

ACEVEDO AM, LAGRAVERE-VICH M, AL-JEWAIR T (2021) Diagnostic accuracy of lateral cephalograms and cone-beam computed tomography for the assessment of sella turcica bridging. *Am J Orthod Dentofacial Orthop*, 160(2): 231-239.

ALKOFIDE EA (2007) The shape and size of the sella turcica in skeletal Class I, Class II, and Class III Saudi subjects. *Eur J Orthod*, 29(5): 457-463.

ARAMAKI T, IKEDA T, USUI A, FUNAYAMA M (2017) Age estimation by ossification of thyroid cartilage of Japanese males using Bayesian analysis of postmortem CT images. *Leg Med (Tokyo)*, 25: 29-35.

AXELSSON S, STORHAUG K, KJAER I (2004) Post-natal size and morphology of the sella turcica. Longitudinal cephalometric standards for Norwegians between 6 and 21 years of age. *Eur J Orthod*, 26(6): 597-604.

BAIDAS LF, AL-KAWARI HM, AL-OBAIDAN Z, AL-MARHOON A, AL-SHAHRANI S (2018) Association of sella turcica bridging with palatal canine impaction in skeletal Class I and Class II. *Clin Cosmet Investig Dent,* 10: 179-187.

CEDERBERG RA, BENSON BW, NUNN M, ENGLISH JD (2003) Calcification of the interclinoid and petroclinoid ligaments of sella turcica: a radiographic study of the prevalence. *Orthod Craniofac Res*, 6(4): 227-232.

DURÃO AR, ALQERBAN A, FERREIRA AP, JACOBS R (2015) Influence of lateral cephalometric radiography in orthodontic diagnosis and treatment planning. *Angle Orthod*, 85(2): 206-210.

GARVIN HM (2008) Ossification of laryngeal structures as indicators of age. *J Forensic Sci*, 53(5): 1023-1027.

JEWETT CH (1920) Teleroentgenography of the sella turcica with observations on one hundred normal cases. *Am Jour Roentgenol*, 7: 352-355.

KAYA Y, ÖZTAŞ E, GOYMEN M, KESKIN S (2021) Sella turcica bridging and ponticulus posticus calcification in subjects with different dental anomalies. *Am J Orthod Dentofacial Orthop,* 159(5): 627-634.

KIRSCH T, CLAASSEN H (2000) Matrix vesicles mediate mineralization of human thyroid cartilage. *Calcif Tissue Int*, 66(4): 292-297.

LEONARDI R, FARELLA M, COBOURNE MT (2011) An association between sella turcica bridging and dental transposition. *Eur J Orthod,* 33(4): 461-465.

MEYER-MARCOTTY P, REUTHER T, STELLZIG-EISENHAUER A (2010) Bridging of the sella turcica in skeletal Class III subjects. *Eur J Orthod,* 32(2): 148-153.

MÜLLER F (1952) Die Bedeutung der Sellabruecke für das Auge. *Klin Monatsbl Augenheilkd*, 120: 298-302.

MUPPARAPU M, VUPPALAPATI A (2002) Detection of an early ossification of thyroid cartilage in an adolescent on a lateral cephalometric radiograph. *Angle Orthod*, 72(6): 576-578.

MUPPARAPU M, VUPPALAPATI A (2005) Ossification of laryngeal cartilages on lateral cephalometric radiographs. *Angle Orthod*, 75(2): 196-201.

SATHYANARAYANA HP, KAILASAM V, CHITHARANJAN AB (2013) Sella turcica - Its importance in orthodontics and craniofacial morphology. *Dent Res J (Isfahan),* 10(5): 571-575.

SCRIBANTE A, SFONDRINI MF, CASSANI M, FRATICELLI D, BECCARI S, GANDINI P (2017) Sella turcica bridging and dental anomalies: is there an association? *Int J Paediatr Dent*, 27(6): 568-573.

SULEYMAN KB, KARAMAN A, YASA Y (2019) Relationship between sella turcica bridging and cephalometric parameters in adolescents and young adults. *Oral Radiol*, 35(3): 245-250.

TABATABAEE SM, VASHEGHANI FARAHANI M, ALIMOHAMMADI A, SHEKARCHI B (2020) Investigating the association between chronological age and thyroid cartilage ossification using CT imaging. *Med J Islam Repub Iran*, 34: 130.

The outcome of ketogenic diets on the liver and the protecting role of atorvastatin: A histological, immunohistochemical and ultrastructural study

Sherif M. Zaki[1], Shereen A. Fattah[1], Mai Abdou Y. Ahmed[2], Hanan D. Yassa[2]

[1] *Department of Anatomy and Embryology, Faculty of Medicine, Cairo University, Cairo, Egypt*

[2] *Department of Anatomy and Embryology, Faculty of Medicine, Beni-Suef University, Beni-Suef , Egypt*

SUMMARY

The current study investigated structural and functional modifications of the liver following long-term ketogenic diet (KD) and every-other-day ketogenic diet (EODKD) usage. The probable role of atorvastatin (ATO) in the adjustment process was also investigated. It was carried out on 24 Sprague-Dawley rats, which were divided into four groups: control, KD, EODKD, and ATO. Various biochemical, histological, and immunohistochemical analysis were performed on the liver. The blood was tested for aspartate aminotransferase(AST),alanineaminotransferase (ALT), triglycerides, cholesterol, inflammatory markers, Bax, BCL2, NLRP3 inflammasome, and oxidative stress markers.

KDs induced damages to the liver mainly due to oxidative stress (increase TBARS, MDA/decrease SOD/GSH) and inflammation. In addition, the hepatic triglycerides and cholesterol levels are decreased. The KD group was worse off than the EODKD group. ATO administered concurrently with KD preserved liver architecture, reduced oxidative stress, normalized NLRP3, and further reduced intrahepatic triglycerides and cholesterol levels. Both KD and EODKD cause structural liver damage that is accompanied by an elevation of hepatic markers (AST and ALT) and a decrease in hepatic triglycerides, hepatic cholesterol, and serum cholesterol. KD has a more destructive effect. Oxidative stress, inflammation, and high fat concentrations are contributing factors to hepatic injury in these diets. ATO with KD is beneficial.

Keywords: Ketogenic diet – Every other day ketogenic diet – Liver – Atorvastatin – Rat

LIST OF ABBREVIATIONS:

BAX: Bcl-2-associated X protein.

BCL2: *B-cell lymphoma 2*.

CD11b: cluster of differentiation molecule 11b.

GSH: Glutathione.

HMG-CoA reductase: 3-hydroxy-3-methylglutaryl-Coenzyme A reductase.

MDA: Malondialdehyde.

NAFLD: non-alcoholic fatty liver disease.

NLRP3: The NACHT, LRR and PYD domains-containing protein 3.

Corresponding author:
Mai Abdou Yousef Ahmed. Department of Anatomy and Embryology, Faculty of Medicine, Beni-Suef University, Beni-Suef, Egypt. Phone: 002-01002934523. E-mail: maiabdou28@yahoo.com

Submitted: April 8, 2022. **Accepted:** May 15, 2022

https://doi.org/10.52083/XTZB3175

SDS- PAGE: sodium dodecyl sulfate- polyacrylamide gel electrophoresis.

SOD: superoxide dismutase.

TBARS: Thiobarbituric Acid Reactive Substances.

INTRODUCTION

The ketogenic diet (KD) has gained popularity among the public and scientific communities as a way to lose weight (Bolla et al., 2019). Additionally, they can alleviate several neurological illnesses, including Parkinson's disease, traumatic brain injury, Alzheimer's disease, autism, and Lou Gehrig's disease (Deng-Bryant et al., 2011; Hertz et al., 2015; Shaafi et al., 2016). KDs with very low carbohydrates can have effective weight-loss interventions that may reduce non-alcoholic fatty liver disease (NAFLD) and visceral adipose tissue, leading to decreased insulin resistance and end-organ damage (Marchesini et al., 2016). Additionally, very low-carbohydrate KDs are used as adjunctive therapy for brain cancer (Garbow et al., 2011). As a final note, the every-other-day KD (EDOKD) keeps seizures under control better (Hartman et al., 2013).

The KD is characterized by a high fat intake, moderate-to-low protein intake, and very low carbohydrate intake (<50 g) (Barrea et al., 2022). The fat-to-non-fat ratio in KD is 4:1 (Milder et al., 2010). After using KDs for a few days, the production of energy is dependent upon burning fat, with increased production of ketone bodies (Paoli et al., 2013). In addition, KDs promote the oxidation of dietary and adipose lipids (Barañano and Hartman, 2008).

However, these diets can pose several problems. In one study, mice fed with a KD over a period of 12 weeks accumulated hepatic lipids sequentially. The mice eventually developed endoplasmic reticulum stress, macrophage accumulation, cellular damage, and steatosis (Garbow et al., 2011). However, no research has been yet conducted on the specific structural and functional changes in the liver related to long-term KD.

Atorvastatin (ATO) was the most popular lipid-lowering drug in the early 2000s. It works by inhibiting the enzyme HMG-CoA reductase, a key component of cholesterol synthesis. This drug belongs to the statins family, which are applied as lipid-decreasing agents (Kogawa et al., 2019). Recently, some researchers reported promising results of ATO in the treatment of fatty liver disease (Gómez-Domínguez et al., 2006). However, studies are lacking on whether ATO prevents the damaging effects of KDs on the liver.

The purpose of the present research is to investigate the relationship between structural and functional liver changes following long-term KD and EODKD use. In addition, the causal mechanisms in hepatic affection were examined. The probable role of ATO in the adjustment process was also investigated.

MATERIAL AND METHODS

Twenty-four Sprague-Dawley rats weighing 150-200 g were used. They were housed in standard cages and acclimatized in the laboratory for two weeks before starting the study.

In keeping with the ethical standards set by the National Institutes of Health guide for the care and use of laboratory animals, this work was approved by the Ethics Committee at Cairo University (2545/2020).

Our rats were monitored for morphological and behavioural changes every day, and their health profiles were recorded. Four groups of six rats each were arranged:

- Control group: rats were fed standard chow (SC) (Holland et al., 2016).
- KD group: rats were fed KD (Holland et al., 2016).
- EODKD group: in the first 24 hours, the rats fasted. They then accessed KD every other day (second, fourth, sixth, etc.). Thus, they alternated fasting and feeding days (Hartman et al., 2013).
- ATO group: ATO was given concomitant with KD (Ji et al., 2011). ATO was purchased from the EIPICO Chemical Company in Cairo, Egypt, and given via gastric gavage in doses of 6 mg/kg/day (Schmechel et al., 2009).The essential nutrients of SC and KD were presented in Table 1 (Holland et al., 2016).

Table 1. Sources of macronutrients for each diet.

	KD	SC
Calories, g	5.2	3.1
CHO, % of calories	10.3	58
Protein, % of calories	20.2	24
Fat, % of calories	69.5	18
Fatty acid breakdown, % of fat • **Saturated fat** • **Monounsaturated** • **Polyunsaturated fat**	 70 13 17	 16 23 61
Cholesterol, % by weight	Not specified	Traces

Ketogenic diet (KD); Fat: MCT oil, flaxseed oil, and canola oil; Protein: casein as well as added L-cysteine; Carbohydrate: maltodextrin and cellulose; Standard chow (SC); Fat: soybean oil; Protein: soybean meal and corn gluten with added L-lysine and L-methionine; Carbohydrate: ground wheat and ground corn.

We measured the body weight (BW) of the rats at the beginning and at the end of the experiment. Blood was taken from the tail of the rats for biochemical analysis, followed by their sacrifice after 8 weeks.

The liver was dissected and weighted for calculating the relative body weight. Parts of the liver were processed for histological study, and other parts were processed for electron microscopy study and western blot analysis.

Light microscopic study

Hematoxylin & Eosin (H&E) and Masson's trichrome stained: specimens were fixed in 10 % neutral buffered formalin and were processed to prepare 5 µm thick paraffin sections (Suvarna et al., 2019).

Analysis of the blood parameters

The plasma aspartate aminotransferase (AST) and alanine aminotransferase (ALT) levels were measured according to Monteiro et al. (2016).

An analysis of hepatic triglycerides, hepatic cholesterol and serum cholesterol was performed using the commercially available kit according to Schwartz and Wolins (2007).

Hepatic oxidative markers

Malondialdehyde (MDA) and Thiobarbituric Acid Reactive Substances (TBARS) were assessed conferring to the method of Oktay et al. (1995).

Glutathione (GSH) content and superoxide dismutase (SOD) activity were evaluated corresponding to Weydert and Cullen (2010) using the commercial kit (Biodiagnostic, Egypt).

Immunohistochemical study

Paraffin sections were dewaxed, rehydrated, and incubated in 3% hydrogen peroxide solution for 30 minutes to block endogenous peroxidase activity. In the next step, heat-mediated antigen retrieval was performed, and tissue antigen was retrieved using a microwave. The tissue sections were then cleaned and immersed for 5 minutes in phosphate buffered saline (PBS). Following PBS removal, serum was applied to the sections for 30 minutes at room temperature.

1. **Caspase-3:** the sections were incubated with primary anti-active caspase-3 antibody (Cat #: ab208161, Abcam, Cambridge, MA, USA), followed by secondary antibody labelled streptavidin biotin (LSAB) kit, Dako Carpentaria, CA, USA) (Bancroft and Gamble, 2008).
2. **Bax, Bcl-2:** The sections were incubated with the primary antibody Bcl-2, Bax (anti-human Bcl-2 protein, DakoCytomation, Denmark), followed by the secondary antibody (biotinylated link universal from the commercial kit LSAB: DakoCytomation, Denmark). The positive reaction for Bcl-2 and Bax showed a brown color of the cytoplasm (Panasiuk et al., 2006).

Image analysis and morphometric measurements

The content of collagen fibres and the expression of Bcl-2 and Bax were achieved using Leica LAS V3.8 image analyser computer system (Switzerland).

Western Blot

The liver was homogenized in Radioimmunoprecipitation assay (RIPA) buffer and centrifuged. Proteins were then loaded onto precast SDS-PAGE gels, then transferred to polyvinylidene difluoride (PVDF) membranes. The membranes were incubated with rabbit anti-NLRP3 (1:500), ra-

bbit anti-β-actin (1:2000), and rabbit anti-CD11b antibody (1:2000). Then, the membranes were incubated with secondary antibodies. Immunoreactive proteins were imaged by an excellent chemiluminescent substrate (ECL) kit (GE Healthcare, Amersham, UK using iBright Imaging System (Yang et al., 2017; Qu et al., 2019).

Electron Microscopic examination

The sections were set according to Hayat (2000) and shot using a Joel, 100 CX II TEM.

Statistical analysis

We used SPSS 22 to conduct our analysis. We estimated the statistical significance of the data using ANOVA followed by a Bonferroni pairwise comparison.

RESULTS

Losses in the liver weight and body weight in the KD and EODKD groups

The mobility and health status of the groups were generally good. We detected no mortality in each group.

At the beginning of the study, the body weight (BW) was 180±15.6 g. At the end of the study, the BW increased in control and ATO groups to 250±15 and 220.1±13.1 respectively while it decreased in KD and EODKD groups to 154.4±10.6 and 164.8±12.9 respectively (Table 2, Bar chart 1).

A significant decrease of the relative liver weight was detected in KD and EODKD groups to 0.1±0.07 and 0.17±0.06 respectively as compared to the control group. The weights in ATO and control groups were comparable 0.3±0.01, 0.4±0.01 respectively (Table 3, Bar chart 2).

Table 2. Comparison of the body weight among the studied groups. The body weight at the beginning of the study was 180±15.6 g.

Body weight (g)	I-Control		II-KD		III-EODKD	IV-ATO
Mean ±SD	250±15		154.4±10.6		164.8±12.9	220.1±13.1
F-value	22.6					
Overall P-value	0.01					
Pairwise comparisons	II&I 0.01*	III&I 0.03*	IV&I 0.01*	III&II 0.5	IV&II 0.04*	IV&III 0.9

*= p-value significant

Bar chart 1. Comparison of the body weight among the studied groups.

Table 3. Comparison of the relative liver weight among the studied groups.

Relative liver weight	I-Control		II-KD		III-EODKD	IV-ATO
Mean ±SD	0.4±0.01		0.1±0.07		0.17±0.06	0.3±0.01
F-value	37.8					
Overall P-value	<0.001*					
Pairwise comparisons	II&I <0.01*	III&I 0.011*	IV&I 0.987	III&II 0.002*	IV&II <0.01*	IV&III 0.014*

*= p-value significant

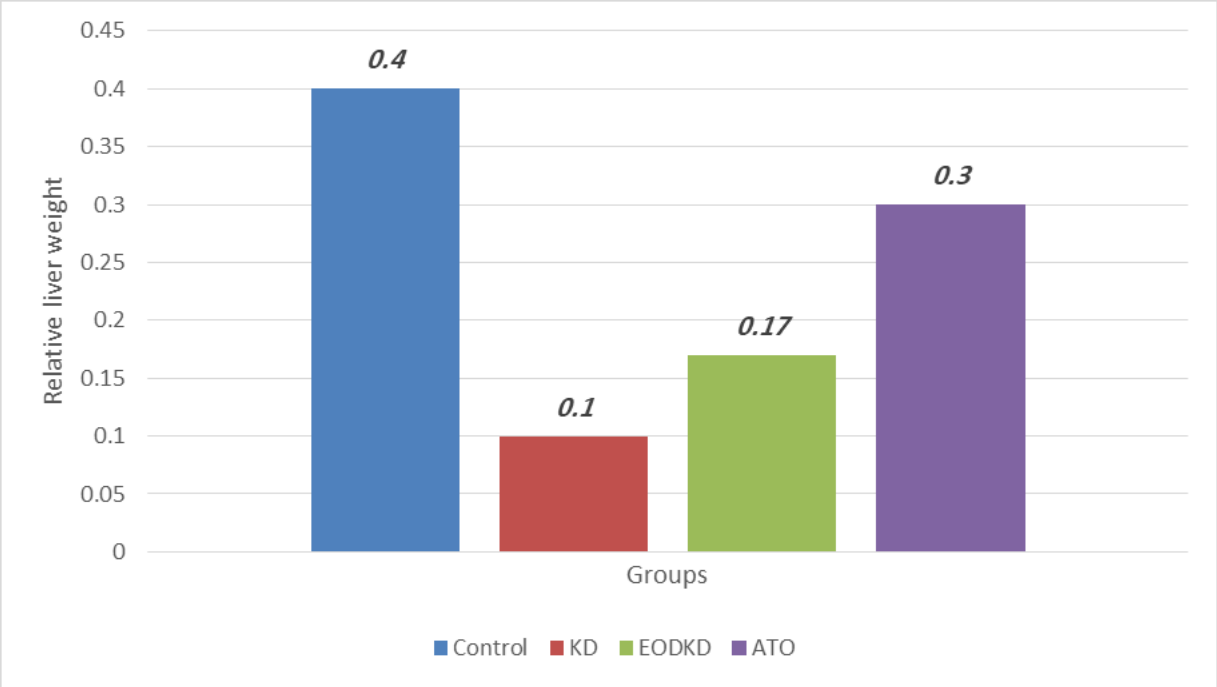

Bar chart 2. Comparison of the relative liver weight among the studied groups.

Hepatic structural affection in the KD and EODKD groups

Normal hepatocyte architecture was observed around central veins in the control group (Fig. 1-A). KD hepatocytes exhibited pyknotic nuclei and congested central vein associated with mononuclear inflammatory cells in the KD group (Fig. 1-B). Hepatocytes with vacuolated cytoplasm associated with mononuclear inflammatory cells around dilated central vein in the EODKD group (Fig. 1-C). The ATO group showed normal hepatocyte patterns (Fig. 1-D).

Hepatocytes with vacuolated cytoplasm and dilated hepatic sinusoids in both KD and EODKD groups (Figs. 2-A, B)

A normal histological pattern was seen in the control group (Fig. 3-A). The portal veins were dilated and congested, hepatocytes with pyknotic nuclei and cytoplasmic vacuoles were seen in both KD and EODKD groups (Figs. 3- B, C). In the ATO group, the hepatocytes regain the normal histological pattern (Fig. 3-D).

Dilated, congested portal veins and hepatocytes with vacuolated cytoplasm were observed in both KD and EODKD groups (Figs. 4-A, B)

Collagen fibre content increased in the KD and EODKD groups

Collagen fiber content was minimal in the control group (Fig. 5-A). The fiber content increased significantly around the congested portal veins in the KD group (> two-fold) (Fig. 5-B, Table 4) and in the EODKD group (> one-fold) (Fig. 5-C, Table 4) in comparison to the control group. Compared to the EODKD group, the fiber content in the KD group was 30% higher (Table 4). The collagen fibres in the ATO group were minimal (Fig. 5-D).

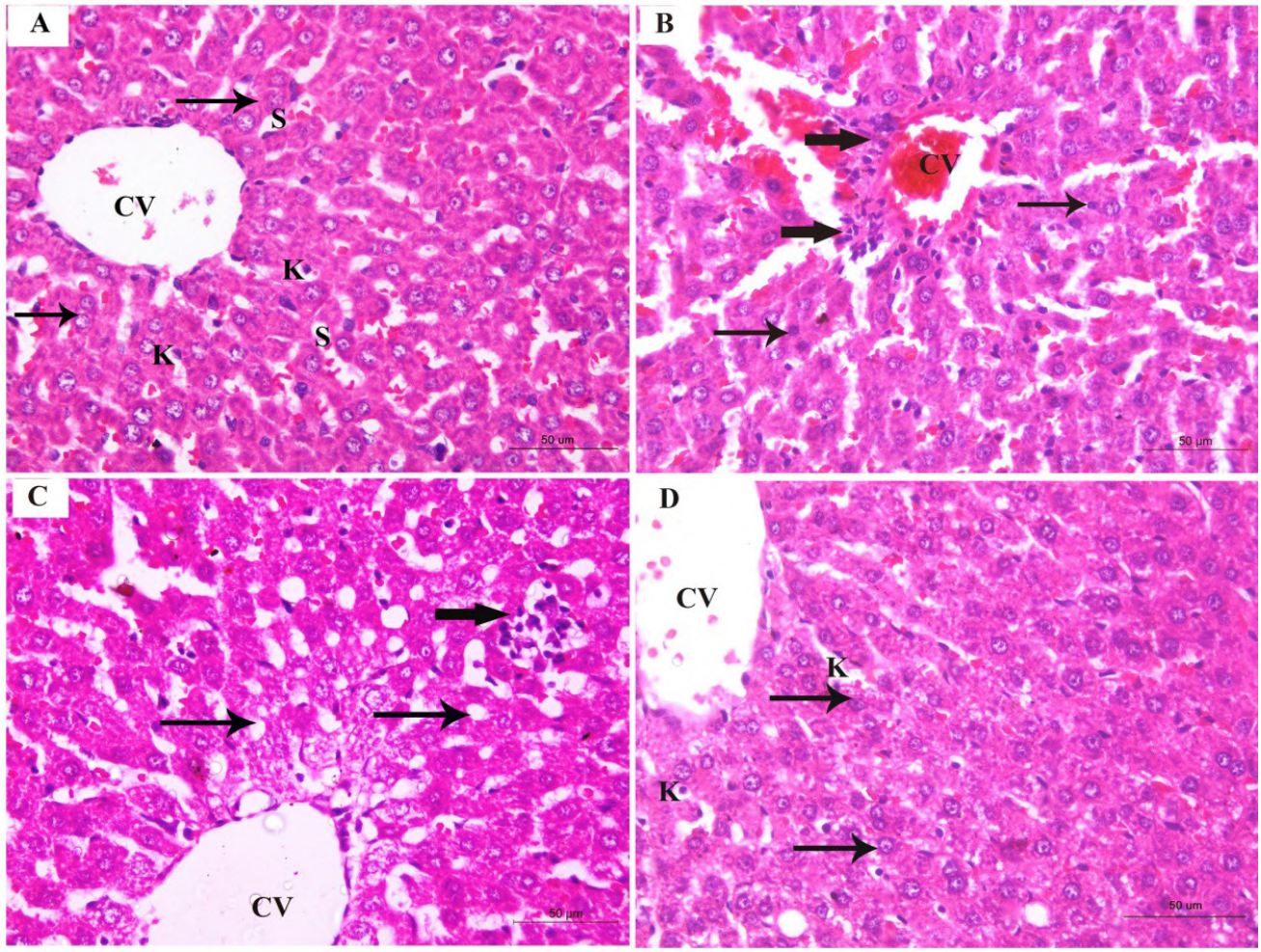

Fig. 1.- Sections around central veins. **A:** interconnected branching plates of hepatocytes (arrows) spreading from a central vein (CV) in the control group. Note blood sinusoids (S) and Von-Kupffer cells (K). **B:** Pyknotic hepatic cell nuclei (thin arrows), dilated congested central vein (CV), and mononuclear inflammatory cells (thick arrows) in the KD group. **C:** Hepatocytes with vacuolated cytoplasm (thin arrows) and inflammatory cellular aggregation (thick arrow) near a central vein (CV) in the EODKD group. **D:** Normal hepatocytes (arrows), Von-Kupffer cells (K), and slightly dilated central vein (CV) in the ATO group. H&E staining. Scale bars: A,B = 50 µm; C,D = 60 µm.

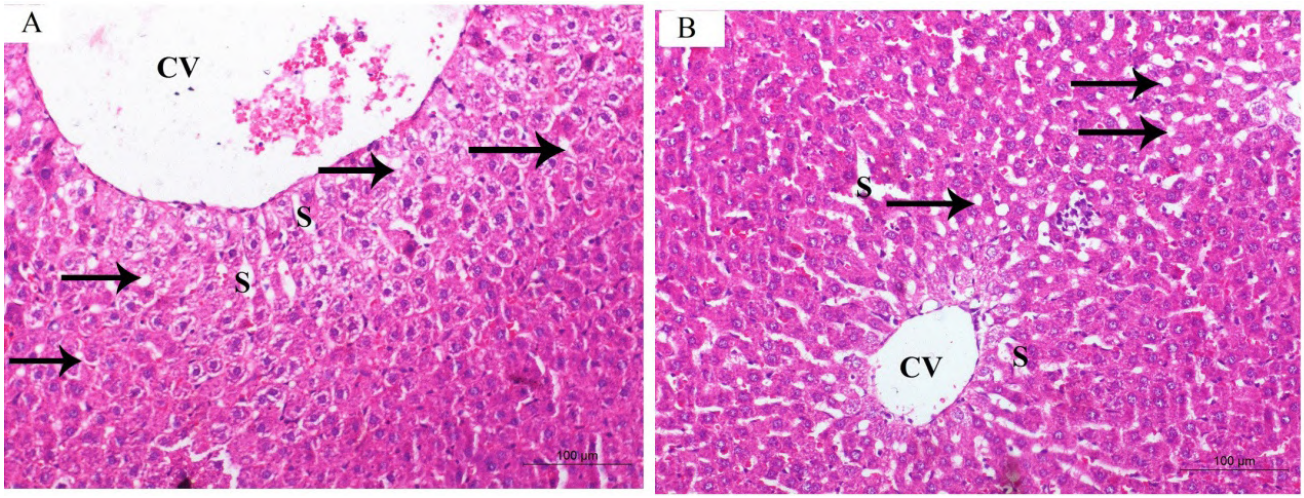

Fig. 2.- Sections around central veins. **A:** Dilated, congested central vein (CV), dilated hepatic sinusoids (S) and hepatocytes with vacuolated cytoplasm (arrows) in the KD group. **B:** hepatocytes with vacuolated cytoplasm (arrows) and dilated hepatic sinusoids (S) in the EODKD group. H&E staining. Scale bars = 100 µm.

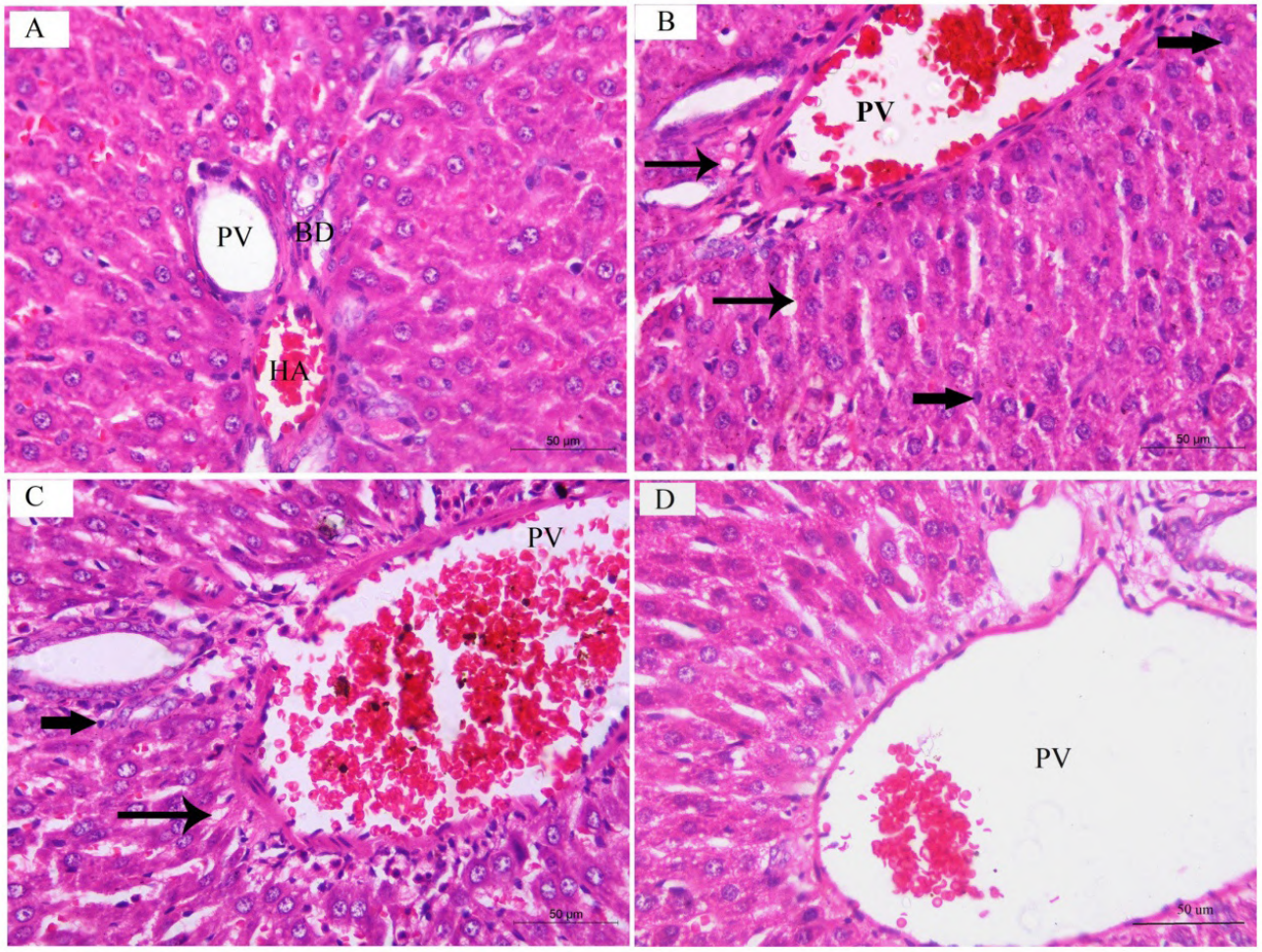

Fig. 3.- Sections around portal areas. Note hepatic artery (H), portal vein (PV), and bile ductule (BD). **A:** Normal architecture of the control. **B:** Pyknotic hepatic cell nuclei (thick arrows) and vacuolated cytoplasm (thin arrows) in the KD group. Note the portal vein is dilated and congested. **C:** Dilated and congested portal vein, hepatocytes with pyknotic nuclei (thick arrows) and vacuolated cytoplasm (thin arrow) in the EODKD group **D:** Normal hepatocytes and dilated portal vein in the ATO group. H&E staining. Scale bars A-D = 50 µm.

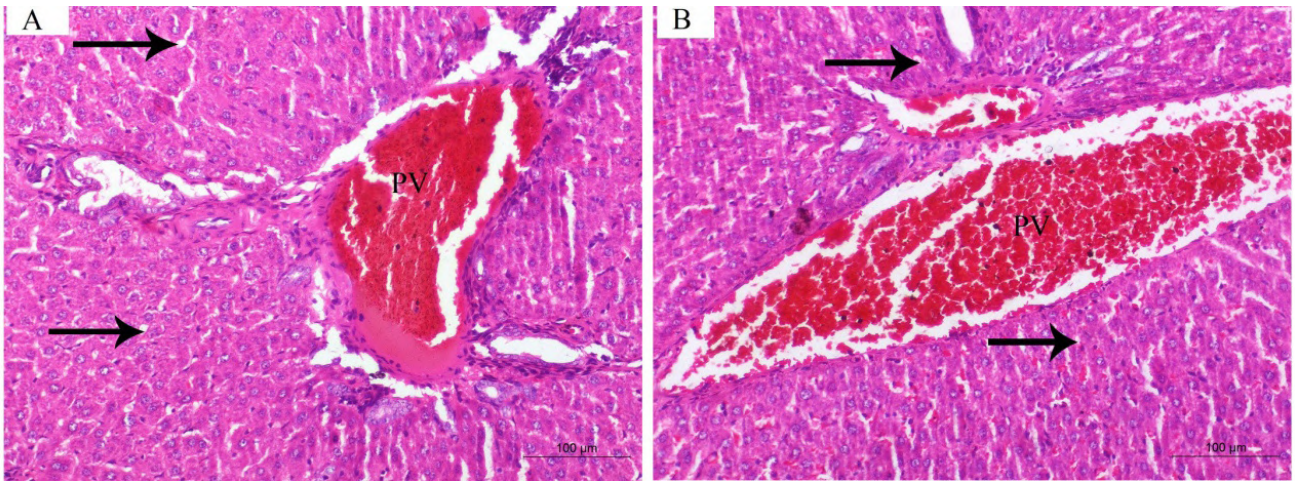

Fig. 4: A: Dilated, congested portal vein and vacuolated cytoplasm (arrows) in the KD group. **B:** Hepatocytes with vacuolated cytoplasm (arrows) in the EODKD group. Note the portal vein is dilated and congested. H&E staining. Scale bars = 100 µm.

Apoptosis was more prevalent in the KD and EODKD groups

Caspase-3 immunoreaction was minimal and comparable in control and ATO groups (Figs. 6-A, D, Table 4). Increased expression of apoptotic response was detected in the KD group (230%) (Fig. 6-B, Table 4) and EODKD (176%) group (Fig. 6-C, Table 4) when compared to the control group. The response in the KD group was 22 % higher than in the EODKD group (Table 4).

Table 4. Caspase3, Bcl2, Bax, Bcl2/Bax ratio and content of collagen fibers in the studied groups.

Group		Caspase 3	Bcl-2	Bax	Bcl-2/Bax ratio	Content of collagen fibers
Control	Mean ±SD	1.3±0.3	6.2±2.4	0.3±0.1	20.5±6.7	3.4±0.7
KD	Mean ±SD	4.3 ±0.4	2.2±0.3	3.5±0.2	0.43±0.01	11.1±0.9
	Versus control	0.001*	0.009*	0.001*	0.001*	0.001*
	Versus EODKD	0.563	0.952	0.019*	0.010*	0.005*
	Versus ATO	0.003*	0.001*	0.001*	0.001*	0.001*
EODKD	Mean ±SD	3.5±0.5	2.9±1.2	2.3±0.6	2.2±0.3	8.5±1.3
	Versus control	0.006*	0.001*	0.004*	0.003*	0.013*
	Versus KD	0.563	0.952	0.019*	0.010*	0.005*
	Versus ATO	0.001*	0.002*	0.005*	0.042*	0.014*
ATO	Mean ±SD	1.7 ±0.4	5.8±0.5	0.8±0.1	11.7±1.5	3.5±0.8
	Versus control	0.332	0.994	0.436	0.057	0.999
	Versus KD	0.003*	0.001*	0.001*	0.001*	0.001*
	Versus EODKD	0.001*	0.002*	0.005*	0.042*	0.014*

*= p-value significant

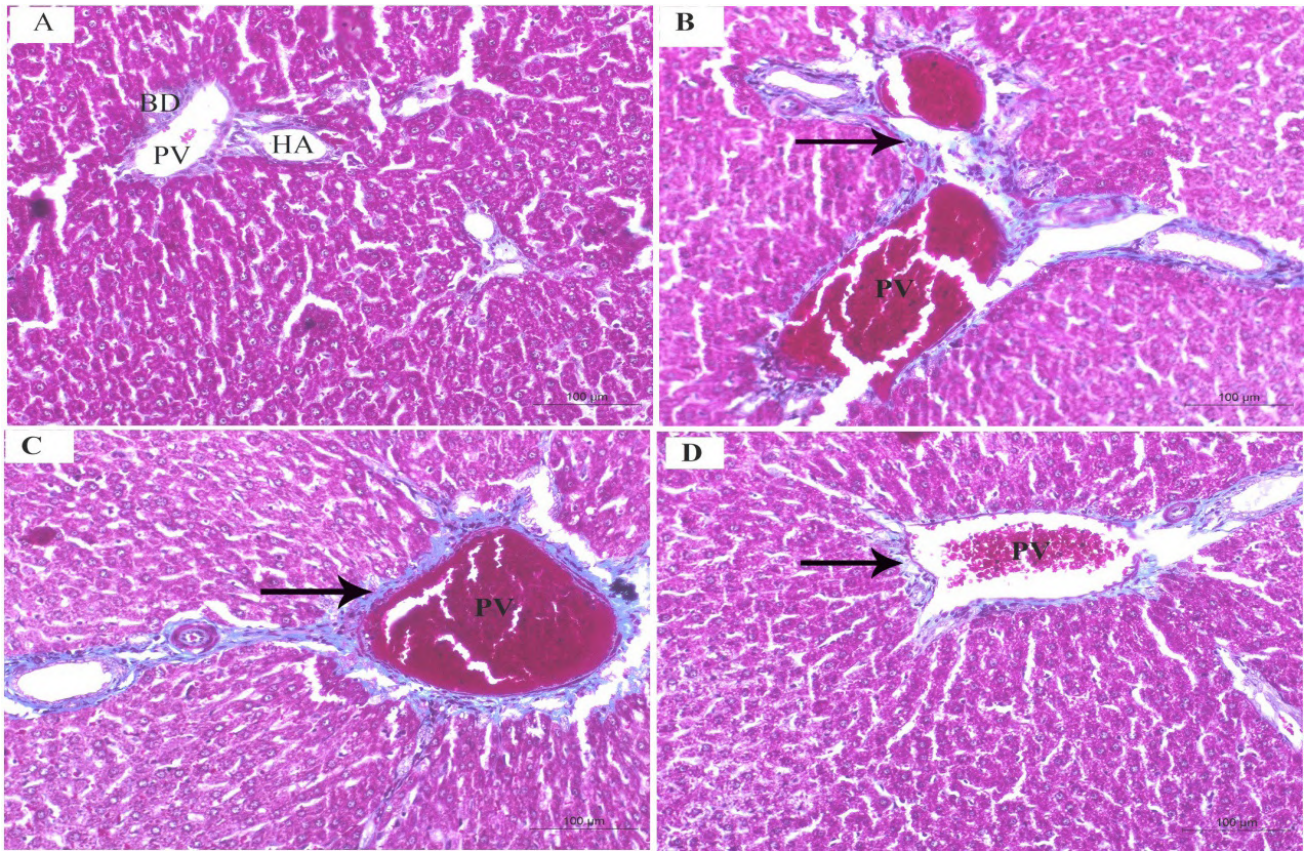

Fig. 5.- Collagen fibres (arrows) around the periportal area. Note the portal vein radical (PV), the hepatic artery (HA), and the bile ductule (BD). **A:** Negligible amount of collagen fibres in the control. **B:** The KD group exhibited more collagen deposition around congested portal vein (arrow). **C:** A relative increase in collagen deposition (arrow) around congested portal veins within the EODKD group. **D:** There are a few collagen fibres in the ATO group (arrow). Masson's trichrome. Scale bars A-D = 100 µm.

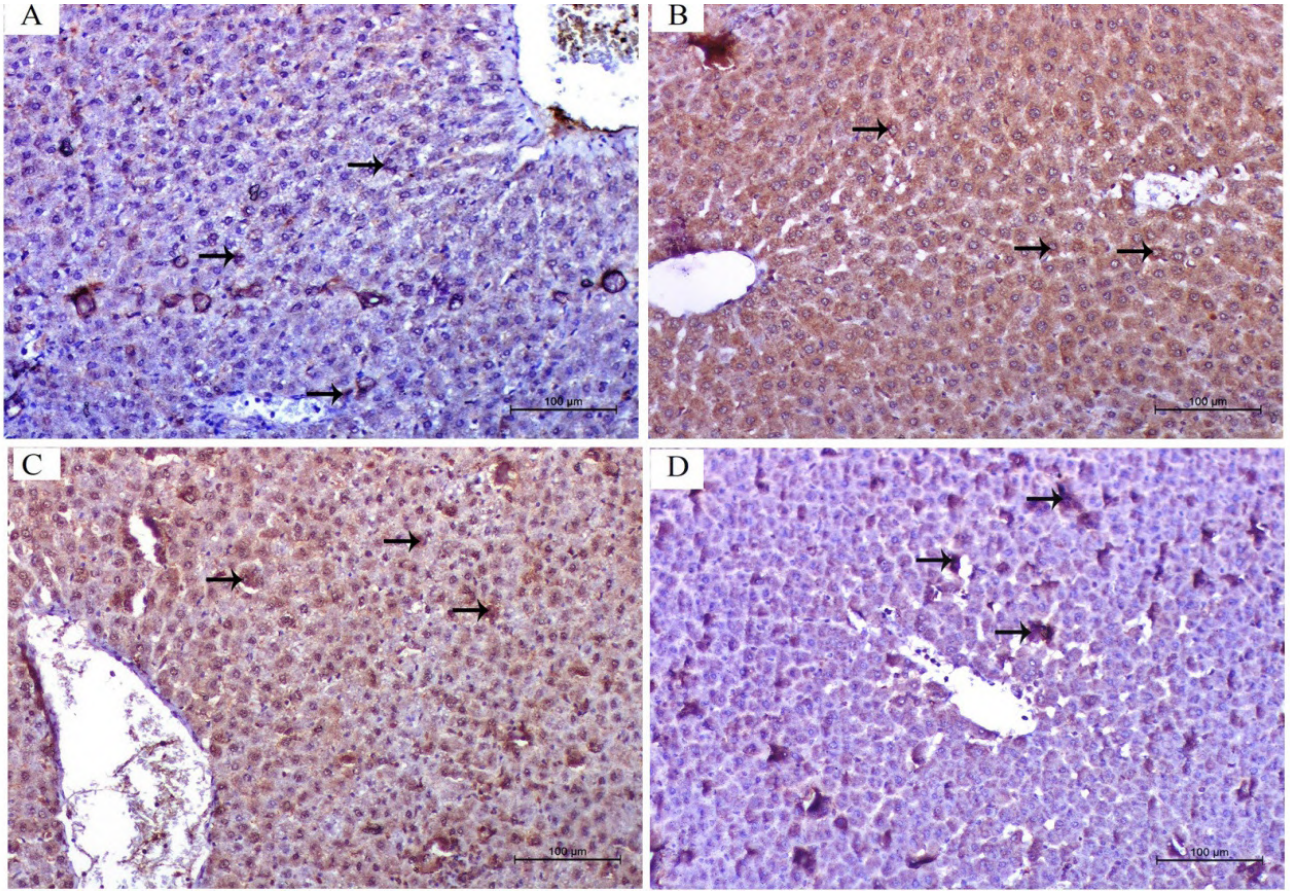

Fig. 6.- Immunoreaction of caspase 3 (arrows). **A:** A slight active expression of apoptotic reaction in the control group. **B:** increased expression of apoptotic reaction in the KD group. **C:** Apoptosis expression was less intense in the EODKD group. **D:** The ATO group showed a slight active reaction. Caspase 3 immunostaining. Scale bars A-D = 100 µm.

The BAX immunoreaction was minimal in the control group (Fig. 7-A, Table 4). A significant increase in the apoptotic reaction was observed in the KD group (> ten-fold) (Fig. 7-B, Table 4) and EODKD group (> six-fold) (Fig. 7-C, Table 4) as compared to the control group. The reaction in the KD group was 50% higher than that in the EODKD group (Table 4). ATO group shows minimal expression reaction (Fig. 7-D).

By comparison with the control group, the BCL2 immunoreaction was reduced in the KD and EODKD groups by 30% and 50%, respectively (Figs. 8-B, C, Table 4). However, the difference was not significant, since the last two groups were closely related (Table 4). The reaction in the ATO group was similar to the control group (Figs. 8-A, D, Table 4).

In comparison with the control group, the Bcl2/Bax ratio was 20-fold lower in the KD group and ten-fold lower in the EODKD group. The ratio in the KD group was four-fold lower than the EODKD group. Comparatively to the control group, the ratio dropped to 45% using ATO (Table 4).

Liver ultrastructural degeneration in the KD and EODKD groups

Control and ATO groups displayed classic hepatic architectures ((Figs. 9A, F). Hepatocytes from the KD and EODKD groups displayed degenerative nuclear changes, as well as mitochondria with lost cristae and ruptured outer membranes. Rarefied cytoplasm with prominent lysosomes was also observed (Figs. 9 B-E).

Enhanced hepatic enzyme markers and reduced hepatic triglycerides and cholesterol in the KD and EODKD groups

The levels of hepatic triglycerides were significantly lower in the KD and EODKD groups compared with the control group. In the KD group, they were 14% lower than those in the EODKD group. With ATO, they were 45% lower than those in the control group (Table 5).

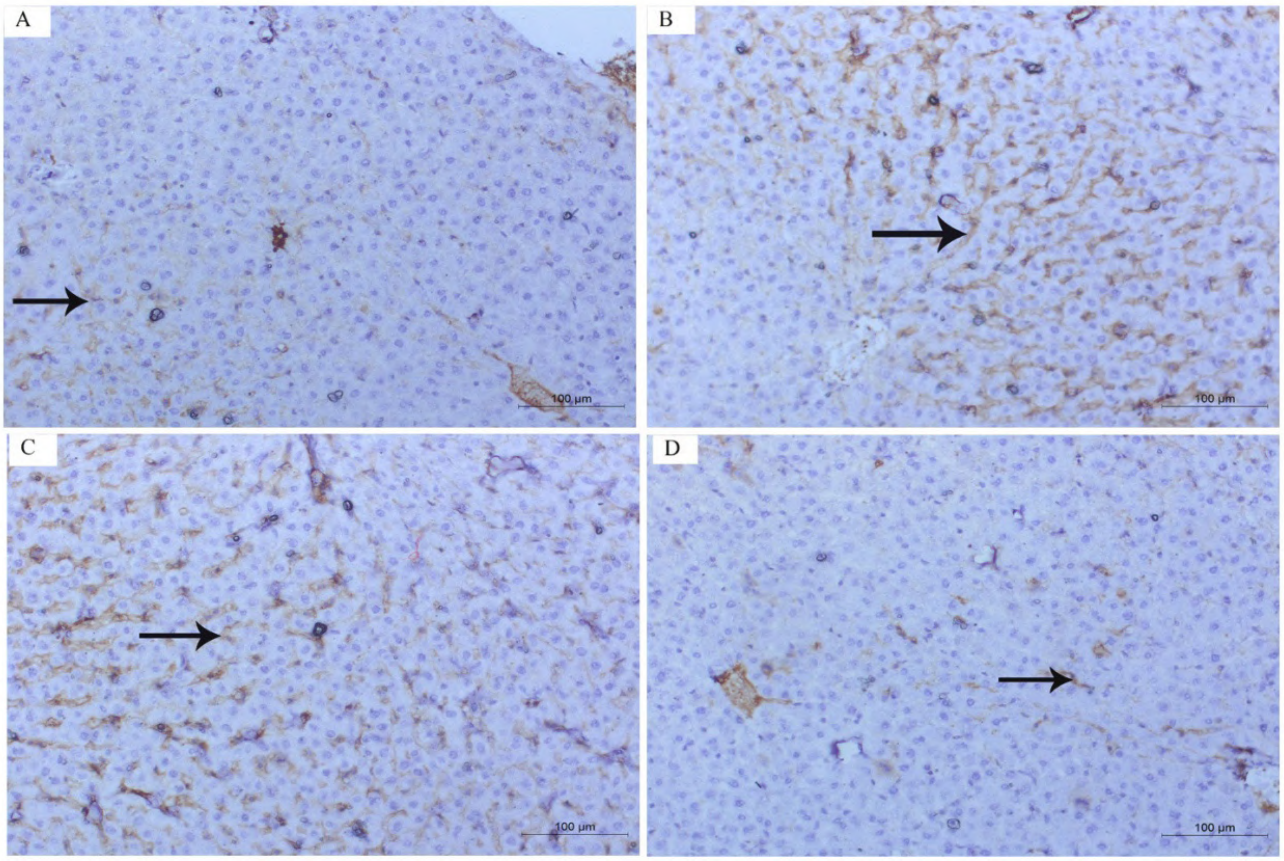

Fig. 7.- Immunoreaction of BAX (arrows). **A:** slight active expression of apoptotic reaction in the control group. **B:** A greater expression of apoptosis in the KD group. **C:** EODKD cells expressed fewer apoptotic reactions. **D:** ATO group shows minimal expression reaction. BAX immunostaining. Scale bars A-D = 100 µm.

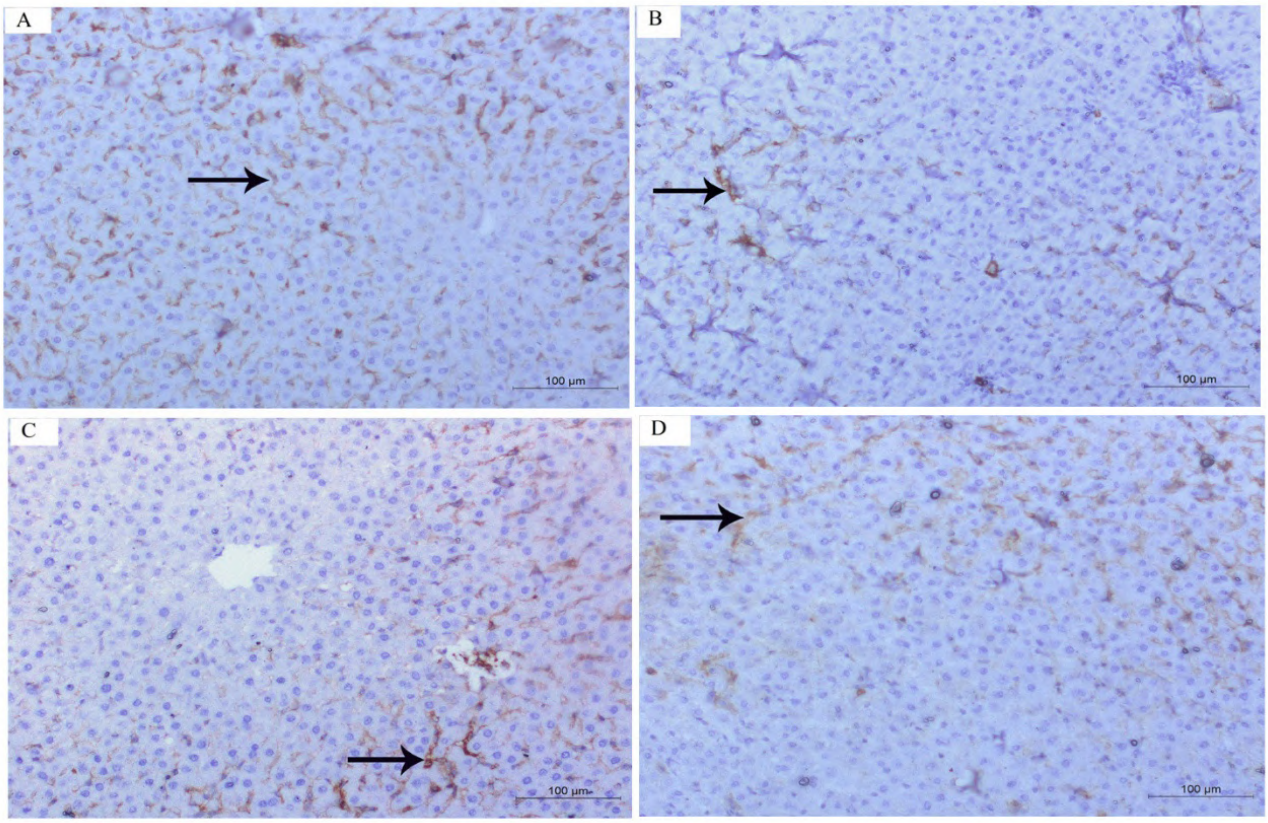

Fig. 8.- Immunoreaction of BCL2 (arrows). **A**: Normal reaction of the control group. **B**: The KD group showed a marked decrease in reaction. **C**: EODKD showed a less pronounced decrease in reaction. **D**: ATO group reactions were normal. BCL2 immunostaining. Scale bars A-D = 100 µm.

In the KD and EODKD groups, the levels of hepatic cholesterol were 54% and 32% lower than the control group, respectively. In the KD group the levels were 20% lower than the EODKD group. With ATO, the levels were 67% lower than the control group (Table 5).

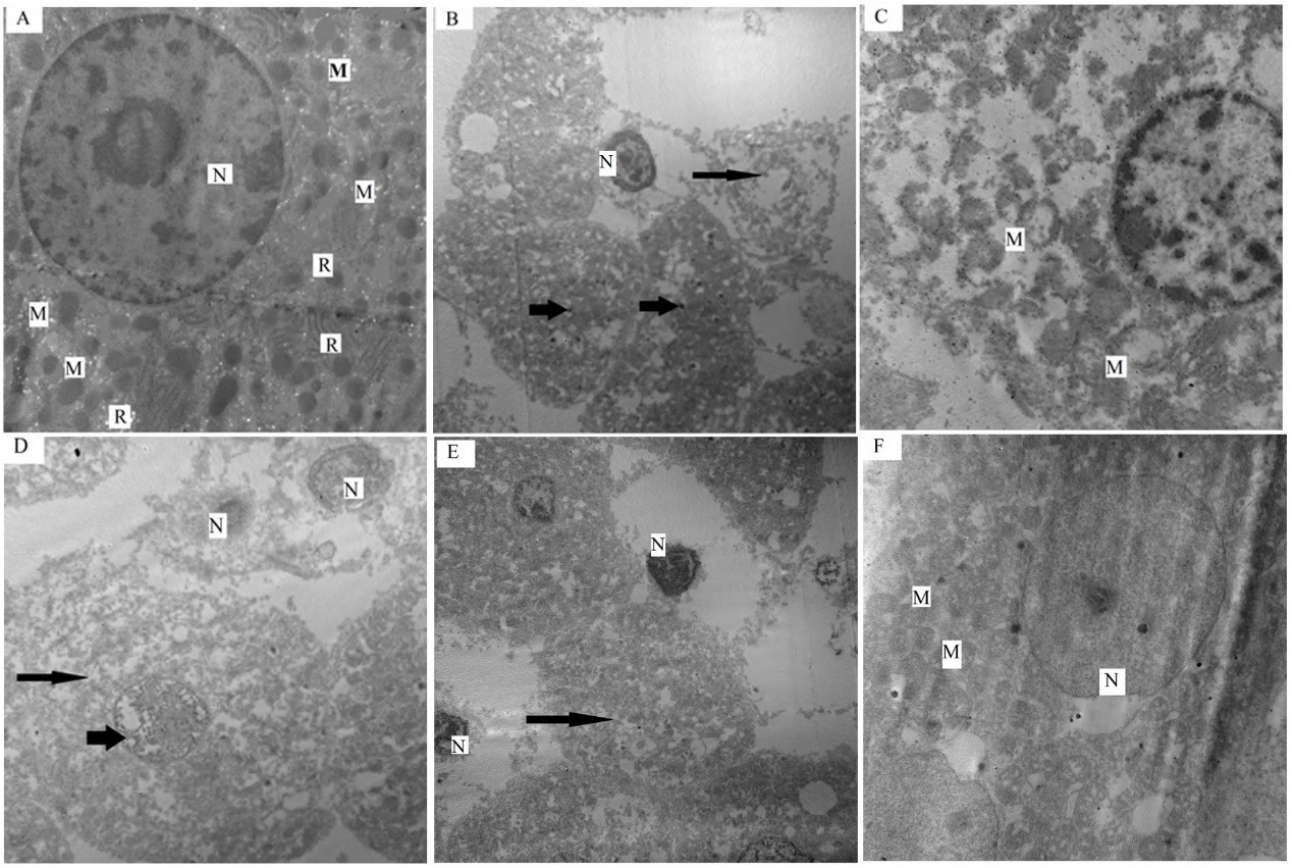

Fig. 9.- A: Classic hepatic architecture in a control rat. Note a hepatic nucleus (N) with a prominent nucleolus, mitochondria (M) of moderate electron density, and rER (R) with the normal organization (x 8000). **B:** rarefied cytoplasm (thin arrow), pyknotic hepatic nucleus (N), and prominent lysosomes (thick arrows) in the KD group (x 3000). **C:** mitochondria (M) with lost cristae and ruptured outer membranes in the KD group (x 8000). **D, E:** hepatocytes with degenerative nuclear changes (thick arrow), pyknotic nuclei (N), and rarefied cytoplasm (thin arrow) in EODKD (x 4000, 3000). **F**: normal hepatic architecture in the ATO group. Note a hepatic nucleus (N) with regular nuclear membrane, mitochondria (M) of moderate electron density (x 6000).

Table 5. Biochemical parameters of the studied groups.

Group		Hepatic triglyceride (mg/g liver)	Hepatic cholesterol (mg/g liver)	Serum cholesterol (mg/dl)	ALT (U/L)	AST (U/L)
Control	Mean ±SD	110±20	37.0±2.8	122±10.5	14.5±3.5	15.0±1.4
KD	Mean ±SD	70.0±18.4	17.0±8.2	90.7±15.6	50.3±5.8	55.3±6.4
	Versus control	0.008*	0.001*	0.003*	0.001*	0.001*
	Versus EODKD	0.03*	0.010*	0.001*	0.011*	0.003*
	Versus ATO	0.002*	0.001*	0.005*	0.001*	0.001*
EODKD	Mean ±SD	80.5±19.6	25.3±9.8	100.0±17.3	34.0±5.3	35.3±3.1
	Versus control	0.003*	0.003*	0.008*	0.010*	0.002*
	Versus KD	0.03*	0.010*	0.003*	0.011*	0.003*
	Versus ATO	0.004*	0.021*	0.002*	0.011*	0.015*
ATO	Mean ±SD	60.9±15.6	12.3±3.2	75.5±12.8	16.7±2.9	21.7±1.5
	Versus control	0.03*	0.02*	0.04*	0.954	0.161
	Versus KD	0.002*	0.001*	0.005*	0.001*	0.001*
	Versus EODKD	0.004*	0.021*	0.002*	0.011*	0.015*

*= p-value significant

The serum cholesterol levels of the KD and EODKD groups were lower than those of the control group by 26 and 18%, respectively, while the levels of the KD group were 11% lower than those of the EODKD group. With ATO, the levels were 38% lower than those of the control group (Table 5).

There was an increase in ALT levels in the KD and EODKD groups as compared to the control group by 250% and 143%, respectively. For the KD group, the level was 32% higher compared to the EODKD group. The levels in ATO and control groups were similar (Table 5).

As compared to the control, the KD and EODKD groups had higher levels of AST by 267% and 134%, respectively. ATO and control groups did not differ in terms of AST levels. The KD group's level was 36% higher compared to the EODKD group's level (Table 5).

Increase oxidative stress in the KD and EODKD groups

In the KD and EODKD groups, there was a 740% (7-fold) and a 520% (5-fold) increase as compared to the control group. MDA levels were 23% higher in the KD group than the EODKD group. The levels in the ATO and control groups were similar (Table 6).

As compared with the control group, TBARS levels in the KD and EODKD groups exhibited 175% and 120% increase, respectively. The level of both in the KD group was 20% higher than in the EODKD group, while levels in the ATO and control groups were similar (Table 6).

SOD levels in the KD and EODKD groups decreased by 46% and 23%, respectively, compared with the control. SOD in the KD group was 44% lower than in the EODKD group. Levels in the ATO and control groups were similar (Table 6).

In the KD and EODKD groups, GSH levels fell 48% and 34%, respectively, in comparison to the control group. In the KD group, GSH levels dropped 28% less than in the EODKD group. In the control group, levels were essentially identical (Table 6).

Increase expression of NLRP3 and CD11b in the KD or EODKD groups

As compared to the control group, the expression level of CD11b in KD and EODKD groups increased 540% (>5 fold) and 340% (> 3-fold), respectively. The level in the KD group was 31% higher compared to the EODKD group. The levels in ATO and control groups were similar (Fig. 10, Table 7).

Table 6. Oxidative/antioxidative markers in the studied groups.

Group		MDA (nmol/mg protein)	TBARS (nmol/mg protein)	SOD (U/mg protein)	GSH (U/mg protein)
Control	Mean ±SD	5.0±1.0	20.0±8.0	84.0±7.3	144.0±12.0
KD	Mean ±SD	42.3±3.5	55.0±5.6	45.0±6.0	74.7±9.5
	Versus control	0.000*	0.01*	0.005*	0.000*
	Versus EODKD	0.022*	0.550	0.008*	0.002*
	Versus ATO	0.000*	0.002*	0.000*	0.001*
EODKD	Mean ±SD	31.3±2.2	44.3±7.0	64.0±3.1	95.0±8.0
	Versus control	0.000*	0.001*	0.000*	0.000*
	Versus KD	0.024*	0.504	0.007*	0.002*
	Versus ATO	0.021*	0.004*	0.006*	0.004*
ATO	Mean ±SD	8.0±7.0	25.0± 6.0	80.0±3.0	135.3±8.4
	Versus control	0.110	0.983	0.376	0.564
	Versus KD	0.000*	0.003*	0.000*	0.001*
	Versus EODKD	0.011*	0.003*	0.005*	0.002*

*= p-value significant

In the KD and EODKD groups, NLRP3 expression levels were 250% (2.5-fold) and 160% (>1.5-fold), respectively, compared to the control group. In the KD group, the expression levels were 24% higher than in the EODKD group. In the ATO group, the expression levels were like those of the control group (Fig. 10, Table 7).

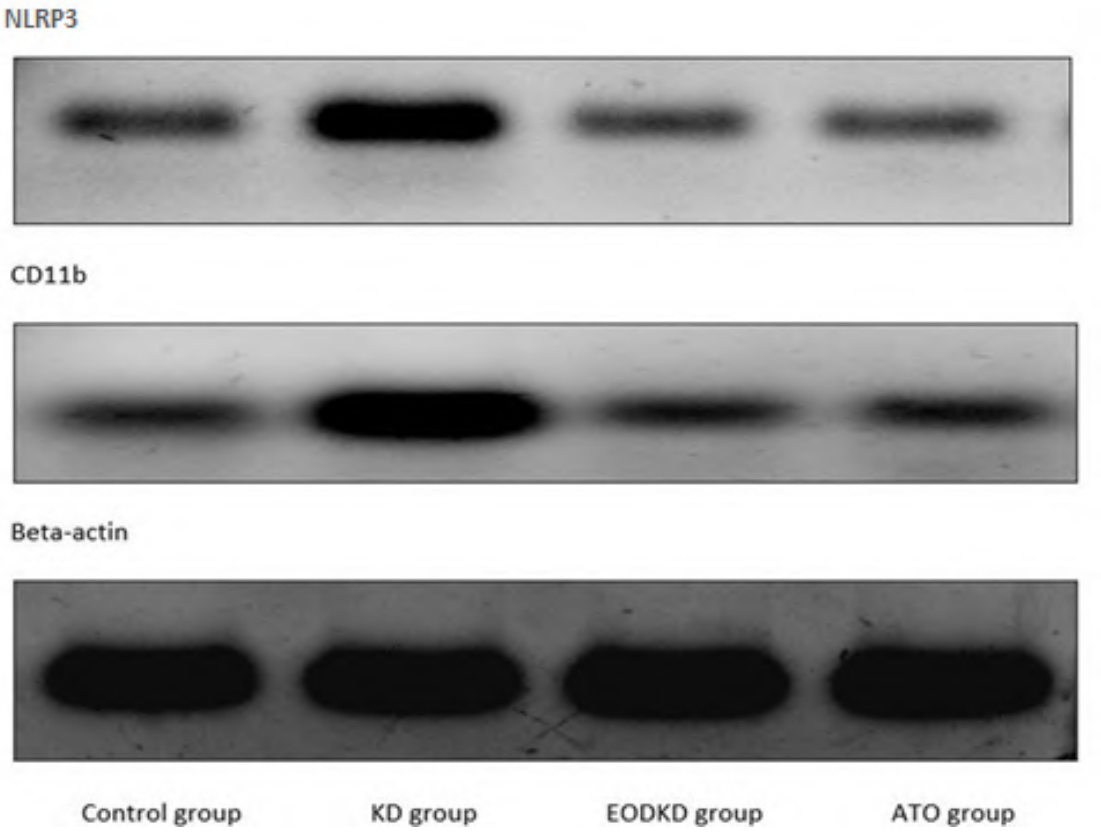

Fig. 10.- Expression levels of NLRP3 and CD11b by Western blot. B-actin was used as a control. The expression of both genes increased in the KD group, while it is decreased in EODKD with more decrease in the ATO group

Table 7. CD11b and NLRP3 levels among the different groups.

Group		CD11b level	NLRP3 level
Control	Mean ±SD	1.0±0.02	1.5±0.2
KD	Mean ±SD	6.4±0.8	5.3±0.4
	Versus control	0.001*	0.001*
	Versus EODKD	0.011*	0.021*
	Versus ATO	0.001*	0.001*
EODKD	Mean ±SD	4.4±0.5	4.0±0.3
	Versus control	0.008*	0.004*
	Versus KD	0.011*	0.021*
	Versus ATO	0.030*	0.003*
ATO	Mean ±SD	2.1±0.01	1.8±0.1
	Versus control	0.251	0.089
	Versus KD	0.001*	0.001*
	Versus EODKD	0.030*	0.003*

*= p-value significant

DISCUSSION

At the end of this study, both KD and EODKD groups had lost weight by 14% and 8%, respectively. This weight loss may be the result of modulating resting energy expenditure by these diets (Krieger et al., 2006), or by reducing insulin levels (Westman et al., 2007), or by loss of appetite consequence to ketosis (Sumithran et al., 2013). Researchers suggest that KDs are responsible for weight loss because they promote ketogenesis, which may enhance mitochondrial fat oxidation and bioenergetic signalling (Miller et al., 2020). Increased gluconeogenesis (energy demand) caused by carbohydrate restriction is also a contributing factor (Fine and Feinman, 2004). Still others believe the diets were metabolically effective (Feinman and Fine, 2007). Kump and Booth (2005) found that KD-fed animals showed a 17% increase in energy expenditure compared with standard chow-fed mice, concluding that KD caused an increase in thermogenesis independent of physical activity. In a study by Frommelt et al. (2014), rats fed a KD for 4 weeks exhibited higher levels of gross energy in urine than rats fed standard chow.

After 22 weeks of KD in mice, there is no weight loss (Ellenbroek et al., 2014). According to other reports, after 18 weeks of KD, the mice's weight returned to baseline and then slowly increased (Douris et al., 2015). We were unable to verify both findings in our study due to its relative shortness.

The relative liver weight of the KD and EODKD groups decreased by 75% and 57%, respectively, compared to the control group. This may be caused by the depletion of liver glycogen (Bian et al., 2014). Many studies have shown that weight loss influences liver health and liver fat percentage. A 5% weight loss decreased hepatic fat by 28-40% (Thomas et al., 2006; Kantartzis et al., 2009).

Both KD and EODKD result in structural liver damage (apoptosis, cytoplasmic vacuolation, inflammatory cellular infiltration, congestion of the portal & central veins and hepatic sinusoids). The biochemical liver markers (ALT and AST) were elevated. The elevation of these markers indicates severe liver damage (Monteiro et al., 2016). ALT and AST were elevated more than two-fold in the KD group and more than one-fold in the EODKD group (being higher in the KD group by 32% and 36%). The medium protein content of KD and EODKD may contribute to the described injury pattern (Garbow et al., 2011).

KD and EODKD are associated with vacuolation of hepatocytes. Vacuolation of hepatocytes is defined as microvesicular and macrovesicular steatosis. The macrovesicular steatosis detected in both groups may be ascribed to abnormalities in the delivery, metabolism, synthesis, and export of lipids (Brunt and Tiniakos, 2005). The decrease in the hepatic triglyceride levels, hepatic cholesterol levels, and serum cholesterol levels in EODKD and KD groups supports this assumption. Many studies reported a decrease in these biomarkers in rats fed a KD (Holland et al., 2016). Furthermore, cytoplasmic vacuolation may be attributed to lipid peroxidation as oxidative stress damage cell membranes, as well as membranes of cell organelles leading to an increase in their permeability and disturbance of the concentrations of the ions in the cytoplasm and cell organelles (Panasiuk et al., 2006). Oxidative stress was obviously noticed in KD and EODKD groups (elevation of oxidative markers and flat antioxidant), being higher in the KD group. It is demarcated as the shift between oxidants and antioxidants in favor of oxidants (Bocarsly et al., 2010). Oxidative stress and KDs are controversial issues. Some studies report the oxidative stress and antioxidant effects of KDs (Rhyu et al., 2014). In other studies, researchers have shown that KDs reduce oxidative stress through Nrf2 (nuclear factor-erythroid factor 2-related factor 2) signaling and by suppressing the NF-κB (nuclear factor kappa-light-chain-enhancer of activated B cells) signaling pathway (Lu et al., 2018).

The periportal areas that are affected by KD and EODKD had inflammation around them. Inflammation in absenteeism of infection is now considered a major mechanism for liver injury (Kubes and Mehal 2012; Hoque et al., 2013). Sterile inflammation is started when the damaged hepatocytes expose the intracellular molecules that are recognized by the innate immune system. Kupffer cells become activated and trigger an inflammatory response through common

pathways involving the NLRP3 inflammasome (Rock et al., 2010). The expression level of NLRP3 in KD and EODKD groups displayed 2.5 and 1.5-fold higher linked to the control group (being 24% higher in the KD group). Activation of the NLRP3 inflammasome results in the production of pro-inflammatory cytokines, chemokines with the subsequent recruitment of neutrophils, and cell death (Broderick et al., 2015). Another possible factor that can trigger sterile inflammation is the sustained supply of high concentrations of fat to periportal hepatocytes (the cells receive more fat than can be oxidized) (Borradaile et al., 2006). The increased apoptosis that observed in KD and EODKD groups could provide other possible explanation of this inflammation (Wang et al., 2008).

Apoptosis was identified in KD and EODKD groups. The outline of the apoptotic signal pathway finally meets a common mechanism driven by caspases. Caspase-3 is the major destroyer of apoptosis, thus helping cell survival (Ma et al., 2014). The value of the caspase 3 is distinctly increased in the KD and EODKD groups.

The caspases mechanism is controlled by the Bcl-2 family (Adams and Cory, 1998). This family is classified into Bcl-2 subfamily, Bax subfamily and Bik and Bid subfamily. The Bcl-2 employs anti-apoptotic activity, while Bax applies proapoptotic activity (Tsujimoto, 1998). The Bax reaction increased with KD ten-fold and with EODKD six-fold. Contrary, the expression of BCL2 decreased in KD and EODKD groups by 30% and 50%. Bcl2/Bax ratio decreased with KD twenty-fold and with EODKD ten-fold. Bcl2/Bax ratio expresses the danger of the cell to apoptosis (Tsujimoto, 1998) as seen in KD and EODKD groups.

The content of collagen fibers in periportal areas increased in the KD group by more than two-fold, and in the EODKD group by more than one-fold (being higher in the KD group by 30%). KD is known to cause hepatic fibrosis in some cases (Brunt and Tiniakos, 2005). The developed liver fibrosis during liver damage causes an irreversible distortion of the normal hepatic architecture (Sokol, 2002). Oxidative stress and chronic inflammation are involved in such progress (Poli, 2000).

The concomitant use of ATO with KD protects liver architecture. Moreover, the biological hepatic markers (AST and ALT) were of their normal levels. ATO provides its protective effect through decreasing the oxidative stress (oxidative/antioxidative markers were matching the control group), normalization expression of NLRP3 (absence of sterile inflammation) and inhibition HMG-CoA reductase (Kogawa et al., 2019), which plays a key role in the production of cholesterol in the body (marked decrease of intrahepatic triglyceride level compared to KD and EODKD groups).

CONCLUSIONS

Both KD and EODKD result in structural liver damage that is accompanied by an elevation in hepatic markers (AST and ALT) along with a decrease in hepatic triglyceride, hepatic cholesterol, and serum cholesterol. KD has a more significant effect. There are several factors contributing to hepatic injury in these diets, including oxidative stress, sterile inflammation, low protein content, and high fat concentrations. ATO in conjunction with KD is beneficial.

ACKNOWLEDGEMENTS

The authors wish to thank Professor Dr. Laila Ahmed Rashed professor of Biochemistry, Faculty of Medicine, Cairo University for her great effort in this thesis.

REFERENCES

ADAMS JM, CORY S (1998) The Bcl-2 protein family: arbiters of cell survival. *Science*, 281(5381): 1322-1326.

BANCROFT JD, GAMBLE M (2008) Theory and practice of histological techniques. 6th ed. Churchill Livingstone Elsevier, China, pp 433-472.

BARAÑANO KW, HARTMAN AL (2008) The ketogenic diet: uses in epilepsy and other neurologic illnesses. *Curr Treat Options Neurol*, 10(6): 410-419.

BARREA L, CAPRIO M, TUCCINARDI D, MORICONI E, DI RENZO L, MUSCOGIURI G, COLAO A, SAVASTANO S (2022) Could ketogenic diet "starve" cancer? Emerging evidence. *Critical Rev Food Sci Nutrit*, 62(7): 1800-1821.

BIAN H, HAKKARAINEN A, LUNDBOM N, YKI-JÄRVINEN H (2014) Effects of dietary interventions on liver volume in humans. *Obesity (Silver Spring)*, 22(4): 989-995.

BOCARSLY ME, POWELL ES, AVENA NM, HOEBEL BG (2010) High-fructose corn syrup causes characteristics of obesity in rats: increased body weight, body fat and triglyceride levels. *Pharmacol Biochem Behav*, 97(1): 101-106.

BOLLA AM, CARETTO A, LAURENZI A, SCAVINI M, PIEMONTI L (2019) Low-carb and ketogenic diets in type 1 and type 2 diabetes. *Nutrients*, 11(5): 962.

BORRADAILE NM, HAN X, HARP JD, GALE SE, ORY DS, SCHAFFER JE (2006) Disruption of endoplasmic reticulum structure and integrity in lipotoxic cell death. *J Lipid Res*, 47(12): 2726-2737.

BRODERICK L, DE NARDO D, FRANKLIN BS, HOFFMAN HM, LATZ E (2015) The inflammasomes and autoinflammatory syndromes. *Annu Rev Pathol*, 10: 395-424.

BRUNT EM, TINIAKOS DG (2005) Pathological features of NASH. *Front Biosci*, 10: 1475-1484.

DENG-BRYANT Y, PRINS ML, HOVDA DA, HARRIS NG (2011) Ketogenic diet prevents alterations in brain metabolism in young but not adult rats after traumatic brain injury. *J Neurotrauma*, 28(9): 1813-1825.

DOURIS N, MELMAN T, PECHERER JM, PISSIOS P, FLIER JS, CANTLEY LC, LOCASALE JW, MARATOS-FLIER E (2015) Adaptive changes in amino acid metabolism permit normal longevity in mice consuming a low-carbohydrate ketogenic diet. *Biochim Biophys Acta*, 1852(10 Pt A): 2056-2065.

ELLENBROEK JH, VAN DIJCK L, TÖNS HA, RABELINK TJ, CARLOTTI F, BART E P B BALLIEUX, EELCO J, P DE KONING (2014) Long-term ketogenic diet causes glucose intolerance and reduced β- and α-cell mass but no weight loss in mice. *Am J Physiol Endocrinol Metab*, 306(5): E552-558.

FEINMAN RD, FINE EJ (2007) Nonequilibrium thermodynamics and energy efficiency in weight loss diets. *Theor Biol Med Model*, 4: 27.

FINE EJ, FEINMAN RD (2004) Thermodynamics of weight loss diets. *Nutr Metab (Lond)*, 1(1): 15.

FOSSATI P, PRENCIPE L (1982) Serum triglycerides determined colorimetrically with an enzyme that produces hydrogen peroxide. *Clin Chem*, 28(10): 2077-2080.

FROMMELT L, BIELOHUBY M, MENHOFER D, STOEHR BJ, BIDLINGMAIER M, KIENZLE E (2014) Effects of low carbohydrate diets on energy and nitrogen balance and body composition in rats depend on dietary protein-to-energy ratio. *Nutrition*, 30(7-8): 863-868.

GARBOW JR, DOHERTY JM, SCHUGAR RC, TRAVERS S, WEBER ML, WENTZ AE, EZENWAJIAKU N, COTTER DG, BRUNT EM, CRAWFORD PA (2011) Hepatic steatosis, inflammation, and ER stress in mice maintained long term on a very low-carbohydrate ketogenic diet. *Am J Physiol Gastrointest Liver Physiol*, 300(6): G956-967.

GÓMEZ-DOMÍNGUEZ E, GISBERT JP, MORENO-MONTEAGUDO JA, GARCÍA-BUEY L, MORENO-OTERO R (2006) A pilot study of atorvastatin treatment in dyslipemid, non-alcoholic fatty liver patients. *Aliment Pharmacol Ther*, 23(11): 1643-1647.

HARTMAN AL, RUBENSTEIN JE, KOSSOFF EH (2013) Intermittent fasting: a "new" historical strategy for controlling seizures? *Epilepsy Res*, 104(3): 275-279.

HAYAT MA (2000) Principles and techniques of electron microscopy: biological applications. Cambridge University Press, New York.

HERTZ L, CHEN Y, WAAGEPETERSEN HS (2015) Effects of ketone bodies in Alzheimer's disease in relation to neural hypometabolism, □-amyloid toxicity, and astrocyte function. *J Neurochem*, 134(1): 7-20.

HOLLAND AM, KEPHART WC, MUMFORD PW, MOBLEY CB, LOWERY RP, SHAKE JJ, PATEL RK, HEALY JC, MCCULLOUGH DJ, KLUESS HA, HUGGINS KW, KAVAZIS AN, WILSON JM, ROBERTS MD (2016) Effects of a ketogenic diet on adipose tissue, liver, and serum biomarkers in sedentary rats and rats that exercised via resisted voluntary wheel running. *Am J Physiol Regul Integr Comp Physiol*, 311(2): R337-351.

HOQUE R, FAROOQ A, MEHAL WZ (2013) Sterile inflammation in the liver and pancreas. *J Gastroenterol Hepatol*, 28 Suppl 1(0 1): 61-67.

JI G, ZHAO X, LENG L, LIU P, JIANG Z (2011) Comparison of dietary control and atorvastatin on high fat diet induced hepatic steatosis and hyperlipidemia in rats. *Lipids Health Dis*,10: 23.

KANTARTZIS K, THAMER C, PETER A, MACHANN J, SCHICK F, SCHRAML C, KÖNIGSRAINER A, KÖNIGSRAINER I, KRÖBER S, NIESS A, FRITSCHE A, HÄRING H-U, STEFAN N (2009) High cardiorespiratory fitness is an independent predictor of the reduction in liver fat during a lifestyle intervention in non-alcoholic fatty liver disease. *Gut*, 58(9): 1281-1288.

KOGAWA AC, PIRES AEDT, SALGADO HRN (2019) Atorvastatin: A review of analytical methods for pharmaceutical quality control and monitoring. *J AOAC Int*, 102(3): 801-809.

KRIEGER JW, SITREN HS, DANIELS MJ, LANGKAMP-HENKEN B (2006) Effects of variation in protein and carbohydrate intake on body mass and composition during energy restriction: a meta-regression 1. *Am J Clin Nutr*, 83(2): 260-274.

KUBES P, MEHAL WZ (2012) Sterile inflammation in the liver. *Gastroenterology*, 143(5): 1158-1172.

KUMP DS, BOOTH FW (2005) Sustained rise in triacylglycerol synthesis and increased epididymal fat mass when rats cease voluntary wheel running. *J Physiol*, 565(Pt 3): 911-925.

LU Y, YANG Y-Y, ZHOU M-W, LIU N, XING H-Y, LIU X-X, LI F (2018) Ketogenic diet attenuates oxidative stress and inflammation after spinal cord injury by activating Nrf2 and suppressing the NF-κB signaling pathways. *Neurosci Lett*, 683: 13-18.

MA J, ZOU C, GUO L, SENEVIRATNE DS, TAN X, KWON Y-K, AN J, BOWSER R, DEFRANCES MC, ZARNEGAR R (2014) Novel death defying domain in met entraps the active site of caspase-3 and blocks apoptosis in hepatocytes. *Hepatology*, 59(5): 2010-2021.

MARCHESINI G, PETTA S, DALLE GRAVE R (2016) Diet, weight loss, and liver health in nonalcoholic fatty liver disease Pathophysiology, evidence, and practice. *Hepatology*, 63(6): 2032-2043.

MILDER JB, LIANG LP, PATEL M (2010) Acute oxidative stress and systemic Nrf2 activation by the ketogenic diet. *Neurobiol Dis*, 40(1): 238-244.

MILLER VJ, LAFOUNTAIN RA, BARNHART E, SAPPER TS, SHORT J, ARNOLD WD, HYDE PN, CRABTREE CD, KACKLEY ML, KRAEMER WJ, VILLAMENA FA, VOLEK JS (2020) A ketogenic diet combined with exercise alters mitochondrial function in human skeletal muscle while improving metabolic health. *Am J Physiol Endocrinol Metab*, 319(6): E995-E1007.

MONTEIRO ME, XAVIER AR, OLIVEIRA FL, FILHO PJ, AZEREDO VB (2016) Apoptosis induced by a low-carbohydrate and high-protein diet in rat livers. *World J Gastroenterol*, 22(22): 5165-5172.

OKTAY K, SCHENKEN RS, NELSON JF (1995) Proliferating cell nuclear antigen marks the initiation of follicular growth in the rat. *Biol Reprod*, 53(2): 295-301.

PANASIUK A, DZIECIOL J, PANASIUK B, PROKOPOWICZ D (2006) Expression of p53, Bax and Bcl-2 proteins in hepatocytes in non-alcoholic fatty liver disease. *World J Gastroenterol*, 12(38): 6198-6202.

PAOLI A, RUBINI A, VOLEK JS, GRIMALDI KA (2013) Beyond weight loss: a review of the therapeutic uses of very-low-carbohydrate (ketogenic) diets. *Eur J Clin Nutr*, 67(8): 789-796.

POLI G (2000) Pathogenesis of liver fibrosis: role of oxidative stress. *Mol Aspects Med*, 21(3): 49-98.

QU X, GAO H, TAO L, ZHANG Y, ZHAI J, SUN J, SONG Y, ZHANG S (2019) Astragaloside IV protects against cisplatin-induced liver and kidney injury via autophagy-mediated inhibition of NLRP3 in rats. *J Toxicol Sci*, 44(3): 167-175.

RHYU H-S, CHO S-Y, ROH H-T (2014) The effects of ketogenic diet on oxidative stress and antioxidative capacity markers of Taekwondo athletes. *J Exercise Rehab*, 10(6): 362-366.

ROCK KL, LATZ E, ONTIVEROS F, KONO H (2010) The sterile inflammatory response. *Annu Rev Immunol*, 28: 321-342.

SCHMECHEL A, GRIMM M, EL-ARMOUCHE A, HÖPPNER G, SCHWOERER AP, EHMKE H, ESCHENHAGEN T (2009) Treatment with

atorvastatin partially protects the rat heart from harmful catecholamine effects. *Cardiovasc Res*, 82(1): 100-106.

SCHWARTZ DM, WOLINS NE (2007) A simple and rapid method to assay triacylglycerol in cells and tissues. *J Lipid Res*, 48(11): 2514-2520.

SHAAFI S, NAJMI S, ALIASGHARPOUR H, MAHMOUDI J, SADIGH-ETEMAD S, FARHOUDI M, BANIASADI N (2016) The efficacy of the ketogenic diet on motor functions in Parkinson's disease: A rat model. *Iran J Neurol*, 15(2): 63-69.

SOKOL RJ (2002) Liver cell injury and fibrosis. *J Pediatr Gastroenterol Nutr*, 35 Suppl 1: S7-10.

SUMITHRAN P, PRENDERGAST LA, DELBRIDGE E, PURCELL K, SHULKES A, KRIKETOS A, PROIETTO J (2013) Ketosis and appetite-mediating nutrients and hormones after weight loss. *Eur J Clin Nutr*, 67(7): 759-764.

SUVARNA SK, LAYTON C, BANCROFT JD (2019) Bancroft's theory and practice of histological techniques. Oxford: Elsevier.

THOMAS EL, BRYNES AE, HAMILTON G, PATEL N, SPONG A, GOLDIN RD, FROST G, BELL JD, TAYLOR-ROBINSON SD (2006) Effect of nutritional counselling on hepatic, muscle and adipose tissue fat content and distribution in non-alcoholic fatty liver disease. *World J Gastroenterol*, 12(36): 5813-5819.

TSUJIMOTO Y (1998) Role of Bcl-2 family proteins in apoptosis: apoptosomes or mitochondria? *Genes Cells*, 3(11): 697-707.

WANG Y, AUSMAN LM, RUSSELL RM, GREENBERG AS, WANG XD (2008) Increased apoptosis in high-fat diet-induced nonalcoholic steatohepatitis in rats is associated with c-Jun NH2-terminal kinase activation and elevated proapoptotic Bax. *J Nutr*, 138(10): 1866-1871.

WESTMAN EC, FEINMAN RD, MAVROPOULOS JC, VERNON MC, VOLEK JS, WORTMAN JA, YANCY WS, PHINNEY SD (2007) Low-carbohydrate nutrition and metabolism. *Am J Clin Nutr*, 86(2): 276-284.

WEYDERT CJ, CULLEN JJ (2010) Measurement of superoxide dismutase, catalase and glutathione peroxidase in cultured cells and tissue. *Nat Protoc*, 5(1): 51-66.

YANG Q, BAVI P, WANG JY, ROEHRL MH (2017) Immuno-proteomic discovery of tumor tissue autoantigens identifies olfactomedin 4, CD11b, and integrin alpha-2 as markers of colorectal cancer with liver metastases. *J Proteomics*, 168: 53-65.

Anatomical variants of the uterine artery: 214 angiotomographies

Miguel Á. Vázquez-Barragán[1], José Ramon Ariztegui-Andrade[1], Juan P. Montemayor-Lozano[2], Oscar Vidal-Gutiérrez[1,3], Ricardo Pinales-Razo[2], Ernesto C. Martínez-Avila[4], Rodolfo Morales-Avalos[4]

[1] Department of Gynecology and Obstetrics, University Hospital "Dr. Jose Eleuterio Gonzalez", Universidad Autonoma de Nuevo Leon, Monterrey, Mexico

[2] Department of Radiology, University Hospital "Dr. Jose Eleuterio Gonzalez", Universidad Autonoma de Nuevo Leon, Monterrey, Mexico

[3] Department of Oncology, University Hospital "Dr. Jose Eleuterio Gonzalez", Universidad Autonoma de Nuevo Leon, Monterrey, Mexico

[4] Department of Physiology, School of Medicine, Universidad Autonoma de Nuevo Leon, Monterrey, Mexico

SUMMARY

The aim of the work is to know the changes that the uterine artery undergoes with age, the determination of its origin and its possible variants. Cross-sectional, comparative, descriptive, retrospective study Angiotomographies of the abdomen and pelvis of female patients were obtained, reformatted in 3D, analyzing the uterine arteries (thickness, origin and trajectory). Measurements were carried out by two medical specialists in diagnostic imaging. 107 CT angiograms of patients with a mean age of 56.62±16.97 years (range 1890) were included. The average thickness of the uterine arteries was 2.16 mm (±0.38 mm). Divided by laterality and age groups, they were 2.35 mm, 2.19 mm and 2.36 mm on the right side and 2.19 mm, 2.07 mm and 2.15 mm on the left side, respectively. There was no statistically significant difference in thickness between the three groups (p=0.08). Five types of anatomical variants are described with prevalence of 85.1% in type I, 6.75% in type II, 5.4% in type III, 2.02% in type IV and 0.67% in type V, the latter coming directly from the left ovarian artery. There are five different anatomical variants in our population, Type I is the most predominant. There are no significant morphological changes with age, except for an increase in vascular lesions, mainly atherosclerosis, in people over 50 years of age.

Keywords: Anatomy – Angiotomography – Gynecology – Uterine artery – Variants

INTRODUCTION

The classic anatomy of the uterine artery arises directly from the internal iliac artery, although it can also arise from the umbilical artery. It is the homologue to the artery of the vas deferens in man, and the one that gives the main irrigation to the uterus (Moore et al., 2013; Lockhart, 1959).

Gynecological surgical anatomy mentions that it arises exclusively from the internal iliac artery. However, there are reports of its origin independently, and of a common origin with the internal or vaginal pudendal artery (Rock et al., 2006; Sutton, 1997; Reich et al., 1989).

Corresponding author:
Dr. Ernesto Christopher Martínez Ávila. Department of Physiology, School of Medicine, Universidad Autonoma de Nuevo Leon, Av. Francisco I. Madero, s/n, Col. Mitras Centro, 66460 Monterrey, Nuevo Leon, Mexico. Phone: +528125909069. E-mail: Asistentedeinvestigacion00@gmail.com

Submitted: May 7, 2022. **Accepted:** May 18, 2022

https://doi.org/10.52083/GFWA3583

Hysterectomy is one of the most frequently performed surgical procedures in the United States. The most common indications are uterine fibroids (40.7%), endometriosis (17.7%) and uterine prolapse (14.5%) (ACOG, 2011; Lefebvre et al., 2002; Liu et al., 2006).

The conventional surgical technique via the abdomen is still relevant. However, minimal invasion and the use of natural orifices, such as the vaginal one, are promoted nowadays (Rock et al., 2006; CGP, 2009).

The uterus is pulled cranially and deviates to one side of the pelvis, stretching the inferior ligaments. A curved Heaney clamp is placed perpendicular to the uterine artery, taking care of the vasculature, to divide the ligament. The procedure is repeated on the contralateral side (Rock et al., 2006).

Aging produces changes in the structure and function of the arteries, giving rise to various cardiovascular diseases, such as hypertension, atherosclerosis, coronary disease, among others (Floryn et al., 2005)

The elderly population isthe group with the highest burden of cardiovascular diseases worldwide, especially coronary heart disease and myocardial infarction (Mirea et al., 2012) Atherosclerosis and loss of vascular elasticity can be observed in most elderly patients, but a more exaggerated response has been observed in hypertensive patients (Lahoz et al., 2007).

Hysterectomy is one of the most common gynecological surgical procedures. It is important to know its anatomical variants in relation to the vasculature and the expected changes with age. Our objective was to determine the prevalence of variants in our population, and to stratify the changes according to the age of the patient.

MATERIALS AND METHODS

A descriptive, observational, cross-sectional, comparative study was carried out. Angiotomographies were obtained from the database of the Radiodiagnosis Department of a hospital in Northern Mexico.

Mexican patients who for some reason underwent computed tomography angiography of the abdomen and pelvis were included. All those patients whose reason for study was trauma to the pelvis, hip, findings of congenital malformations of the pelvis, pregnancy, primary and secondary infectious processes of their corresponding organs, or with malformations of female organs were excluded. All those studies whose images did not allow a reconstruction, or whose quality made the evaluation of vascular structures difficult, were eliminated.

The equipment used for the acquisition of the images was the Light Speed VCT Model with 64 slices per rotation (General Electric, Milwaukee, WI), with a continuous scan with a thickness of 2.5 mm. To better visualize the images, reformatting with maximum intensity projection (MIP) and Volume Rendering (VR) were used, with software number 12HW14.6_SP1-1-1V40_H_H64_G_GTL. The reconstructed images were transmitted to workstations "Advantage Workstation AW 4.4" (General Electric, Milwaukee, WI), with a linear precision of 0.01 millimeters. Workstation calibration was predetermined by the manufacturer.

A Carestream Vue PACS Version 12.1.5.6009 workstation was used for the assessment of the uterine arteries, using reconstructions that were stored on a separate workstation.

Reconstructions and measurements were performed independently by 2 radiology experts.

Computed Tomography Angiography (CTA) were studied for their anatomical variant and were classified as type I to V. The internal diameter of the vessel was recorded at its site of origin (M1), and at its ascending portion (M2). The data were recorded in an Excel table to determine their frequencies, mean and standard deviation. Carrying out this analysis did not interfere in any way with the normal protocols for carrying out, storing and delivering the results of the study to the patient or doctor requesting it. No CTA was performed for the purpose of the study, and there was no radiation exposure for the purpose of this investigation.

This research protocol was previously reviewed and approved by the ethics and research committees of the University, with registration GI 17-003.

The sample size was determined using a formula for calculating a prevalence or proportion, with a Z value of 1.96 and a confidence level of 95%, and a precision of 10% expecting a proportion of 50%, a sample of 140 arteries to carry out this study.

RESULTS

107 studies were included, of which 74 (69.16%) could be reconstructed. The remaining 30.84% (n 33) with a mean age of 56.62 ± 16.97 years was included for determination of variants, but not in vessel morphometry due to elimination criteria (Table 1).

Table 1. Reason for elimination of studies in 3D reconstruction for morphometries.

Pathology	Average Ages (years)	Sample (n 33)
Atherosclerosis	58 ± 7.2	17
Hysterectomy	62 ± 9.4	11
Myoma	49 ± 10.2	4
Adnexal mass	48 ± 5.2	1

The patients were stratified into three groups according to their age (Table 2). When comparing the calibers of the uterine arteries between the 18-40 and 41-60 age groups, a statistically significant difference was found (p= 0.04). However, when comparing the three groups through ANOVA, no difference was found between the three groups (p = 0.08), although there was a positive trend.

Table 2. Age groups and measurement of uterine arteries. Ranges expressed in years. Values expressed in millimeters (mm) n: sample size; M1: diameter at its origin; M2: diameter in its ascending portion.

Age ranges	Uterine artery			
	Right		Left	
	M1	M2	M1	M2
18-40 (n 26)	2.41±0.38	2.3±0.49	2.15±0.28	2.23±0.61
41-60 (n 60)	1.97±0.49	2.05±0.41	2.01±0.40	2.13±0.49
60-90 (n 62)	2.36±0.45	2.530.39	2.2±0.39	2.1±0.38
Average	2.14±0.46	2.17±0.42	2.14±0.35	2.15±0.51

Variants of the uterine arteries

From the findings found in the analyzed studies, the following order is proposed for the categorization of the variants in the origin of the uterine arteries.

- Type I. - The origin of the uterine artery is directly from the anterior trunk of the internal iliac artery (Fig. 1).
- Type II. - The origin of the uterine artery comes from the branch of the anterior trunk of the internal iliac artery, called the inferior gluteal/superior vesical artery (Fig. 2).
- Type III. - The origin of the uterine artery is independent and comes directly from the internal iliac artery to one side of the bifurcation of the inferior and superior gluteal arteries (Fig. 3).
- Type IV. - The origin of the uterine artery comes from the umbilical branch of the anterior trunk of the internal iliac artery (Fig. 4).

A unique variant was found, not previously described, which is proposed as a Type V variant (with an origin directly from the ovarian artery, which in turn came from the left renal artery, instead of the abdominal aorta, as classically described).

Table 3 outlines the distribution of the types regardless of whether it is right or left.

Table 3. Categorization of the anatomical variants of the uterine artery.

Variants	Total n 214 (%)	Uterine artery	
		Right n 10 (%)	Left n 107 (%)
I	182 (85.04)	89 (83.17)	93 (86.91)
II	15 (7.00)	9 (8.41)	6 (5.60)
III	11 (5.14)	7 (6.54)	4 (3.73)
IV	5 (2.33)	2 (1.86)	3 (2.80)
V	1 (0.46)	0 (0.00)	1 (0.93)

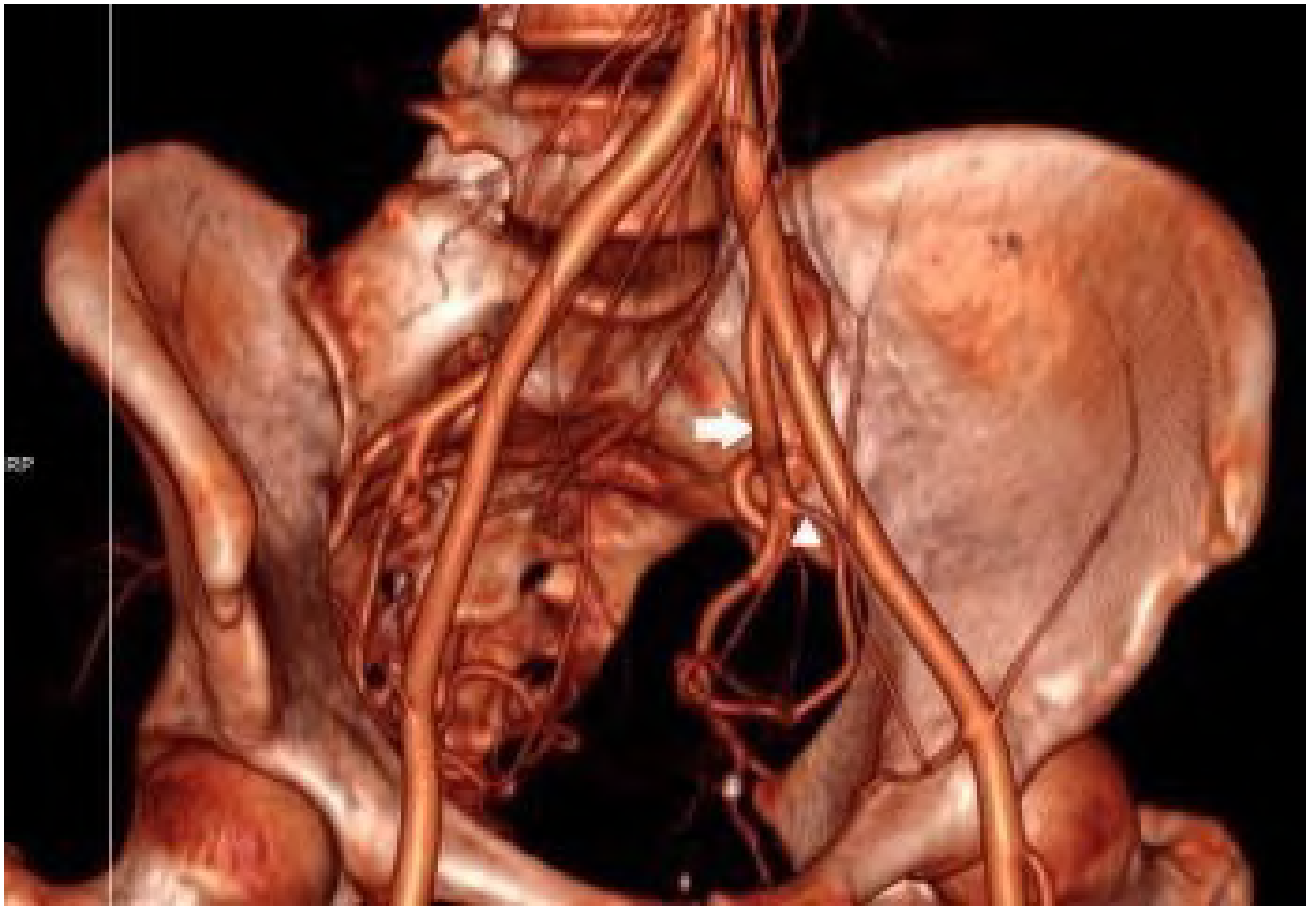

Fig. 1.- The origin of the uterine artery (arrowhead) is directly from the anterior trunk of the internal iliac artery (arrow).

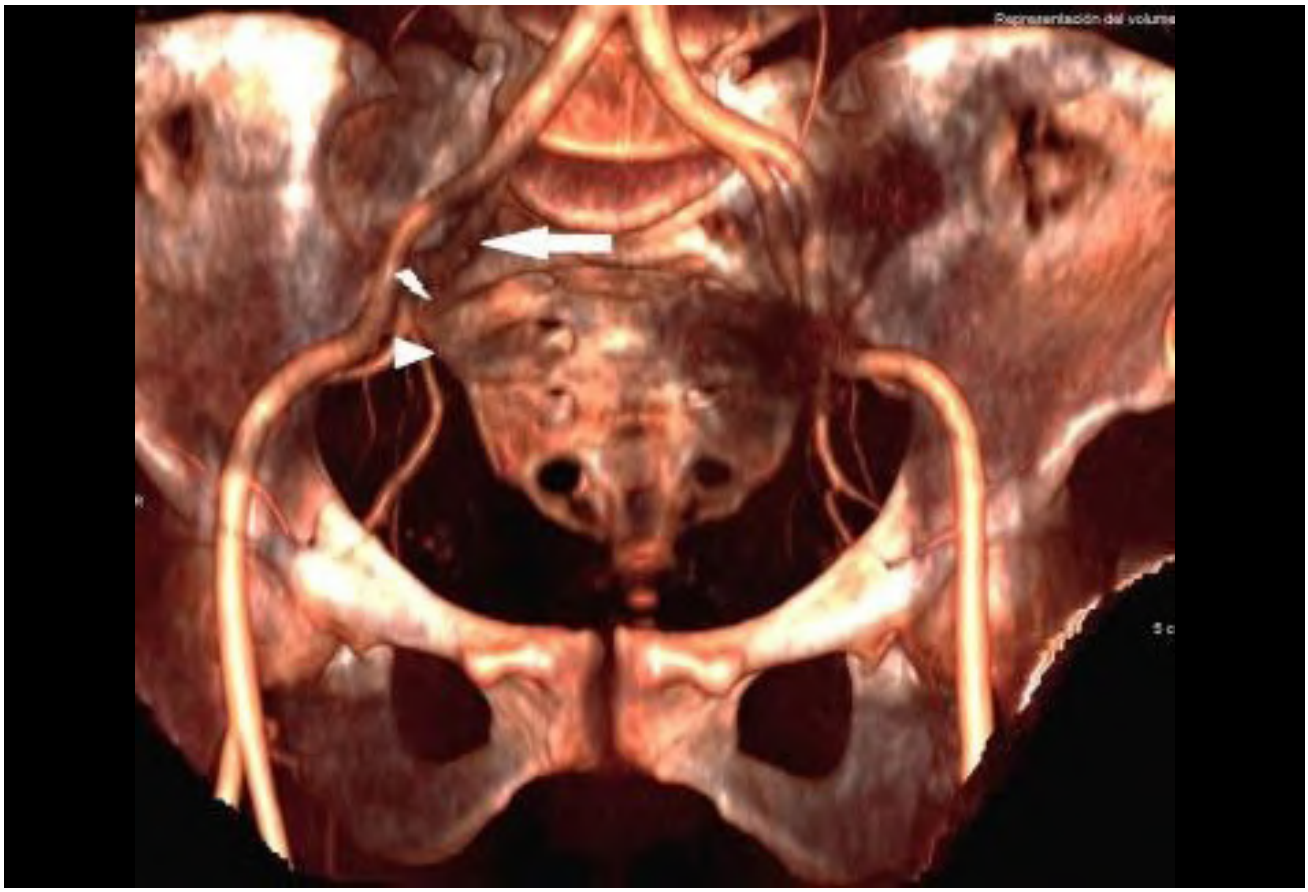

Fig. 2.- The origin of the uterine artery (arrowhead) is independent, and comes directly from the internal iliac artery (arrow) to one side of the bifurcation (Ray) of the inferior and superior gluteal arteries.

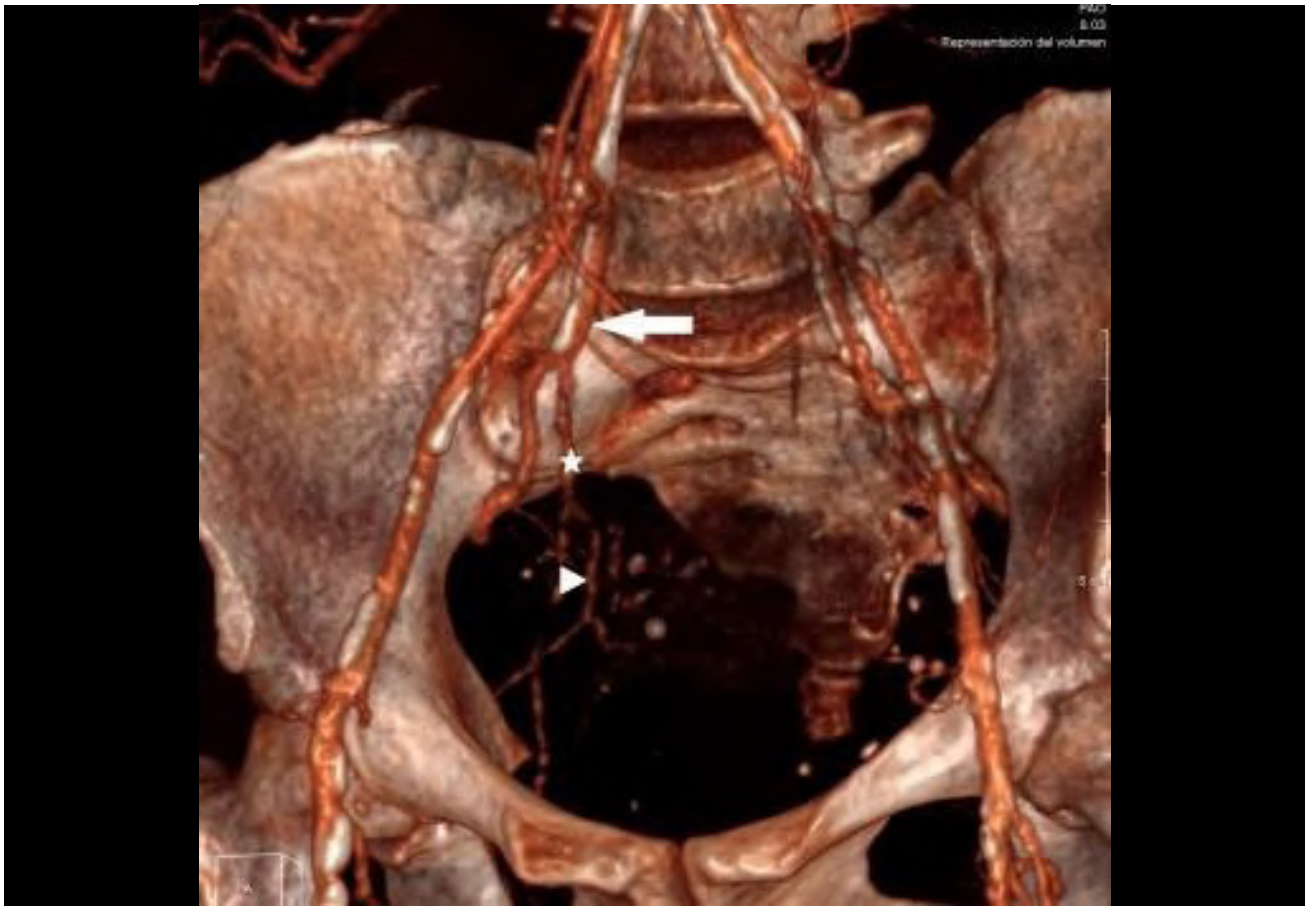

Fig. 3.- The origin of the uterine artery (arrowhead) comes from the branch of the anterior trunk (star) of the internal iliac artery (arrow) called inferior gluteal/superior vesical.

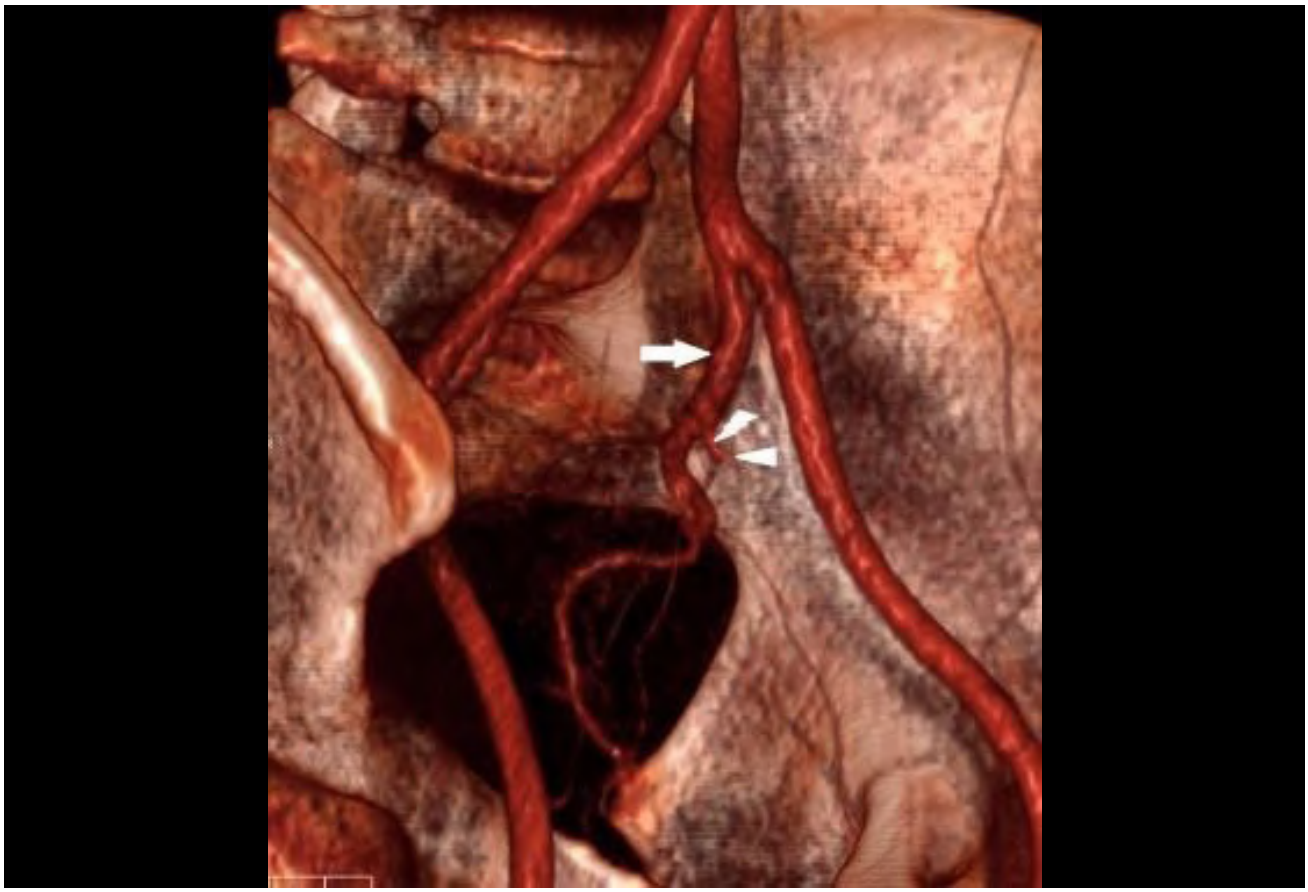

Fig. 4.- The origin of the uterine artery (arrowhead) comes from the umbilical branch (lightning) of the anterior trunk of the internal iliac artery (arrow).

DISCUSSION

Every doctor must have a broad knowledge of human anatomy and how it influences pathologies. This is even more important in surgical procedures, since ignorance can increase injuries. Knowledge of the prevalence of anatomical variations helps to reduce risks (Clayton, 2006).

In this study, we demonstrate that there are anatomical variants in the origin of the uterine artery, the most common being type I, with a prevalence of 85%.

Our study showed that, in 85.04% of cases, the origin of the uterine artery comes directly from the anterior trunk of the internal iliac artery. This is followed in 7.00% of cases by the variant that arises from a branch of the anterior trunk of the internal iliac artery called the inferior gluteal or superior vesical artery. It is reported that the variant called type III in our study, arising as an independent branch of the internal iliac artery, appeared in 5.1% of cases. Likewise, the appearance of the variant in the origin of the uterine artery from a branch of the anterior trunk, called the umbilical or superior vesical artery, was documented in 2.33% of the cases, a much lower proportion, unlike that reported in the study by Arfi et al. (2017), who reported observing this variant in up to 25.6% of cases.

They carried out a study in which they analyzed the anatomy of the arteries that make up the female genital tract, where they used angiography to determine their results, concluding that the best projection for visualizing the uterine artery, when it originated from the anterior division of the internal iliac artery, was the contralateral, oblique-anterior with 20- 30 degrees of inclination (Mori et al., 2010).

Three age groups were formed according to the stage of the woman's fertile life, and the diameters of the arteries were compared in two different portions and independently between the three groups, with no statistically significant findings.

In 2002, Razavi et al. conducted a study in which they analyzed and classified the place where the ovarian arteries anastomose with the uterine arteries in women who underwent uterine fibroid embolization. For this, they used 76 angiographies of female patients, finding variations in the course of the uterine artery, showing a pattern of three different types of anastomoses. In type I, the blood supply of the ovarian artery through the uterus came directly from the uterine artery; in type II, the ovarian artery supplied the fibroids directly; and in type III there was no ovarian artery, and the total blood supply to the ovary came directly from the uterine artery.

Albulescu et al. (2014) carried out a study in which the origin and trajectory of the uterine artery were analyzed in 110 angiographies of female patients, resulting in a classification with 4 types of variants.

A study led by Dr. Alexandra Arfi was conducted in 2017 at Hospital Intercommunal de Cretéil in Paris, France, where 43 3D CTA reconstructions were performed to determine the origin of the uterine artery, and the results were: direct origin of the anterior trunk together with the umbilical artery in 62.7% of cases; from a direct branch of the internal iliac artery in 25.6% of cases; directly from the superior gluteal artery in 9.3% of cases; and from the internal pudendal artery in 2.3% of cases (Arfi et al., 2017).

To our knowledge, this is the first study that, apart from determining the origin of the uterine artery, evaluates its diameters at two different points in a standardized manner. A 3D reconstruction technique is used, which allows the artery to be assessed from all angles, and to determine the incidence of other vascular diseases that affect its morphology.

According to the findings found in our study, the origin of the uterine artery is in the same proportion as that reported in the previously described literature (Wu et al., 2007; Akerman, 2019; Barodka et al., 2011).

It is worth highlighting the finding of a variant that has not been previously described, which was called Type V, and which had its origin in the left ovarian artery, which is a branch of the left renal artery.

Previous series of studies may be difficult to compare due to different descriptions of the

pelvic vascular anatomy in the radiological and surgical literature, with substantial differences in the nomenclature of the branches of the internal iliac artery.

The present study has several limitations. It is a retrospective evaluation of healthy patients, whose specific medical history is unknown, as well as their gynecological history. Nor is the height and weight of the patient taken into consideration.

This study reports five different anatomical variants in the origin of the uterine artery, categorized according to the order of appearance and frequency. The fifth variant is described for the first time and arises directly from the ovarian artery, which in turn arises directly from the left renal artery. Uterine artery diameters were determined at two different sites, without identifying statistically significant findings when grouping patients by different stages of female fertile life. Age is not a factor that favors variability in uterine arterial thickness.

The blood vessels suffer injuries with age, which correlates with the findings found in the analyzed studies of patients over 50 years of age, mainly the incidence of atherosclerosis.

ACKNOWLEDGEMENTS

To all the work team and colleagues of the institution who helped in the preparation of this study.

REFERENCES

AKERMAN AW, BLANDING WM, STROUD RE, NADEAU EK, MUKHERJEE R, RUDDY JM (2019) Elevated wall tension leads to reduced miR-133a in the thoracic aorta by exosome release. *J Am Heart Assoc*, 8(1): e010332.

ALBULESCU D, CONSTANTIN C (2014) Uterine artery emerging variants - angiographic aspects. *Curr Heal Sci J.* 40(3): 214-216.

AMERICAN COLLEGE OF OBSTETRICIANS AND GYNECOLOGISTS (2011) Planned home birth. Commitee Opin. *ACOG,* 476(476): 1-4.

ARFI A, ARFI-ROUCHE J, BARRAU V, NYANGOH-TIMOH K, TOUBOUL C (2017) Three-dimensional computed tomography angiography reconstruction of the origin of the uterine artery and its clinical significance. *Surg Radiol Anat,* 40(1): 85-90.

BARODKA VM, JOSHI BL, BERKOWITZ DE, HOGUE CW, NYHAN D (2011) Review article: implications of vascular aging. *Anesth Analg*, 112(5): 1048-1060.

CLAYTON RD (2006) Hysterectomy. *Best Pract Res Clin Obstet Gynaecol*, 20(1): 73-87.

COMMITTEE ON GYNECOLOGIC PRACTICE (2009) Choosing the route of hysterectomy for benign disease. *Obstet Gynecol*, 118(5): 1156-1158.

FLORY N, BISSONNETTE F, BINIK YM (2005) Psychosocial effects of hysterectomy. *J Psychosom Res*, 59(3): 117-129.

LAHOZ C, MOSTAZA JM (2007) La Aterosclerosis como enfermedad sistémica. *Revista Española de Cardiología*, 60(2): 184-195.

LEFEBVRE G, ALLAIRE C, JEFFREY J, VILOS G, ARNEJA J, BIRCH C, FORTIER M (2002) SOGC clinical guidelines. Hysterectomy. *J Obstet Gynaecol Can*, 24(109): 37-61.

LIU JH, GREER BE, CURTIN J (2006) ACOG Practice Bulletin #65: Management of Endometrial Cancer. *Obstet Gynecol*, 107(4): 952-953.

LOCKHART RD, FRSE CHM (1959) Anatomy of the human body. *Br J Surg*, 47: 208.

MIREA O, DONOIU I, PLEŞEA IE (2012) Arterial aging: a brief review. *Rom J Morphol Embryol,* 53(3): 473-477.

MOORE KL, DAILEY AF, AGUR AMR (2013) Clinically oriented anatomy. Wolters Kluwer Health P, pp 1-1700.

MORI K, SAIDA T, SHIBUYA Y, TAKAHASHI N, SHIIGAI M, OSADA K, TANAKA N, MINAMI M (2010) Assessment of uterine and ovarian arteries before uterine artery embolization: advantages conferred by unenhanced MR angiography. *Radiology*, 255(2): 467-475.

RAZAVI MK, WOLANSKE KA, HWANG GL, SZE DY, KEE ST, DAKE MD (2002) Angiographic classification of ovarian artery-to-uterine artery anastomoses: initial observations in uterine fibroid embolization. *Radiology,* 224(3): 707-712.

REICH H, DECAPRIO J, MCGLYNN F (1989) Laparoscopic hysterectomy. *J Gynecol Surg,* 5(2): 213-216.

ROCK JA, HOWARD W, JI, JONES III (2006) Te Linde: Ginecología Quirúrgica. In: Te Linde. *Ginecología quirúrgica*, p 1226.

SUTTON C (1997) Hysterectomy: a historical perspective. *Baillieres Clin Obstet Gynaecol,* 11(1): 1-22.

WU JM, WECHTER ME, GELLER EJ, NGUYEN TV, VISCO AG (2007) Hysterectomy rates in the United States, 2003. *Obstet Gynecol*, 110(5): 1091-1095.

Variant septation of the sphenoid sinus in adult Nigerians: CT study

Beryl Ominde[1], Joyce Ikubor[2], Wilson Iju[1], Patrick Igbigbi[1]

[1] Department of Human Anatomy and Cell Biology, Delta State University, Abraka, Nigeria
[2] Department of Radiology, Delta State University Teaching Hospital, Oghara, Nigeria

SUMMARY

Preoperative evaluation of the sphenoid sinus septa is mandatory for safe endoscopic endonasal transsphenoidal surgery. This study aimed at elucidating the variant septation of the sphenoid sinus using computed tomographic images of adult patients. This observational study retrospectively evaluated 336 brain Computed Tomographic images of adult patients seen in a Nigerian Teaching Hospital. The study was approved by the Research Committee of the Hospital. The presence, number, location and attachment of the sphenoid sinus septum were studied and recorded. Statistical Package for Social Sciences version 23 was used to analyze the prevalence of the variants and compare them based on gender and side using the Chi-square test. The level of significance was considered at $p<0.05$.

The prevalence of a single complete septum was 179 (53.3%), while double and multiple septa had a frequency of 88 (26.2%) and 69 (20.5%) respectively. The complete septum was predominantly located in the paramedian position (185, 69.3%). The septa attached onto the carotid canal and optic canal in 91 (27.1%) and 46 (13.7%) patients respectively. The multiple and double septa had a high predilection for the carotid (52, 75.4%) and optic (32, 36.4%) canal insertions respectively. These patterns of septation did not show any significant relationship with gender or side ($P>0.05$). The single septum was the most prevalent and frequent in the paramedian location, while multiple and double septa commonly insert onto the carotid and optic channels respectively.

Key words: Sphenoid – Sinus – Septum – Canal – Surgery

INTRODUCTION

The sphenoid sinus (SS) has been described as the most surgically inaccessible sinus, owing to its deep location in the base of the skull (Singh et al., 2019). It is the first paranasal sinus to develop from the third to the fourth month of intrauterine life (Ominde et al., 2021). From birth to three years of age, it exists as a pit in the sphenoethmoidal recess (Degaga et al., 2020; Singh et al., 2022). Thereafter, pneumatization begins and proceeds posteriorly, leading to a visible definitive cavity at puberty (Fasunla et al., 2012; Wani et al., 2019). The sinus continues to expand with age, following the growth of the sphenoid bone. With advancing age, resorption of its bony walls causes further SS expansion (Kusch and Garcia, 2019).

Corresponding author:
Beryl S. Ominde. Department of Human Anatomy, Delta State University, P.M.B. 1, Abraka, Nigeria. Phone: +2347085458946. E-mail: berylominde@gmail.com

Submitted: May 13, 2022. **Accepted:** June 7, 2022

https://doi.org/10.52083/USGL2455

The variant patterns of development and pneumatization of the SS have led to asymmetry in its shape, size, and septation (Wani et al., 2019). The varying aeration consequently contributes to the differences in number and locality of SS septa over and above the inconsistent position of the optic canal that houses the optic nerve and the carotid canal containing the internal carotid artery (ICA) (Ominde et al., 2021). The complete intersinus septum divides the SS into asymmetric compartments, while the incomplete intrasinus/ partial septa are within the sinus but do not divide it completely (Kusch and Garcia, 2019; Singh et al., 2022). The partial septa are a result of resistant pneumatization at the sites of fusion between various bone ossification centers (Ngubane et al., 2018). The SS septa may insert onto the neighbouring ICA canal or optic nerve canal (Secchi et al., 2018; Ismail et al., 2018). Studies in literature have documented the variation in the number, location and attachment of the SS septa in various populations (Famurewa et al., 2018; Wani et al., 2019; Degaga et al., 2020; Dziedzic et al., 2020; Singh et al., 2022;).

The SS serves as a surgical corridor in accessing the structures in the middle and posterior cranial fossa (Singh et al., 2022). Endoscopic endonasal transsphenoidal surgery is indicated in tumors within the sellar, suprasellar, and parasellar regions (Aksoy et al., 2017). During surgery, excessive traction on the septa may cause avulsion of ICA and optic canals, consequently damaging the neurovascular structures (Singh et al., 2019). The awareness of the number and locality of the SS septa is therefore mandatory preoperatively to minimize surgical complications. Computed Tomography (CT) is the imaging modality of choice for assessing the variant complex anatomical framework of the SS, in addition to the presence and extent of sinus disease (Secchi et al., 2018; Ominde and Igbigbi, 2021; Arutperumselvi et al., 2022). This study, therefore, aimed at elucidating the variant septation of the SS in adult patients who underwent CT imaging in a Teaching Hospital in Delta State, Nigeria.

MATERIALS AND METHODS

This research adopted the retrospective cross-sectional design of descriptive nature. Using purposive sampling technique, brain CT images of 336 patients with suspected intracranial tumors or bleeds and chronic headache, who presented to the Radiology Department of a Teaching Hospital within a duration of five years, spanning between 1 June 2015 and 30June 2020 were selected. These non-contrast brain CT studies were conducted using a 64-slice CT scanner (Toshiba Aquilon, Japan, 2009) and stored in the archives of the Department. The settings for image acquisition was at 120 kV and 300 mA in 3 mm thick axial CT slices. According to the protocol adopted by the Department, the axial slices were taken from the base of the skull to the vertex, to ensure the inclusion of the paranasal sinuses, which are also evaluated for incidental sinusitis in patients with a history of headache. Ethical approval was granted (EREC/PAN/2020/030/0371) by the institutions Research Committee prior to accessing the images. Images with adequate exposure, symmetry, and specified age and gender of the patient were used. The study included images of adults aged 20 years and above, owing to the fact that the SS reaches its adult size at 20 years (Ominde et al., 2021). We excluded all the images of patients below 20 years, images with visible craniofacial fractures and congenital anomalies, presence of sinonasal tumors, cysts or infection and evidence of previous sinus surgery or skull base surgery.

Using a slice thickness of 1.5mm and table increment of 1.5mm as the reconstruction parameters, the axial CT slices were reformatted into multiplanar coronal and sagittal sections. All the three views were displayed on bone window to allow accurate evaluation of the variant SS septa. The presence, number, and location of septa in addition to the attachment of the septa onto the carotid and optic canals on each side were assessed. A septum running from one wall of the SS to another and fully compartmentalizing it was regarded as a complete septum. In addition, a septum located within the sinus but failing to completely divide the SS was referred to as a partial septum (Kusch and Garcia, 2019). Data were recorded on datasheets and transferred to Statistical Package for Social Sciences (SPSS), version 23 (IBM® Armonk, New York), for analysis. The data were grouped based on side and gender.

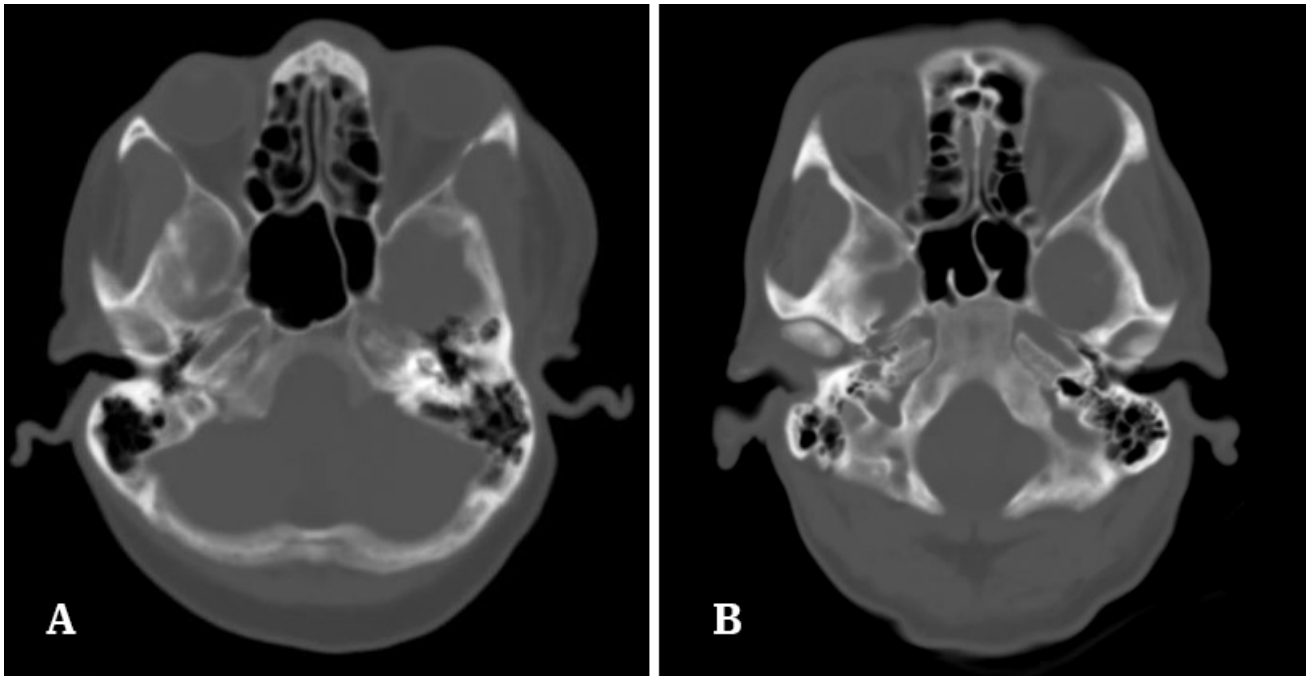

Fig. 1.- Axial CT images depicting the SS septa. **A**: single complete septum located paramedian **B**: Single complete septum with partial septa projecting in the sphenoid sinus bilaterally.

The prevalence of the variants was summarized in percentages based on the groupings. Thereafter, group comparisons were assessed using the Chi-square test, and these were considered significant at $p < 0.05$.

RESULTS

The study used 199 (59.2%) males and 137 (40.8%) females with a mean age of53.29±18.18 years. All the CT images evaluated had at least one sphenoid sinus septum present. The prevalence of a single complete septum was 179 (53.3%) (Fig. 1A). Double septa (comprising one complete and one partial septum) were observed in 88 (26.2%) patients. The remaining 69 patients (20.5%) had multiple septa comprising a single complete septum and ≥2 incomplete septa (Fig. 1B). The number of SS septa had no significant association with gender (P>0.05) (Table 1).

The single complete septum predominantly had a paramedian location (185, 69.3%), while a midline location of the intersphenoid septum was observed in 82 (30.7%) patients. The partial septa were more preponderant within the right SS (88, 56.1%) than the left (69, 43.9%) SS. However, this was not statistically significant (p=0.063).

The attachment of the SS septum onto the carotid canal was observed in 91 patients (27.1%), and commonly occurring unilaterally (62, 18.5%) than bilaterally (29, 8.6%) (Fig. 2A). The unilateral occurrence was higher on the right (42, 12.5%) than on the left (20, 6%) carotid canal. The insertion of the septa onto the optic canal occurred only unilaterally (46, 13.7%) with

Table 1. Number of sphenoid septa based on gender.

Number of septa	Total		Female		Male		P value
	N	%	N	%	N	%	
Single	179	53.3	76	55.5	103	51.8	0.504
Double	88	26.2	32	23.4	56	28.1	0.421
Multiple	69	20.5	29	21.2	40	20.1	0.381
Total	336		137		199		

a higher preponderance on the right (29, 8.6%) than the left (17, 5.1%) optic canal (Fig. 2B). The insertion of the septa onto the optic and ICA canals had no association with side or gender (P>0.05) (Table 2). Table 3 shows the prevalence of septal attachment onto the optic and carotid canals in different study populations. In the evaluation of the patients with SS septa, the prevalence of the septa attaching to the carotid canal was highest in patients with multiple septa (52, 75.4%), followed by double septa (33, 37.5%), and lastly single septum (6, 3.4%). On the other hand, optic canal insertions were predominant in patients with double septa (32, 36.4%), followed by multiple septa (13, 18.8%). Out of the 179 patients with a single SS septum, insertion onto the optic canal was only observed in one patient (0.6%).

DISCUSSION

A single complete inter-sphenoid septum was observed in 53.3% of cases, and this corresponded with the findings of Arutperumselvi et al. (2022) in India. This frequency was lower than 88.2% and higher than 46.9%, documented in previous Nigerian studies in Oyo and the Osun States respectively (Fasunla et al., 2012; Famurewa et al., 2018). Higher frequencies were documented in Ethiopia, India, Poland, and Belgium (Ismail et al., 2018; Wani et al., 2019; Degaga et al., 2020; Dziedzic et al., 2020). Double septa comprising

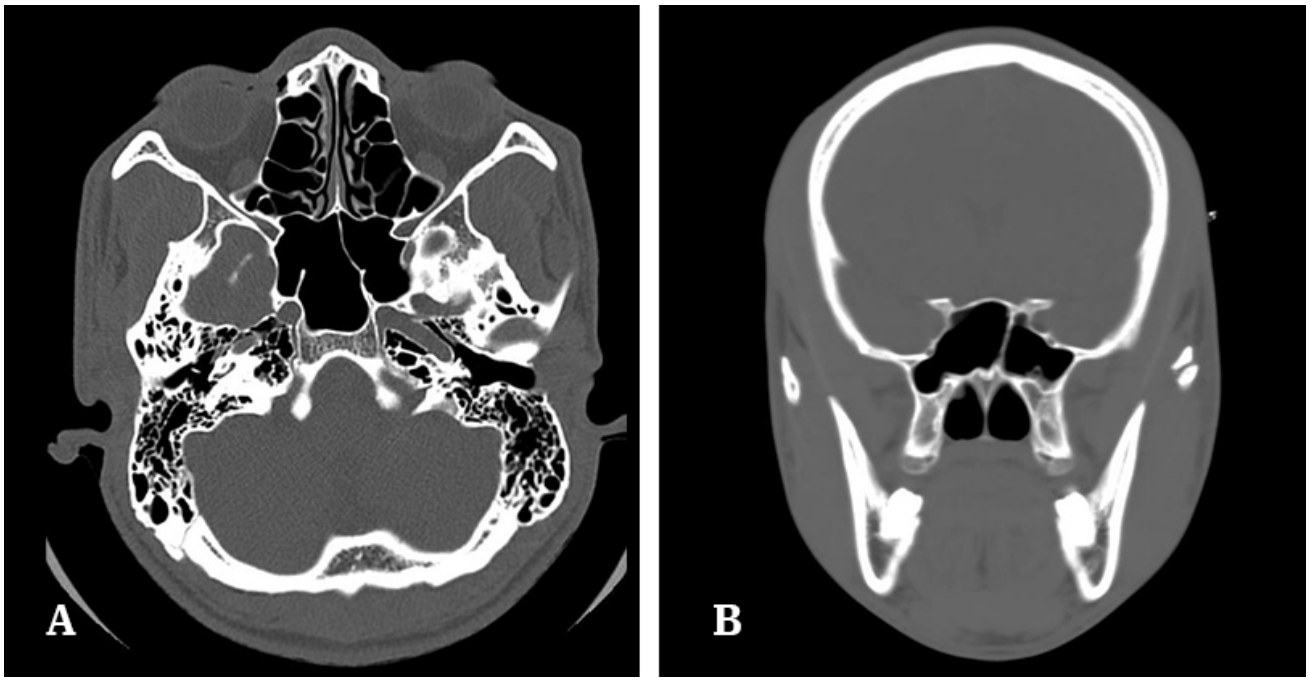

Fig. 2.- Axial CT images showing the sphenoid sinus septa attaching on: **A**: ICA canal bilaterally. **B**: left optic canal.

Table 2. Attachment of the sphenoid septa on to the carotid and optic canals.

Canal	Side	Total		Female		Male		*P value
		N	%	N	%	N	%	
Carotid	Right	71	21.1	28	20.4	43	21.6	0.796
	Left	49	14.6	23	16.8	26	13.1	0.342
	¶P value			0.184		0.149		
Optic	Right	29	8.6	12	8.8	17	8.5	0.945
	Left	17	5.1	4	2.9	13	6.5	0.138
	¶P value			0.247		0.396		

¶ P value for the side differences, * P value for gender differences

Table 3. Attachment of the SS septa onto the optic and carotid canals in different studies.

Author	Country	N	CT slice thickness	Septum attachment (%)	
				Carotid canal	Optic canal
Singh et al. (2022)	India	84	1 mm	29.7	27.4
Fasunla et al. (2012)	Nigeria	110	3 mm	4.5	
Wani et al. (2019)	India	591		Right 6.5 Left 23	0.4
Famurewa et al. (2018)	Nigeria	320	2.5 mm	31.6	
Aksoy et al. (2017)	Turkey	347	3 mm	47.7	17.5
Arutperumselvi et al. (2022)	India	100		20	
Joghataei et al. (2019)	Iran	129		76	
Sumaily et al. (2018)	Saudi Arabia	420	1 mm	16.4	29.4
Current study	Nigeria	336	3 mm	27.1	13.7

one complete and one incomplete septum were observed in 26.2% of cases, and this was higher than reports by Fasunla et al. (2012) and Wani et al. (2019) and lower than the 32% documented by Dziedzic et al. (2020). We observed multiple septa (single complete with ≥2 partial septa) in 20.5% of the patients, and this was lower than the frequency among the Nigerians of Osun State (Famurewa et al., 2018). Furthermore, this frequency was higher than the findings in India, but lower than the reports from Turkey (Aksoy et al., 2017; Wani et al., 2019). The awareness of multiple SS septa is important, since they are commonly seen in acromegaly (Dziedzic et al., 2020). Akin to Aksoy et al., (2017), we did not observe the absence of SS septa. This was contrary to Gibelli et al. (2019), Dziedzic et al. (2020), and Degaga et al. (2020), who documented the absence of SS septa in 21.9%, 2%, and 1% of their studied population respectively.

The location of the single complete septum was predominantly paramedian (69.3%). This was consistent with the reports by Ismail et al. (2018), and contrasted with Famurewa et al. (2018). According to Dziedzic et al. (2020), the low occurrence of the single midline septum infers that another midline anatomical landmark is required during transsphenoidal procedures. The frequency of the incomplete septa was not significantly associated with side of the sinus location. This was conflicting with the findings in Osun State, where the partial septa were predominantly on the left (Famurewa et al., 2018). Similar to the reports by Wani et al. (2019), the number and position of the SS septa were not influenced by gender. Therefore, their variance in the literature could be accredited to differences in genetics, ethnicity, race, environmental and geographical factors which influence the pneumatization patterns of the SS and ethmoid sinuses (Ominde et al., 2021). The awareness of the number of SS septa and their location is essential preoperatively to inform on the possible surgical challenges hence plan for a safe surgical route and technique.

The presence of SS septa attaching onto the carotid canal was observed in 27.1% of the skull images, and with a more frequent unilateral than bilateral occurrence. This prevalence was comparable to 29.7% documented by Singh et al. (2019). Our finding was lower than the 31.6% and higher than the 4.5% documented in previous Nigerian studies (Fasunla et al., 2012; Famurewa et al., 2018). Additionally, higher frequencies have been documented by Aksoy et al. (2017), Joghataei et al. (2019), and Dziedzic et al. (2020), while Dafalla et al. (2017) and Arutperumselvi et al. (2022) reported lower frequencies. Insertion onto bilateral carotid canals was observed in 8.6% of cases and this was slightly higher than the 6.9% and lower than the 14% reported by Famurewa et al. (2018) and Dziedzic et al. (2020), correspondingly.

The frequency of the septum inserting onto the wall of the optic canal (13.7%) was higher than the

observations by Wani et al. (2019) and Gibelli et al. (2019). On the contrary, higher frequencies in Saudi Arabia and India have been reported (Aksoy et al., 2017; Sumaily et al., 2018; Singh et al., 2019). Parallel to the documented reports by Wani et al. (2019), gender had no association with the insertion of SS septa onto the neurovascular canals. The variance in literature could be ascribed to race, ethnicity, genetics besides dissimilarities in the sample size and CT slice thickness used in evaluating the sinuses (Table 3).

Our study reports a higher tendency of the multiple septa to be inserted on to the carotid canal (75.4%), while the double septa are associated with a higher propensity for optic canal insertion. Similarly, Dziedzic et al. (2020) documented that multiple septa of the SS have a high tendency to insert onto the ICA canal. We further observed that the single septum rarely inserts onto the neurovascular canals. From these findings, this study suggests that, after the radiological evaluation for the number of SS septa, it is imperative to evaluate for their possible insertions to the optic and carotid canal preoperatively.

The awareness of the SS septa inserting onto neurovascular canals is important before endoscopic transnasal sphenoidal surgery to avoid excessive traction on the septum during neuro-navigation (Singh et al., 2019). Such septa require removal via drilling rather than fracture (Dziedzic et al., 2020). Avulsion of the bone that forms the canal wall may rupture the ICA, leading to massive bleeding which may be fatal. This is because the complex anatomy and deep location of the SS make it difficult to control the bleeding from the adjacent ICA. Subsequently, this causes retrobulbar hematoma with acute proptosis (Ominde and Igbigbi, 2021). It is recommended that the septum attaching on the ICA canal be drilled at high speed, parallel to the ICA course to avoid its injury (Dziedzic et al., 2020). Injury of the optic nerve by an avulsed SS septum may lead to blindness (Dafalla et al., 2017).

CONCLUSION

The single septum was the most prevalent and frequent in the paramedian location, while multiple and double septa commonly insert onto the carotid and optic channels respectively.

ACKNOWLEDGEMENTS

We would like to acknowledge Priscilla Ejiroghene and Emmanuel Akpoyibo, who assisted with data collection and analysis. We also appreciate the resident doctors in the Radiology Department of the Teaching Hospital for the technical help during data collection process.

REFERENCES

AKSOY F, YENIGUN A, GOKTAS SS, OZTURAN O (2017) Association of accessory sphenoid septa with variations in neighbouring structures. *J Laryngol Otol,* 131: 51-55.

ARUTPERUMSELVI VS, MALAISAMY A, RAMAKRISHNAN KK, YARLAGADDA S, SHARMA PK, THANGARAJAH A, RAJAN SC (2022) A review of common anatomical variants of paranasal sinuses and nasal cavity and its frequency of occurrence as evidenced on multi-detector computed tomography. *Int Arch Integr Med*, 9(1): 8-21.

DAFALLA SE, SEYED MA, ELFADIL NA, ELMUSTAFA OM, HUSSAIN Z (2017) A Computed Tomography-aided clinical report on anatomical variations of the paranasal sinuses. *Int J Med Res Health Sci,* 6(2): 24-33.

DEGAGA TK, ZENEBE AM, WIRTU AT, WOLDEHAWARIAT TD, DELLIE ST, GEMECHU JM (2020) Anatomographic variants of sphenoid sinus in Ethiopian population. *Diagnostics,* 10: 970.

DZIEDZIC T, KOCZYK K, GOTLIB T, KUNERT P, MAJ E, MARCHEL A (2020) Sphenoid sinus septations and their interconnections with parasphenoidal internal carotid artery protuberance: radioanatomical study with literature review. *Videosurgery Miniiv*, 15: 227-233.

FAMUREWA OC, IBITOYE BO, AMEYR SA, ASALEYE CM, AYOOLA OO, ONIGBINDE OS (2018) Sphenoid sinus pneumatization, septation and the internal carotid artery: A computed tomography study. *Niger Med J*, 59: 7-13.

FASUNLA AJ, AMEYE SA, ADEBOLA OS, OGBOLE G, ADELEYE AO, ADEKANMI AJ (2012) Anatomical variations of the sphenoid sinus and nearby neurovascular structures seen on computed tomography of black Africans. *East Cent Afr J Surg*, 17(1): 57-64.

GIBELLI D, CELLINA M, GIBELLI S, CAPELLA A, OLIVIA AG, TERMINE G, SFORZA C (2019) Relationship between sphenoid sinus volume and accessory septation: A 3D assessment of risky anatomical variants for endoscopic surgery. *Anat Rec,* 303: 1300-1304.

ISMAIL M, ABDELHAK B, MICHEL O (2018) Endoscopic sphenoid sinus anatomy in view of transphenoidal surgery: Standardized way-point cadaver dissection. *Egypt J Ear Nose Throat Allied Sci*, 19(2): 38-44.

JOGHATAEI MT, HOSSEINI A, ANSARI MJ, GOLCHINI E, NAMJOO Z, MORTEZAEE K, PIRASTEH E, DEHGHANI A, NASSIRI S (2019) Variations in the anatomy of sphenoid sinus: a computed tomography investigation. *J Pharm Res Int*, 26(3): 1-7.

KUSCH AM, GARCIA VR (2019) Giant pneumatization of sphenoid sinus: Report of four cases and review of literature. *Rev Med Hered,* 30: 45-49.

NGUBANE NP, LAZARUS L, RENNIE CO, SATYAPAL KS (2018) The septation of the sphenoidal air sinus. A cadaveric study. *Int J Morphol*, 36(4): 1413-1422.

OMINDE BS, IGBIGBI PS (2021) Variant neurovascular relations of the sphenoid sinus in adult Nigerians. *Niger Postgraduate Med J*, 28(2): 112-116.

OMINDE BS, IKUBOR J, IGBIBGI PS (2021) Pneumatization patterns of the sphenoid sinus in adult Nigerians and their clinical implications. *Ethiop J Health Sci*, 31(6): 1295-1302.

SECCHI MM, DOLCI RL, TEIXEIRA R, LAZARINI PR (2018) An analysis of anatomic variations of the sphenoid sinus and its relationship to the internal carotid artery. *Int Arch Otorhinolaryngol*, 22(2): 161-166.

SINGH A, MANJUNATH K, SINGH H (2022) Relationship of sphenoid sinus to adjacent structures in South India: a retrospective cross-sectional study. *Egypt J Otolaryngol*, 38: 8.

SINGH BP, METGUDMATH RB, SINGH D, SAXENA U (2019) Anatomical variations of sphenoid sinus among patients undergoing computed tomography of paranasal sinus. *Int J Otorhinolaryngol Head Neck Surg,* 5(4): 888-892.

SUMAILY I, ALDHABAAN S, HUDISE J (2018) Anatomical variations of PNS. Gender and age impact. *Glob J Otolaryngol*, 14(1): 007-0014.

WANI AH, SHIEKH Y, PARRY AH, QAYOOM Z (2019) Anatomical variations of intra-sphenoid sinus septations in a sample of Kashmiri population: a non-contrast computed tomography study. *Int J Res Med Sci*, 7(5): 1445-1449.

Cadaveric study of morphology of caudate lobe of the liver in North Indian population

Ruchi Sharma[1], Yogesh Yadav[2], Pankaj Wadhwa[3], Ashish Gautam[4], Nisha Kaul[1]

[1] *Santosh Medical college, Ghaziabad, Uttar Pradesh- 201204, India*

[2] *Noida International Institute of Medical Sciences, Noida, Uttar Pradesh - 201301, India*

[3] *Department of Pharmaceutical Chemistry, School of Pharmaceutical Sciences, Lovely Professional University, Phagwara, Punjab – 144 411, India*

[4] *Yashoda Super Specialty Hospital, Ghaziabad, Uttar Pradesh- 201001, India*

SUMMARY

The caudate lobe is a vertically elongated central projection from posterior surface of liver. It is bordered on the right by the groove for the inferior vena cava (IVC), on the left by the fissure for the ligamentum venosum, and on the bottom by the porta hepatis. It is continuous on the superior aspect with the upper part of the right limb of the fissure for the ligamentum venosum. The morphology of the caudate lobe was studied in 100 cadaveric human livers (15-70 years old) stored in 10% formaldehyde, regardless of gender, obtained from the department of anatomy at Santosh Medical College in Ghaziabad. The caudate lobe was observed in a variety of shapes. Vertical fissures extending upward from the lower border of the caudate lobe were seen in 52% of the liver specimens, while accessory caudate fissures extending downward from the upper border were seen in 9% and accessory transverse fissures were seen in 3% cases. Caudate notch was horizontal in 11% of liver specimens. The papillary process was visible in 27% of the liver specimens; a hook shape of the papillary process was seen in one liver specimen. Caudate process was present in 18% of the cases. Linguiform process was observed in 46% of cadaveric liver specimens.

As observed, the incidences of morphological variations of the caudate lobe are very high, so it is critical for both radiologists and surgeons to keep these variations in mind when making diagnoses and planning surgeries for a favourable clinical outcome.

Key words: Accessory fissure – Caudate lobe – Cadaveric liver – Cadaveric morphology – Vertical fissure – Papillary process – Linguiform process

INTRODUCTION

The fold of peritoneum and ligaments anatomically separate the liver into four lobes (Standring et al., 2005), with the caudate lobe as a left lobe being one of them (Chavan and Wabale, 2014; Sagoo et al., 2018). “Lobus Exiguus” is the first name of the caudate lobe, given by Adrien van den Spiegel in 1622; Glisson renamed it as “Spiegel’s lobe” in 1654; and in 1957 it was renamed “segment 1” by Couinaud (Gardner

Corresponding author:
Dr Pankaj Wadhwa. Department of Pharmaceutical Chemistry, School of Pharmaceutical Sciences, Lovely Professional University, Phagwara, Punjab – 144 411, India. E-mail: pankajwadhwa88@gmail.com
Dr Ruchi Sharma. Santosh Medical college, Ghaziabad, Uttar Pradesh-201204, India. Email: ruchi65sharma@gmail.com. Phone: +91-9968232704

Submitted: April 21, 2022. **Accepted:** June 14, 2022

https://doi.org/10.52083/EUZM3304

et al., 2019). The caudate lobe is a vertically elongated midline projection from the posterior surface of the liver (Sibulesky, 2013). It is bound on the right by the groove for the inferior vena cava (IVC), on the left by the fissure for the ligamentum venosum, on the bottom by the porta hepatis, and on the top by the superior surface of the right upper end of the fissure for the ligamentum venosum (Dodds et al., 1990; Sagoo et al., 2018). The caudate lobe proper and the caudate process are two portions of the caudate lobe that are joined by the caudate isthmus, a thin parenchymal bridge (Gardner et al., 2019; Sarala et al., 2015). The first part is Spiegel's lobe (Couinaud's segment 1) to the left of IVC, and the second part is paracaval portion (caudate process), which extends anterior and to the right of IVC and connects the right lobe (Chavan and Wabale, 2014; Gardner et al., 2019; Sagoo et al., 2018). The papillary process is a small, rounded projection formed by the medial inferior part of the caudate lobe (Joshi et al., 2009). The caudate lobe gets its name from the fact that it frequently produces a tail-like process known as papillary process, rather than because of its caudal location (Sadanandan and Varghese, 2017). It is a distinct part of the liver ,with its own vascular and biliary drainage system (Sarala et al., 2015). It has intriguing characteristics, especially in a case of cirrhosis (Sadanandan and Varghese, 2017). The complex anatomy of the caudate lobe makes cross-sectional images difficult to interpret, especially when the papillary process is enlarged or involved in diseases (Auh et al., 1984; Chavan and Wabale, 2014; Sadanandan and Varghese, 2017). The development of the caudate lobe is a complicated process. Both the right and left lobes of the liver give rise to the caudate lobe. Dodds and his colleagues proposed a theory to explain the development of the liver's caudate lobe. According to their findings, as the liver enlarges in the second trimester, the liver and mesentery of the ductus venosus rotate rightward, causing a small portion of the liver, the caudate lobe, to emerge (Dodds et al., 1990). In another study, Joshi et al. (2009) discovered rectangular shape in 58 % of the cases, triangular in 8%, irregular in 20%, a pear shape in 10%, and other shapes (square, heart, inverted flask, etc.) in 4%.

For localised benign tumours of the caudate lobe, lobectomy is the treatment of choice (Xu and Huang, 2010). Safe resection of the caudate lobe is still a challenge for surgeons. Thus, knowledge of the variations in the caudate lobe anatomy aids anatomists and radiologists in better analysing CT, MRI, and other imaging studies to avoid misdiagnosis, as well as surgeons in planning surgeries with favourable clinical outcomes and in diagnostic imaging. The goal of this study is to investigate the morphology of the caudate lobe of the human liver, as well as its variation.

MATERIALS AND METHODS

This study was conducted on 100 formalin fixed human livers (15-70 years) irrespective of sex, obtained from the department of anatomy, Santosh Medical College Ghaziabad.

Inclusion criteria: all cadaveric liver specimen included in this study had normal anatomical features.

Exclusion criteria: liver specimen with diseased and features of damaged, hepatic surgery or tumours were excluded from this study.

The shape, variation in the papillary and caudate processes, the existence of fissures, and the presence and absence of the linguiform process were all investigated in the gross anatomy of the caudate lobe (pons hepaticus). Complete pons hepaticus occurs when the IVC's retrohepatic section is entirely covered from its posterior end. When the pons hepaticus was partially completed, it covered the posterior portion of the IVC's retro hepatic section.

RESULTS AND OBSERVATIONS

In the present study, a total of 100 embalmed specimen of cadaveric human liver were studied. On examining the caudate lobe, it was found that there were no livers with caudate agenesis. The majority of caudate lobes in all livers are rectangular in shape (62%), followed by irregular (18%), pyriform (12%), triangular (3%), dumbbell (3%), horse shoe shape (1%), and like slit 1 (1%) shaped caudate lobes, as mentioned in Table 1.

Table 1. Representing the caudate lobe's shape-based classification.

SHAPE OF CAUDATE LOBE		
TYPE OF SHAPE	**NUMBERS OF LIVER SPECIMEN**	**% AGE OF LIVER SPECIMEN**
Rectangular	62	62
Irregular	18	18
Pyriform	12	12
Dumbbell	03	03
Triangular	03	03
Horseshoe	01	01
Slit Like	01	01

In Table 2, the characteristics of the cadavers such as age, sex and weight is also described for selected liver specimens.

The vertical caudate fissure extending upward from the lower border was observed in 62 % of the cadaveric liver specimens (Fig. 1A). The

Table 2. Showing the basic characteristics of the cadavers.

SERIAL NUMBER	AGE (IN YEARS)	SEX (M/F)	WEIGHT(GM)
1.	15	M	1445
2.	23	M	1772
3.	27	M	1680
4.	37	M	1789
5.	37	F	1810
6.	39	M	1867
7.	42	M	1787
8.	44	M	1850
9.	46	M	1759
10.	46	F	1450
11.	47	F	1278
12.	48	M	1800
13.	48	F	1722
14.	49	F	1786
15.	49	M	1789
16.	49	M	1850
17.	50	M	1745
18.	50	F	1590
19.	51	F	1353
20.	51	F	1366
21.	52	M	1484
22.	52	M	1722
23.	52	F	1452
24.	53	F	1588
25.	53	M	1668
26.	53	F	1670
27.	54	M	1737
28.	54	F	1756
29.	55	F	1775
30.	55	F	1637
31.	55	F	1437
32.	56	M	1900

SERIAL NUMBER	AGE (IN YEARS)	SEX (M/F)	WEIGHT(GM)
33.	57	F	1400
34.	57	F	1345
35.	57	F	1436
36.	57	M	1787
37.	57	F	1638
38.	57	M	1735
39.	57	F	1190
40.	58	M	1762
41.	58	M	1236
42.	58	M	1543
43.	58	F	1735
44.	58	F	1647
45.	58	M	1670
46.	58	M	1785
47.	59	M	1788
48.	59	F	1686
49.	59	M	1432
50.	60	M	1690
51.	60	F	1545
52.	60	M	1715
53.	61	M	1566
54.	61	F	1434
55.	62	M	1764
56.	62	F	1544
57.	63	M	1578
58.	63	M	1732
59.	63	M	1460
60.	64	M	1745
61.	64	F	1230
62.	64	F	1373
63.	65	M	1792
64.	65	M	1800
65.	65	F	1158
66.	65	F	1830
67.	65	F	1120
68.	66	F	1710
69.	66	F	1562
70.	66	M	1570
71.	66	F	1563
72.	66	M	1637
73.	66	F	1379
74.	66	M	1784
75.	67	M	1700
76.	67	M	1745
77.	67	F	1690
78.	67	F	1627
79.	67	F	1162
80.	67	M	1763
81.	68	M	1800
82.	68	M	1764
83.	68	F	1672

SERIAL NUMBER	AGE (IN YEARS)	SEX (M/F)	WEIGHT(GM)
84.	68	F	1736
85.	68	F	1050
86.	69	M	1675
87.	69	M	1630
88.	69	F	1565
89.	69	M	1530
90.	69	F	1320
91.	69	M	1465
92.	69	M	1647
93.	70	M	1445
94.	70	M	1045
95.	70	M	1257
96.	70	M	1761
97.	70	M	1576
98.	70	M	1645
99.	70	F	1753
100.	70	M	1680

accessory caudate fissure (Fig. 1C), which extends downwards from the upper border, was detected in 9% of liver specimens, as were the accessory transverse fissure (Fig. 1B), which was seen in 3% of liver specimens, and the accessory oblique fissure, which has been seen in 6% liver specimens. At the inferior border of the caudate lobe, 11% of liver specimens had horizontal caudate notches (Fig. 1G). In 15% of cadaveric liver specimens, the accessory fissure was visible between the caudate process and the duodenal impression. There was a link between the vertical inferior fissure in the caudate lobe and the accessory fissure present between the duodenal impression and the caudate process in 5 of the 15 liver specimens. The papillary process (Figs. 1C and 1H) was prominent and visible in 27% of the livers, with 16 of them being very prominent. In 18% of the cadaveric liver specimens, a prominent caudate process (Figs. 1C and 1H) was also observed. The shape of the papillary process in one specimen is similar to a hook (Fig. 1I), for which there is no existing description and no comparable finding in the literature. As shown in Table 3, pons hepaticus and linguiform process were found in 58% of cadaveric liver specimens, covering the retro-hepatic IVC to varying degrees.

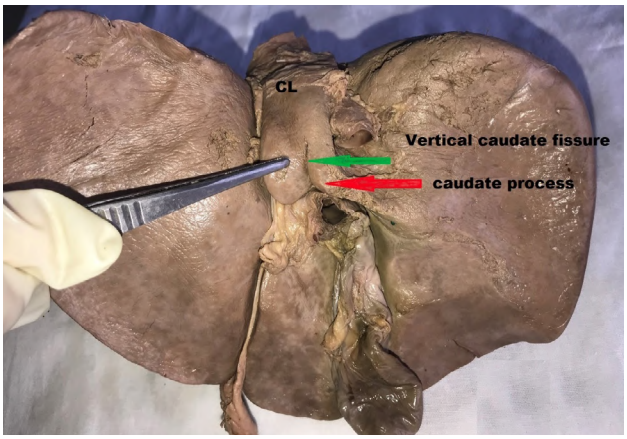

1A: The caudate lobe (CL) is shown in its rectangular shape, with forceps on the papillary process.

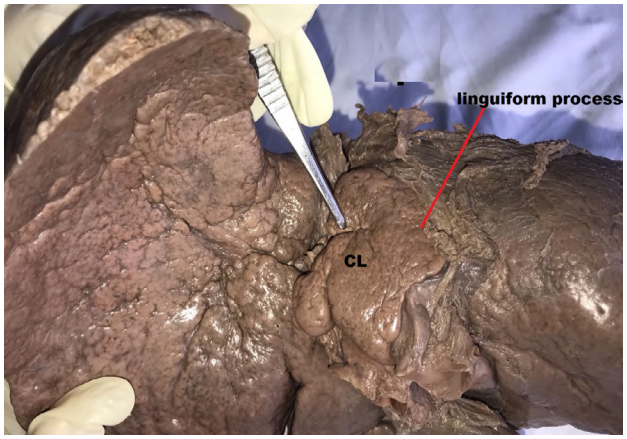

1B: Showing irregular shape of caudate lobe; forceps is on accessory transverse fissure on caudate lobe.

Fig. 1.- A-B: Represents the cadaveric morphology of the liver's caudate lobe.

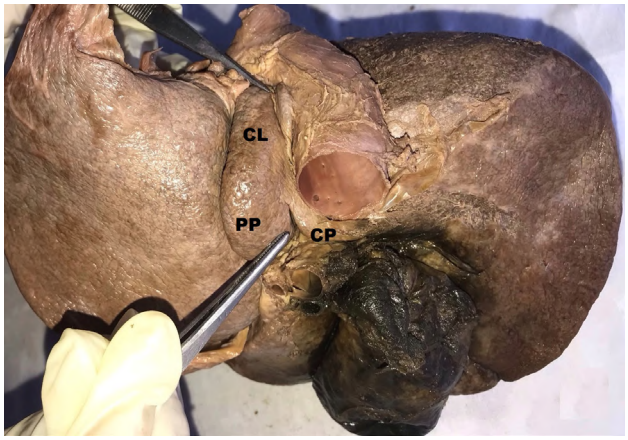

1C: Representing pyriform shape of caudate lobe (CL); Prominent papillary process (PP); Caudate process (CP); Upper forceps is pointing on accessory caudate fissure (vertical) extending downward from upper border of caudate lobe.

1D: Demonstration of triangular shape of caudate lobe (CL).

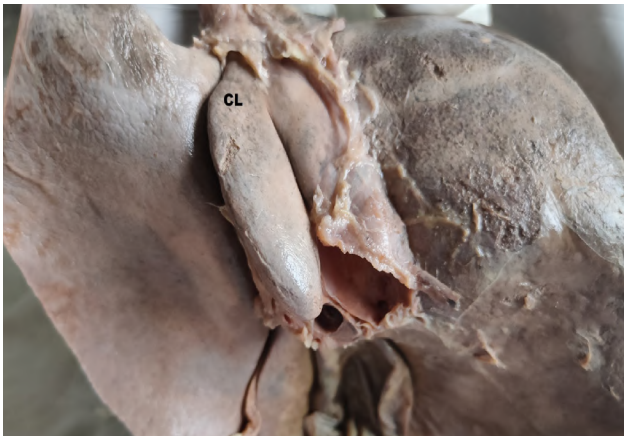

1E: Showing horseshoe shape caudate lobe (CL).

1F: Representing forceps on vertical caudate fissure.

1G: Displaying the caudate notch.

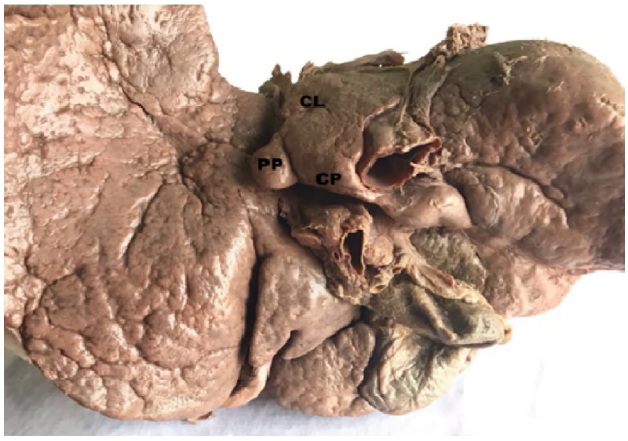

1H: Representing caudate lobe (CL); Papillary process (PP); Caudate process (CP).

Fig. 1.- C-H: Represents the cadaveric morphology of the liver's caudate lobe.

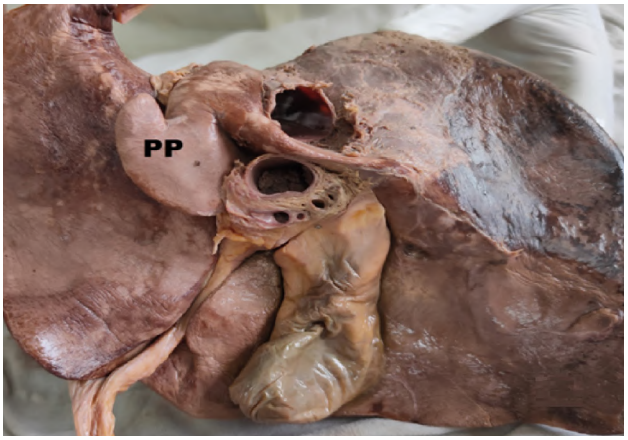

1I: Representing a papillary process with a hook shape (PP).

1J: Here the arrow is on the linguiform process, which covers the retro hepatic IVC, and the forceps is inserted into the IVC.

Fig. 1.- I-J: Represents the cadaveric morphology of the liver's caudate lobe.

Table 3. Representing the caudate lobe's shape-based classification.

PONS HEPATICUS / LINGUIFORM PROCESS	NUMBERS OF LIVERS	% AGE OF LIVER
COMPLETE	16	16
PARTIAL	42	42
ABSENT	42	42

DISCUSSION

According to Sagoo and colleagues, the rectangular shape of the caudate lobe was found in the majority of cases in NWI population livers, and it was the least common in UKC population livers. According to the group, 60 % of NWI people and 80 % of UKC people have a well-developed caudate process (Sagoo et al., 2018). Wabale and his co-workers (Chavan and Wabale, 2014) discovered a notch at the inferior edge of the caudate lobe in 54% of livers. In 21.4% of the livers, Michael and colleagues (Gardner et al., 2019) observed an inferior caudate notch, and 19.6% of the livers had a vertical caudate fissure. Sarala and her colleagues revealed a notch separating the caudate lobe from the caudate process in 31% of livers, and a vertical fissure extending upward from the inferior border in 30% of instances (Sarala et al., 2015). Chavan and his colleagues observed no papillary process in any of their study groups, but many others have reported a 52% prevalence of papillary process in the UKC population (Chavan and Wabale, 2014; Dodds et al., 1990; Gardner et al., 2019; Sagoo et al., 2018; Sarala et al., 2015; Sibulesky, 2013). In addition, Joshi and co-workers discovered a vertical caudate fissure in 30% of the livers and notching along the inferior border of the caudate lobe in 18% of the livers (Joshi et al., 2009). Auh et al. (1984) also reported variability in the caudate process in a North American study. According to Reddy and his colleagues, rectangular shapes were found in 78.75% of the livers, pear shapes in 16.25%, and other shapes in one or two livers. In 35% of the livers, they discovered a vertical fissure extending upward from the lower border of the caudate lobe (Reddy et al., 2017). They also discovered caudate processes in all of the examined livers, which were of varying thickness. Aside from that, they discovered a prominent papillary process in 46.25 % of the cases; papillary process is very prominent in 18.9 % of the cases (Reddy et al., 2017; Sahni et al., 2000).

There have also been reports of the presence of a caudate notch in 18% of livers and a vertical caudate fissure in 30% of livers (Mamatha et al., 2014; Saxena et al., 2016). Mittal and his researchers (2021) observed that the caudate lobes had

a rectangular shape in the majority of these cases, a pear-shaped caudate lobe with a crack along its superior border in 2% of cases, and a small caudate lobe in 8% of cases. In 8% of the patients, the researchers identified a significant papillary process. Various investigations have also documented the occurrence of rectangular, irregular, pear-shaped dumbbell-shaped livers, triangular livers, and pyriform (Contractor et al., 2019; Mittal et al., 2021; Singh et al., 2017; Syamala et al.,). The presence of an accessory lobe or caudate lobe duplication has also been discovered in various reports (Aktan et al., 2001; Sadanandan and Varghese, 2017). Notches were also found in 50% of the caudate lobe of the liver in patients undergoing hepatectomy, according to Kogure et al. (2000). Several other researchers discovered a hepatic vein in the caudate notch. As a result, the caudate lobe proper can be distinguished from the paracaval portion by using the caudate notch as a landmark, and the presence of an underlying vein can be identified in liver resection surgeries involving the caudate lobe (Gardner et al., 2019; Kogure et al., 2000). Phad and their group members reported notch and fissures separating papillary process from rest of caudate lobe in 2.5% cases. They also observed enlarge papillary process in 5% cases (Phad et al., 2014). A fissure separates the papillary process from the caudate process of the liver, according to Dev et al. (2014). The papillary process's continuity with the caudate lobe and the characteristics of the liver, on the other hand, make it easier to distinguish between the papillary process and extrahepatic paracaval mass (Dev et al., 2014). In the majority of cases, Syamala and colleagues reported papillary process. They recently discovered prominent papillary process in 27% of cases, with papillary process being very prominent in 16% of livers. In one of the caudate lobes of the liver, the shape of the papillary process is hook-like. On imaging, the large papillary process can mimic a mass lesion in the pancreatic head region or enlarge the periportal lymph node, and it can also mimic a pancreatic tumour if it extends to the left and the stomach is displaced to the anterior side (Syamala et al.). In various other reports, hepatocaval shunt performance is also hampered. In the majority of cases, different research groups observed a linguiform process (Chaudhari et al., 2017).

The sound knowledge of normal and variation in anatomy of liver is important. The incidences of morphological variations of the caudate lobe are very high, so it is very important for both radiologist and for surgeons to keep these variations in mind while making diagnosis to avoid any confusion, and in planning surgeries for favourable clinical outcome. In our study, a prominent caudate process was found in 18% of the livers. The presence of the caudate process is important to know in order to avoid diagnostic ambiguity because it can mimic neoplastic disease on cross-sectional imaging. The presence of a well-developed caudate process may obstruct the hanging manoeuvre, which is performed during major liver resection surgeries and involves passing the surgical instrument through the space anterior to the retro-hepatic IVC. During liver resection surgeries, the presence of a linguiform process makes the retro hepatic approach difficult. Due to the linguiform process, which makes IVC repair difficult in trauma patients, surgeries are extremely difficult. The shape of caudate lobe, presence of caudate fissure and notch, presence of linguiform process, prominent papillary process and variable caudate process have been described in detail in the present study, and it is expected that it would help surgeons in hepatobiliary surgeries, liver transplant surgeries, as well as radiologists in proper interpretation of CT and USG.

CONCLUSION

In the current study, rectangular shapes were found in 62 percent of caudate lobes, followed by irregular shapes (18%) and others (20%). However, we found no evidence of an accessory caudate lobe or caudate duplication in our research. We also found a vertical caudate fissure in 52% of the livers, and a horizontal caudate notch in 11% of the cases. The current study found a linguiform process in 58 percent of patients, with varying degrees of involvement of the retro hepatic IVC.

REFERENCES

AKTAN Z, SAVAS R, PINAR Y, ARSLAN O (2001) Lobe and segment anomalies of the liver. *J Anat Soc India,* 50(1): 15-16.

AUH YH, ROSEN A, RUBENSTEIN WA, ENGEL IA, WHALEN JP, KAZAM E (1984) CT of the papillary process of the caudate lobe of the liver. *Am J Roentgenol,* 142(3): 535-538.

CHAUDHARI HJ, RAVAT MK, VANIYA VH, BHEDI AN (2017) Morphological study of human liver and its surgical importance. *J Clin Diagn Res,* 11(6): AC09.

CHAVAN N, WABALE R (2014) Morphological study of caudate lobe of liver. *Indian J Basic Appl Med Res,* 3(3): 20411.

CONTRACTOR J, KODIYATAR B, VANIYA V (2019) A morphological study of caudate lobe in human cadaveric liver. *Sch Int J Anat Physiol,* 2: 128-131.

DEV G, SHARMA R, SHARMA B (2014) Hepatic papillary process - An anatomic variant of liver. *JK Science,* 16(4): 184.

DODDS WJ, ERICKSON SJ, TAYLOR AJ, LAWSON TL, STEWART ET (1990) Caudate lobe of the liver: anatomy, embryology, and pathology. *Am J Roentgenol,* 154(1): 87-93.

GARDNER MT, CAWICH SO, ZHENG Y, SHETTY R, GARDNER DE, NARAYNSINGH V, PEARCE NW (2019) Morphology of the caudate lobe of the liver in a Caribbean population. *Italian J Anat Embryol,* 124(3): 364-376.

JOSHI S, JOSHI S, ATHAVALE S (2009) Some interesting observations on the surface features of the liver and their clinical implications. *Singapore Med J,* 50(7): 715.

KOGURE K, KUWANO H, FUJIMAKI N, MAKUUCHI M (2000) Relation among portal segmentation, proper hepatic vein, and external notch of the caudate lobe in the human liver. *Ann Surg*, 231(2): 223.

MAMATHA Y, MURTHY C, PRAKASH B (2014) Study on morphological surface variations in human liver. *Int J Health Sci Res*, 4: 97-102.

MITTAL A, GOYAL GL, KAMATH VG (2021) Variations in hepatic segmentation on the surface of liver-a cadaveric study. *JK Science: J Med Educ Res*, 23(1): 43-46.

PHAD VV, SYED S, JOSHI R (2014) Morphological variations of liver. *Int J Health Sci Res,* 4(9): 119-124.

REDDY N, JOSHI S, MITTAL P, JOSHI S (2017) Morphology of caudate and quadrate lobes of liver. *J Evol Med Dental Sci,* 6(11): 897-902.

SADANANDAN R, VARGHESE S (2017) Morphology of caudate lobe of liver. *J Evol Med Dental Sci,* 6(90): 6268-6273.

SAGOO MG, ALAND RC, GOSDEN E (2018) Morphology and morphometry of the caudate lobe of the liver in two populations. *Anat Sci Int,* 93(1): 48-57.

SAHNI D, JIT I, SODHI L (2000) Gross anatomy of the caudate lobe of the liver. *J Anat Soc India*, 49(2): 123-126.

SARALA H, JYOTHILAKSHMI T, SHUBHA R (2015) Morphological variations of caudate lobe of the liver and their clinical implications. *Int J Anat Res*, 3(2): 980-983.

SAXENA A, AGARWAL KK, JAKHWAL C, SINGH S, DAS AR (2016) Some variable facts of liver: embryological and clinical perspective. *Int J Anat Radiol Surg,* 5(1): 64-67.

SIBULESKY L (2013) Normal liver anatomy. *Clin Liver Dis,* 2(Suppl 1): S1.

SINGH R, SINGH K, MAN S (2017) Duplicate caudate lobe of liver with oblique fissure and hypoplastic left lobe of liver. *J Morphol Sci,* 30(4): 309-311.

STANDRING S, ELLIS H, HEALY J, JOHNSON D, WILLIAMS A, COLLINS P, WIGLEY C (2005) Gray's anatomy: the anatomical basis of clinical practice. *Am J Neuroradiol*, 26(10): 2703.

SYAMALA G, VEERNALA P, SHRAVYA ECA (2019) Descriptive study of morphological variations of thyroid gland in adult human cadavers in Siddhartha Medical College, Vijayawada. *J Dental Med Sci*, 18(8): 44-47.

XU L-N, HUANG Z-Q (2010) Resection of hepatic caudate lobe hemangioma: experience with 11 patients. *Hepatobil Pancreatic Dis Int: HBPD INT,* 9(5): 487-491.

Presence of duodenal diverticula in cadaveric study

Alexander Zahariev, María Ignatov, Santiago Pose, Gustavo A. Ugon

Departamento de Anatomía, Facultad de Medicina, Universidad de la República, Montevideo, Uruguay

SUMMARY

The duodenal diverticulum is a common entity, being the second in frequency among digestive tract and mostly asymptomatic. It could be found during endoscopic or surgical procedures, making procedures on the biliary tract more difficult. The objective of this study is to assess the prevalence of duodenal diverticula in cadaveric material and compare findings with the reviewed literature. An observational descriptive study was carried out. 70 in-situ and ex-situ duodenum-pancreatic blocks were dissected from human adult corpses previously fixed in formaldehyde solution. The presence of duodenal diverticula was studied by establishing its prevalence, number, location in relation to the duodenal parts and edges, and the relationship with the major duodenal papilla (MDP).

Regarding the prevalence, 16 (22,8%) duodenal diverticula were found in the analysed cases. These predominated in the descending part of the duodenum (D2). All of them were unique and were located on the mesenteric edge. Regarding their relationship with MDP, there was a predominance of the intradiverticular papilla. The duodenal diverticulum is a frequent entity and the prevalence reported in literature is different within each type of study (cadaveric, ERCP and CT). Our results evidence the highest prevalence if compared to other cadaveric studies analysed. In our study, as well as in the reviewed literature, duodenal diverticula are mostly located in the D2, in relation to MDP.

Key words: Duodenal diverticula – Periampullary diverticula – Duodenal papilla

INTRODUCTION

Duodenal diverticula were initially described in the 18th century by Chomen (1710) and Morgagni (1761) as a finding during cadaveric dissections, without understanding yet their clinical implications. The first reports on the living were made after 1912 in the course of surgery and duodenal radiological examinations (Gru, 1954).

Duodenal diverticula are a frequent entity, being the second in frequency among the digestive tract. Their approximate prevalence varies between 5% and 27% in cadaveric population and through endoscopic studies, knowing that they are found in lower proportion when assessed by imaging studies (Mahajan et al., 2004; Brunicardi et al., 2010; Acuña et al., 2002).

They are defined as a sacculation composed of different layers of the duodenal wall that herniate due to a parietal defect. There are two types: congenital and acquired.

Corresponding author:
Alexander Zahariev. Palermo 5819, Montevideo, Uruguay 11400. Phone: +598 94 667 066. E-mail: alexanderzahariev97@gmail.com

Submitted: May 10, 2022. **Accepted:** May 18, 2022

https://doi.org/10.52083/GYTJ2419

Congenital diverticula are evaginations of the duodenal wall that form during embryologic development. They are made up of all layers of duodenum.

Acquired diverticula can arise by traction (adhesions to other organs) or by propulsion (parietal weakness on the point of passage of the vessels and excretory ducts through the muscular layers). These are the most frequent and are formed by mucosa and submucosa, being predisposed to perforation (Valencia, 2014).

They are mostly asymptomatic; when symptomatic, biliopancreatic symptoms are most frequent and are related to their location, representing a challenge on their diagnosis. Most frequent complications are: obstructive jaundice, perforation, duodenal obstruction and digestive bleeding (Brinucardi et al., 2010; Mathis and Farley, 2007). Diverticula can be found during endoscopic or surgical procedures and their presence implies a more complex procedure, with greater morbidity.

The aim of this study is to search for duodenal diverticula in cadaveric material, assess their prevalence and compare our findings with the reviewed literature.

MATERIAL AND METHODS

An observational descriptive study was carried out. It consisted in the dissection in-situ and ex-situ of 70 duodenum-pancreatic blocks from human adult corpses previously fixed in formaldehyde solution. The age of corpses was in the range from sixty-five to seventy-five years old. Systematically, we dissected the common biliary duct and any biliary pathologies found during dissection were excluded from the sample. We were not able to identify the sex of each of the samples because we did ex-situ dissections, for which we were provided just with the duodenum-pancreatic block. Therefore, our data do not allow to consider differences between males and females.

The duodenum was opened longitudinally at its free edge and the presence of duodenal diverticula was assessed.

We recorded prevalence of duodenal diverticula, number (single or multiple), location and relation to duodenal parts and to its edges (mesenteric or antimesenteric). To assess the location, the duodenum was divided in four parts as described by classic authors. We also considered superior and inferior duodenal flexure (SDF and IDF respectively).

Location of the major duodenal papilla (MDP) in relation to the duodenal diverticulum (Dd) was also recorded, describing two types: intradiverticular (MDP within the diverticulum) or juxtadiverticular (MDP near the diverticulum). Duodenal diverticula not located in the same duodenal part as the MDP were excluded from this classification.

The material used to carry out this work was donated under a written consent to the Deparment of Anatomy.

RESULTS

We found 16 (22,8%) duodenal diverticula in the total of analysed cases (Table 1). All of them were located at the mesenteric edge, mainly in the descending part of duodenum (D2) (Figs. 1 and 2).

Table 1. Analysed variables and results are expressed as absolute frequency and percentual relative frequency. D2: Descending part of duodenum; IDF: Inferior duodenal flexure; D3: Horizontal part of duodenum; D4: Ascending part of duodenum; MDP: Major duodenal papilla.

VARIABLE	N = 70
Prevalence	16 (22,8%)
Unique/multiple	Unique: 100%
Location:	
In relation to duodenum	D2: 13 (81,25%) IDF: 1 (6,25%) D3: 1 (6,25%) D4: 1 (6,25%)
In relation to duodenal edge	Mesenteric edge: 100%
Location of MDP in relation to diverticula	Intradiverticular: 8 (62%)
	Juxtadiverticular: 5 (38%)

Of the 13 diverticula situated in D2, the MDP was located in 8 cases (62%) intradiverticular and in 5 (38%) cases juxtadiverticular.

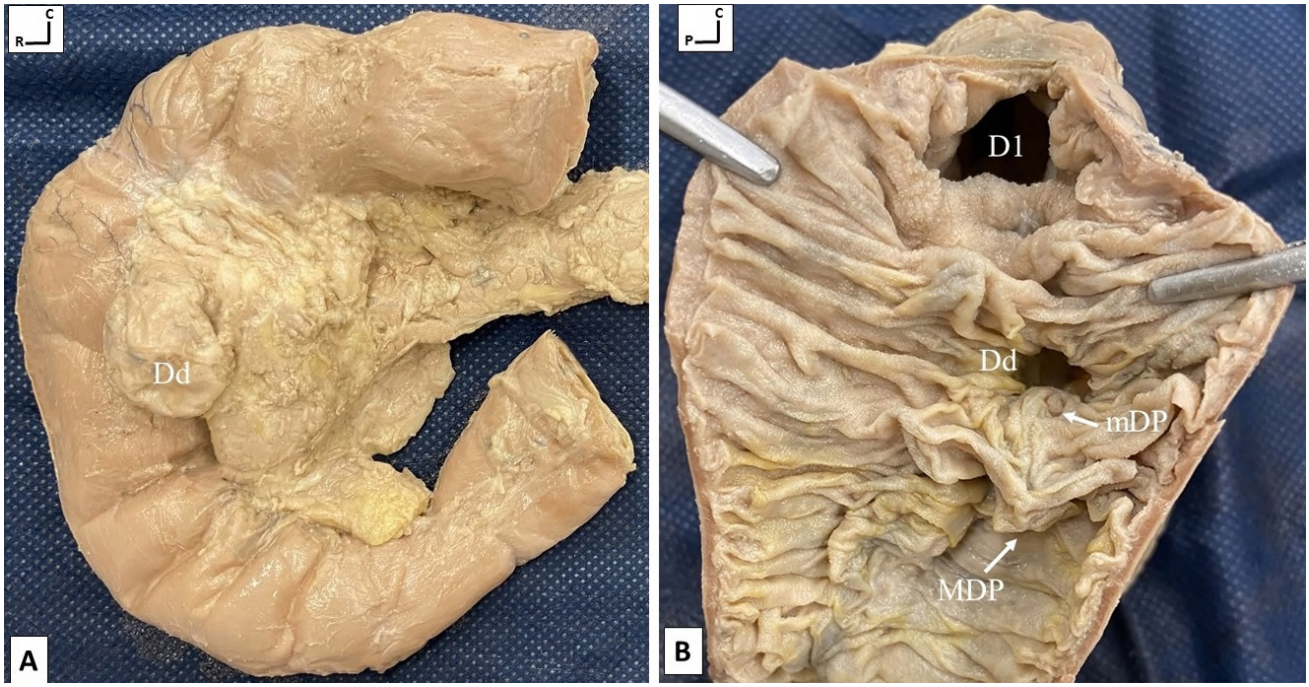

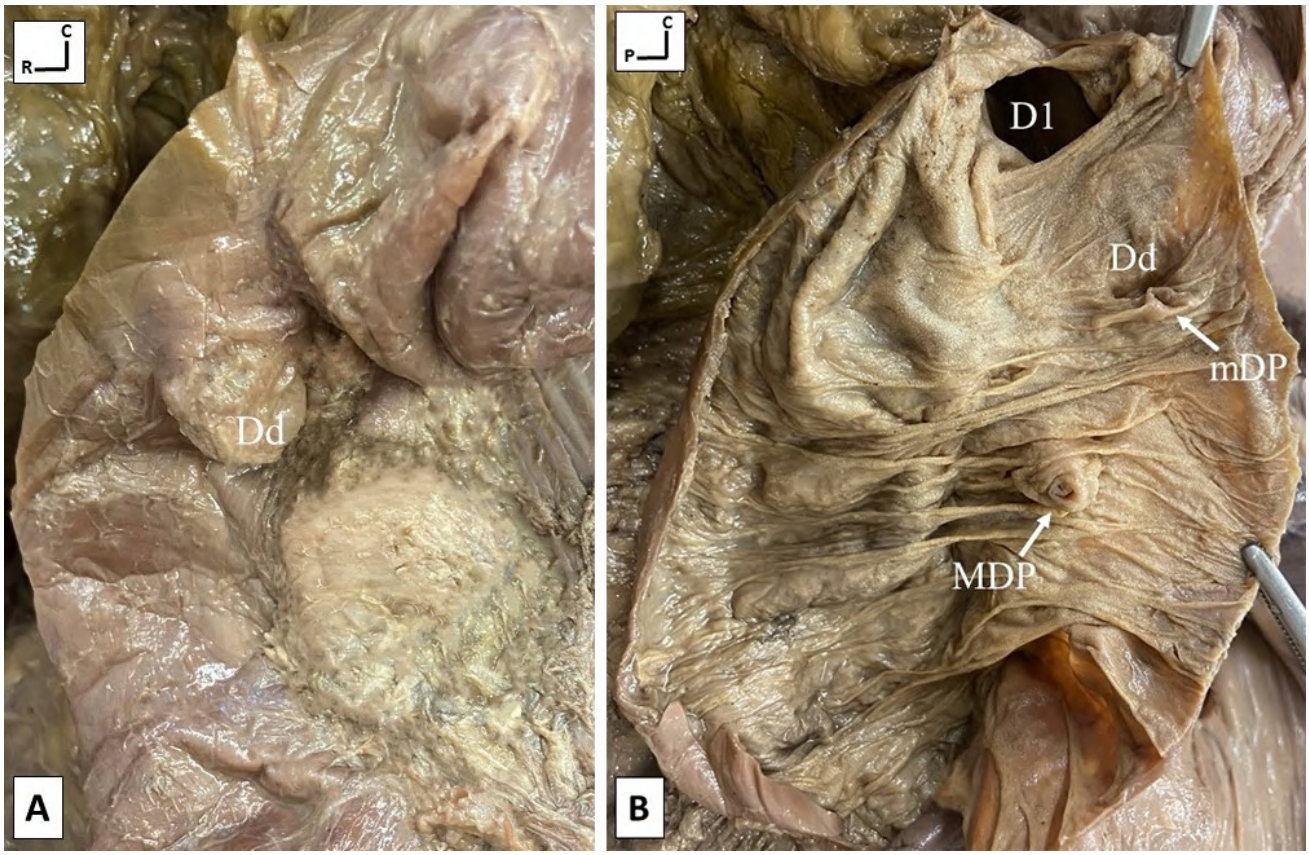

Figs. 1 and 2.- Duodenum-pancreatic block. Fig. **1A** and **2A**: Anterior view of the duodenum-pancreatic block. A duodenal diverticulum is observed in the descending part of duodenum and mesenteric edge. Fig. **1B** and **2B**: Longitudinal opening of duodenum was made through the antimesenteric edge of the descending part of duodenum. Orifice of duodenal diverticulum and its relationship with major and minor duodenal papilla can be observed. Dd: Duodenal diverticulum; D1: Superior part of duodenum; MDP: Major duodenal papilla; mDP: Minor duodenal papilla.

DISCUSSION

Prevalence of duodenal diverticula varies according to different types of studies (cadaveric, ERCP and CT), and also in each type of study (Table 2).

Regarding the prevalence of duodenal diverticula in corpses (Baldwin, 1911; Boileau, 1935; Ackermann, 1943; Poppel and Jacobson, 1956; Dowdy et al., 1962; Sakthivel et al., 2013), there are differences in the reviewed literature, our study showing the highest prevalence. Considering that prevalence increases with age (Boileau, 1935; Motta-Ramírez et al., 2010), our results may be explained because of the age of the corpses. Cadaveric studies that report the age of corpses (Baldwin, 1911; Boileau, 1935; Sakthivel et al., 2013) have a wide age range, including young subjects. This could explain their lower prevalence.

The bibliography that studies duodenal diverticula with ERCP or CT have biggest series, but also reports different prevalence.

In ERCP, the prevalence described is among 11%-38% (Acuña et al., 2002; Boix et al., 2006; Ospina Nieto, 2007; Ozogul et al., 2014;). This method is biased, because it does not evaluate the entire duodenum, so duodenal diverticula located distal from MDP may be not reported.

Concerning prevalence observed in CT studies (Wiesner et al., 2009; Motta-Ramírez et al., 2010; Rekha et al., 2016; Yilmaz et al., 2019), it is lower than the other types of studies reviewed. This can be explained because visualization of duodenal diverticula with CT is difficult, increasing diagnostic sensitivity with the use of oral and intravenous contrast (Esteban et al., 2014; Rangan and Thomas Lamont, 2020). However, using contrast does not assure their visualization (Stone et al., 1989). Stone et al. (1989) found 10 duodenal diverticula in 14 abdominal CT with oral and intravenous contrast in patients that had a previous diagnosis of duodenal diverticula with upper gastrointestinal barium examination.

In the discussed literature, most diverticula were unique (Table 3) and located predominantly in D2 (Table 4), at least half of them being juxtapapillary (Boileau, 1935; Dowdy et al., 1962; Ozogul et al., 2014; Rekha et al., 2016).

ERCP studies do not assess the entire duodenum, so this could be a bias while registering the presence of unique or multiple diverticulum and location of diverticula in the duodenum.

Concerning the location of diverticula in relation to the duodenal edge, both in the literature review (Rekha et al., 2016; Ackermann, 1943; Sakthivel et al., 2013; Skandalakis, 2013) and in our results, these were located in the mesenteric edge. Boileau

Table 2. Prevalence of duodenal diverticula. ERCP: Endoscopic retrograde cholangiopancreatography; CT: Computed Tomography.

Type of study	Authors (year)	Nº	Prevalence
Cadaveric	Baldwin (1911)	105	14 (13,3%)
	Boileau (1935)	133	15 (11,3%)
	Ackermann (1943)	50	11 (22%)
	Poppel (1956)	100	4 (4%)
	Dowdy (1962)	100	10 (10%)
	Sakthivel (2013)	120	5 (4,2%)
ERCP	Acuña (2002)	100	11 (11%)
	Boix (2006)	400	131 (38%)
	Ospina (2007)	508	122 (24,4%)
	Ozogul (2014)	2327	274 (11,7%)
CT	Wiesner (2009)	1010	33 (3,3%)
	Motta-Ramírez (2010)	12704	50 (0,5%)
	Rekha (2016)	565	47 (8,3%)
	Yilmaz (2019)	2910	157 (5,4%)

et al. (1935) found 1 of the 15 diverticula in the antimesenteric edge.

Regarding the location of MDP in relation to duodenal diverticula, we observed in the reviewed literature that there is a slight predominance of juxtadiverticular MDP (Acuña et al., 2002; Boix et al., 2006; Ospina Nieto, 2007; Ozogul et al., 2014;). In contrast, our study showed a predominance of MDP located intradiverticularly (Table 1). This may have clinical implications in procedures that involve MDP.

Table 3. Unique or multiple diverticula reported in the reviewed literature. ERCP: Endoscopic retrograde cholangiopancreatography; CT: Computed Tomography.

Variable	Type of study	Authors	Results (%)
Unique/multiple diverticula	Cadaveric	Baldwin (1911)	Unique: 93%
			Multiple: 7%
		Ackermann (1943)	Unique: 72,7%
			Multiple: 27,3%
	ERCP	Acuña (2002)	Unique: 81,8%
			Multiple: 18,2%
		Ospina (2007)	Unique: 83%
			Multiple: 17%
	CT	Motta-Ramírez (2010)	Unique: 86%
			Multiple: 14%
		Rekha (2016)	Unique: 89,3%
			Multiple: 10,7%

Table 4. Location of duodenal diverticula. ERCP: Endoscopic retrograde cholangiopancreatography; CT: Computed Tomography. SDF: Superior duodenal flexure; D2: Descending part of duodenum; IFD: Inferior duodenal flexure; D3: Horizontal part of duodenum; D4: Ascending part of duodenum.

Type of study	Authors	Nº of diverticula	Location
Cadaveric	Baldwin (1911)	15 (14 specimens)	D2: 9 (60%)
			D3: 5 (33,3%)
			D4: 1 (6,7%)
	Boileau (1935)	20 (15 specimens)	SDF: 1 (5%)
			D2: 14 (70%)
			IDF: 2 (10%)
			D3: 3 (15%)
	Ackermann (1943)	14 (11 specimens)	D2: 5 (35,7%)
			IFD: 1 (7,1%)
			D3: 5 (35,7%)
			D4: 3 (21,5%)
	Dowdy (1962)	10	D2: 10 (100%)
	Sakthivel (2013)	5	D2: 3 (60%)
			D3: 2 (40%)
ERCP	Acuña (2002)	11	D2: 11 (100%)
	Ozogul (2014)	274	D2: 274 (100%)
CT	Rekha (2016)	52 (47 patients)	D2: 47 (90,4%)
			D3: 5 (9,6%)

We highlight that we found 2 duodenal diverticula in relation to minor duodenal papilla which were located on the edge of the diverticulum (Figs. 1B and 2B). Baldwin (1911) also found in 1 specimen 2 diverticula in relation to minor duodenal papilla.

As for the limitations, we were not able to identify the sex of each of the samples, and our data do not allow to consider differences between both sex. We emphasize that greater series have been made in living subjects, with the bias that ERCP and CT have, previously commented.

CONCLUSIONS

Duodenal diverticula are a frequent entity. Prevalence differs according to different types of studies (cadaveric, ERCP and CT). Our results evidence the highest prevalence compared to cadaveric studies reviewed. In our study, as well as in the reviewed literature, they are mostly located in D2 in relation to MDP, with a similar distribution of intradiverticular/juxtapapillar MDP.

ACKNOWLEDGEMENTS

"The authors sincerely thank those who donated their bodies to science so that anatomical research and teaching could be performed. Results from such research can potentially increase scientific knowledge and can improve patient care. Therefore, these donors and their families deserve our highest respect".

REFERENCES

ACKERMANN W (1943) Diverticula and variations of the duodenum. *Ann Surg,* 117(3): 403-413.

ACUÑA R, LEÓN F, FRIDMAN L, ALCÁNTARA A, ÁLVAREZ J (2002) Prevalencia del divertículo duodenal y su morbimortalidad en la colangiografía endoscópica retrógrada. *Revista Mexicana de Cirugía Endoscópica,* 3(3): 117-122.

BALDWIN W (1911) Duodenal diverticula in man. *Anat Rec*, 5: 121-140.

BOILEAU JC (1935) On the frequency and age incidence of duodenal diverticula. *Can Med Assoc J,* 33(3): 258-262.

BOIX J, LORENZO-ZUÑIGA V, AÑAÑOS F, DOMENÈCH E, MORILLAS R, GASSULL M (2006) Impact of periampullary duodenal diverticula at endoscopic retrograde cholangiopancreatography: a proposed classification of periampullary duodenal diverticula. *Surg Laparosc Endosc Percutan Tech,* 16(4): 208-211.

BRUNICARDI C, ANDERSEN D. BILLIAR T, DUNN D, HUNTER J, MATTHEWS J, POLLOCK R (2010) Intestino delgado. *Schwartz Principios de Cirugía*. 9th edit. McGraw-Hill interamericana, Madrid, pp 1004-1006.

DOWDY G, WALDRON G, BROWN W, TEXAS H (1962) Surgical anatomy of the pancreatobiliary ductal system. *Arch Surg*, 84: 93-110.

ESTEBAN R, CASTAÑÓN R, FLORES G, SÁNCEZ J, PINTO B, REBOLLEDO M (2014) Divertículos duodenales y enfermedad biliopancreática. *Radiología,* 56: 411.

GRU I (1954) Diverticulosis duodenal. *Rev Fac Med,* 22(11-12): 486-490.

MAHAJAN SK, KASHYAP R, CHANDEL UK, MOKTA J, MINHAS SS (2004) Duodenal diverticulum: review of literature. *Indian J Surg,* 66(3): 140-145.

MATHIS K, FARLEY D (2007) Operative management of symptomatic duodenal diverticula. *Am J Surg.* 93: 305-308.

MOTTA-RAMÍREZ GA, ORTÍZ-LEÓN JL, URBINA DE LA VEGA F, MEJÍA-NOGALES RE, BARINAGARRENTERIA-ALDATZ R (2010) La enfermedad diverticular duodenal como hallazgo incidental detectado por tomografía computarizada. *Rev Gastroenterol Mex,* 75(2): 165-170.

OSPINA NIETO J (2007) Impacto verdadero del diverticulo periampular en la CPRE. *Rev Col Gastroenterol,* 22(4): 297-301.

OZOGUL B, OZTURK G, KISAOGLU A, AYDINLY B, YILDIRGAN M, ATAMANALP S (2014) The clinical importance of different localization of the papilla associated with juxtapapillary duodenal diverticula. *Can J Surg,* 57(5): 337-341.

POPPEL M, JACOBSON H (1956). Roentgen aspects of the papilla of Vater. *Am J Digest Dis,* 1(2): 49-58.

RANGAN V, THOMAS J (2020) Small Bowel diverticulosis: pathogenesis, clinical management, and new concepts. *Curr Gastroenterol Rep,* 22(4): 1-7.

REKHA B, CHANDRAMOHAN A, CHANDRAN S, JAYASEELAN V, SUGANTHLY J (2016) Contrast enhanced computed tomographic study on the prevalence of duodenal diverticulum in Indian population. *J Clin Diagn Res*, 10(4): AC12-5.

SAKTHIVEL S, KANNAIYAN K, THIAGARAJAN S (2013) Prevalence of duodenal diverticulum in South Indians: a cadaveric study. *ISRN Anat*, 2013:767403.

SKANDALAKIS J (2015) Intestino delgado. *Bases anatómicas y embriológicas de la cirugía*. Marbán, Madrid, pp 710-711.

STONE E, BRANT W, SMITCH G (1989) Computed tomography of duodenal diverticula. *J Comput Assist Tomogr*, 13(1): 61-63.

VALENCIA M, OTEGI I, CUCO S, EGEA P, RIAÑO M, DIFALGO M, LÓPEZ A, PARRA J (2014) Diverticulitis duodenal perforada. *Revista Portuguesa de Cirugía*, 31: 41-47.

WIESNER W, BEGLINGER CH, OERTLI D, STEINBRICH W (2009) Juxtapapillary duodenal diverticula: MDCT findings in 1010 patients and proposal for a new classification. *JBR-BTR*, 92(4): 191-194.

YILMAZ E, KOSTEK O, HEREKLIOGLU S, GOKTAS M, TUNCBILEK N (2019) Assessment of duodenal diverticula: computed tomography findings. *Curr Med Imaging Rev*, 15(10): 948-955.

A1-A2 anterior cerebral artery fenestration. A case report of a rare anatomical variant

Dmitri V. Hovrin[1], Ilya V. Senko[2], Gerald Musa[3], Dimitri K.T. Ndandja[3], Rossi E.B. Castillo[3], Gennady E. Chmutin[3]

[1] Department of Neurosurgery, City clinical hospital № 7 named after S.S Yudina, Moscow, Russia

[2] Federal Center of Brain and Neurotechnologies, Federal Medical and Biological Agency of Russia, Moscow

[3] Department of Neurosurgery and Neurological Diseases, Peoples Friendship University of Russia (RUDN University), Moscow, Russia

SUMMARY

Cerebral vascular anatomical variations are not uncommon in the human population. Their prevalence is not exactly known, as most of them are incidentally diagnosed on angiography or postmortem dissections. We present a rare fenestration of the A1 segment of the anterior cerebral artery presenting with a ruptured saccular aneurysm.

A 42-year-old hypertensive patient presented unconscious following a ruptured saccular aneurysm. The computer tomography angiography showed a fenestration of the right A1 segment of the anterior cerebral artery (ACA). The medial segment of the A1 was communicating with the left ACA via the Anterior communicating artery, while the lateral segment was directly joining the A2 segment of the same side. Intraoperatively, the two segments were identified as separate vascular structures not sharing adventitia, and of equal caliber. The aneurysm arising from the bifurcation was clipped. The patient recovered with no neurological deficits. Many vascular anomalies like fenestrations and bifurcations are underdiagnosed, as many of them remain asymptomatic and are discovered incidentally on postmortem dissection or angiography for other pathologies. This has led to a paucity of cases to determine the prevalence in the human population. Good knowledge of the vascular anatomy variations and associated risk of aneurysm is important for the vascular neurosurgeons.

Keywords: Anterior cerebral artery – Fenestration – Bifurcation – Anatomical variants – Vascular anatomy

INTRODUCTION

Many different vascular anomalies have been described in the brain, some of which can be found in the arteries that form the circle of Willis and are related to congenital disorders (Enyedi et al., 2021; Dumitrescu et al., 2021). One of these rare variants is fenestration, or partial duplication.

Corresponding author:
Gerald Musa MBCHB. Department of Nervous Diseases and Neurosurgery, Peoples' Friendship University of Russia (RUDN University), Potapovskaya Roscha 7k2, Moscow, Russia. Phone: +7 9778275213. E-mail: gerryMD@outlook.com, ORCID: 0000-0001-8710-8652

Submitted: May 8, 2022. **Accepted:** June 14, 2022

https://doi.org/10.52083/LXNM1800

Fenestrations, according to the literature, are more frequent in the posterior circulation (Nyasa et al., 2021; Tanaka, 2017). They are usually silent and asymptomatic, and as a result are most commonly discovered incidentally on cadaver dissections and angiography for other pathologies (Fredon et al., 2021; Krystkiewicz et al., 2021). Fenestration, or partial duplication of the anterior cerebral artery, is almost always accompanied by the presence of an aneurysm. Fenestrations have been described in the A1 segment of the anterior cerebral artery, although the most frequently affected segment of the anterior circulation is the Anterior communicating artery (Acom) (Mamadaliev et al., 2019; Trandafilovic et al., 2021). As with all other vascular disorders, cerebral angiography is invaluable in their accurate diagnosis (Mahajan et al., 2020).

The incidence of arterial fenestrations in the brain ranges from 0.3% to 0.9% in angiography and 0.14% in cadaver dissections, according to the literature (Guo et al., 2018; Iqbal, 2013). Its prevalence in the A1 region is 0-4%, as described in anatomical studies, and 0.058%, as described in angiographic studies (Makowicz et al., 2013). The distal A1 segment is described as the most frequently associated with fenestrations in dissections of cadavers. Various theories have been reported to explain the association between aneurysms and fenestrations, including: Vascular wall weakness (Iwabuchi et al., 2018), and failure of fusion of the plexiform multi-channel network of vessels that develop into major arteries during fetal life (Krystkiewicz et al., 2021; Kwon et al., 2013; Mahajan et al., 2020; Makowicz et al., 2013).

In this article, we present a case of a rare A1 fenestration terminating in the A2 segment with a proximal saccular aneurysm. To the best of our knowledge, this type of fenestration has been described once in a cadaver dissection without an associated aneurysm. The case report below is presented according to the CARE checklist.

CASE DESCRIPTION

A 42-year-old female patient presented to the emergency department with sudden loss of consciousness following a severe headache. She was a known hypertensive on medication, with a history of recurrent headaches. On examination, her GCS was 9, BP 165/100mmHg. She had left hemiparesis. An urgent CT showed intracerebral and intraventricular hemorrhage with no midline shift (Fig. 1A). CTA showed a fenestrated left A1 with a saccular aneurysm at the proximal end of the fenestration (Fig. 1B).

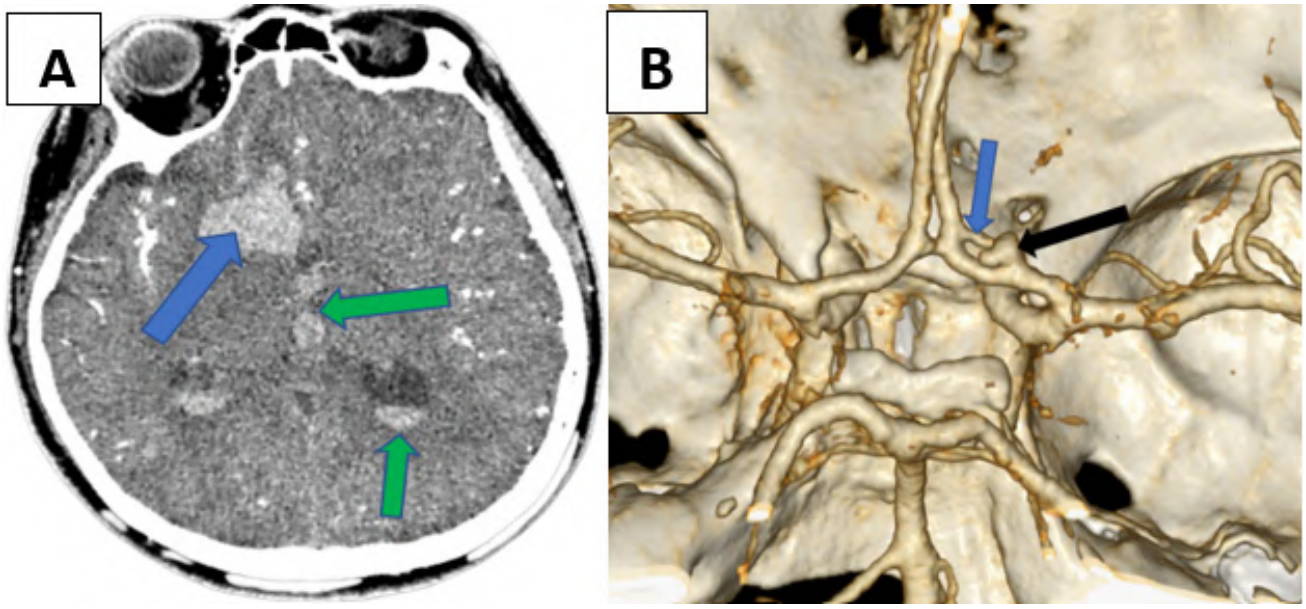

Fig. 1.- A- Preoperative CT brain showing a right frontal intracerebral hematoma (blue arrow) and Fischer grade 4 subarachnoid hemorrhage. **B**- Preoperative CTA shows a fenestrated right A1 connecting to the right A2 (blue arrow) with a saccular aneurysm (black arrow) arising from the origin of the fenestration.

The patient was stabilized in the intensive care unit for 48 hours. On the second day post admission, she underwent aneurysm clipping. Intraoperatively, the partial duplication of the right A1 was visualized (Fig. 2A) with an aneurysm arising at the origin of the partial duplication (Fig. 2B).

The aneurysm was successfully clipped with no intraoperative complications (Fig. 2C).

The post-operative period was uneventful, and the patient was discharged on the fourteenth day post-operative with no neurological deficit. At 3-month follow-up, the patient remained asymptomatic without any restriction to daily activities.

There were no diagnostic challenges faced in this patient, as the neuroimaging performed was adequate.

Endovascular services at the time the patient presented were not available at the institution. As a result, an endovascular approach was not an option.

DISCUSSION

Thomas Willis in 1664 described the complete cerebral vascular circuit, the so-called circle of Willis, and described it as a network of arterial vascular anastomosis, located at the base of the skull (Nyasa et al., 2021; Dumitrescu et al., 2021).

The cerebral arterial circulation is divided into an anterior and posterior system. The anterior circulation includes the internal carotid arteries, which give rise to the anterior cerebral arteries, which are connected via the anterior communicating artery, and the middle cerebral arteries. The posterior circulation includes the paired vertebral arteries, which merge giving rise to the basilar artery. The basilar artery gives rise to the anteroinferior and superior cerebellar arteries, and the posterior cerebral arteries (Tanaka, 2017). The posteroinferior cerebellar arteries arise directly from the vertebral arteries before they form the basilar artery. The anterior and posterior systems communicate through the posterior communicating arteries (Makowicz et al., 2013).

The anterior cerebral artery (ACA) presents both clinically significant and incidental variations in its anatomy. Previous studies have found a significant difference in the prevalence of these anatomical variants amongst different ethnic groups (Jiménez Sosa et al., 2017).

A study by Makowicz et al. (2013) revealed that the presence of these atypical variants of cerebral vessels is associated with an increased risk of ischemic event and/or aneurysm formation. The typical complete variant of ACA is seen in only 30-57 % of the population (López-Sala et al., 2020).

Almost all the variants of ACA and its branches have been described in the literature. Several authors have classified variants of ACA and its branches: A1, Acom, and A2 (Jiménez Sosa et al., 2017; Kayembe et al., 1984). Some of the described variants are illustrated in Fig. 3. We have added

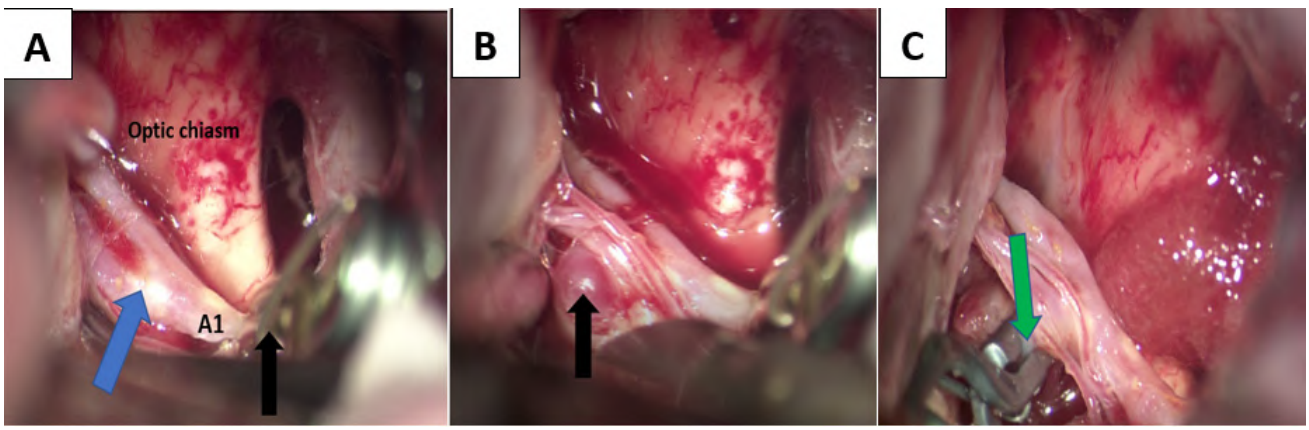

Fig. 2.- A- Intraoperative exposure of the A1 segment after placement of temporary clip (black arrow). Notice the abnormal bifurcation of A1 (blue arrow). **B**- The saccular aneurysm (black arrow) seen arising posteriorly at the A bifurcation. **C**- Shows the view after aneurysm clipping with the 2 branches of A1 clearly visible.

the variant described in this case report: i.e., A1-A2 fenestration.

The variations seen in the ACA include: reduction in caliber (Hypoplasia), complete absence (aplasia), the same artery with different and independent origin (Duplication, triplication), and fenestration, which occurs when vessels duplicate forming two channels corresponding to a single path, with each channel having its own endothelium and tunica media but possibly sharing the tunica adventitia and, most importantly, reuniting distally (López-Sala et al., 2020). Fenestration is also referred to as partial duplication (Guo et al., 2018).

A duplication occurs with two distinct arteries with separate origin that do not converge distally. It is most often seen in MCA variants. Duplication of A1 segment of ACA occurs in up to 4% of normal subjects in cadaveric studies (Perlmutter and Rhoton, 1976). ACA Trifurcation is the occurrence of 3 segments and prevalence in A2 with the third branch arising from Acom in 2-13% of cases. Hypoplasia of ACA and Aplasia both account for 31.2% and 10.6% respectively (López-Sala et al., 2020; Makowicz et al., 2013).

We describe a relatively rare variant of ACA, complete fenestration or partial bifurcation of the right A1. The term bifurcation is used cautiously instead of fenestration, as the two segments did not share an adventitia and connected to the A2 segment, as opposed to the classic fenestration, which merges with the same arterial segment and shares an adventitia.

Fenestration of the right A1 resulted in two separate A1 branches, a medial and lateral segment, with the medial segment connecting to the left A2 via the Acom and the lateral segment directly connecting into the A2 on the same side. Sonda and Basso (2015) reported a similar type of partial bifurcation of A1 in a cadaveric dissection, but in their case it was associated with a duplication of Acom. The association of fenestration with aneurysms has been described in literature. Makowicz et al. (2013) attribute this to a focal smooth muscle defect in arterial intima media at a bifurcation site, a so-called “medial” defect. This, in addition to hemodynamic turbulences at the bifurcation site, increases the risk of aneurysm formation and subsequent rapture.

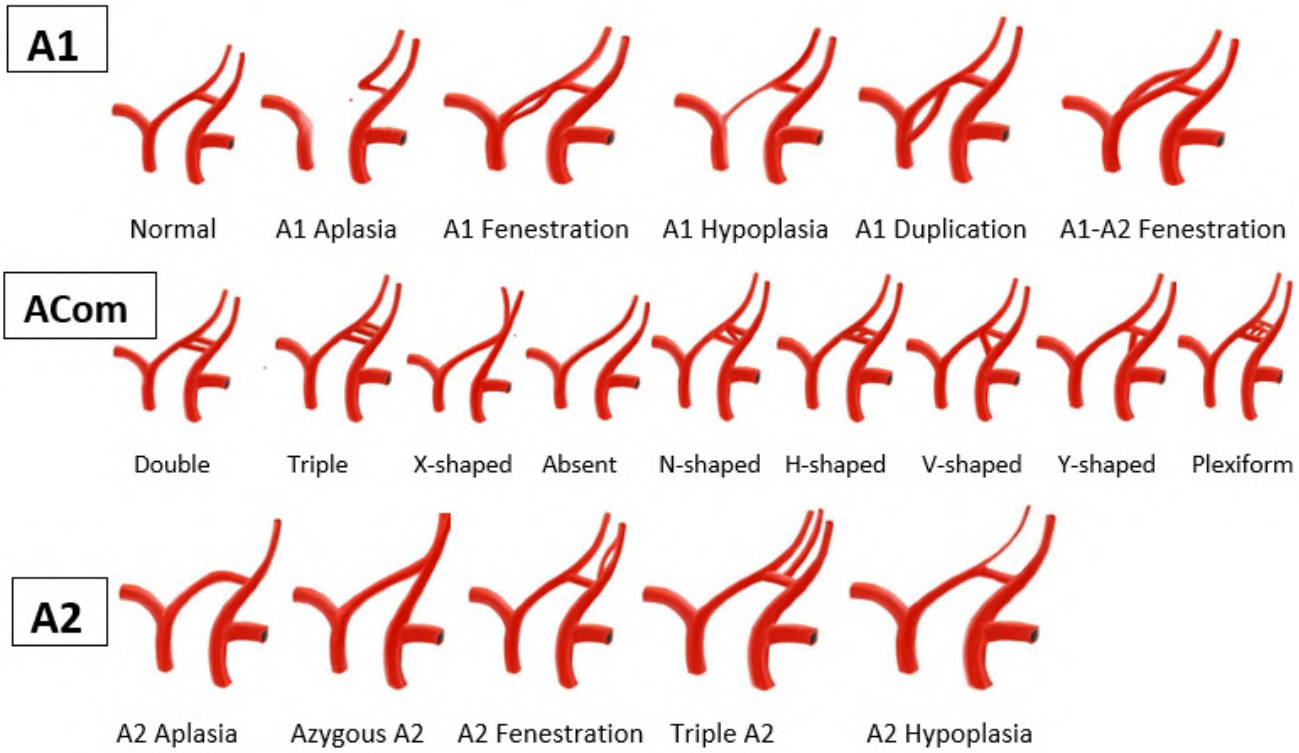

Fig. 3.- Pictural presentation of the many anatomical variations of the Anterior Cerebral Arteries (ACA). They have been grouped into A1, ACom, and A2 (Drawings by Dr. Musa Gerald).

Many cases of fenestrations are asymptomatic and go undiagnosed. Our patient presented with a raptured saccular aneurysm, which was managed with standard microsurgical techniques with very good neurological outcome.

CONCLUSION

Many vascular anomalies like fenestrations and bifurcations are underdiagnosed, as many of them remain asymptomatic and are discovered incidentally on postmortem dissection or angiography for other pathologies. This has led to paucity of cases to determine the prevalence in the human population. A good knowledge of the vascular anatomy variations and associated risk of aneurysm is important for the vascular neurosurgeons.

ACKNOWLEDGEMENTS

The publication was carried out with the support of the Peoples Friendship University of Russia (RUDN) Strategic Academic Leadership Program.

ETHICS APPROVAL AND CONSENT TO PARTICIPATE

Written informed consent was obtained from the patients' caregivers. Consent for publication of this case report and accompanying images was obtained from the patients' caregivers.

REFERENCES

DUMITRESCU AM, COSTEA CF, FURNICĂ C, TURLIUC MD, CUCU AI, BOGDĂNICI CM, TURLIUC Ş, DUMITRESCU GF, SAVA A (2021) Morphological aspects of the vasculogenesis and angiogenesis during prenatal edification of the circle of Willis: a review. *Rom J Morphol Embryol,* 62: 679-687.

ENYEDI M, SCHEAU C, BAZ RO, DIDILESCU AC (2021) Circle of Willis: anatomical variations of configuration. A magnetic resonance angiography study. *Folia Morphol (Warsz)*. doi: 10.5603/FM.a2021.0134.

FREDON F, BAUDOUIN M, HARDY J, KOUIRIRA A, JAMILLOUX L, TAIBI A, MABIT C, VALLEIX D, ROUCHAUD A, DURAND-FONTANIER S (2021) An MRI study of typical anatomical variants of the anterior communicating artery complex. *Surg Radiol Anat,* 43: 1983-1988.

GUO X, GAO L, SHI Z, LIU D, WANG Y, SUN Z, CHEN Y, CHEN W, YANG Y (2018) Intracranial arterial fenestration and risk of aneurysm: a systematic review and meta-analysis. *World Neurosurg,* 115: e592-e598.

IQBAL S (2013) A comprehensive study of the anatomical variations of the circle of Willis in adult human brains. *J Clin Diagn Res,* 7: 2423-2427.

IWABUCHI N, SAITO A, FUJIMOTO K, NAKAMURA T, SASAKI T (2018) Unruptured saccular aneurysm arising from the fenestrated A1 segment of the anterior cerebral artery: report of 2 cases. *Case Rep Neurol,* 10: 140-149.

JIMÉNEZ SOSA MS, CANTÚ GONZÁLEZ JR, MORALES AVALOS R, DE LA GARZA CASTRO O, QUIROGA GARZA A, PINALES RAZO R, ELIZONDO RIOJAS G, ELIZONDO OMAÑA RE, GUZMÁN LÓPEZ S (2017) Anatomical variants of anterior cerebral arterial circle: a study by multidetector computerized 3D tomographic angiography. *Int J Morphol,* 35: 1121-1128.

KAYEMBE KN, SASAHARA M, HAZAMA F (1984) Cerebral aneurysms and variations in the circle of Willis. *Stroke,* 15: 846-850.

KRYSTKIEWICZ K, CISZEK B, SZYLBERG L, TOSIK M, HARAT M (2021) Morphological analysis of cerebral artery fenestrations and their correlation with intracranial aneurysms. *World Neurosurg,* 156: E85-E92.

KWON WK, PARK KJ, PARK DH, KANG SH (2013) Ruptured saccular aneurysm arising from fenestrated proximal anterior cerebral artery: case report and literature review. *J Korean Neurosurg Soc,* 53: 293-296.

LÓPEZ-SALA P, ALBERDI N, MENDIGAÑA M, BACAICOA M-C, CABADA T (2020) Anatomical variants of anterior communicating artery complex. A study by computerized tomographic angiography. *J Clin Neurosci,* 80: 182-187.

MAHAJAN A, BANGA V, CHATTERJEE A, GOEL G (2020) Infraoptic course of anterior cerebral artery coexistence with double fenestration of proximal A2 segment of anterior cerebral artery with associated dysplastic anterior communicating artery aneurysm treated with stent-assisted coiling. *Asian J Neurosurg,* 15: 247-249.

MAKOWICZ G, PONIATOWSKA R, LUSAWA M (2013) Variants of cerebral arteries–anterior circulation. *Polish J Radiol,* 78: 42.

MAMADALIEV D, KATO Y, TALARI S, MEWADA T, YAMADA Y, KEI Y, KAWASE T (2019) Unilateral fenestrated A1 segment of anterior cerebral artery multiple aneurysms: case reports and literature review. *Asian J Neurosurg,* 14: 957-960.

NYASA C, MWAKIKUNGA A, TEMBO L, DZAMALALA C, IHUNWO AO (2021) Distribution of variations in anatomy of the circle of Willis: results of a cadaveric study of the Malawian population and review of literature. *Pan Afr Med J,* 38: 11.

PERLMUTTER D, RHOTON AL (1976) Microsurgical anatomy of the anterior cerebral-anterior communicating-recurrent artery complex. *J Neurosurg,* 45: 259-272.

SONDA I, BASSO LS (2015) Fenestrated A1 segment of right anterior cerebral artery associated to duplicated anterior communicating artery. *Anatomy,* 9.

TANAKA M (2017) Functional vascular anatomy of the brain. *Neurol Med Chir (Tokyo),* 57: 584-589.

TRANDAFILOVIC M, VASOVIC L, VLAJKOVIC S, MILIC M, DREVENSEK M (2021) Double unilateral fenestration of the anterior cerebral artery in the pre-communicating segment: a report of a unique case. *Folia Morphol (Warsz)*. doi: 10.5603/FM.a2021.0088.

Perceptions of students and teachers about traditional and active didactic strategies in a veterinary anatomy course

Ricardo A. Barreto-Mejía[1], Nurvey E. Cano-Marín[2], Rubén H. Torres-Gómez[2], Sara Quiceno-Zapata[1], Lynda J. Tamayo-Arango[1]

[1] Grupo de Investigación CIBAV, Escuela de Medicina Veterinaria, Facultad de Ciencias Agrarias, Universidad de Antioquia, Medellín, Colombia

[2] Grupo de investigación EDUSALUD, Facultad de Medicina, Universidad de Antioquia, Medellín, Colombia

SUMMARY

Active learning strategies were gradually implemented in the veterinary anatomy course at the University of Antioquia. In the cohort of the second semester of 2018, in the first module (musculoskeletal system), we used the traditional methodology (master classes both in theory and in practice), and active teaching strategies were used in the rest of the course. Faculty perceived some dissatisfaction among the students with this change. The objective of this work was to understand the perceptions of students and teachers about the traditional and active didactic strategies of the course, during this academic period through semi-structured interviews and focus group. The students perceived the combination of traditional learning strategies with active strategies as ideal. The traditional approach seems more comfortable to them, because the teacher provides all the information. However, they saw rote learning and the large amount of information as a disadvantage. They perceived that formative assessment allows for the consolidation of knowledge. The teachers highlighted the importance of using several methods that allow for adapting to the different learning styles of the students. In addition, they considered that their role is to guide students so that, through analysis, interpretation and research processes, they learn to build their knowledge. We conclude that students are highly dependent on traditional learning strategies, so it is necessary to stimulate the use of tools supported by constructivism. Also, more administrative support should be given for faculty to have the training and enough paid time for the preparation and application of active learning strategies.

Keywords: Veterinary anatomy – Traditional class – Anatomy education – Active methodologies – Teaching strategies

INTRODUCTION

The new educational approaches that are based on active learning theories and outcomes have generated the need to implement new pedagogical practices that allow for a deeper understanding

Corresponding author:
Lynda J. Tamayo-Arango. Escuela de Medicina Veterinaria, Facultad de Ciencias Agrarias, Universidad de Antioquia UdeA, Calle 67 Nº 53 - 108, Medellín, Colombia. E-mail: lynda.tamayo@udea.edu.co

Submitted: November 8, 2021. **Accepted:** May 9, 2022

https://doi.org/10.52083/QGYD9761

of veterinary anatomy, where students put into practice their knowledge and skills to solve anatomical problems (Van Ginneken and Vanthournout, 2005). Active learning methods based on constructivist strategies outperform passive strategies, at least in the initial stage of learning (Kooloos et al., 2020), making them effective learning tools for teaching veterinary medicine (Diamond et al., 2020). Active learning methods include all the learning activities that engage students in the educative process and that make them reflect continuously about their learning (Bonwell and Eison, 1991), which allows the development of higher order abilities in the students, increase retention of knowledge and enable better performance in tests (Bristol et al., 2019). On the other side, traditional strategies include all the activities in which the student is a passive receptor of the knowledge, while the teacher has the active role in the teaching and learning process (Vitorino et al., 2020).

The Veterinary Anatomy course at the Faculty of Agrarian Sciences of the University of Antioquia has a systemic approach, with a simultaneous study of the comparative anatomy of domestic animals (canines, equines, swine and ruminants). The teaching and learning process has historically been characterized by the use of a traditional approach. However, as of the 2015 curricular reform, other teaching strategies began to be gradually introduced, since the new curricular guidelines are based on outcomes and are based on active learning.

During the second academic semester of 2018, active learning methodologies were implemented with greater intensity in all modules, except for the first module (locomotor system), in which only the traditional methodology was used, consisting in lectures and demonstrative explanations in practical sessions (Fig. 1). During this period, some of the students expressed certain dissatisfaction with the strategies used, since they were adapted to traditional methodologies in which the student does not challenge himself to have an active attitude during learning.

Within the teaching methodologies supported by the active learning tools, the following were included: the reviewing of a reading material by the students prior to the class, elaboration of concept maps in small groups of students, briefing sessions (Lachman and Pawlina, 2015), formative assessment and dissection –the latter because it allows the students to integrate knowledge, to solve problems and to develop logical thinking through doing (Cake, 2006).

In addition, at the end of each class session, feedback was given to the students, with the help of the results of the formative assessment. Also, teachers presented the learning objectives at the beginning of each module, so the students could be clear about what is intended for them to learn.

In order to change the rote memory approach, activities of formative assessment were set up. Students were allowed to review the results of the quiz, study and present them again, until obtaining clarity in the anatomical concepts

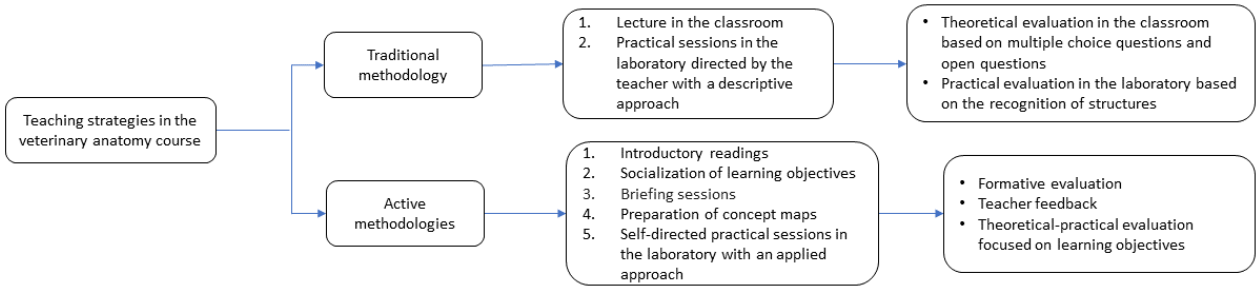

Fig. 1.- Flow chart showing the teaching strategies and assessment tools used in the course.

through constant feedback from the teacher. The partial exams were replaced by an evaluation focused on learning objectives and theoretical-practical questions (objective structured practical evaluation -OSPE- type) with 3 minutes for the resolution of the questions (Yaqinuddin et al., 2013), and the implementation of extended matching items was part of the changes.

During the practical sessions, students were asked to search the structures that were related to the topics addressed during the theoretical class in the cadavers and other anatomical specimens, making use of anatomy texts and a study guide. The teacher guided the students in the identification of the structures when there are difficulties or doubts in the recognition. Finally, a review of the structures was carried out on the cadaver, in which students and teachers participated at the same time, relating each structure to its specific function.

In order to inquire the students and teachers' interpretations regarding the new methodologies, it was proposed to understand the perceptions of students and teachers about the didactic strategies of the veterinary anatomy course of the Faculty of Agricultural Sciences during the second academic period of 2018.

MATERIALS AND METHODS

Qualitative descriptive research oriented in the hermeneutical paradigm for understanding the perceptions about the didactic strategies of the veterinary anatomy course was carried out with a group of students and teachers of the undergraduate veterinary medicine of the University of Antioquia. This study was approved by the Bioethics committee of the Faculty of Medicine, University of Antioquia.

The potential participants were 52 students who took the Veterinary Anatomy course during the second academic semester of 2018 and 5 teachers. A call was made via email to all students, inviting them to participate in the research on a voluntary basis, they were made aware of the dynamics of the research and the objectives of the project. The sample was intentionally non-probabilistic based on the interest of the researcher. The inclusion criterion was to have finished the course during the indicated academic period and the exclusion criterion was to be a repeating student. Semi-structured interviews and a focus group were carried out. Of the total population, 13 students were interviewed (25%). The number of students was determined according to the concept of theoretical saturation, that is, the point at which data collection and information analysis did not generate new information (Victoroff and Hogan, 2006). The focus group was carried out with 3 students (5.8%).

Three of the teachers (60%) voluntarily participated in this research. The principal investigator (RBM) was excluded from the interviews to avoid bias.

All participants filled out the informed consent form endorsed by the Bioethics committee of the Faculty of Medicine, University of Antioquia. There was no financial remuneration for participation in this study.

The interviews were conducted by a veterinary medicine student with knowledge in qualitative research (SQZ), who was previously trained by one of the research advisors (NCM, Magister in higher education in health with experience in qualitative studies). The training was focused on theoretical and practical aspects of the semi-structured interview.

At the beginning of the interviews, each participant was informed of the research objectives, the definition of perception and a contextualization related to the learning strategies used, where the traditional didactic strategy was called methodology 1 and the active methodological strategies were called methodology 2. All interviews and the focus group were duly recorded.

After collecting the information, each interview was transcribed verbatim in Microsoft Word. Each participant was assigned a code in order to protect his/her identity. Using the Atlas.ti version 7.5.4 program, the information collected was analyzed to categorize the perceptions of the participants from three pre-established categories: traditional method, active method and perception. The pre-established categories were defined based on

the literature review. An open categorization was carried out, from which new categories emerged that made possible to deepen the understanding of perceptions. Finally, the results were triangulated by comparing the data from the interviews of the students and teachers, the focus group, and the scientific literature (Fig. 2).

The validity of this research is supported by the textual transcription of each interview and the exhaustive categorization and triangulation of the information from the collected data and documents from the scientific literature.

RESULTS

The data obtained shows that, although students had a greater predilection for the use of the traditional learning methodology, it seemed ideal for them to learn in a veterinary anatomy course that also alternates the use of active strategies. Similarly, teachers stated that anatomy teaching should use various methods that allow adapting to the different learning styles of students.

Regarding traditional teaching, four main categories were identified: lectures, memorization,

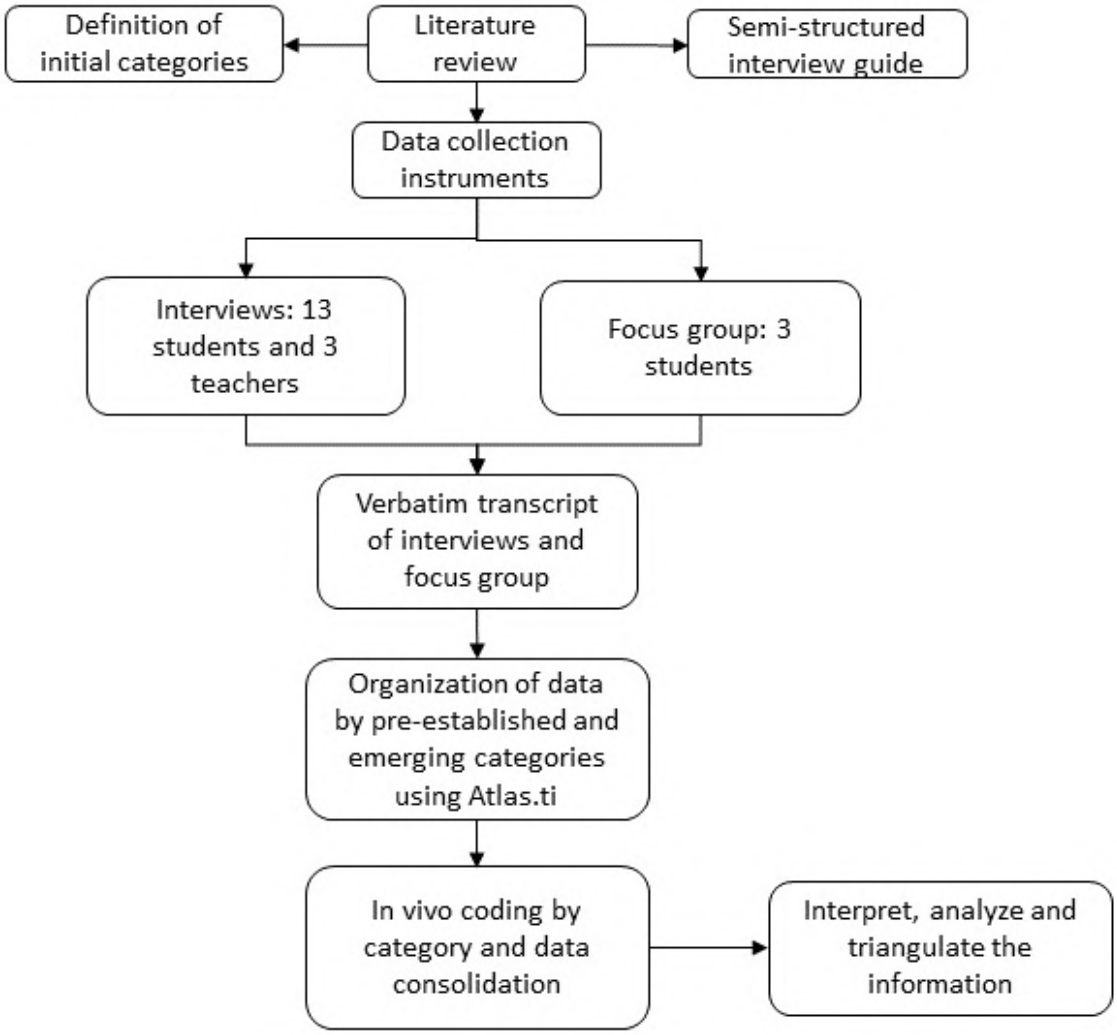

Fig. 2.- Flow chart showing the collection and analysis of the information.

density of the topics and assessment. Lectures were valued positively; in general, the students expressed that this is a learning strategy that allows for the explanation of detailed theoretical aspects of a structure or a topic in depth. In addition, they considered that it is comfortable, since the teacher provides all the necessary information. However, they considered rote learning, the amount of information handled in the development of the lecture and the assessment to be the main drawbacks in this methodology.

For teachers, lectures allowed for a good handling of the information, because it makes possible to present a topic in an orderly manner, it provides quick information to the student and it allows for the presentation of concepts that may be complex for the student. However, it is an unattractive teaching methodology, in which the learner becomes a very passive individual and gets used to being given facts without the need to do any learning effort. They stated that it is one of the most frequently used methodological strategies, but it is necessary to select its content and make appropriate use of it, since students lose their attention when a lecture becomes too extensive. Teachers also considered thematic density to be one of the main difficulties of lectures. Related to active learning strategies, in the open categorization of student interviews, four main categories emerged: formative assessment, concept maps, briefing sessions, and clarity of concepts. The students considered that the formative assessment allowed them to consolidate their knowledge or reinforce concepts not yet understood.

Regarding the concept maps, this tool was identified as favorable for the learning process, although there were some negative comments related to the time given for the completion of the task (approximately 20 minutes), difficulties in relation to team work and, finally, a personal factor related to the learning style (one student that thought that in this way he does not learn).

Briefing sessions were also evaluated positively, since they tended to give context to the anatomy by integrating anatomical knowledge with common basic clinical aspects of veterinary medical practice. Finally, in this type of strategy, the lack of understanding of anatomical concepts stood out as the main difficulty, since the students felt that the teacher did not offer them a theoretical class as such. Although most students considered that active strategies are based on the construction of knowledge autonomously, the general perception is that with the traditional method they obtained greater learning.

Teachers considered that the implementation of new didactic strategies other than lectures requires adequate training in pedagogical aspects and that experience is a fundamental aspect for the proper development of these methodologies. They also mentioned that it helps arouse student interest. They considered that when teaching strategies have specific learning objectives, the student is clear about what to learn and what can be assessed. Explicit learning objectives also guide the teacher in the teaching (content prioritization) and assessment process. Teachers believed that it was satisfactory to work with these teaching and learning strategies, and considered that their role is to act as a guide so that students, through a process of analysis, interpretation and research, learn to build their knowledge. However, they stated that the time required for the implementation of active learning strategies is one of the most challenging aspects. Although the opinion of the teachers about the briefing sessions agrees with that reported by the students, they highlighted that the strategy is difficult to elaborate.

DISCUSSION

In this study we analyzed the perception of students and teachers about the didactic strategies that were used during the second academic period of 2018 in the veterinary anatomy course of the Faculty of Agrarian Sciences of the University of Antioquia.

The preference of students for the traditional didactic strategies are in accordance with a previous study in which a large part of students perceived that they learn better with lectures than with teaching activities based on active learning (Vitorino et al., 2020), although constructivism-based learning methods have been shown to

improve student performance on short-term exams compared to traditional teaching methods (McGreevy and Church, 2020; Michael, 2006). In addition, it has been observed that students give less educational value to teaching strategies that generate anxiety and some active learning techniques tend to generate more anxiety than lectures (Hood et al., 2020), and a perception of increased workload (Silverthorn, 2020). However, other studies have shown that active learning strategies improved student satisfaction with positive effects on student learning (Dooley et al., 2018; Keegan et al., 2012; Monahan and Yew, 2002). Anatomy students perceived team-based learning as a more rewarding and enjoyable learning strategy than regular lectures-based teaching (Inuwa, 2012; Ozkadif and Ekencastn, 2012).

The reasons that support the predilection of traditional methodologies for learning anatomy could be related to the limited experience and pedagogical training of the teachers in charge of the course in the implementation of active methodological strategies (Morzinski, 2005; Moore et al., 2002).

Students have a resistance to change to new learning methods, even more when traditional teaching approaches are the main strategy used in primary and middle education (Schwerdt and Wuppermann, 2011). Lectures are the most frequently used methodology in the teaching of students in higher education (Schmidt et al., 2015) and, in the case of veterinary anatomy, this approach prevails today (Ozkadif and Ekencastn, 2012). Student resistance to new teaching methods is one of the challenges when trying to migrate from a traditional to a student-centered teaching model (Silverthorn, 2020). It is necessary that students take greater responsibility in their learning process, however, some of them decide to assume a passive role (Bohaty et al., 2016).

Regarding the benefits of multimodal teaching for different learning styles perceived by teachers in this study is consistent with Hauer and Quill (2011), who stated that several teaching approaches facilitate the achievement of knowledge, skills and attitudes in students. In addition, when veterinary anatomy students combined various study methods, they obtained better academic performance (Ward and Walker, 2008), and when lectures were used in conjunction with active learning strategies, students paid greater attention to classes (Bunce et al., 2010). Likewise, medical students considered that learning was carried out actively with group interactions with the use of a multimodal teaching strategy for learning anatomy (structured practical sessions) (Akeel, 2021). This author highlighted the importance of incorporating multimodal teaching strategies in contemporary curricula, since these adapt more easily to the learning styles of students (Edgell, 2011) and help to maintain student interest (McGreevy and Church, 2020).

In contrast, the perceptions of the students are immersed in a dependence on traditional learning methods. All this supports the idea of continuing on focusing the teaching of veterinary anatomy through a great variety of didactic strategies that promote the autonomy of the student in the acquisition of their knowledge (Sugand et al., 2010; Dooley et al. 2018).

Among the main difficulties perceived by students about the traditional strategies, learning by rote stands out, in accordance with what has been reported in other studies, which reported that the main method for the appropriation of anatomical terminology is memorization (Santos-Treto et al.,2010; Ortiz and Merchan, 2012), mainly because they are required to reproduce verbatim in assessments (Ortiz and Merchan, 2012). Memory learning hinders long-term retention process, much more when functional and practical relationships with veterinary practice that provide context and application are not established (Ward and Walker, 2008). Learning by rote has been related with negative aspects in academic performance in contrast with deep learning approaches (Ward and Walker, 2008; Castañeda, 2015). Therefore, we highlight the need for implementing different teaching strategies in veterinary anatomy courses to stimulate deep learning approaches that are related to the understanding of information and long-term learning.

Formative assessment without a rote memorization approach helps to reduce the tension and

stress of the students. The fact that the teachers keep learning objectives in mind, allows assessment methods to remain aligned with the teaching strategies (Biggs and Tang, 2015). Our positive students` perceptions on formative assessment are in accordance with Bhattacharjee (2020), who reported the creation of formative evaluation strategies in veterinary anatomy course through the use of social networks. Formative assessment allows the teacher to know the difficulties in student learning or the objectives not yet reached (Ruze et al., 2020).

The negative opinions of the students regarding the use of concept maps agree with the study reported by Diwakar et al. (2007), due to the limited time for its elaboration and the predilection for individual work. Sufficient time (on average 3 hours) is required for the process to develop in an analytical and conscientious way to obtain quality results and favor meaningful learning (Diwakar et al., 2007).

In accordance to Vitorino et al. (2020), the lack of comprehension of the anatomical concepts when active strategies were used could be attributed to a high dependence on learning through traditional methods, due to a difficulty in recognizing the key concepts in content.

The positive perception of the use of the briefing sessions for both students and teachers lies in the benefit of giving context to the anatomical knowledge by the integration with common basic clinical aspects of veterinary medical practice. Veterinary anatomy students have considered the necessity to implement clinical aspects as a teaching strategy (Küçükaslan et al., 2019). Briefing sessions seek to develop clinical reasoning skills in students through clear objectives based on the understanding of basic anatomical concepts, reflection and critical thinking (Lachman and Pawlina, 2015). Veterinary medicine students need to develop higher-order skills such as reflection and critical thinking from the most basic courses, such as anatomy, to achieve a deeper learning (Bohaty et al., 2016; Kim et al., 2013).

Finally, although the purpose of the focus group was to expand the amount of information collected to ensure better understanding of the topic, the number of participants could limit the discussion regarding the perceptions of the students and the possibility of obtaining more significant information in terms of diversity and quality that could be of interest for the study. For Mishra (2016), although focus groups with only three participants can be successfully implemented, there is a risk of having a limited discussion. Otherwise, having large focus groups could interfere with the amount of information collected.

CONCLUSION

We conclude that students are highly dependent on traditional teaching strategies for learning anatomy, which makes necessary to diversify the teaching strategies that allow for the adaptation to the different learning styles of the students. This would help to stimulate the development of autonomy in students so that they can assume a true commitment in their learning process; motivation to seek information in a variety of literature sources, even beyond those reported by the teacher; inquiry and discussion among peers, so that the acquisition of knowledge becomes a construction rather than a one-way transmission.

Likewise, this research showed the importance of reflection about pedagogical and curricular aspects by teachers, implementing new didactic strategies in order to strengthen the teaching and learning process. This endeavor must be supported by an administrative commitment focused on the implementation of policies that strengthen pedagogical training programs and including extra hours for preparation of classes in the work plans.

Study limitations

From the methodology proposed in this research, it was thought to carry out 3 focus groups to have a better understanding of the studied phenomenon. However, due to the quarantine decreed by the National Government of Colombia since March 2020 for the Covid-19 pandemic, a single focus group could be carried out. It was not possible to interview the teachers who taught the traditional methodology due to time constraints. It would

have been interesting to know their position on traditional and active teaching strategies. In this study, the perceptions of a group of students and teachers about the didactic strategies of the veterinary anatomy course at the University of Antioquia were assessed, so it is necessary to take precautions when generalizing the results. Not all teachers had the same level of training in teaching and assessment strategies related to active modalities.

REFERENCES

AKEEL MA (2021) Exploring students' understanding of structured practical anatomy. *J Taibah Univ Sci*,16: 318-327.

BHATTACHARJEE S (2020) # anatomymcq - A pilot study on using the Twitter survey tool as a formative assessment strategy. *MedEdPublish*, 9: 1-21.

BIGGS J, TANG C (2015) Constructive alignment: an outcomes-based approach to teaching anatomy. In: Chan LK, Pawlina W (eds). *Teaching anatomy: A practical guide*. 1ª Ed. Springer International Publishing, New York, pp 31-38.

BOHATY BS, REDFORD GJ, GADBURY-AMYOT CC (2016) Flipping the classroom: assessment of strategies to promote student-centered, self-directed learning in a dental school course in pediatric dentistry. *J Dent Educ*, 80: 1319-1327.

BONWELL CC, EISON JA (1991) Active learning: creating excitement in the classroom. ERIC Clearinghouse on Higher Education, Washington.

BRISTOL T, HAGLER D, MCMILLIAN-BOHLER J, WERMERS R, HATCH D, OERMANN MH (2019). Nurse educators' use of lecture and active learning. *Teach Learn Nurs*, 14: 94-96.

BUNCE DM, FLENS EA, NEILES KY (2010) How long can students pay attention in class? A study of student attention decline using clickers. *J Chem Educ*, 87: 1438-1443.

CAKE MA (2006) Deep dissection: motivating students beyond rote learning in veterinary anatomy. *J Vet Med Educ*, 33: 266-271.

CASTAÑEDA LA (2015) Enseñanza de la anatomía orientada al desarrollo de competencias en la carrera de Bioingeniería. Universidad Nacional del Litoral, Santa Fe: Argentina. Tesis de Maestría en didáctica de las Ciencias Experimentales. 127 p.

DIAMOND KK, VASQUEZ C, BORRONI C, PAREDES R (2020) Exploring veterinary medicine students' experiences with team-based learning at the Universidad Andrés Bello. *J Vet Med Educ*,47: 421-429.

DIWAKAR V, ERTMER PA, NOUR AY (2007) Helping students learn veterinary physiology through the use of concept maps. *J Vet Med Educ*, 34: 652-657.

DOOLEY LM, FRANKLAND S, BOLLER E, TUDOR E (2018) Implementing the flipped classroom in a veterinary pre-clinical science course: Student engagement, performance, and satisfaction. *J Vet Med Educ*, 45: 195-203.

EDGELL H (2011) Teaching anatomy with multiple techniques. *Teaching Innovation Projects*, 1: 1-5.

HAUER J, QUILL T (2011) Educational needs assessment, development of learning objectives, and choosing a teaching approach. *J Palliat Med*, 14: 503-508.

HOOD S, BARRICKMAN N, DJERDJIAN N, FARR M, GERRITS RJ, LAWFORD H, HULL K (2020) Some believe, not all achieve: the role of active learning practices in anxiety and academic self-efficacyin first-generation college students. *J Microbiol Biol Educ*, 21: 7-11.

INUWA IM (2012) Perceptions and attitudes of first-year medical students on a modified team-based learning (TBL) strategy in anatomy. *Sultan Qaboos Univ Med J*, 12: 336-343.

KEEGAN RD, BROWN GR, GORDON A (2012) Use of a simulation of the ventilator-patient interaction as an active learning exercise: comparison with traditional lecture. *J Vet Med Educ*, 39: 359-367.

KIM K, SHARMA P, LAND SM, FURLONG KP (2013) Effects of active learning on enhancing student critical thinking in an undergraduate general science course. Innov High Educ, 38: 223-235.

KOOLOOS JG, BERGMAN EM, SCHEFFERS MA, SCHEPENS-FRANKE AN, VORSTENBOSCH MA (2020) The effect of passive and active education methods applied in repetition activities on the retention of anatomical knowledge. *Anat Sci Educ*, 13: 458-466.

KÜÇÜKASLAN Ö, ERDOĞAN S, BULUT İ (2019) Turkish undergraduate veterinary students' attitudes to use of animals and other teaching alternatives for learning anatomy. *J Vet Med Educ*, 46: 116-127.

LACHMAN N, PAWLINA W (2015) Choosing between lecture and briefing sessions. In: Chan LA, Pawlina W (eds). *Teaching anatomy: A practical guide*. 1ª Ed. Springer International Publishing, New York, pp 89-96.

MCGREEVY KM, CHURCH FC (2020) Active learning: Subtypes, intra-exam comparison, and student survey in an undergraduate biology course. *Sci Educ*, 10: 1-15.

MICHAEL J (2006) Where's the evidence that active learning works? *Adv Physiol Educ*, 30(4): 159-167.

MISHRA L (2016) Focus group discussion in qualitative research. *Techno Learn*, 6: 1-5.

MONAHAN CM, YEW AC (2002) Adapting a case-based, cooperative learning strategy to a veterinary parasitology laboratory. *J Vet Med Educ*, 29: 186-192.

MOORE DA, LEAMON MH, COX PD, SERVIS ME (2002) Teaching implications of different educational theories and approaches. *J Vet Med Educ*, 29: 117-123.

MORZINSKI JA (2005) Mentors, colleagues, and successful health science faculty: lessons from the field. *J Vet Med Educ*, 32: 5-11.

ORTIZ SRS, MERCHÁN NYT (2012) Significado del aprendizaje y la enseñanza de la anatomía: contribuciones desde las percepciones de los estudiantes. *Zona Próxima*, 17: 24-37.

OZKADIF S, EKECASTN E (2012) Modernization process in veterinary anatomy education. *Energy Educ Sci Technol-PT B*, 4: 957-962.

RUZE A, AMUTI S, LIPAN N, LIU F (2020) A new holistic assessment system and its impacts on student performance in regional anatomy. *Int J Morphol*, 38: 863-868.

SANTOS-TRETO Y, MARZABAL-CARO Y, WONG-CORRALES LA, FRANCO-PÉREZ PM, RODRÍGUEZ-BLANCO K (2010) Factores asociados al fracaso escolar en estudiantes de medicina del Policlínico Facultad Vicente Ponce Carrasco. *Revista Médica Electrónica*, 32: 0-0.

SCHMIDT HG, WAGENER SL, SMEETS GA, KEEMINK LM, VAN DER MOLEN HT (2015) On the use and misuse of lectures in higher education. *Health Prof Educ*, 1: 12-18.

SCHWERDT, G, WUPPERMANN AC (2011) Is traditional teaching really all that bad? A within-student between-subject approach. *Econ Educ Rev*, 30: 365-379.

SILVERTHORN DU (2020) When active learning fails... and what to do about it. In: Mintzes J, Walter E (eds). *Active learning in college science: the case for evidence-based practice*. 1ªEd. Springer Nature; Switzerland, pp 985-1001.

SUGAND K, ABRAHAMS P, KHURANA A (2010) The anatomy of anatomy: a review for its modernization. *Anat Sci Educ*, 3: 83-93.

VAN GINNEKEN CJ, VANTHOURNOUT G (2005) Rethinking the learning and evaluation environment of a veterinary course in gross anatomy: the implementation of an assessment and development center and an e-learning platform. *J Vet Med Educ*, 32: 537-543.

VITORINO RW, FORNAZAIRO CC, FERNANDES EV (2020) Evaluation of performance and perception of learning in teaching human anatomy: traditional method vs constructivist method. *Int J Morphol*, 38: 74-77.

VICTOROFF KZ, HOGAN S (2006) Students' perceptions of effective learning experiences in dental school: a qualitative study using a critical incident technique. *J Dent Educ*, 70: 124-132.

WARD PJ, WALKER JJ (2008) The influence of study methods and knowledge processing on academic success and long-term recall of anatomy learning by first-year veterinary students. *Anat Sci Educ*, 1: 68-74.

YAQINUDDIN A, ZAFAR M, IKRAM MF, GANGULY P (2013) What is an objective structured practical examination in anatomy? *Anat Sci Educ*, 6: 125-133.

Online assessment vs Traditional assessment: perception of medical teachers in a tertiary level teaching hospital in South India

Anitha Nancy[1], Jeneth B. Raj[1], Joe D. Anton[1], Aravinthan S[2], Balachandra V. Adkoli[3]

[1] Mahatma Gandhi Medical College & Research Institute, Sri Balaji Vidyapeeth (Deemed to be University), Puducherry-607402, India

[2] PSP Medical College, Dr. MGR University, Tamil Nadu, India

[3] Sri Balaji Vidyapeeth (Deemed to be University), Puducherry-607402, India

SUMMARY

The use of e-assessment has increased in higher education over the last two decades, which means that medical teachers are required to work by adapting to the increasing usage of technology. Because of the automated marking and feedback, online tests are viewed as highly efficient, fast, and reliable. The online assessment was not used for formative/summative assessment except in fewer renowned institutions in our country. But it had increased recently in all educational setups because of the COVID-19 pandemic. This study aims to know the perception of preclinical faculty on the advantages and disadvantages of using online internal assessment when compared to the traditional method. A cross-sectional survey was done using Google form with standard and validated questionnaires with Likert scale scoring (1- strongly disagree, 2- disagree, 3- neutral, 4- agree, and 5- strongly agree) for preclinical medical faculty to assess their perception of online vs traditional assessment method. The result was analyzed by descriptive statistics. Out of 45 responses, only 50% were competent to handle the online assessment, but the other 50% were confident though not competent due to lack of training. 96% of faculty agreed that paper correction load is reduced in online aptitude tests. But nearly 40% agreed that aptitude tests can assess only the student's knowledge in the cognitive domain. In our study, we found that not all the faculty preferred to switch from the conventional method. However, they show their willingness to adopt a blended teaching and assessment method.

Keywords: Online assessment – Traditional assessment – ICT – Google form survey

INTRODUCTION

In this digital era, several changes are emerging in education, because technology is being used in human activities other than education. The need for technology integration in education becomes the core factor of quality education. Computer Assisted Learning/ Teaching/Instruction/Assess-

Corresponding author:
Dr. Anitha Nancy T. Associate Professor, Department of Anatomy, Mahatma Gandhi Medical College & Research Institute, Sri Balaji Vidyapeeth (Deemed to be University), Puducherry-607402, India. Phone: 8903139965. E-mail: ancyjean2010@gmail.com

Submitted: February 9, 2022. **Accepted:** June 2, 2022

https://doi.org/10.52083/CPSZ4396

ment, e-learning, e-assessment, online/virtual learning environment, education apps, and AI in education have emerged steadily (Zafar and Hussain, 2020). In addition, the delivery method in online learning environments also allows for opportunities in assessment which are unique to this type of learning environment (Baleni, 2015). The use of e-assessment/online tests has increased in education over the last 20 years. This is due to decreased resources for teaching and increased student numbers, meaning that academics are required to do more with less while adapting to the increasing usage of technology in teaching (Nicol, 2007; Donelly, 2014). The potential of technology has been employed to benefit the challenge of heavy academic workloads in teaching and for assessment, with the use of e-assessment providing a way to avoid disjunction between teaching and assessment modes (Gipps, 2005). In other words, the growth in the use of Information and communication technology (ICT) as a teaching mode necessitates their growth as a mode of assessment. Because of the automated grading and instant feedback, online tests are viewed as highly efficient, fast, and reliable, making them useful where large numbers of learners are concerned (Bakerson and Rodriguez-Campos, 2006); online tests specifically ask for computer-assisted assessment where the deployment and marking are automated (Davies, 2010). Online tests have been used within learning management systems (LMS) either purely online or in mixed-mode delivery extensively during Covid-19 lockdown time to medical students in our institution. So, it is important to know the faculty's views regarding changes in educational techniques, and it should be taken into serious consideration to ensure a smooth and successful transition, which was the aim of our study. Because their perceptions remain critical, technological measures taken to solve problems in education may end up as substandard solutions.

MATERIALS AND METHODS

The study subjects of this project were preclinical medical faculty in our institution. It was a cross-sectional type of study. It was done for the duration of 1 month from the date of Institute Human Ethical Committee approval by the volunteer recruitment process. The online Google form survey questionnaire was distributed to all 60 preclinical medical faculty of our university(Anatomy, 22; Physiology, 20; Biochemistry, 18), and the data were obtained. A universal sampling method was used and whoever responded to the questionnaire within the duration of the study project was taken as a study sample.

This study's purpose was explained in detail to the study participants at the beginning of the questionnaire. A set of valid questionnaires used earlier by Baleni (2015) was used in this survey with modifications, and the newly added questions were validated by face validation, peers and subject expert validation. The survey questions were grouped under two categories: 1) Demographic details and 2) Perception of faculty on the advantages and disadvantages of online assessment compared to the traditional method. Pre-defined questions were asked to know their experience in handling online assessments and the type of training they underwent to handle it. Close-ended questionnaire (15) was scored by the Likert scale ranging from Strongly Agree (SA), Agree (A), Not Sure (NS), and Disagree (DA) to Strongly Disagree (SDA) using the descriptive and inferential statistics. Advantages of online assessment were assessed in Q. No. 1,3,4,5 & 7. Disadvantages of online assessment were assessed in Q. No. 2,6,8,12,13 & 14. Perception of faculty in handling newer technology was assessed in Q. No. 9,10,11 & 15. The anonymity of the faculty and the confidentiality of the results were strictly maintained. All data were entered into an online Google form questionnaire sheet and then into an Excel spreadsheet (MS Excel 2011).

RESULTS

At the end of the one month, out of 60 preclinical faculty members, 45 (Anatomy- 20, Physiology- 15 and Biochemistry- 10) i.e., 75%, gave their consent and responded to both predefined and close-ended questions. Out of 45 responses, only 35 faculty members had disclosed their age, ranging from 28-52 years. There was equal participation from both male and female faculty. There was

equal participation of faculty from tutors to professors in all 3 preclinical departments (Professor, 7; Associate Professor, 14; Assistant Professor, 17; and Tutor, 7). Participation ranged from junior faculty with less than one year of experience in teaching to senior faculty who had more than 20 years of experience.

Experience and training to conduct online assessments

Pre-defined questions were asked to know their experience in handling online assessments and the type of training they underwent to handle them, and out of 45 responses 98% of faculty agreed that they had experience in conducting/ handling a minimum of 3 online tests. 50% of faculty mentioned attending various Faculty Development Programs (FDP). 63% felt that they need to have a trial assessment (Table 1).

Table 1. Questions for experience and training to conduct online assessment.

No	Questions	YES	NO
1.	Conducted/handled a minimum of 3 online tests	98%	2%
2.	Received any formal training in medical education practices	50%	50%
3.	Competent to handle the newer technology first time	50%	50%
4.	Is the online trial test comfortable in handling the newer technology?	63%	37%

Advantages of online assessment

Q. No. 1, 3, 4, 6 and 7 stated the advantages of online assessment and 40.7% of faculty have positively responded (A and SA) to reduced paper correction load and grading the paper was easy in aptitude test by 96.1% of faculty. 33.4% of faculty were feeling comfortable using online assessments. 74.1% of faculty agreed that constructive and immediate feedback is possible (Table 2).

Table 2. Advantages of Online assessment.

No	Questionnaires	Likert Scale Scoring				
		SA	A	NS	DA	SDA
1.	Online assessment paper correction load reduced	7.4	33.3	22.2	37.1	-
2.	Easy for Aptitude test	40.7	55.6	3.7	-	-
3.	Time is reduced in grading the online test	7.4	40.7	22.2	29.6	7.4
4.	Comfortable to use online assessment	3.8	29.6	25.9	29.6	11.1
5.	Timely, constructive and personalized feedback can motivate the students	14.8	59.3	18.5	3.9	3.5

SA- Strongly Agree, A- Agree, NS- Neutral, DA-Disagree, SDA-Strongly Disagree

Disadvantages of online assessment

Q. No. 2, 6, 8, 12, 13 and 14 stated the disadvantages of online assessment over traditional methods, like difficulty to download and correcting essay questions. 62.9% agreed to it and 88.9% agreed that they lacked personal connection with students during the online assessment. 40.7% of faculty agreed that online assessment can test only the knowledge component in the cognitive domain, that the major disadvantage was cheating, and that more time is required by the faculty to develop a standard online test – this was agreed by nearly 95-98% of faculty (Table 3).

Table 3. Disadvantages of Online assessment.

No	Questionnaires	Likert Scale Scoring				
		SA	A	NS	DA	SDA
1	Challenging to grade essay questions	14.8	48.1	7.5	29.6	-
2	Students have taken preparation for online tests seriously	-	-	11.1	70.4	18.5
3	Lack of Personal connection with students	18.5	70.4	3.7	7.4	-
4	Assess only lower-order thinking	3.7	37	29.6	29.6	-
5	Cheating is a major drawback in online assessment	59.3	40.7	-	-	-
6	Additional time is required to design quality test items	48.1	48.1	3.8	-	-

SA- Strongly Agree, A- Agree, NS- Neutral, DA-Disagree, SDA-Strongly Disagree

Perception of faculty in handling newer technology

Q. No. 9, 10, 11 & 15 concerned the perception of pre-clinical faculty on the reliability of the newer technology and also the willingness to update and adapt to the new digital world. Only 11% of faculty agreed on the reliability of the newer technology. 70% felt that lack of training would make them incompetent in handling the digital era. 75% did not prefer online assessment over the traditional method. But 80% showed their willingness to adapt the blended teaching and assessment methodology (Table 4).

Table 4. Perception of faculty in handling newer technology.

No	Questionnaires	Likert Scale Scoring				
		SA	A	NS	DA	SDA
1.	The technology used is reliable	-	11.1	44.4	29.6	14.8
2.	Is it necessary to be competent in ICT	18.5	51.9	11.1	14.8	3.7
3.	Prefer to use the online assessment method over the traditional method?	-	15.4	7.6	46.2	30.8
4.	Adoption of the blended method of assessment is essential at present	29.6	59.3	11.1	-	-

SA- Strongly Agree, A- Agree, NS- Neutral, DA-Disagree, SDA-Strongly Disagree

DISCUSSION

COVID-19 pandemic situation has made all health science universities develop effective online teaching and assessment tools (Kumar, 2018) Faculty's perception of online assessment compared to the conventional method is very important, because they were the one who was planning, scheduling, and conducting the online assessment during this COVID 19 pandemic time and are also experienced in conducting multiple conventional assessment methods to the students.

The majority of faculty agreed that they had experience in conducting/handling a minimum of 3 online tests. The question was asked to know about their training to handle newer technology and received a positive response from the half of faculty. And this faculty (mostly Professors, Associate Professors and Senior Assistants) were attending various Faculty Development Program (FDP) organized by the institution, Medical Education Unit (MEU) of their parent institute, or another nodal and regional center. But the other half of the faculty group had not received any training. This may be due to the selection process where senior faculty were always picked up for any training. Because of the lack of training, most of the faculty were not feeling competent to handle the newer technology.

Advantages of online assessment

From the perception of our faculty, the advantages of online assessment where paper correction load is reduced, grading online aptitude is easy and immediate constructive feedback will motivate the learner to perform well, which were in accordance with the study by Zafar and Hussain (2019), which stated that the technology integration by faculty is becoming important and vital in all kinds of education; and also in accordance with the study done by Baleni (2015), which stated that the benefits of online assessment were student commitment, faster feedback, and lecturers also benefited with less marking time.

Disadvantages of online assessment

Assessing low order thinking, extra time and effort is needed to prepare a well-designed online test, lack of personal connection, cheating and plagiarism by students were very common disadvantages of an online assessment, which was in accordance with the study results of Baleni (2015), Khan and Khan (2019) and Mukhtar et al. (2020). In the cognitive domain, only the knowledge component was tested, and more time is required by the faculty to develop a standard online assessment to test the higher-order thinking of the students, which was agreed upon by nearly 50% of the faculty; and this result was in accordance with the study result of Boitshwarelo et al. (2017).

Perception of faculty in handling newer technology

Lack of training and updates in ICT would make them incompetent in handling the digital era. Our result was in accordance with a study done by Khan and Khan (2019), which stated that when teachers lacked the technological skills and confidence to conduct online assessments, it had a negative influence on students.

So, from our study, we found that it was difficult for the important stakeholders of education like teachers, who did not prefer the switch from conventional to online methods in the form of learning or assessment, even though the advantages of online methods overweigh the traditional method. But they show their willingness to adapt to the blended learning method, and it can change their mindset to accept the 21st-century outcome-based education.

The limitations of our study were questionnaire-based, as it gave us only the percentage of people who agreed or disagreed in Likert scale scoring. Including other types of tools in educational research like Focus Group Discussion (FGD) and In-depth interviews might have given more insight into the advantages and disadvantages of online assessment by the faculty. Besides, the study was done only on preclinical faculty. Thus, the result may not truly reflect the perception of all medical faculty in clearer and broader aspects.

But from our study, we would like to recommend that online assessment can be acceptable for teachers if they are trained and equipped in handling newer technology. The administrations should: 1) improve their infrastructure in technical aspects and standardize them; 2) set up online monitoring committee and employ tracking software to check the progress of the program; 3) train the faculty in ICT by conducting FDPs for all the faculty involved in the process. And faculty should have: 1) professional responsibility to update themselves by attending FDPs, and also 2) to plan and design online proctored examinations with Standard Operating Procedure (SOP).

ACKNOWLEDGEMENTS

We thank Dr. M. Shivasakthy, Professor, Deputy Director of the Centre for Health Professional Education and Dr. C.K. Lakshmidevi, Professor, Head of the Anatomy Department, for permitting us to conduct the study and supporting us to complete it successfully.

REFERENCES

BAKERSON M, RODRIGUEZ-CAMPOS L (2006) The evaluation of internet usage within the graduate-level classroom. *Int J Learning*, 13: 15-72.

BALENI Z (2015) Online formative assessment in higher education: Its pros and cons. *Electronic J e-Learning*, 13(4): 228-236.

BOITSHWARELO B, REEDY AK, BILLANY T (2017) Envisioning the use of online tests in assessing twenty-first-century learning: a literature review. *Res Practice Technol Enhanced Learning,* 12: 1-16.

DAVIES S (2010) Effective assessment in a digital age. *Bristol: JISC InnovationGroup.https://www.webarchive.org.uk/wayback/archive/20140614115719/http://www.jisc.ac.uk/media/documents/programmes/elearning/digiassass_eada. pdf.*

DONNELLY C (2014) The use of case-based multiple-choice questions for assessing large group teaching: Implications on student's learning. *Irish J Acad Practice*, 3(1): 12-15.

GIPPS CV (2005) What is the role of ICT-based assessment in universities? *Studies Higher Educ*, 30(2): 171-180.

KHAN S, KHAN RA (2019) Online assessments: Exploring perspectives of university students. *Educ Inform Technol*, 24: 661-677.

KUMAR S (2018) Awareness, benefits and challenges of e-learning among the students of Kurukshetra University Kurukshetra: A study. *Int J Inform Dissemin Technol*, 8(4): 227-230.

MUKHTAR K, JAVED K, AROOJ M, SETHI A (2020) Advantages, limitations and recommendations for online learning during COVID-19 pandemic era. *Pak J Med Sci*, 36(COVID19-S4): COVID19-S27-S31.

NICOL D (2007) E-assessment by design: using multiple-choice tests to good effect. *J Further Higher Educ*, 31(1): 53-64.

ZAFAR DR, HUSSAIN MD (2020) Technological pedagogical content knowledge (TPCK) and its implication in teacher education. *JRR*, V(XXXVI): 41-46.

European Journal of Anatomy